Spatiotemporal Dynamics of Cytoskeletal and Chemosensory Proteins in the Bacterium *Rhodobacter sphaeroides*

Sheng-Wen Chiu

Linacre College, University of Oxford

A THESIS SUBMITTED FOR THE DEGREE OF DOCTOR OF PHILOSOPHY

HILARY TERM 2014

Abstract

Spatiotemporal Dynamics of Cytoskeletal and Chemosensory Proteins in the Bacterium *Rhodobacter sphaeroides*

Sheng-Wen Chiu
Linacre College, University of Oxford
Submitted for the degree of Doctor of Philosophy, Hilary Term 2014

The discovery of the prokaryotic cytoskeleton has revolutionized our thinking about spatial organisation in prokaryotes. However, the roles different bacterial cytoskeletal proteins play in the localisations of diverse biomolecules are controversial. Bacterial chemotaxis depends on signalling through large protein clusters and each cell must inherit a cluster on cytokinesis. In *Escherichia coli* the membrane chemosensory clusters are polar and new static clusters form at pre-cytokinetic sites, ensuring positioning at new poles after cytokinesis and suggesting a role for the bacterial FtsZ and MreB cytoskeletons. *Rhodobacter sphaeroides* has both polar, membrane-associated and cytoplasmic, chromosome-associated chemosensory clusters. This study sought to investigate the roles of FtsZ and MreB in the partitioning of the two chemosensory clusters in *R. sphaeroides*. The relative positioning between the two chemosensory systems, FtsZ and MreB in *R. sphaeroides* cells during the cell cycle was monitored using fluorescence microscopy. FtsZ forms polar spots after cytokinesis, which redistribute to the midcell forming nodes from which gradients of FtsZ extend circumferentially to form the Z-ring. The proposed node-precursor model might represent a common mechanism for the formation of cytokinetic rings. The MreB cytoskeleton continuously reorganizes between patchy and filamentous structures, and colocalises with FtsZ at midcell. Membrane chemosensory proteins form individual dynamic unit-clusters with mature clusters containing about 1000 $CheW_3$ proteins. These unit-clusters diffuse randomly within the membrane but have a higher propensity for curved regions like cell poles. Membrane clusters do not colocalise with FtsZ and MreB and appear excluded from the Z-ring vicinity. The bipolar localisation of membrane clusters is established after cell division via random diffusion and polar trapping of clusters. The cytoplasmic chemosensory clusters colocalise with FtsZ at midcell in new-born cells. Before cytokinesis one cluster moves to a daughter cell, followed by the second moving to the other cell. FtsZ and MreB do not participate in the positioning of cytoplasmic clusters. Therefore the two homologous chemosensory clusters use different mechanisms to ensure partitioning, and neither system utilizes FtsZ or MreB for positioning.

Declaration

The work in this thesis was undertaken in the Department of Biochemistry at the University of Oxford. Work was performed between October 2010 and October 2013 under the supervisions of Prof. Judith P. Armitage and Prof. Mark C. Leake. All the work in this thesis is my own unless stated and has not been submitted for a degree at this or any other university.

Relevant Publications

S.W. Chiu and M.C. Leake. 2011. Functioning Nanomachines Seen in Real-Time in Living Bacteria Using Single-Molecule and Super-Resolution Fluorescence Imaging. *International Journal of Molecular Sciences* 12: 2518–2542.

S.W. Chiu, M.A.J. Roberts, M.C. Leake, and J.P. Armitage. 2013. Positioning of Chemosensory Proteins and FtsZ through the *Rhodobacter sphaeroides* Cell Cycle. *Molecular Microbiology* 90: 322–337.

I. Llortente-Garcia, T. Lenn; H. Erhardt; O. Harriman, L.N. Liu, A. Robson, **S.W. Chiu**, S, Matthews, N. Willis, C. Bray, S.H. Lee, J. Y. Shin, C. Bustamante, J. Liphardt, T. Friedrich,C. Mullineaux, M.C. Leake. 2014. Single-molecule *In Vivo* Imaging of Bacterial Respiratory Complexes Indicates Delocalised Oxidative Phosphorylation. *Biochimica et Biophysica Acta – Bioenergetics*, 1837: 811–824.

Acknowledgements

Endless thanks to my supervisors Judith P. Armitage and Mark C. Leake, for giving me the opportunity and the freedom to do exciting research, and for all their guidance and support. Thanks to Mark A. J. Roberts, Kathryn Scott, George Wadhams, and Nicolas Delalez for all their kind help and advice. I also appreciate all of the other members of the Armitage and Leake groups for their support, especially to David Wilkinson, Christopher W. Jones and Nelly Dubarry. Special thanks to Micron Oxford for help with microscopy.

I am grateful for the Scholarship for Studying Abroad from Ministry of Education, Taiwan and the EPA Cephalosporin Scholarship from Linacre College. Thanks to Department of Biochemistry (Oxford), American Society for Microbiology, British Biochemical Society, British Society for Cell Biology, Howard Hughes Medical Institute, Institute of Physics, John Innes Centre, Linacre College, and Society for General Microbiology for the financial supports which sent me to wonderful conferences to enjoy the enthusiasm of brilliant scientists.

Thanks to *Rhodobacter sphaeroides*, although your awfully slow growth makes time-lapse study a nightmare, I think that's also why the amazing FtsZ precursors could be easier to see in you.

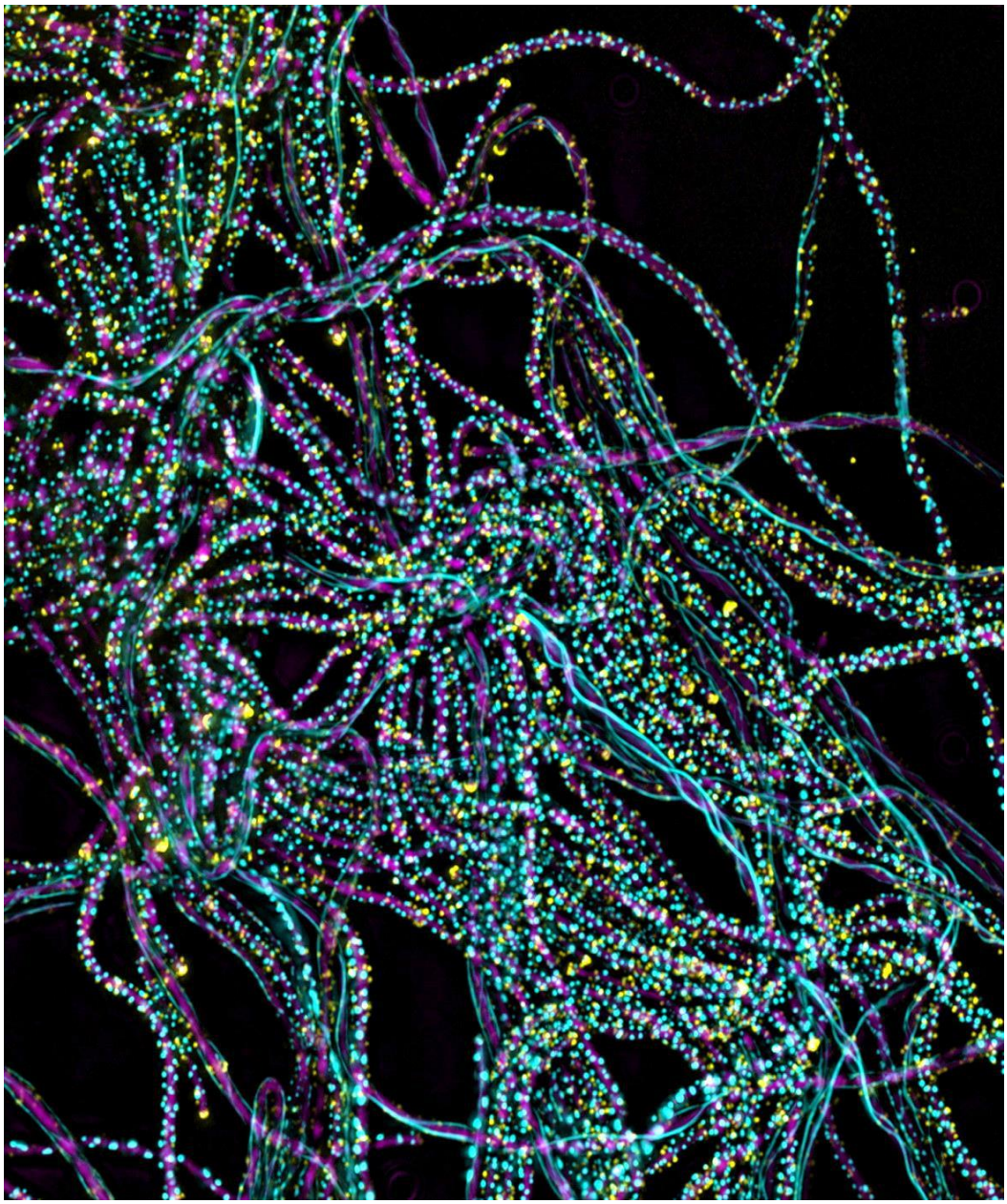

Filamentous *Rhodobacter sphaeroides* cells (magenta) expressing FtsZ–CFP and CheW$_3$–YFP.

"Nature composes some of her loveliest poems for the microscope and the telescope."

—*Where the Wasteland Ends*, Theodore Roszak.

Abbreviations

2D	Two dimensional
3D	Three dimensional
Ap^R	Ampicillin resistance
ATP	Adenosine triphosphate
AU	Arbitrary unit
bp	Base pair
CCD	Charge-coupled device
CFP	Cyan fluorescent protein
*che*Op	Chemotaxis operon
CTP	Cytidine triphosphate
DAPI	4′,6-diamidino-2-phenylindole
DIC	Differential interference contrast
EDTA	Ethylenediaminetetraacetic acid
Em	Emission
Ex	Excitation
FRAP	Fluorescence recovery after photobleaching
FRET	Förster resonance energy transfer
GDP	Guanosine diphosphate
GFP	Green fluorescent protein
GTP	Guanosine triphosphate
ICM	Intracytoplasmic membrane
IPTG	Isopropyl-β-D-thiogalactopyranoside
Km^R	Kanamycin resistance
LB	Luria-Bertani
Mb	Megabase
MSD	Mean squared displacement
NA	Numerical aperture
NTPs	Nucleotide triphosphates
OD_{600}	Optical density at 600 nm
OD_{700}	Optical density at 700 nm
oriC	Origin of replication
PALM	Photoactivatable localisation microscopy
PBP	Penicillin-binding protein
PBS	Phosphate buffered saline
PCR	Polymerase Chain Reaction
pN	Pico newton (N)

PS	Photosystem
RFP	Red fluorescent protein
SD	Standard deviation
SDS	Sodium dodecyl sulphate
STED	Stimulated emission depletion
TBE	Tris-borate-EDTA buffer
ter	Terminus of replication
Tris	2-amino-2-(hydroxymethyl)-1,3-propandiol
YFP	Yellow fluorescent protein

Table of Contents

Chapter 1. Introduction

Many researchers presently studying our simpler organisms are deeply concerned about the future of prokaryote research… We believe that some journals no longer consider developments in prokaryotic biology worthy of reporting…

— *What will be the fate of research on prokaryotes?* Charles Yanofsky

1.1 Bacterial Cell Biology

To see a world in a grain of a bug

In 1991, Charles Yanofsky wrote an editorial in *Cell* to express his concern about the fate of research on prokaryotes (Yanofsky, 1991). At that moment, the joys in these prokaryotes—amorphous bags containing homogeneous solution of biomolecules (Losick and Shapiro, 1999)—seems to be exhausted. Just in the same year, Bi and Lutkenhaus (1991) published a landmark paper for the discovery that the bacterial cell division protein FtsZ assembles into a ring-like structure (the Z-ring) at cytokinetic sites. This paper demonstrated that a cytoplasmic protein can localise to a particular site in the bacterial cell and its location is pertinent to its role in cytokinesis. This finding, together with further studies, gave rise to the notion that FtsZ is a tubulin homologue (Bermudes et al., 1994; Erickson, 1995; Lowe and Amos, 1998). Shapiro and colleagues later showed that chemoreceptors in *Caulobacter crescentus* (Alley et al., 1992) and *Escherichia coli* (Maddock and Shapiro, 1993) localise to the cell poles as huge clusters. Their observations indicate that the bacterial cytoplasmic membrane is not uniform and protein complexes can localise to particular regions of the membrane. The underlying themes of these findings—bacterial cell division, chemotaxis,

cytoskeleton, and protein localisation—are still the frontiers of microbiology. Moreover, even after two decades of fruitful studies, some essential puzzles remain unanswered for FtsZ and chemosensory clusters.

It is now clear that the interior of a bacterium is not an amorphous, unstructured amalgamation containing a homogeneous solution of biomolecules, as had been the received until very recently (Errington, 2003; Losick and Shapiro, 1999). We are now entering a new phase, where dramatic advances in bacterial cell biology continually increase our appreciation of how the whole bacterial cell has an exquisitely organized and dynamic subcellular architecture (Gitai, 2005; Goley, 2013). Work in multiple bacterial species has demonstrated that a whole set of biomolecules occupy specific subcellular locations and exhibit dynamic behaviours (Dworkin, 2009; Govindarajan et al., 2012; Morris and Jensen, 2008; Nevo-Dinur et al., 2012; Norris et al., 2007; Rudner and Losick, 2010; Shapiro et al., 2009; Vendeville et al., 2010). Therefore, characterising spatial dynamics is essential to clearly understand biological processes even in the "simple" bacteria.

The power of direct visualization earns microscopy a special place in life sciences, and indeed the development of bacterial cell biology has greatly relied on microscopy (Chiu and Leake, 2011; Gitai, 2009; Kentner and Sourjik, 2010; Lewis, 2004; van Teeffelen et al., 2012). Owing to its relative ease of implementation and ability to image cells under native living conditions without the need for harsh treatments, fluorescence microscopy is among the most versatile and accessible methods for direct observation (Gitai, 2009). The development of fluorescent proteins as molecular tags over the past two decades has provided a revolutionary tool for cell biology by allowing several proteins to be simultaneously monitored in living cells (Chudakov et al., 2010; Hinner and Johnsson, 2010; Kremers et al., 2011; Shaner et al., 2005; Shaner et al., 2007; Snapp, 2009). The concomitant progresses in small organic fluorescent dyes, nanocrystals ("quantum dots"), and small genetic encoded tags including fluorescent amino acids further expend the toolbox of biologists (Giepmans et al., 2006; Hinner and Johnsson, 2010). The application of these fluorescent probes in bacteria has made it routine to visualize the dynamic localisation of proteins, DNA, RNA, lipids, and peptidoglycans in living bacterial cells (Foss et al., 2011; Golding and Cox, 2004; Southward and Surette, 2002; Wang et al., 2008b). In parallel to the developments in fluorescent labelling are the advances in digital photography (Eils and Athale, 2003), three-dimensional (3D) imaging (Gerlich and Ellenberg, 2003), fluorescence recovery after photobleaching (FRAP) (Lippincott-Schwartz et al., 2003), Förster resonance energy transfer (FRET) (Padilla-Parra and Tramier, 2012), and single-cell time-lapse imaging (Brehm-Stecher and Johnson, 2004), to

name just a few. These techniques have been proven invaluable to bacterial cell biology (Brehm-Stecher and Johnson, 2004; Chiu and Leake, 2011; Gitai, 2009; Kentner and Sourjik, 2010). In the past few years, large-scale, high-throughput imaging has been adapted for bacterial cell biology and yielded some exciting discoveries (Gerding et al., 2007; Goley et al., 2010; Kitagawa et al., 2006; Werner et al., 2009). Since most bacteria studied are just a few fold larger than the diffraction limit of conventional microscopy, it is no doubt that super-resolution/single-molecule fluorescence imaging (Biteen, 2012; Biteen and Moerner, 2010; Chiu and Leake, 2011; Coltharp and Xiao, 2012; Gahlmann and Moerner, 2014) and cryo-electron tomography (Milne and Subramaniam, 2009; Tocheva et al., 2010) have brought unprecedented insights to this field.

Spatial organisation in bacteria

After decades of dissecting bacterial cells into their molecular constituents, we are now trying to put them back together. How do genes and their products perform biological functions in space and time? How do bacteria generate, maintain, and reproduce their spatial organization? Advances in bacterial cell biology have expended the study of spatial organisation into diverse aspects and levels, from individual molecules to subcellular architecture, from cell differentiation to multicellularity. Bacterial cells have signature shapes (Young, 2006), intrinsic polarity (Dworkin, 2009), and specifically positioned macromolecular assemblies (Govindarajan et al., 2012). Each cell division is a challenge: a newborn bacterial cell has to complete huge intersecting tasks to divide. Not only must it double in size, replicate and segregate its genome, and position its division machinery at the right place, a bacterial cell must also copy its structural framework. It is crucial that all these tasks are spatially and temporally coordinated. Indeed, bacterial spatial organisation is controlled by multi-component regulatory networks, involving localised protein complexes and dynamic cytoskeletal structures (Haeusser and Levin, 2008; Thanbichler, 2010).

Protein localisation in bacteria

Who?

Which proteins in bacteria have non-uniform localisation patterns? In *C. crescentus*, ~10% of its proteome exhibit non-uniform subcellular localisation (Werner et al., 2009). Proteins belonging to many diverse functional categories are

positioned specifically: cell motility, signal transduction, cell division and DNA partitioning, DNA replication/recombination/repair, cell envelope biogenesis, and intracellular trafficking and secretion (Govindarajan et al., 2012; Laloux and Jacobs-Wagner, 2014; Morris and Jensen, 2008; Rudner and Losick, 2010; Shapiro et al., 2009; Vendeville et al., 2010). It should be noted that localisation of proteins varies with growth conditions, cell cycle stages and differentiation (Morris and Jensen, 2008; Rudner and Losick, 2010; Shapiro et al., 2009; Vendeville et al., 2010). Typical localisation patterns observed are filamentous structures/extended arrangements (helices, rings, curved lines) (Cabeen and Jacobs-Wagner, 2010; Govindarajan et al., 2012; Pilhofer and Jensen, 2013) as well as foci with anterior/posterior or dorsal/ventral positioning (Shapiro et al., 2009).

Why?

Dynamic protein localisation facilitates bacterial behaviours as diverse as aging, cell division, chemotaxis and motility, differentiation, gene expression, genome maintenance, interactions with hosts, macromolecular partition and transport, metabolism, morphogenesis, and multicellular phenomenon (Garcia Vescovi et al., 2010; Govindarajan et al., 2012; Rudner and Losick, 2010; Shapiro et al., 2009; Thanbichler, 2010). To perform miscellaneous biological processes with small genomes, temporal and spatial regulations can provide economic solutions to bacteria. Besides, some "design principles" can be envisioned for spatial regulation in bacteria:

1. Directions in space:

Polarity/directionality is the most common spatial pattern in all living systems (Nelson, 2003). Polarity is the cornerstone of growth and division, even spherically symmetrical bacterial cells must break symmetry in order to divide (Dworkin, 2009; Margolin, 2009). By altering the direction of cell-wall growth, cells can differentiate into different progenies (e.g. spores and mycelia) or make cell extensions that possess specialized functions (e.g. stalks). Besides cell shape, directionality is apparent in the motion of bacteria, which depends on polarized organelles in many cases (Kirkpatrick and Viollier, 2010).

2. Coordination:

Spatial coupling enhances the efficiency and specificity of reaction pathways by (1) increasing local concentrations of all components that further improve substrate/intermediate channelling; (2) facilitating reaction flux control (Govindarajan et al., 2012; Morris and Jensen, 2008; Wilson and Gitai, 2013). Physically colocalised systems are expected to be more noise-free than systems composed of randomly diffusing components. Polar localisation of proteins can

produce a cellular gradient of activity (e.g. MinCDE) or confine an activity to a discrete cellular location (e.g. proteolytic control of DNA replication initiation inhibitor) (Shapiro et al., 2009).

Scaffolding/clustering provides a means for fine control in cell signalling (Kholodenko et al., 2010). First, the generation of a cascade can be terminated by spontaneous disassembly of a protein cluster without requiring biochemical modification of many components. Second, proteins can be used for different functions in a context-dependent manner, offering a combinatorial repertoire for a huge diversity originated from a small pool of components.

3. Geometric power—form and function:

Many bacterial proteins adopt helical distributions (Govindarajan et al., 2012). Why should nature chose a helix? Helices have a structure with a repetition along a screw axis. The repetition has constant radius and axial pitch. These characteristics give a helix some distinctive features: equivalence, symmetry, economy and stability (Galloway, 2010). Equivalence implies a symmetrical balance of forces (or any kind of effects). The equivalence of a helix results in a constant torsion at every point, and hence stability. The helical packing of molecules also has the advantage that it can accommodate any cell shape. The helix can compress or relax to adapt to the changes of cell geometry or alter its localisation. It is arguably a very efficient way to uniformly distribute molecules throughout the cell without having to produce an enormous total mass of biological material (Galloway, 2010).

How?

What mechanisms govern subcellular protein localisation? Three ultimate approaches seem to form the basis of all mechanisms. **Self-assembly processes** can create and maintain dynamic patterns from constituent components in a spontaneous manner, without external impetus (Rudner and Losick, 2010), exemplified by the oscillating MinCDE system and other bacterial cytoskeletons (Cabeen and Jacobs-Wagner, 2010; Rudner and Losick, 2010; Shapiro et al., 2009). This mechanism can work without positional cues (Rudner and Losick, 2010; Shapiro et al., 2009).

Geometric cues largely depend on the geometric differences between the cell pole and the lateral site of a rod-shaped cell. Uneven distributions of membrane phospholipids with different curvatures in each region exhibit landmarks for the localisation of primary protein anchors (Dworkin, 2009; Govindarajan et al., 2012; Rudner and Losick, 2010; Shapiro et al., 2009). Using self-assembly and geometric cues, the *Bacillus subtilis* protein DivIVA can establish similar polar localisation

even in *E. coli* or the fission yeast *Schizosaccharomyces pombe* (Ramamurthi, 2010; Strahl and Hamoen, 2012).

Bacterial cells tightly coordinate chromosome segregation and cytokinesis to ensure faithful transmission of genetic materials and spatial organisation to their daughter cells (Haeusser and Levin, 2008; Thanbichler, 2010). To this end, bacteria have developed mechanisms that monitor the cell-cycle-dependent spatial dynamics of chromosome to select the cell-division site and control the timing of divisome assembly (Haeusser and Levin, 2008; Thanbichler, 2010). Thus beyond a vehicle of genetic information, the **chromosome/nucleoid** also actively participates in the shaping of spatial organisation of the cell (Ptacin and Shapiro, 2013). A well-known example is nucleoid occlusion, which prevents the assembly of divisome in the close vicinity of the nucleoid (Wu and Errington, 2011). Current studies also show a sophisticated communication between chromosome segregation and cell division: by coupling the spatial distribution of the FtsZ-modifier MipZ to chromosome organization, the divisome can form at the midcell at the right time (Kiekebusch et al., 2012; Thanbichler and Shapiro, 2006). Recent advances in imaging technologies have revealed that the nucleoid has specific and dynamic organizations within the cell (Berlatzky et al., 2008; Fisher et al., 2013; Toro and Shapiro, 2010; Wang et al., 2011). The self-replicating nature (Youngren et al., 2014) and robustness (Wiggins et al., 2010) of this organisation make it a good "template" for protein localisation (Campos and Jacobs-Wagner, 2013; Ptacin and Shapiro, 2013). In brief, this could be via an interaction with a specific chromosomal locus (Campos and Jacobs-Wagner, 2013; Ptacin and Shapiro, 2013), or a passive steric hindrance/crowding effect (Laloux and Jacobs-Wagner, 2014).

All other protein localisation approaches probably exert their functions based on the above three mechanisms. **Diffusion-and-capture** may be the most widely used secondary mechanism, in which proteins diffuse throughout the cell until encountering their anchors (Bardy and Maddock, 2007; Laloux and Jacobs-Wagner, 2014; Rudner and Losick, 2010; Shapiro et al., 2009). Hence, a localised anchor (e.g. DivIVA or lipid domains) can capture and localise other proteins. Bacterial cytoskeletons can serve as intracellular tracks or scaffolds for the localisation of a host of proteins (de Boer, 2010; Rudner and Losick, 2010; Shaevitz and Gitai, 2010). We can consider cytoskeletons-based localisation as a variation of diffusion-and-capture. Proteins can also be **positioned at the cytokinetic site**, so after cell division they are localised at the cell pole readily. This is illustrated by the association of the polar landmark TipN with the divisome in *C. crescentus* (Laloux and Jacobs-Wagner, 2014). Each round of

cytokinesis defines a new pole versus an old pole, each has a different age and developmental history (Bardy and Maddock, 2007; Dworkin, 2009; Macara and Mili, 2008). Besides, the polar and lateral cell envelopes have different compositions. Therefore, **different affinities for pole- or lateral site-specific elements** of the cell envelope could localise proteins to different regions (Laloux and Jacobs-Wagner, 2014).

1.2 Bacterial Chemotaxis

Evolution is the best judge of biological importance. The importance of taxis is illustrated by the diverse mechanisms utilized by bacteria to perform tactic behaviours (Armitage and Scott, 2013; Krell et al., 2011). Among them, chemotaxis is the best studied example. In addition to moving to an optimum environment, bacterial chemotaxis is important for symbiosis, pathogenesis, and biofilm formation (Porter et al., 2011a; Wadhams and Armitage, 2004). The "wheel" in bacterial chemotaxis, the flagellum, is a large membrane-spanning nanomachine generated from choreographed expression and assembly of ~50 genes/proteins (Erhardt et al., 2010; Sowa and Berry, 2008). The flagellar motor is powered by H^+ or Na^+ ion flux and can change its rotatory direction or frequency. This nanomachine is so exquisite that its existence was used to against the theory of evolution (Pallen and Matzke, 2006). If the "wheel" is so exquisite, no doubt that the "driver", the chemosensory pathway, is very sophisticated (Hazelbauer et al., 2008; Sourjik and Armitage, 2010; Sourjik and Wingreen, 2012). The bacterial chemosensory pathway is one of the best-studied model systems of signal transduction (Sourjik and Wingreen, 2012) and a paradigm for systems biology (Baker et al., 2006; Tu, 2013). Researches on two bacterial models have greatly contributed to our understandings of chemotaxis: *E. coli* and *Rhodobacter sphaeroides*.

The *E. coli* dogma

The chemosensory signal transduction pathway

The *E. coli* chemotactic machinery has been extensively characterised (Sourjik and Armitage, 2010; Sourjik and Wingreen, 2012). The chemosensory pathway (Fig. 1.1) starts with transmembrane chemoreceptors, which detect chemoeffectors and transmit signals to regulate the autophosphorylation of the cytoplasmic histidine kinase, CheA. The adaptor CheW facilitates the interactions between CheA and receptors. CheA transfers phosphoryl groups to the response regulator CheY. CheY-P released from the receptor complex diffuses to the flagellar motor and promotes a switch in the rotational direction of flagella (Porter et al., 2011a; Sourjik and Armitage, 2010; Sourjik and Wingreen, 2012).

E. coli has four chemoreceptors, ***m***ethyl-accepting ***c***hemotaxis ***p***roteins (MCPs), which form homodimers that span the cytoplasmic membrane (Hazelbauer et al., 2008; Hazelbauer and Lai, 2010). MCPs dimers are long (~ 37 nm) structures composed of α-helical coiled-coils (Hazelbauer et al., 2008; Liu et

al., 2012). The diverse periplasmic domain of MCPs is responsible for chemoeffector sensing. A change in ligand binding is transmitted from the periplasmic domain across the cell membrane to the cytoplasmic signaling domain. The cytoplasmic domain is conserved across all bacterial species. The chemoreceptor homodimers form trimers-of-dimers with other MCPs. The number of receptors differs, with Tsr (***t***axis to ***s***erine and ***r***epellents) and Tar (***t***axis to ***a***spartate and ***r***epellents) being high-abundance and Trg (***t***axis to ***r***ibose and ***g***alactose) and Tap (***ta***xis to di***p***eptides) being low-abundance receptors. CheA and CheW stabilize the trimers-of-dimers arrangement (Hazelbauer et al., 2008; Wadhams and Armitage, 2004). Bacteria adapt to a background level of chemoeffectors by both rapid signal termination and by resetting the receptors to a non-signalling state. This adaptation depends on the degree of methylation of specific, conserved glutamate residues in the cytoplasmic signalling domain of an MCP. Methyl groups are transferred to MCPs by the constitutively active methyltransferase CheR, and they are removed by the methylesterase CheB (Fig. 1.1) (Wadhams and Armitage, 2004).

CheA functions as a dimer that phosphorylates two response regulator proteins, CheY and CheB. In response to decreased attractant binding, the *E. coli* MCPs promote tumbling by activating CheA autophosphorylation. Phosphorylated CheA transfers phosphate group to CheY and CheB. CheY-P is released from the chemosensory cluster and diffuses to the flagellar motor, where it binds to FliM and FliN of the switch complex and promotes a switch in the rotational direction (from anticlockwise to clockwise) (Porter et al., 2011a; Wadhams and Armitage, 2004).

CheW is an 18 kDa protein composed of two SRC-homology-3 (SH3) like domains. In eukaryotes, SH3 domain mediates the assembly of specific protein complexes. It is found in many proteins that are involved in signal transduction (Mayer, 2001). CheW interacts with both CheA and MCPs, and is required for the formation of the quaternary MCP–CheW–CheA complex (Li et al., 2013a; Liu et al., 2012). CheW has no known catalytic activity and is therefore thought to be a scaffold protein that transduces the signals generated by the MCPs to CheA. However, the primary sequence of CheW is highly conserved, and in many species there are several homologues that are involved in chemotaxis, suggesting CheW may have other roles than a simple scaffold protein (Porter et al., 2011a; Wadhams and Armitage, 2004).

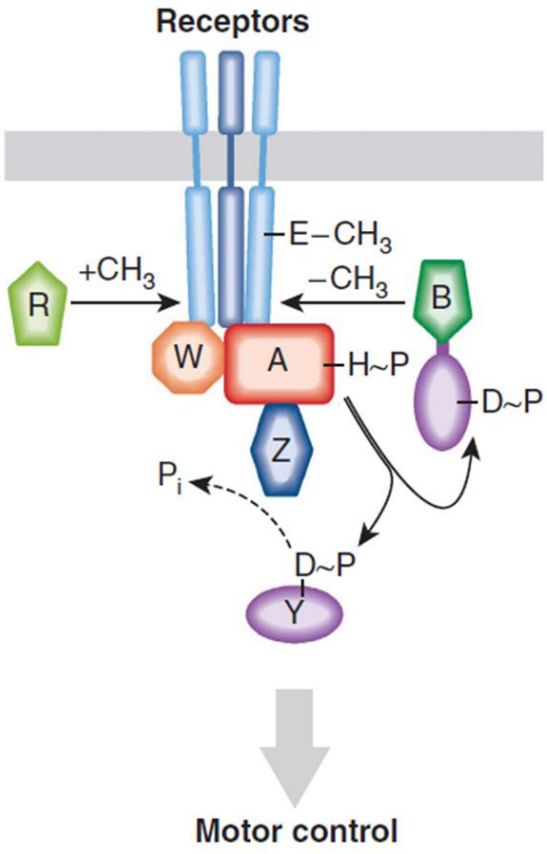

Figure 1.1. Schematics of the *E. coli* chemosensory pathway. Receptors sense and transmit signals to regulate the activity of the cytoplasmic histidine kinase CheA. Different types of receptor dimers (light or dark blue) form mixed trimers. The binding and regulation of CheA by receptors are aided by CheW. CheA transfers phosphate group to CheY (a response regulator controlling flagellar motor) and CheB (a methylesterase controlling the adaptation of receptors). Receptors are methylated on glutamate residues by the methyltransferase CheR. CheY is dephosphorylated by the phosphatase CheZ to allow rapid signal termination. Receptors, CheA, and CheW form a stable signalling core, to which CheB, CheR, CheY and CheZ dynamically localise. From Sourjik and Armitage (2010).

Spatial organisation of the *E. coli* chemosensory system

Clustering of chemosensory proteins

Thousands of chemosensory proteins, including receptor trimers-of-dimers, CheA and CheW, form large membrane chemosensory clusters at the cell poles and smaller clusters along the cell body (Fig. 1.2) (Briegel et al., 2009; Hazelbauer et al., 2008; Sourjik and Armitage, 2010). The formation of membrane chemosensory clusters is universal in prokaryotes (Gestwicki et al., 2000). Fluorescence microscopy and cryo-electron tomography suggest a preferential polar/subpolar localisation of these clusters in bacterial species studied so far (Briegel et al., 2009; Porter et al., 2011a).

Receptor trimers-of-dimers self-assemble into roughly hexagonal arrays in the membrane chemosensory clusters (Fig. 1.3). Clusters are further stabilized by the association of CheA and CheW. The chemosensory arrays are not perfectly regular structures and the hexagonal arrangement appears to be frequently distorted. All other chemosensory proteins localise to the clusters by interacting with either chemoreceptors or CheA. The core of the cluster (chemoreceptors,

CheA, and CheW) is stable, with no chemoreceptors exchange between clusters for >30 min (Sourjik and Armitage, 2010).

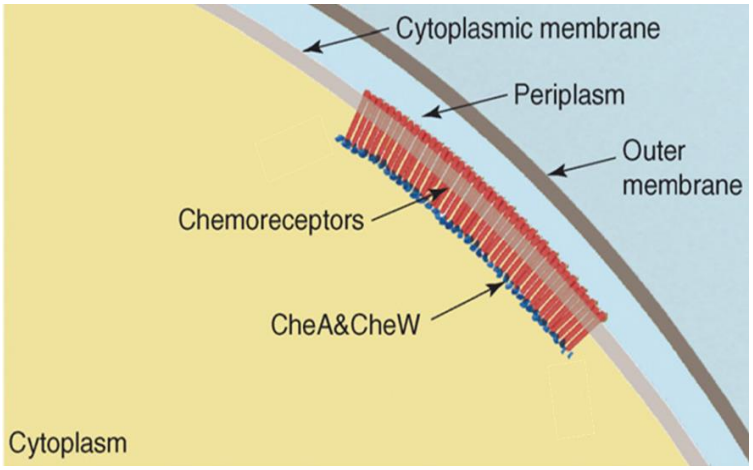

Figure 1.2. Schematics of the membrane chemosensory cluster based on cryo-electron tomography images of *E. coli*. Chemoreceptors (red) and the CheA/CheW layer (blue) form clusters near the cell pole. These clusters occur in cells containing chemoreceptors, CheA and CheW, but not in cells lacking any one of these proteins. Adapted from Hazelbauer et al. (2008) and Zhang et al. (2007).

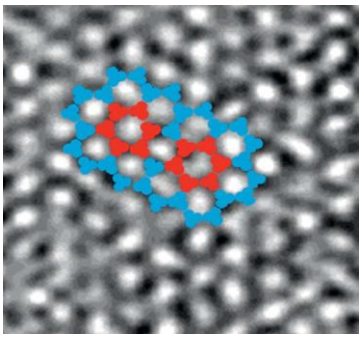

Figure 1.3. A cryo-electron tomography image of the conserved hexagonal architecture in membrane chemosensory clusters. Cartoon illustrates fitting of trimers-of-dimers into the hexagonal lattice. One circle represents one receptor dimers. Six trimers-of-dimers enclose one hexagon (red). Adapted from Sourjik and Armitage (2010).

The formation of chemosensory clusters is believed to possess two important functions based on cooperative interactions: (1) amplification and integration of chemotactic stimuli (2) scaffolding protein partners, thus enhancing the efficiency and specificity of the chemosensory pathway (Hazelbauer et al., 2008; Sourjik and Armitage, 2010).

The *Rhodobacter sphaeroides* version of chemotaxis

The α-proteobacterium *R. sphaeroides* is tactic towards a wide range of different stimuli, including oxygen, light, some amino acids, certain sugars, and organic acids (e.g. succinate and propionate). The chemotaxis of *R. sphaeroides* to most attractants depends on energy taxis/metabolic sensing, in which transport and metabolism of the attractants are required for sensing (Porter et al., 2011a). Energy taxis is used by diverse bacterial species and has the advantage of

allowing migration towards those environments that are optimal for metabolism rather than those merely having a high concentration of a particular attractant (Alexandre, 2010). In contrast to the *E. coli* bidirectional flagellar motor, *R. sphaeroides* has a single unidirectional stop–start motor (Pilizota et al., 2009). *R. sphaeroides* responses to a reduction in an attractant, and CheY-P binding causes the motor to stop. Upon ceasing to rotate, the flagellar filament changes its conformation from helical to coiled form, leading to cell reorientation (Armitage et al., 1999).

The chemosensory systems in *R. sphaeroides* represent a higher level of complexity, reflecting its physiological versatility (Fig. 1.4) (Porter et al., 2008, 2011a; Sourjik and Armitage, 2010). It is an emerging model organism for studying signal transduction complexity found in many bacteria and more complex cells (Porter et al., 2011a). *R. sphaeroides* has three major operons encoding chemosensory proteins, two of which (*che*Op$_2$ and *che*Op$_3$) are expressed under laboratory conditions. The chemosensory proteins in the two expressing operons including two CheA homologues, three CheW homologues, three CheY homologues, two CheB homologues, and two CheR homologues (Porter et al., 2008, 2011a). The *R. sphaeroides* chemosensory proteins form an *E. coli*-like conventional membrane-associated pathway with nine membrane-spanning chemoreceptors (MCPs), and a second novel cytoplasmic pathway with four soluble chemoreceptors (***t***ransducer-***l***ike ***p***roteins, Tlps). *R. sphaeroides* requires both pathways for chemotaxis. Separation of chemosensory proteins may enable tuning of responses to independently sensed external and internal conditions (Porter et al., 2008, 2011a; Sourjik and Armitage, 2010).

The membrane chemosensory system

Previous studies have showed that membrane chemosensory clusters in *R. sphaeroides* have bipolar localisation similar to *E. coli* (Fig. 1.5) (Harrison et al., 1999; Wadhams et al., 2000; Wadhams et al., 2003). These clusters are composed of the MCPs and the *che*Op$_2$-encoded proteins CheA$_2$, CheW$_2$, CheW$_3$ and CheR$_2$. Cluster formation depends on CheA$_2$, CheW$_2$, CheW$_3$ and the MCPs (Martin et al., 2001; Wadhams et al., 2005). CheA$_2$-P can phosphorylate all of the *R. sphaeroides* response regulators, meaning that the membrane cluster can influence the cytoplasmic cluster (Fig. 1.4) (Porter and Armitage, 2002).

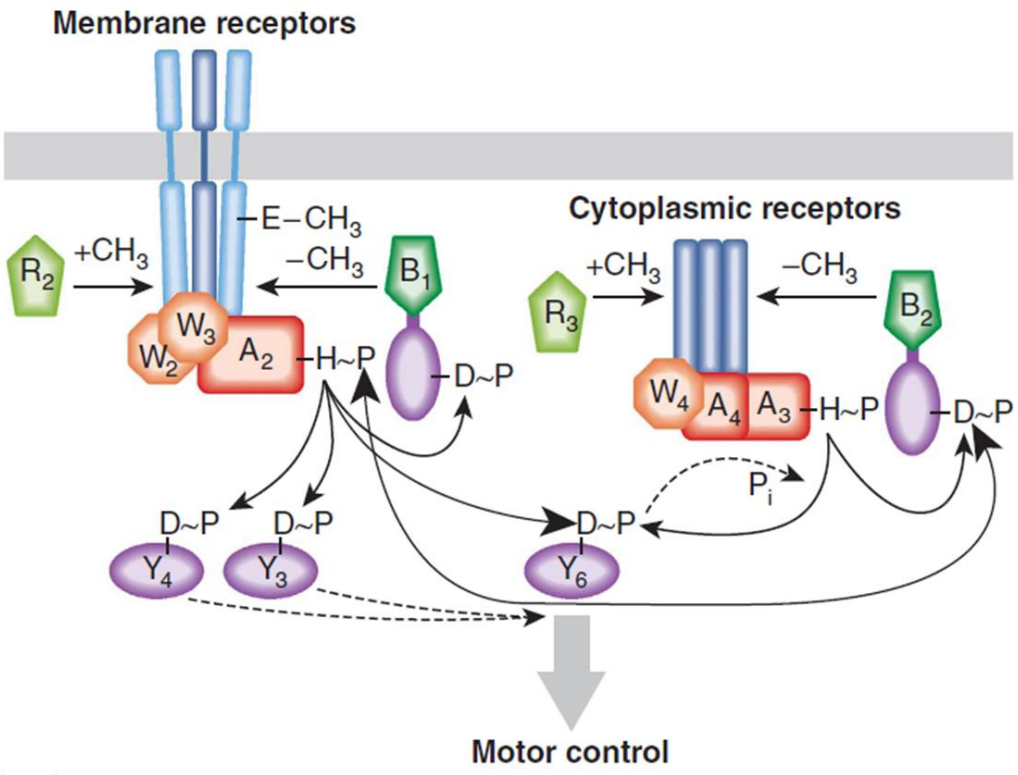

Figure 1.4. Schematics of the *R. sphaeroides* chemosensory pathways. Attractants are thought to be sensed by the transmembrane receptors, which regulate $CheA_2$ activity. Internal signals reflecting the metabolic state of the cell are thought to be sensed by the cytoplasmic receptors, regulating $CheA_3$ and $CheA_4$. $CheY_6$ alone is capable of stopping the flagellar motor, but requires either $CheY_3$ or $CheY_4$ to support full chemotaxis. The reversible phosphotransfer between $CheA_2$ and $CheB_2$ is indicated by the bi-sided arrow. From Sourjik and Armitage (2010).

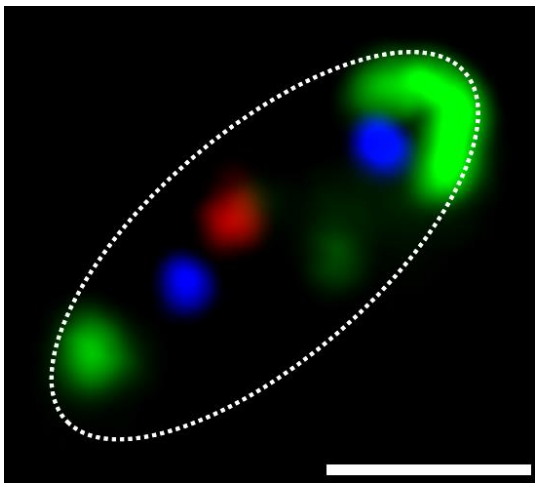

Figure 1.5. Localisations of membrane (green) and cytoplasmic (blue) chemosensory clusters in *R. sphaeroides*. Dashed line: cell outline. Green: membrane clusters marked by YFP–$CheW_3$; blue: cytoplasmic clusters marked by TlpT–CFP; red: the cytokinetic site marked by FtsZ–RFP. Scale bar: 1 μm.

The membrane and cytoplasmic chemosensory clusters each contain dedicated chemoreceptors plus a set of CheW, CheA and CheR proteins. Strikingly, protein homologues are found in both types of cluster (Wadhams et al., 2005; Wadhams et al., 2003). Therefore, the interactions between proteins within the same cluster type must be highly specific. For CheA homologues, the specificity is determined by contacts made between the CheA P5 domain and the other components of the cognate cluster. Intriguing, *R. sphaeroides* CheA homologues can complement equivalent deletions in *E. coli*, but they do not function when they are artificially targeted to the "wrong" clusters (Scott et al., 2010).

The cytoplasmic chemosensory system

The cytoplasmic cluster localises at (pre)cytokinetic sites (Fig. 1.5) and comprises the cytoplasmic receptors (Tlps) lacking transmembrane regions and the *che*Op$_3$-encoded proteins CheA$_3$, CheA$_4$, CheW$_4$ and CheR$_3$ (Wadhams et al., 2005; Wadhams et al., 2003). Cluster formation requires the cytoplasmic chemoreceptors along with CheW$_4$ and either CheA$_3$ or CheA$_4$ (Wadhams et al., 2005). As the membrane chemosensory clusters, there are thousands of chemoreceptors and associated proteins in the cytoplasmic clusters. Intriguingly, cytoplasmic clusters contain trimers-of-receptor-dimers organised in hexagonal arrays similar to those of membrane clusters (Briegel et al., 2014). However, it is unclear how chemosensory proteins form a quaternary complex in the absence of a membrane scaffold. One possibility is that the cytoplasmic clusters can use the nucleoid as a supporting matrix, as proposed for other cytoplasmic macromolecular assemblies (Galán et al., 2011; Henry and Crosson, 2013). Any mutation that causes cytoplasmic cluster disassembling also impedes normal chemotaxis. Therefore, each cell must inherit both the membrane and cytoplasmic clusters for proper chemotaxis.

The ligands of the cytoplasmic chemoreceptors are unknown. Nevertheless, chemotaxis towards many attractants (e.g. alanine, ammonia, glutamate and sugars) requires their transport and metabolism, suggesting common metabolites derived from these chemoeffectors could be the ligands (Porter et al., 2011a). Thus the cytoplasmic clusters might participate in energy taxis.

The cytoplasmic chemosensory cluster regulates the activity of two unusual CheA homologues, CheA$_3$ and CheA$_4$. CheA$_4$ is an N-terminally truncated CheA homologue, while CheA$_3$ has the centre region replaced by a novel ~ 800-amino acid sequence possessing phosphatase activity (Porter and Armitage, 2002). CheA$_4$ phosphorylates CheA$_3$ and CheA$_3$-P acts as a phosphodonor for CheY$_6$ and

$CheB_2$ (Porter and Armitage, 2004). Therefore, the cytoplasmic cluster can influence the phosphorylation state of only two response regulators, comparing to all for the membrane cluster.

Positioning of chemosensory clusters

The membrane chemosensory clusters

The polar/subpolar localisation of membrane chemosensory clusters is universal in prokaryotes (Briegel et al., 2009; Gestwicki et al., 2000; Porter et al., 2011a). In addition to enhance chemosensory signalling (Ringgaard et al., 2011; Ringgaard et al., 2014; Sourjik and Armitage, 2010), the polar localisation of chemosensory proteins may facilitate communications between the chemosensory machinery and the general phosphotransferase system (PTS), thus coordinate their actions and generate an optimal metabolic response (Govindarajan et al., 2012).

Three mechanisms have been proposed for the polar localisation of membrane chemosensory clusters mainly based on the studies of *E. coli* and vibrios. The **stochastic self-assembly/cytokinetic site-anchoring** (Fig. 1.6) mechanism suggests newly synthesized chemosensory proteins either join existing clusters or nucleate new ones (Greenfield et al., 2009; Thiem and Sourjik, 2008; Wang et al., 2008a). In the stochastic self-assembly process, cluster nucleation is distance-dependent and away from existing clusters (Fig. 1.6 A). This results in a periodic distribution of clusters along the cell body, with the cluster size decreasing in the order of old-pole, new-pole, midcell, quarters and so on. This mechanism ensures an even positioning of membrane chemosensory clusters at (pre)cytokinetic sites, so they readily localise at the new poles after cell division (Fig. 1.6 B) (Greenfield et al., 2009; Thiem and Sourjik, 2008; Wang et al., 2008a). However, the stochastic self-assembly process cannot explain why lateral clusters keep static at these sites (Fig. 1.6 B, arrowheads). An anchor, like a cytoskeletal structures, is proposed to attach lateral clusters at (pre)cytokinetic sites (Thiem et al., 2007; Thiem and Sourjik, 2008). The identity of this putative anchor is unknown, but Thiem et al. (2007) showed that it is not the *E. coli* MreB or MinCDE cytoskeletal systems. Movement of polar clusters is also restricted by unknown mechanisms, possibly the specific membrane curvature or lipid composition of the cell pole (Rudner and Losick, 2010). In this stochastic self-assembly/cytokinetic site-anchoring mechanism, the positioning and formation of new clusters is coupled.

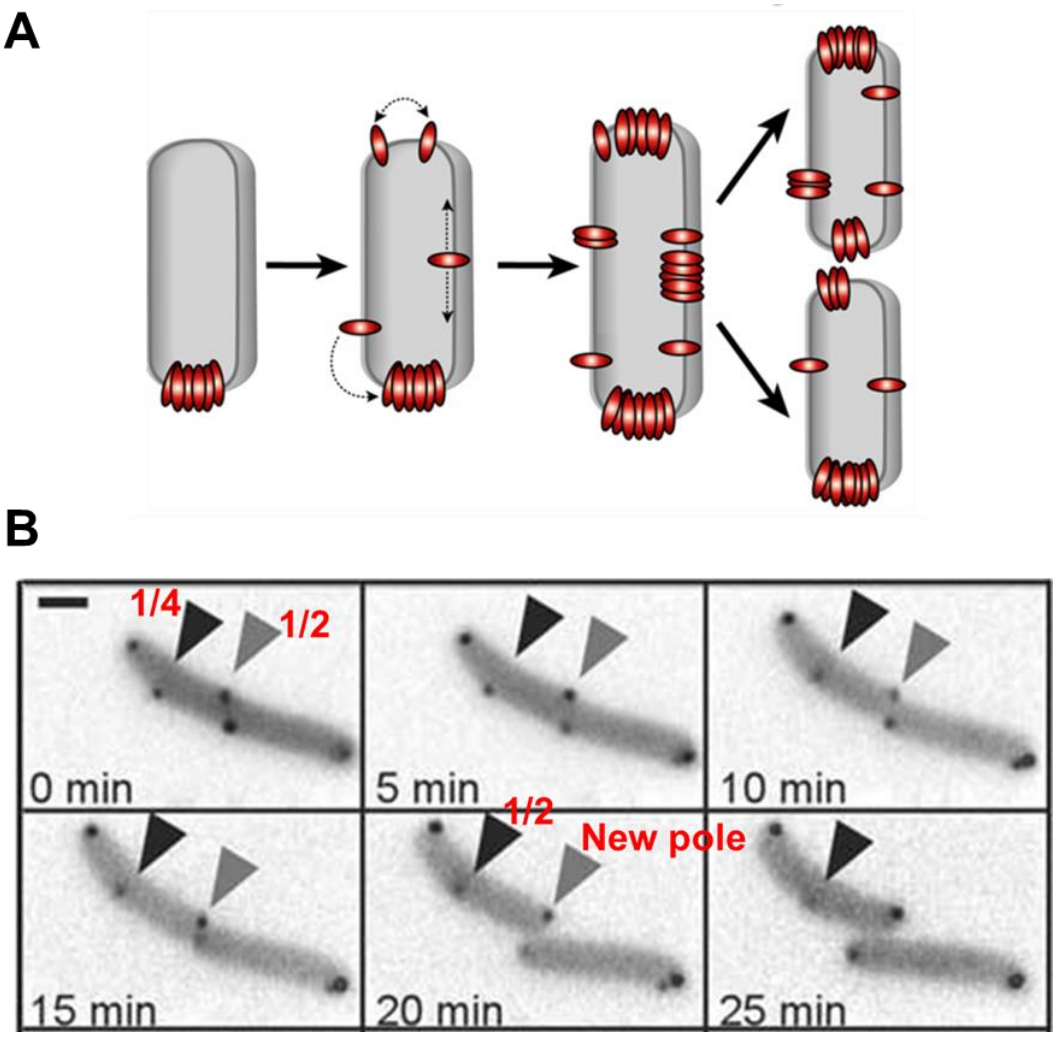

Figure 1.6. The stochastic self-assembly/cytokinetic site-anchoring mechanism for membrane chemosensory clusters. **(A)** Schematics of the stochastic self-assembly by which cluster locations are maintained. Cluster nucleation is most likely to occur where the density of unclustered receptors is high, which occurs far from any existing cluster. So new clusters form primarily at locations that are furthest from large existing clusters. Therefore, a cell with one polar cluster will tend to form the next large cluster at the opposite pole, yielding a bipolar localisation. A cell with clusters at both poles will tend to form new clusters at the midcell (the location furthest from both poles). Adapted from Greenfield et al. (2009). **(B)** Time-lapse images of growing *E. coli* cells with membrane chemosensory clusters marked by YFP–CheR. Grey arrows indicate a lateral cluster that is initially positioned at ~ 1/2 of the cell length and becomes polar after the next cell division (20 min, "new pole"). Black arrows indicate a lateral cluster that is initially positioned at ~ 1/4 of the cell length and becomes polar two generations later (not shown). It becomes a midcell cluster at 20 min. Scale bar: 1 μm. Adapted from Thiem et al. (2007).

An alternative **helical insertion diffusion–capture** mechanism suggests that newly synthesized chemoreceptors are inserted in the membrane in a helical fashion via the general protein translocation machinery (Sec) (Shiomi et al., 2006). The chemoreceptors then migrate to and form large clusters at the cell poles. However, it is difficult to explain the observed localisation patterns (e.g. static lateral clusters in Fig. 1.6 B) by this mechanism.

Waldor and colleagues showed in three reports that a third **ParPC-mediated diffusion–capture** mechanism occurs in some polar-flagellated bacteria (e.g. vibrios). In *Vibrio cholerae* and *V. parahaemolyticus*, the localisation of membrane chemosensory clusters shows a unipolar-to-bipolar transition during the cell cycle: newborn cells have chemosensory clusters locate at the old pole, and then new clusters appear at the new pole before cytokinesis (Ringgaard et al., 2011). A multidomain polar anchor, HubP (***hub*** of the ***p***ole), anchors three ParA-like ATPases (section 1.5) to the cell poles and, through them, controls polar localisation of the chromosome origin, the chemosensory machinery, and the flagellum (Yamaichi et al., 2012). One of these ParA-like proteins, ParC (***par***titioning ***c***hemotaxis), is encoded within chemotaxis operons of many polar-flagellated γ-proteobacteria (Ringgaard et al., 2011). ParC interacts (probably indirectly) with HubP (Yamaichi et al., 2012). HubP partially relocalises from the poles to the midcell prior to cytokinesis, thereby enabling endurance of the polar anchorage in future daughter cells. Unknown mechanisms delay the recruitment of ParC by HubP, so ParC does not localise at the new poles in newborn cells (Yamaichi et al., 2012). ParC further recruits ParP to the "mature" new poles (Ringgaard et al., 2014). ParP sequesters chemosensory clusters at the cell poles via capturing and preventing the dissociation of CheA. ParP binds CheA via a CheW-like domain. Remarkably, a tripartite (ParC–ParP–CheA) interaction network coevolves in certain polar-flagellated γ-proteobacteria (Ringgaard et al., 2014).

Waldor and colleagues suggested that in vibrios the ParPC anchor modifies the otherwise stochastic self-assembly process of chemosensory protein assembly and localisation (Ringgaard et al., 2014). However, membrane chemosensory proteins form randomly localised clusters in the absence of ParC and ParP, without any preference to the cell pole (Ringgaard et al., 2014). Although it is plausible to assume that the stochastic self-assembly process, which only depends on simple physicochemical principles, as the "default" mechanism for chemosensory cluster positioning in bacteria, the inconsistent localisation patterns of chemosensory clusters in vibrios challenge its universality. Nevertheless, the ParC–ParP–CheA module shows that by amending the

well-established CheA–CheW interaction, the formation and positioning of membrane chemosensory clusters can be tightly controlled according to the cell cycle stages.

The *R. sphaeroides* cytoplasmic chemosensory clusters

The *R. sphaeroides* cytoplasmic chemosensory clusters localise approximately at the midcell. After duplication, clusters appear equi-positioned at about the one-quarter and three-quarter cell positions (Thompson et al., 2006), a pattern reminiscent of that seen for certain plasmids (Gerdes et al., 2010; Lutkenhaus, 2012). Partitioning of cytoplasmic chemosensory clusters requires homologues of plasmid and chromosome DNA partitioning proteins PpfA (ParA homologue) and TlpT (ParB analogue) (Roberts et al., 2012; Thompson et al., 2006). PpfA is encoded within *cheOp*$_3$, immediately upstream of *tlpT*. PpfA controls both the number and positioning of cytoplasmic chemosensory clusters. Cells lacking *ppfA* or containing mutants with defects in dimerization, ATPase, or DNA-binding activities show aberrant positioning of the cytoplasmic cluster and rarely contain more than a single cluster. After cell division, the two daughter cells inherit either a single cytoplasmic cluster or no cluster at all (Roberts et al., 2012; Thompson et al., 2006). Although the daughter cell lacking a cytoplasmic cluster eventually synthesizes a new one, the delay could cause a reduction in chemotaxis, which is deleterious in the harsh natural environment (Porter et al., 2011a).

There is growing evidence that ParA homologues are involved in the spatial regulation of several other protein complexes, including the carboxysomes (Savage et al., 2010), cellulose biosynthesis complex (Le Quéré and Ghigo, 2009), type IV secretion system components (Atmakuri et al., 2007), type IV pilus machinery (Perez-Cheeks et al., 2012), and the polar membrane chemosensory clusters in vibrios mentioned above. Strikingly, current studies demonstrate an important role of the nucleoid in ParA-mediated DNA and protein complex partitioning, probably via a cellular landmark or polymerisation matrix function of the nucleoid (Gerdes et al., 2010; Jain et al., 2012; Lutkenhaus, 2012; Roberts et al., 2012; Szardenings et al., 2011). It is therefore possible that the partitioning of cytoplasmic chemosensory clusters is co-ordinated with cell division via the nucleoid (Roberts et al., 2012).

PpfA is distributed across the whole nucleoid in *R. sphaeroides* with bright foci coinciding with the cytoplasmic chemosensory clusters. These bright foci are not seen for the dimerisation, ATP-binding, and DNA-binding mutants of PpfA, as well as in a mutant lacking the N-terminal domain of TlpT. These data are consistent with the hypothesis that the N terminus of TlpT interacts with PpfA

and may act as a ParB analogue (Roberts et al., 2012). However, no filamentous structures or oscillations were seen for PpfA, leaving the mechanism by which PpfA partitions the cytoplasmic cluster unclear.

Like *R. sphaeroides*, many other bacteria also have cytoplasmic chemoreceptors (Porter et al., 2011a). In *Myxococcus xanthus*, the cytoplasmic chemoreceptors FrzCD localise in a helical pattern that span the length of the cell (Mauriello et al., 2009), while in *Pseudomonas aeruginosa* and *Sinorhizobium meliloti* the cytoplasmic chemoreceptors colocalise with the membrane chemoreceptors at the cell poles (Porter et al., 2011a). The functions and mechanisms for these different localisation patterns of cytoplasmic chemoreceptors are unclear. Nevertheless, a recent comparative bioinformatics study has shown that 37% of bacterial species with sequenced genomes encode a PpfA homologue in one of their chemotaxis gene clusters, and 86% of these species also have putative cytoplasmic chemotaxis receptor homologues (Hamer et al., 2010). This observation suggests that a similar mechanism is used by other bacteria to partition their cytoplasmic chemosensory clusters.

1.3 *Rhodobacter sphaeroides*

The purple non-sulfur photosynthetic bacterium *R. sphaeroides* is an emerging model organism for studying complex signal transduction pathways and other aspects of bacterial cell biology (Chiu et al., 2013; Mackenzie et al., 2007; Porter et al., 2008, 2011a). *R. sphaeroides* belongs to the α-3 subgroup of the Proteobacteria (Imhoff, 2006; Imhoff, 2008) and exhibits high physiological versatility (Imhoff, 2006; Madigan and Jung, 2008; Overmann and Garcia-Pichel, 2006). Transitions between different growth modes are affected by diverse environmental factors, and oxygen tension is among the most influential ones (Imhoff, 2006; Overmann and Garcia-Pichel, 2006). In the presence of oxygen, *R. sphaeroides* grows by aerobic respiration. In the absence of oxygen, it preferably grows photoheterotrophically (in the presence of light), but can grow either using anaerobic respiration (in the dark and in the presence of appropriate electron acceptors), or fermentation (with appropriate substrates). Organic acids are the preferred carbon source and electron donor for aerobic and photoheterotrophic growth (Imhoff, 2006; Madigan and Jung, 2008; Overmann and Garcia-Pichel, 2006). In general, *R. sphaeroides* lives in aqueous environments like eutrophic ponds, lakes, sewage, stagnant waters, and waste lagoons (Imhoff, 2006; Madigan and Jung, 2008; Overmann and Garcia-Pichel, 2006). There is a vertical stratification of oxygen concentrations, light availability, and variable sources and kinds of electron donors in these niches. Therefore, a great metabolic versatility is advantageous in such habitats. Intriguingly, circadian clock genes and rhythmicity of gene expression may exist in *R. sphaeroides* helping this bacterium to adjust to different environmental factors (Choudhary et al., 2008; Min et al., 2005).

Cellular and developmental biology of *R. sphaeroides*

Signal transduction

Bacterial chemotaxis is one of the most investigated signal transduction mechanisms. Studies focus on bacterial species other than the classic *E. coli* and *Salmonella* models have revealed a significant diversity in the chemotaxis mechanisms (Porter et al., 2008, 2011a). The physiological versatility of *R. sphaeroides* is reflected in the complexity of its chemosensory systems (see section 1.2). For example, it was found that *R. sphaeroides* strain 2.4.1 contains 452 signal transduction domains in a total of 295 proteins, so ~7% of its proteins are dedicated to signal transduction (Mackenzie et al., 2007). Therefore, the diverse

tatic behaviours, and the complex, integrated and spatially regulated chemosensory pathways of *R. sphaeroides* make it a superior model for studying signal transduction.

Differentiation according to metabolic states

In addition to the complex chemosensory systems, the metabolic versatility of *R. sphaeroides* is achieved through a flexible gene expression network which is accompanied by differentiations of cellular morphologies and subcellular architecture (Arai et al., 2008; Chory et al., 1984; Kiley and Kaplan, 1988; Mackenzie et al., 2007; Pemberton et al., 1998; Slovak et al., 2005; Zeilstra-Ryalls et al., 1998). When growing photoheterotrophically, *R. sphaeroides* produces the photosystem (PS) and exhibits an increase in invaginations of the cytoplasmic membrane (Fig. 1.7). The formation of the intracytoplasmic membrane (ICM) provides a substantial propagation in the overall area of the cellular membranes that houses the PS photosynthetic apparatus (Kiley and Kaplan, 1988; Niederman, 2006; Pemberton et al., 1998; Zeilstra-Ryalls et al., 1998). A reduction in oxygen tension is both necessary and sufficient to induce production of the ICM, as ICM is unnecessarily produced under anaerobic dark growth conditions (Kiley and Kaplan, 1988; Zeilstra-Ryalls et al., 1998). While oxygen availability is the major factor controlling PS induction, light intensity determines the extent of ICM formation and the abundance of different PS components (Kiley and Kaplan, 1988; Pemberton et al., 1998; Zeilstra-Ryalls et al., 1998). Besides the profound alteration of the cytoplasmic membrane, photoheterotrophic cells change their morphology from rod-shape (aerobically grown cells) to coccobacillus (Chory et al., 1984; Slovak et al., 2005). The extents of morphological change and ICM formation are inversely related to the incident light intensity, with low light levels producing more spherical shape and ICM (Kiley and Kaplan, 1988; Pemberton et al., 1998; Slovak et al., 2005; Zeilstra-Ryalls et al., 1998).

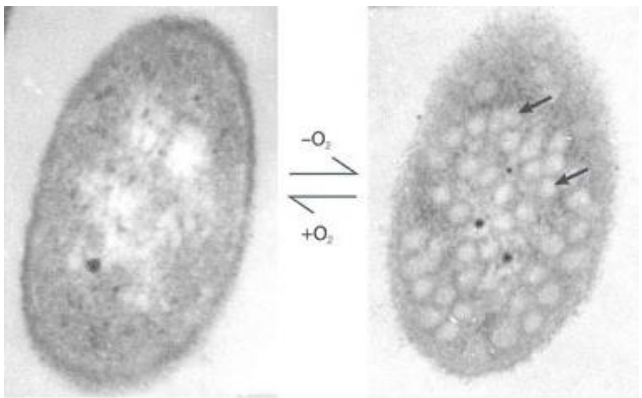

Figure 1.7. The transition of *R. sphaeroides* from an aerobic to photoheterotrophic environment triggers regulatory events that result in the formation of ICM (arrows). From O'Connell (2005) and image courtesy of Chris Mackenzie, The University of Texas Health Science Center, USA.

Electron microscopy has demonstrated that the ICM system in different bacteria can assume diverse ultrastructural morphologies, including tubules, lamellae (single, paired or stacked), radiation or interconnected vesicles (Overmann and Garcia-Pichel, 2006). Using cryo-electron tomography, Tucker et al. (2010) discovered a hereto unrecognized ultrastructural complexity within the *R. sphaeroides* ICM. The ICM does not consist entirely of a succession of vesicular structures connected at their necks as proposed before, but instead undergoes budding and becomes fully detached vesicular organelles. These vesicles are capable of carrying out the light-harvesting and light-driven energy transduction activities for anoxygenic photosynthesis, representing true bacterial membrane-bound organelles (Niederman, 2010; Tucker et al., 2010). It is calculated that approximately 15% of the cytoplasm of photoheterotrophic *R. sphaeroides* cells contains vesicles (~800 ICM vesicles per cell).

The dramatic rearrangements of cytoplasmic membrane pose a great challenge to *R. sphaeroides* photoheterotrophic cells. How do cells maintain subcellular architecture under this circumstance? The flagellum always localises in the non-photosynthetic cytoplasmic membrane (Armitage and Schmitt, 1997). The localisation of the bacterial actin homologue MreB appears to be independent of the extensive cytoplasmic membrane rearrangements and consequent reorganisation of the cytoplasm that occurs in photoheterotrophic cells (Slovak et al., 2005). Moreover, the ICM has its own unique protein composition (Woronowicz and Niederman, 2010). These observations suggest that cytoplasmic membrane invaginations must be demarcated within specific regions to prevent interference in some housekeeping functions. The rich information obtained from the studies of *R. sphaeroides* ICM, including data from electron microscopy, atomic force microscopy, crystallography, spectroscopy and proteomics, lays a ground for the investigations of membrane invaginations and vesicle formation, as well as maintenance of subcellular architecture in differentiated cells. In addition to ICM, gas vesicle proteins are encoded in the genome of *R. sphaeroides* (Choudhary et al., 2008). Gas vesicles can play an important role in the flotation of *R. sphaeroides* according to light intensity (Choudhary et al., 2008). Therefore, *R. sphaeroides* may possess two organelle systems that cooperate. The eukaryote-like behaviour of ICM (Niederman, 2010) also makes *R. sphaeroides* a promising model to study spatial regulation of membrane proteins during membrane differentiation.

A tale of two chromosomes

The first bacterium to be revealed as possessing multiple chromosomes was *R. sphaeroides* (Suwanto and Kaplan, 1989). All *R. sphaeroides* strains tested have two chromosomes, although the number of plasmids varied (Nereng and Kaplan, 1999). There is also a wide divergence between the two chromosomes among different *R. sphaeroides* strains (Nereng and Kaplan, 1999). Among the five sequenced strains, the size of chromosome I ranges from 2.49 to 3.22 Mbp, while that of chromosome II from 0.88 to 1.30 Mbp (Choudhary et al., 2007; Lim et al., 2009; Porter et al., 2011b). Genomic analyses have revealed an ancient association of the two chromosomes and significant dispersal of essential genes between them (Mackenzie et al., 2007). Chromosome II-specific DNA sequences have evolved rapidly, while chromosome I-specific DNA sequences have remained highly conserved (Choudhary et al., 2007). It has been suggested that chromosome II is mainly involved in the evolution of strain-specific genetic variants (Mackenzie et al., 2007).

The discovery and subsequent studies of bacterial genomes consisting of multiple chromosomes raise many interesting questions of bacterial cell biology. For example, how are multiple chromosomes organized and segregated? It is suggested that distinct mechanisms capable of discriminating between and interacting with the two *V. cholerae* chromosomes exist. In *E. coli* the *oriC* is positioned at the midcell, while the *oriC* is localised at the old pole in *C. crescentus* (Reyes-Lamothe et al., 2012; Toro and Shapiro, 2010). Localisations of *V. cholerae oriCI* (polar) and *oriCII* (midcell) are reminiscent of *C. crescentus* and *E. coli oriC*s, respectively (Fiebig et al., 2006; Fogel and Waldor, 2005). Polar localisation of *oriC*s seems to be conserved in α-proteobacteria (Kahng and Shapiro, 2003). In *R. sphaeroides*, *oriCI* localises to the cell pole and has a cell cycle-dependent localisation pattern similar to *C. crescentus*, while *oriCII* is positioned at the midcell (Nelly Dubarry, personal communication). Therefore, the localisation patterns of *oriCI* and *oriCII* are reminiscent to those of *V. cholerae* (Fiebig et al., 2006; Fogel and Waldor, 2005). The two *R. sphaeroides* chromosomes each encodes a *parABS* system, which is likely to participate in the segregation of the cognate chromosome (Nelly Dubarry, personal communication).

Condensation of the nucleoid by the binding of nucleoid-associated proteins plays an important role in the spatial regulation of chromosomes in many bacterial models (Browning et al., 2010; Dillon and Dorman, 2010; Reyes-Lamothe et al., 2012). However, *R. sphaeroides* chromosomes do not condense (Thompson et al., 2006). Nucleoid-associated proteins involved in chromosome compaction like

MukBEF, Fis, and Lrp are absent in *R. sphaeroides* (Mackenzie et al., 2007), which may account for the absence of condensed nucleoid.

To summarise, *R. sphaeroides* is among the best studied species of versatile metabolic capability and complex chemosensory systems. Combining the intricate multipartite genome and membrane differentiation it provides a unique model with accessible genetic tools for bacterial cell biology. By studying *R. sphaeroides*, we may not only discover some exclusive mechanisms, but also reveal certain universal insights in bacterial cell biology.

1.4 The Bacterial Cytoskeleton

The cytoskeleton plays a central role in the spatiotemporal organisation of eukaryotic cells. The three major components of the eukaryotic cytoskeleton are actin filaments, microtubules, and intermediate filaments. This complex and dynamic filamentous network controls a multitude of processes, including cell division, morphogenesis, polarity, transcription, cell movement and intracellular transport (Alberts et al., 2007). The three eukaryotic cytoskeletal systems are assembled from monomer subunits, which are polymerised to form long linear polymers (protofilaments). Efficient polymerisation also requires nucleation. Because of the "head-to-tail" fashion of polymer assembly, actin filaments and microtubules are polar, with plus- and minus-ends differ topologically and kinetically. Subunit addition occurs much more rapidly at the plus-end than at the minus-end. Lateral interactions between protofilaments are important for the dynamic properties and formation of higher-order structures of the cytoskeleton. The dynamics of actin and tubulin polymerisation are also modulated by binding/hydrolysis of nucleotide triphosphates (NTPs): ATP for actin and GTP for tubulin. Dynamic polymerisation and polarity are the two key features that allow actin and tubulin to achieve their specific functions (Alberts et al., 2007).

For decades, microscopic studies had failed to detect cytoskeletons in prokaryotes. The lack of a cytoskeleton in prokaryotes was once considered a major difference between prokaryotes and eukaryotes. This erroneous view has now been completely overthrown with the discoveries of bacterial homologues of the three major eukaryotic cytoskeletal proteins and the identifications of bacteria-specific cytoskeletal proteins (Cabeen and Jacobs-Wagner, 2010; Gitai, 2005). Bacterial cytoskeletal proteins relevant to this study are reviewed below.

FtsZ: a tubulin homologue

Analyses of conditional mutants in *E. coli* have identified numerous proteins involved in bacterial cytokinesis. Many of these mutants are called *fts* (***f***ilamentous ***t***emperature-***s***ensitive) since they form filaments at nonpermissive temperatures due to the inhibition of cell division. Among these genes, *ftsZ*, is present in nearly all bacteria, many archaea, and eukaryotic organelles like chloroplasts and mitochondria (Gilson and Beech, 2001). The smooth morphology (i.e. no signs of constriction) of *ftsZ* mutants suggests that FtsZ is required for the earliest step in septation (Begg and Donachie, 1985). It is now clear that FtsZ is a tubulin homologue. FtsZ is the most critical component of the

bacterial cytokinetic machinery (divisome), which forms a ring-like structure (the Z-ring) at cytokinetic sites to establish a scaffold that sequentially recruits other divisome members. The Z-ring then constricts to initiate cytokinesis (Adams and Errington, 2009; de Boer, 2010; Erickson et al., 2010).

Biochemical properties of FtsZ

Structures of FtsZ monomer and protofilament

Despite a low level of sequence conservation, the tertiary structure of FtsZ is very similar to that of tubulin (Lowe and Amos, 1998). FtsZ subunits also assemble into tubulin-like protofilaments by stacking vertically (Oliva et al., 2004). The crystallographic structures of FtsZ show that it has two globular domains: an N-terminal GTPase domain and a C-terminal domain. The two domains are arranged around a central helix (Aylett et al., 2011; Lowe, 1998; Lowe and Amos, 1998). The C-terminal domain of FtsZ is more variable among different bacteria. Important features present in the C-terminal domain include highly conserved "synergy" residues believed to regulate GTP-hydrolysis upon FtsZ polymerisation and loop structures that are possibly involved in calcium binding (Lowe and Amos, 1998). Therefore, like tubulin, FtsZ is a self-activating GTPase. The regions required in *E. coli* FtsZ for direct interactions with FtsA and ZipA are also present in the C-terminal domain (Adams and Errington, 2009; Erickson et al., 2010). Tubulin's C terminus, like that of FtsZ, is unstructured, charged, and the binding site for many microtubule-associated proteins (Nogales, 2000).

In vitro, FtsZ self-assembles into single-stranded protofilaments that are straight, curved, or ring-shaped (Fig. 1.8). The protofilaments can be further bundled into higher-order structures like sheets, asters, or tubules by crowding agents or multivalent cations. Microtubule-like arrangements have not been observed for FtsZ protofilaments. The significances of these different FtsZ structures *in vivo* are unclear (Cabeen and Jacobs-Wagner, 2010; Michie and Löwe, 2006).

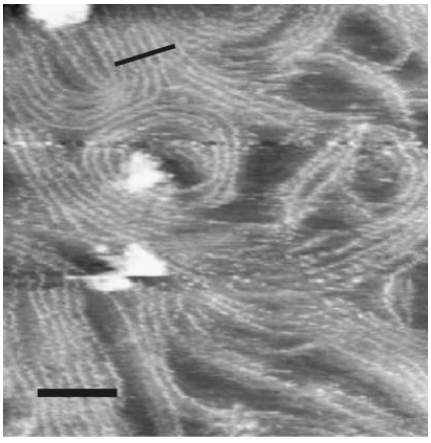

Figure 1.8. An atomic force microscopy image of *in vitro* FtsZ filaments formed in the presence of GMPCPP (a nucleotide analogue which hydrolyses more slowly than GTP). Scale bar: 100 nm. From Mingorance et al. (2005).

Polymerisation and dynamics of FtsZ assemblies

In vitro, FtsZ shows cooperative assembly into dynamic protofilaments and higher-order structures in the presence of GTP. There are at least two major transitions during the assembling process. The initial phase for protofilaments formation occurs at a critical concentration of ~0.5–1 μM (the intracellular concentration of FtsZ is 3–10 μM), and the second transition at ~3 μM, which might represent the formation of higher-order structures. Although lateral interactions between protofilaments have been proposed to participate in the formation of these higher-order structures, current studies argued that lateral bonds do not exist between FtsZ protofilaments. FtsZ polymerisation depends on GTP binding but not hydrolysis, and GTP hydrolysis is probably a rate-limiting step in the assembly/disassembly cycle. *In vitro*, GTP hydrolysis promotes the disassembly of protofilaments and thus limits the length of protofilaments (Adams and Errington, 2009; Erickson et al., 2010).

In vivo FRAP studies have shown that the Z-ring is a very dynamic structure that constantly remodels, with an average half time of recovery of ~10 s in different bacteria (Adams et al., 2011; Anderson et al., 2004; Charbon et al., 2011; Geissler et al., 2007; Specht et al., 2013; Willemse et al., 2011). This dynamics is driven by the GTPase activity of FtsZ. Accordingly, GTP hydrolysis mutants of FtsZ stabilize polymers *in vivo* by reducing subunit turnover, while GTP binding mutants do not possess such effect (Adams and Errington, 2009; Erickson et al., 2010). The polymerisation of FtsZ is also regulated by FtsZ-interacting proteins (see below).

Functions of FtsZ

Cytokinesis

Bacterial cytokinesis is driven by a complex macromolecular machinery variously referred to as divisome, septasome, Z-ring, or septal ring (de Boer, 2010). At the end of cytokinesis, two new cell poles will be formed at each cytokinetic site, therefore all of the cell envelope layers must be remodeled during this process. Bacterial cytokinesis can be roughly split into three general steps (Adams and Errington, 2009; de Boer, 2010; Lutkenhaus et al., 2012; Rico et al., 2013). First step is the selection of the cytokinetic site and the concurrent assembly of the proto-Z-ring. In the second step, which usually occurs after a considerable lag, the remaining divisome proteins are added to the proto-Z-ring to form the mature divisome. Third, the divisome is activated to perform constriction/septation. In the case of constriction in Gram-negative bacteria, septal peptidoglycan synthesis/splitting, cytoplasmic membrane invagination/

fission, and outer membrane invagination/fission must occur simultaneously in a coordinated manner (de Boer, 2010; Lutkenhaus et al., 2012).

FtsZ forms the proto-Z-ring which serves as a scaffold to recruit and position other divisome components (de Boer, 2010; Lutkenhaus et al., 2012). One of the primary functions of these divisome proteins is to carry out septal-specific cell wall production. Among them, the transpeptidase FtsI/PBP3 is specifically required for septal peptidoglycan synthesis (de Boer, 2010; Egan and Vollmer, 2013). Whether or not FtsZ actively exerts a constrictive force that directs cell invagination and inward peptidoglycan growth during cytokinesis has long been debated (Erickson et al., 2010). Strong evidence for FtsZ as a force generator has come from a series of *in vitro* reconstitution experiments. In their pioneering study, Osawa et al. (2008) reconstituted Z-rings inside multilamellar liposomes using purified FtsZ–YFP modified with a membrane tether. In the presence of GTP, the modified FtsZ assembles into rings that constrict liposomes, indicating that membrane-associated FtsZ can generate force by itself. Similar constriction could be seen when FtsZ was tethered to the liposome membrane via FtsA (Osawa and Erickson, 2013). Moreover, membrane-tethered FtsZ on the outside of liposomes produces concave depressions and tubules (Osawa et al., 2009). Although these observations are consistent with force generation by FtsZ, it is unclear how FtsZ does so.

Two classes of models have emerged from *in vitro* and *in vivo* studies to describe how FtsZ can generate constrictive force (Fig. 1.9). The first class proposes that FtsZ protofilaments exert a bending force on the cytoplasmic membrane as they are undergoing a straight-to-curved conformational change (Erickson et al., 2010; Sun and Jiang, 2011). GTP hydrolysis is thought to drive this straight-to-curved conformational change of FtsZ protofilaments (Lu et al., 2000). Mathematical modelling suggests that such a GTP hydrolysis-induced bending can generate a force ranging from 5.2 pN per protofilament to 30 pN per polymerised FtsZ monomer (Allard and Cytrynbaum, 2009; Erickson et al., 2010; Hsin et al., 2012; Li et al., 2013b). Although these estimated values of constrictive force are very different, they are all sufficient to direct inward peptidoglycan growth, considering the estimated force (1–8 pN) required (Drew et al., 2009; Lan et al., 2007). Based on the crystal structure of a GDP–bound *Mycobacterium tuberculosis* FtsZ protofilament, Li et al. (2013b) provides the structural basis for force generation by protofilament bending. However, a comparison of FtsZ structures from multiple species in different nucleotide-bound states argued against the existence of a hydrolysis-induced conformational change (Oliva et al., 2007). Besides, an *E. coli* FtsZ mutant that displays minor GTPase activity can still

divide (Mukherjee et al., 2001).

The second model proposes that condensation/sliding of FtsZ protofilaments would decrease the circumference and constrict the Z-ring (Erickson, 2009; Sun and Jiang, 2011). In this model, lateral interactions among protofilaments could be responsible for the variety of higher-order structures observed *in vitro* (Oliva et al., 2007). Additionally, lateral interactions can spontaneously condense FtsZ protofilaments into the Z-ring and generate constrictive force (Erickson, 2009; Lan et al., 2009; Sun and Jiang, 2011). The force is generated by relative sliding of pairs or small bundles of FtsZ protofilaments that interact transiently. Mathematical modelling suggests that 8–50 pN of force could be produced (Lan et al., 2009). This model is supported by electron cryo-tomography of *in vivo* and *in vitro* architecture of the Z-ring (Jan Löwe, personal communication).

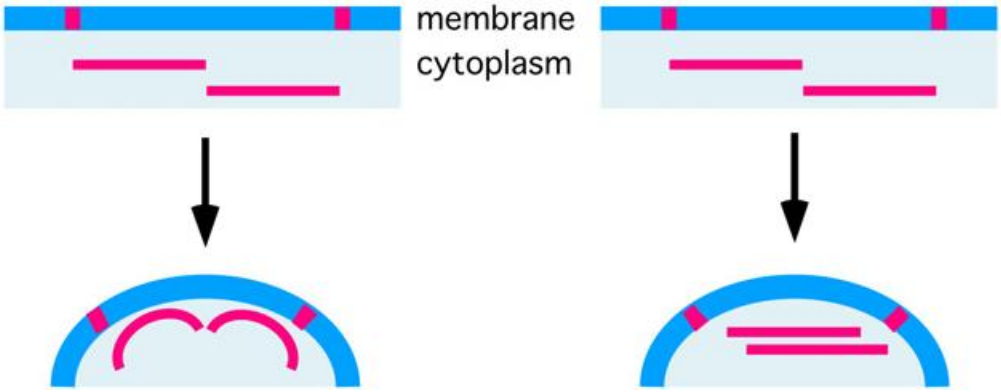

Figure 1.9. Schematics of the bending (left) and condensation/sliding (right) models of force generation by the Z-ring during constriction. FtsZ protofilaments are shown as long purple rods. See the text for more details. From Natale et al. (2013).

Morphogenesis

FtsZ is important for bacterial cell shape by coordinating cell growth, cell division, and cell size (Margolin, 2009). In addition to septum formation, FtsZ also participates in sidewall growth by recruiting the peptidoglycan-synthesis machinery, and facilitates its even distribution (Aaron et al., 2007; Varma et al., 2007; Varma and Young, 2009; Vats and Rothfield, 2007). Under certain circumstances, improper FtsZ function destroys the structural integrity of the cell (Varma and Young, 2004). FtsZ also contributes to the shape of the cell poles (Margolin, 2009).

Another means to affect cell shape is via the control of cell size. Regulation of Z-ring's activity by nutritional inputs can determine the cell length, which

consequently modifies cell shape (Margolin, 2009). In *B. subtilis*, UgtP, a diacylglycerol glucosyltransferase that negatively regulates FtsZ assembly, delays Z-ring formation and thus produces larger cells in rich medium (Weart et al., 2007). More extensive inhibition of cell division results in filamentous cells. Filamentation is a widespread morphological differentiation that is important for bacterial stress adaptation, multicellularity, and pathogenesis (Justice et al., 2008; Young, 2006). Upregulation of proteins preventing Z-ring formation (e.g. MinC and SulA) might be responsible for cell filamentation (Justice et al., 2008; Pearson et al., 2010; Young, 2006). Switching the positioning and formation of the Z-ring from midcell to asymmetric during sporulation can also result in morphological differentiation (Ben-Yehuda and Losick, 2002).

Positioning and assembly of the Z-ring

Protein modulators of FtsZ assembly

The polymerisation of FtsZ is regulated by diverse FtsZ-interacting proteins (Adams and Errington, 2009; Huang et al., 2013; Kirkpatrick and Viollier, 2011). Stabilizers/scaffolders promote Z-ring formation and facilitate its maintenance during cytokinesis. Destabilizers prevent FtsZ assembly at inappropriate locations or stages and ensure that FtsZ assemblies are dynamic enough to respond to the signals governing cytokinesis. Shapers provide further control by modifying the conformations and higher-order structures of FtsZ protofilaments. Together they form a regulatory network that dictates the spatiotemporal regulation of cytokinesis. Some of these proteins are discussed below.

Negative regulation in positioning

Proto-Z-ring formation establishes the location of future cytokinetic sites and must be tightly controlled to prevent aberrant septation. Since the cellular concentration of FtsZ in bacteria is higher than the critical concentration for polymerisation (Erickson et al., 2010), it is essential to inhibit FtsZ polymerisation at undesired locations. In *B. subtilis* and *E. coli*, this is achieved by the combined action of the Min system that inhibits polar Z-ring formation and by the nucleoid occlusion system that prevents the formation of Z-rings over the nucleoid (Fig. 1.10) (den Blaauwen, 2013; Monahan et al., 2014). But an unidentified positive signal that links the initiation of DNA replication to Z-ring formation has been proposed (Monahan et al., 2014; Wu and Errington, 2011). The Min system consists of the FtsZ polymerisation inhibitor MinC, which is localised to the cytoplasmic membrane via association with the ATPase MinD. In *E. coli* the third protein MinE actively displaces the MinCD complex from the cytoplasmic

membrane. The molecular interactions occurring between the three Min proteins on the membrane produces a dynamic pole-to-pole oscillation of MinCDE in a helical-like pattern, with a time-averaged polar distribution. This polar distribution prevents FtsZ to polymerise at the cell poles (Fig. 1.10) (Shih and Zheng, 2013). In *B. subtilis* DivIVA recruits MinCD to the cell poles via the bridging protein MinJ (Bramkamp and van Baarle, 2009; Monahan et al., 2014).

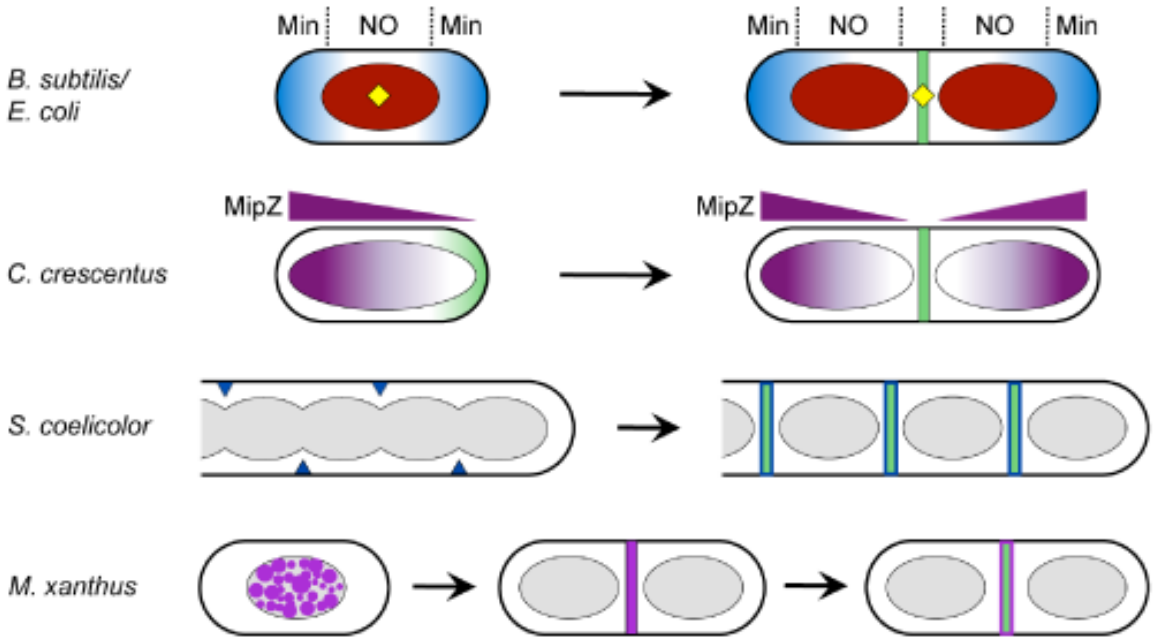

Figure 1.10. Diverse mechanisms for the regulation of Z-ring positioning. In *B. subtilis* and *E. coli*, the Min system (blue) and nucleoid occlusion (NO; red) influence Z-ring positioning by inhibiting FtsZ (green) assembly. Chromosome segregation creates a nucleoid-free gap at the midcell. A putative positive signal (yellow), whose activation is linked to the initiation of DNA replication, may also play a role in positioning the Z-ring at the midcell. In newborn *C. crescentus* cells, the FtsZ inhibitor MipZ (purple) is recruited to the old pole by ParB and non-specifically binds to DNA, forming a polar gradient that constrains FtsZ to the new pole. Chromosome replication and segregation set up a bipolar MipZ gradient that displaces FtsZ from the new pole and directs Z-ring formation to the midcell. In sporulating hyphae of *S. coelicolor*, SsgB (dark blue) localises to cytokinetic sites and recruits FtsZ to form the Z-ring. In newborn *M. xanthus* cells, PomZ (magenta) exhibits a patchy localisation pattern over the nucleoid. After chromosome segregation, PomZ localises at the midcell and recruits FtsZ to form the Z-ring. See the text for more details. From Monahan and Harry (2013).

Thanedar and Margolin (2004) showed that in *E. coli*, FtsZ molecules outside of the Z-ring also localise in a helix-like pattern and oscillate rapidly within this pattern. The period of this oscillation is similar to that of the Min proteins. Strikingly, Bisicchia et al. (2013) show that MinCDE drive a counter-oscillation of early-cell-division proteins ZapA, ZapB, and ZipA, along with FtsZ. They propose that FtsZ forms protofilaments at the cell pole where the MinC concentration is the lowest and serves as a scaffold to recruit ZapA, ZapB, and ZipA. The resulting complexes are disassembled by MinC and reform within the MinCDE oscillation period before accumulating at the midcell to form the Z-ring.

Cytokinesis is also inhibited in the vicinity of the nucleoid by the nucleoid occlusion system (Fig. 1.10) (Monahan et al., 2014; Wu and Errington, 2011). Nucleoid occlusion spatiotemporally couples cytokinesis with chromosome replication and segregation, thus prevents the chromosome from being bisected by the septum. In cells at earlier stages of the cell cycle, the nucleoid occupies the midcell region and inhibits Z-ring formation there. At later cell cycle stages, chromosome segregation results in a nucleoid occlusion-free zone at the midcell and allows Z-ring formation.

The nucleoid occlusion effectors are Noc in *B. subtilis* and SlmA in *E. coli*, and the two proteins have no sequence or structural similarity. Septa form over unsegregated nucleoids under certain conditions in *Δnoc* and *ΔslmA* cells, resulting in bisection of the chromosome, while overproduction of these proteins leads to longer cells (Bernhardt and de Boer, 2005; Wu and Errington, 2004). These genes are not essential in their respective hosts and show synthetic-lethal phenotypes in cells with defectives in the Min system. Interestingly, cytokinesis in *noc min* and *slmA min* double mutants is severely inhibited rather than uncontrolled septum formation along the length of the cell. This phenotype raises the possibility that the Min and nucleoid occlusion systems are required to sequester FtsZ to the midcell, so FtsZ can reach a sufficient concentration to perform its functions (Wu and Errington, 2011).

Noc (Wu et al., 2009) and SlmA (Cho et al., 2011; Tonthat et al., 2011) associate with the nucleoid through their cognate DNA-binding domains that recognize specific chromosomal sequences. These specific DNA sequences are sparse or absent near the terminus region of the chromosome, which occupies a midcell position during the late stages of chromosome segregation in *B. subtilis* and *E. coli*, results in a temporal coupling of cytokinesis and DNA partitioning. SlmA affects Z-ring formation via a disruption in protofilament polymerisation or higher-order structure formation (Cho et al., 2011; Tonthat et al., 2011; Tonthat et al., 2013). How Noc influences Z-ring formation is still unclear (Wu and

Errington, 2011).

In the α-proteobacterium *C. crescentus*, chromosome replication/segregation and cytokinesis are coordinated via MipZ, a ParA-like ATPase that binds DNA nonspecifically (Fig. 1.10) (Kiekebusch et al., 2012; Thanbichler, 2010; Thanbichler and Shapiro, 2006). Shortly after the initiation of DNA replication, the duplicated *oriC* regions are rapidly partitioned to opposite cell poles (Thanbichler and Shapiro, 2006). The *parS* motifs cluster near the *oriC* region are recognized by ParB, and MipZ is recruited to ParB (Kiekebusch et al., 2012; Thanbichler and Shapiro, 2006). As a consequence, segregation and polar attachment of the ParB–*parS* complexes produce a bipolar gradient of MipZ, with concentration higher at the two cell poles and lower at the midcell (Thanbichler and Shapiro, 2006). MipZ directly interacts with FtsZ and inhibits the GTP-dependent polymerisation of FtsZ (Thanbichler and Shapiro, 2006). In this way, Z-ring formation is positioned at the midcell. It should be noted that FtsZ remains at the new pole in newborn *C. crescentus* cells (Thanbichler and Shapiro, 2006). The duplication and segregation of the *oriC* regions, and thus the ParB–*parS* complexes, partition the MipZ gradient to the new pole which disassembles the polar FtsZ assemblies. The ATPase activity of MipZ acts as molecular switch, together with MipZ's DNA-binding ability, establish an FtsZ-inhibiting gradient (Kiekebusch et al., 2012). Intriguingly, the expression of *ftsZ* and *mipZ* might be coregulated by DNA methylation (Gonzalez and Collier, 2013).

Positive regulation in positioning

In sporulating *Streptomyces coelicolor*, FtsZ is recruited to the cytokinetic site via an interaction with the membrane-associated protein SsgB, which promotes FtsZ polymerisation *in vitro* (Fig. 1.10) (Willemse et al., 2011). The localisation of SsgB is further controlled by SsgA (Willemse et al., 2011). SsgA and SsgB are only present in *Actinomycetes*. Nevertheless, another positive regulation system was identified in *M. xanthus* (Fig. 1.10) (Treuner-Lange et al., 2013). Purified *M. xanthus* FtsZ has GTPase activity *in vitro* but does not form detectable protofilaments, suggesting a positive regulator might be required for Z-ring formation in *M. xanthus*. The ParA-like protein PomZ displays a cell cycle-regulated localisation: PomZ accumulates at the cytokinetic site after chromosome segregation, but prior to FtsZ. PomZ interacts with FtsZ *in vitro*. Therefore, PomZ might couple Z-ring formation to cell cycle progression.

Accessory proteins in Z-ring formation

FtsZ does not show any direct affinity for the cytoplasmic membrane. Therefore, certain membrane anchors are required for Z-ring formation. FtsA is the most conserved FtsZ-interacting protein that belongs to the actin/Hsp70/sugar kinase superfamily. FtsA tethers FtsZ to the membrane via its C-terminal amphipathic helix. In both *E. coli* and *B. subtilis* the maintenance of a correct ratio of FtsZ to FtsA is crucial for cytokinesis. In addition to proto-Z-ring assembly, FtsA also promotes Z-ring integrity during cytokinesis and participates in the recruitment of downstream divisome proteins (Adams and Errington, 2009; Huang et al., 2013; Rico et al., 2013). Intriguingly, a current report showed that FtsA can cause fragmentation of FtsZ polymers which may facilitate the formation of highly dynamic Z-rings (Loose and Mitchison, 2014). ZapA is another highly conserved FtsZ-interacting protein that localises to the midcell dependent on a direct interaction with FtsZ and remains dynamically associated with the divisome. ZapA promotes Z-ring stability probably via aligning small FtsZ assemblies that consist of multiple FtsZ protofilaments. ZapB, a less conserved FtsZ-interacting protein, might function in a similar way (Buss et al., 2013). In *E. coli* FtsA and ZipA collaborate in anchoring FtsZ to the membrane. ZipA is a transmembrane protein found in γ-proteobacteria. ZipA is dispersed throughout the cytoplasmic membrane until it is recruited to the assembling Z-ring by a direct interaction with FtsZ. ZipA seems to be required to recruit an essential divisome protein FtsK that links cytokinesis and chromosome segregation. EzrA is a negative regulator of Z-ring assembly in Gram-positive bacteria with a low GC content. EzrA also participates in maintaining the dynamic nature of the Z-ring (Adams and Errington, 2009; Huang et al., 2013; Rico et al., 2013).

SepF, a conserved protein in Gram-positive bacteria and cyanobacteria, participates in Z-ring formation and influences the structure of FtsZ protofilament bundles (Adams and Errington, 2009; Huang et al., 2013; Kirkpatrick and Viollier, 2011; Rico et al., 2013). *In vitro*, SepF forms ring-like structures with a consistent diameter, which are able to arrange FtsZ protofilaments into tubules of identical diameter. Mutations in SepF that abolish ring formation also disrupt cell division *in vivo* (Gündoğdu et al., 2011). This observation indicates the importance of higher-order structures of protofilaments in Z-ring formation. This idea was further reinforced by the discovery that a *C. crescentus* protein, FzlA, can influence the curvature of FtsZ protofilaments. FzlA is conserved in γ-proteobacteria. Overproduction of FzlA leads to the formation of hyperstable FtsZ foci and antagonizes the inhibitory effect of MipZ. FzlA is necessary for cell envelope invagination. Based on these observations, it is

proposed that FzlA-induced protofilament curvature might adjust the diameter of the Z-ring and generate a constriction force during cytokinesis (Goley et al., 2010). Intriguingly, a current study found that the toxin YeeV (CbtA) encoded in a toxin–antitoxin system can bind to both FtsZ and MreB, leading to a morphological change and cell lysis in *E. coli* (Tan et al., 2011).

***In vivo* structure of FtsZ assemblies**

Under conventional fluorescence microscopy, the Z-ring looks like a closed ring that has more or less even distribution of FtsZ (Erickson et al., 2010; Meier and Goley, 2014). Besides, FtsZ also forms arcs, helices, or spots in bacterial cells. The biological significances of these different structures are discussed in more details in Chapter 3. In brief, they may represent the dynamic behaviour of the Z-ring, or the precursors/remnants of the Z-ring.

Li et al. (2007) employed electron cryo-tomography to obtain the first super-resolution image of *in vivo* FtsZ structures. They found that FtsZ protofilaments, each of 40–120 nm long, are loosely scattered around the midcell of *C. crescentus*. A set of studies utilising super-resolution fluorescence microscopy further allows the visualization of fluorescently labelled FtsZ in live bacteria (Chiu and Leake, 2011; Gahlmann and Moerner, 2014; Meier and Goley, 2014). Fu et al. (2010) used photoactivated localisation microscopy (PALM) to characterise the *in vivo* structure of the Z-ring in *E. coli*. They found that in addition to the ring-like conformation, the Z-ring also adopts a novel compressed helical configuration with variable length and pitch. Besides, the conformation of the Z-ring is dependent on FtsZ expression level. The Z-ring is ~110 nm thick, and is composed of loose bundles of FtsZ protofilaments that randomly overlap with each other in both longitudinal and radial directions of the cell. These loose bundles can accommodate additional protofilaments. Similar observations were made by stimulated emission depletion (STED) microscopy (Jennings et al., 2011). PALM further showed that FtsZ protofilaments laterally associate to form "FtsZ clusters" (Buss et al., 2013). These FtsZ clusters are corralled at the midcell through the combined action of ZapA and ZapB, resulting in larger continuous structures (e.g. a ring).

PALM was also used to observe different FtsZ assemblies in *C. crescentus* cells at different cell cycle stages (Biteen et al., 2012; Holden et al., 2014). 3D-PALM of hundreds of synchronized *C. crescentus* cells during different cell cycle stages suggests that Z-ring is a patchy band, and rarely as a continuous ring, supporting a model whereby FtsZ protofilaments are randomly distributed within the Z-ring and interact only weakly (Holden et al., 2014). Holden et al.

(2014) also found that Z-ring constriction can be divided into two phases: a first slower, linear phase and a second rapid phase. The radial and axial thicknesses of the Z-ring change little over the cell cycle, and are in the range of 50–100 nm (Holden et al., 2014).

3D-structured illumination microscopy (SIM) of FtsZ in *B. subtilis* and *Staphylococcus aureus* provided the only super-resolution time-lapse analysis of the Z-ring so far (Strauss et al., 2012). Strauss et al. (2012) showed that the Z-ring is very dynamic and composed of a heterogeneous distribution of FtsZ in a bead-like arrangement. Other divisome components also adopt a bead-like localisation pattern at the cytokinetic site.

Collectively, super-resolution imaging of FtsZ in different bacteria depict the Z-ring as a heterogeneous, frequently discontinuous structure composed of short protofilaments (Fig. 1.11). Improvement in the spatial and temporal resolution of microscopy, as well as a direct dissection of the effects of FtsZ-interacting proteins on Z-ring organisation *in vivo* via super-resolution imaging, may further provide exciting insights.

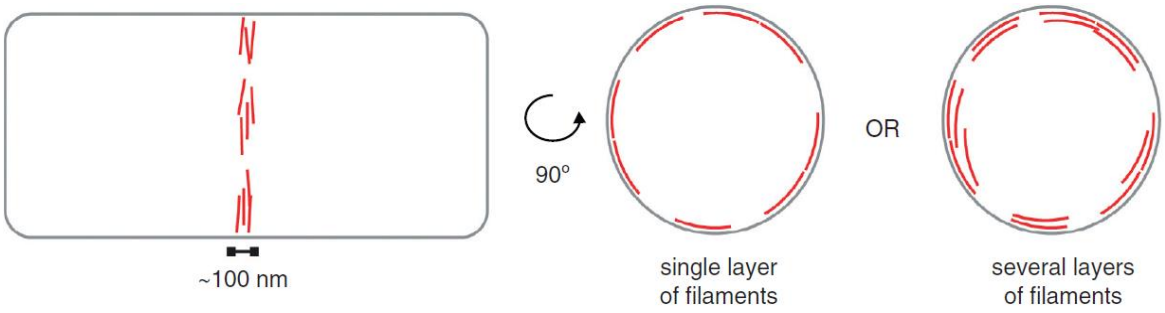

Figure 1.11. Model for organisation of protofilaments in the Z-ring. Short (~100 nm long) protofilaments (red) form loose clusters/bundles (~100 nm wide) that align at the midcell and frequently have gaps between them (left). The Z-ring might either comprise a single layer of protofilaments (middle) or multiple layers of several filaments deep in the radial direction (right). From Meier and Goley (2014).

Chemical modulators of FtsZ

FtsZ, being the most conserved prokaryotic cell division protein, is a promising target for new antibiotics (Foss et al., 2011; Sass and Brötz-Oesterhelt, 2013). Numerous inhibitors of tubulin are known, and since tubulin and FtsZ are homologues, it is possible that some of these inhibitors could affect FtsZ. To exploit this possibility, Yu and Margolin (1998) tested the effect of tubulin assembly inhibitors on FtsZ polymerisation. They found that tubulin inhibitors

like colchicine, colcemid, benomyl, and vinblastine, have no effect on the *in vitro* assembly of FtsZ into polymers. However, the hydrophobic fluorescent probe 5,5′-bis-(8-anilino-1-naphthalenesulfonate) (bis-ANS) inhibited FtsZ assembly. Sarcina and Mullineaux (2000) latter showed that tubulin assembly inhibitors thiabendazole and 2-methyl-benzimidazole cause cell elongation in *E. coli* and cyanobacteria, presumably through the effect on FtsZ. White et al. (White et al., 2002) screened synthetic inhibitors (2-alkoxycarbonylaminopyridines) of tubulin and two compounds were found to inhibit FtsZ polymerisation. Ruthenium red, which completely inhibits tubulin assembly, induces the bundling of FtsZ protofilaments (Santra et al., 2004).

Chemicals outside the tubulin inhibitor repertoire are also tested for their FtsZ inhibitory effects. Wang et al. (2003) screened extracts of microbial fermentation broths and plants, leading to the identification of viriditoxin as a broad-spectrum antibacterial agent that block FtsZ polymerisation. More recently, Margalit et al. (2004) reported the identification of five structurally diverse compounds, together named Zantrins, which destabilize the FtsZ protofilaments or induce filament hyperstability through increased lateral association. These effects are reminiscent of that of the tubulin inhibitors colchicine and Taxol, respectively. To date, dozens of FtsZ inhibitors have been identified through different approaches, some of them are effective antibiotics in *in vivo* models of human infection (Foss et al., 2011; Sass and Brötz-Oesterhelt, 2013). Mechanisms of action of these FtsZ inhibitors can be categorized into three general groups: perturbing the assembly/disassembly dynamics of FtsZ, modulating the GTPase activity of FtsZ, and disrupting the structural integrity of FtsZ (Sass and Brötz-Oesterhelt, 2013).

Various ligands that bind to tubulin have dramatic effects on the dynamics of microtubule (Downing, 2000). The interactions of tubulin with their ligands have made great interest in fields from basic cell biology to clinical application. Therefore, chemical inhibitors are promising tools for studying the functions of FtsZ, as illustrated in a current study (Adams et al., 2011).

MreB: an actin homologue

A multitude of cell shapes is encountered in the prokaryotic world. The shape of a bacterial cell is often a conserved trait and has been widely used as a taxonomic criterion (Young, 2006, 2010). This suggests that bacterial morphology is genetically determined, but how is DNA sequence information translated into

morphology? In most bacteria, cell shape maintenance requires the external cell wall whose rigidity and strength are primarily conferred by peptidoglycan (murein) (Nanninga, 1998; Vollmer and Holtje, 2001; Young, 2003). This is illustrated in the classical experiment in which the isolated murein sacculi reflect the specific shape of the cells from which they have been prepared, indicating that the sacculus itself contains information related to cell shape (Fig. 1.12) (Holtje, 1998; Weidel et al., 1960). Furthermore, the degradation of the peptidoglycan of normal rod-shaped *E. coli* cells with lysozyme results in a spherical morphology (Henning et al., 1972). Consistent with these, mutations in several genes involved in peptidoglycan metabolism and cell wall synthesis have been shown to alter the cell morphology of various bacteria (Carballido-López and Formstone, 2007; Osborn and Rothfield, 2007). The involvement of the cell wall in morphogenesis and the lack of obvious intracellular filaments led to the assumption that cell-walled bacteria are devoid of a cytoskeleton that supports cell shape. However, the machinery responsible for cell wall synthesis is highly conserved, and no apparent chemical difference has been identified in cell walls from bacteria with diverse shapes. It is difficult to explain how the murein sacculus by itself could generate so many different morphologies.

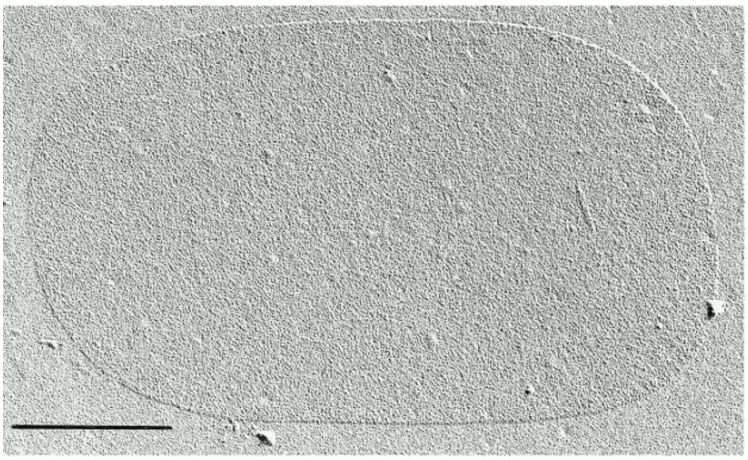

Figure 1.12. Electron micrograph of an isolated *E. coli* murein sacculus. Scale bar: 0.5 μm. From Holtje (1998).

Recent studies on MreB have revolutionized this field. The *mreB* gene was first identified in *E. coli* (Wachi et al., 1987) as a target for mutations that confer resistance to mecillinam. It is located within the *mre* (***m****u****r****e*in formation gene cluster ***e***) region that is associated with cell-shape determination (Doi et al., 1988; Wachi et al., 1989; Wachi et al., 1987; Wachi and Matsuhashi, 1989). *B. subtilis* has three *mreB*-like genes: *mreB* (Levin et al., 1992; Varley and Stewart, 1992), *mreBH*

(Winters et al., 1996) and *mbl* (***m***re***B***-***l***ike) (Abhayawardhane and Stewart, 1995). Disruptions of *mreBH* and *mbl* also have effects on cell shape (Abhayawardhane and Stewart, 1995; Defeu Soufo and Graumann, 2003; Jones et al., 2001).

Errington and colleagues (Jones et al., 2001) later showed that MreB and Mbl form dynamic, helical filaments beneath the cytoplasmic membrane in *B. subtilis*. They recognized that MreB is conserved widely throughout the eubacterial lineage, and is exclusively found in noncocci bacteria (Daniel and Errington, 2003; Jones et al., 2001). In rod-shaped, curved, or spiral bacteria, there is usually at least one *mreB* gene. Exceptions are found in two distinct groups of rod-shaped bacteria: gram-negative bacteria of the *Agrobacterium/Rhizobium* group and gram-positive bacteria of the *Mycobacterium/Corynebacterium* group, are rod shaped but do not contain *mreB* homologues (Daniel and Errington, 2003). This striking correlation between nonspherical shape and the presence of *mreB* homologues points to an important role for MreB proteins in controlling bacterial cell shape. This insight that actin-like proteins are able to form filaments which are involved in determining bacterial cell shape provides a unifying view: actin cytoskeletons shape bacterial cells, just as in eukaryotic cells. Encouraged by the predicted structural similarity (Bork et al., 1992) and the clear functional parallels in shape-determination to actin, van den Ent et al. (2001) solved the crystal structure of MreB from *Thermotoga maritima*. They found that MreB polymerises easily under mild conditions with a strict requirement for ATP. Electron microscopy of the polymers revealed straight and curved filaments and small two-dimensional sheets. The atomic structures of MreB monomer and protofilament resemble those of actin (Fig. 1.13) (van den Ent et al., 2001). It is now widely accepted that MreB is a prokaryotic actin homologue.

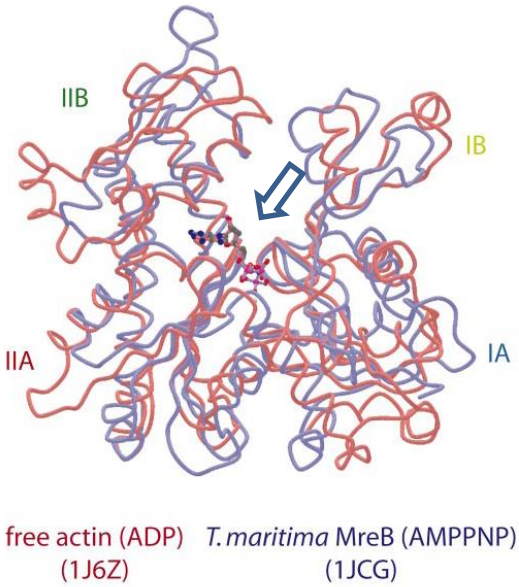

Figure 1.13. Superposition of monomeric actin and MreB. Despite their very low sequence identity (16%), the two proteins have essentially the same fold. PDB entry codes for the crystal structures are in parentheses. Arrow: the nucleotide-binding site. Adapted from Löwe et al. (2004).

Biochemical properties of MreB

Structures of MreB monomer and protofilament

van den Ent et al. (van den Ent et al., 2001) found that in the presence of ATP or GTP, purified *T. maritima* MreB assembles into linear protofilaments and bundles of protofilaments *in vitro*. The longitudinal spacing in the protofilaments is 51 Å, comparable to the 55 Å spacing between polymerised actin subunits. MreB forms two-stranded thin filaments similar to filamentous actin (F-actin), but the strands do not twist around each other. MreB contains two domains (I and II), which are subdivided into two subdomains (A and B) (Fig. 1.13). The subdomains IA, IB, IIA and IIB are also in the same positions as the corresponding subdomains in actin (Fig. 1.13). The nucleotide-binding site is in the interdomain cleft (Fig. 1.13, arrow). MreB shows exactly the same topology (i.e. secondary structural elements) as actin in these domains in a structure-based sequence alignment of MreB and actin. Moreover, the 3D structure of MreB can be superimposed on the structure of actin (Fig. 1.13) (van den Ent et al., 2001).

MreB polymerisation

Esue et al. (2005) studied the *in vitro* assembly of His-tagged *T. maritima* MreB triggered by ATP and compared it to the well-studied assembly of actin. Their results showed that ultrastructure and polymerisation of MreB protofilaments depend critically on temperature and MreB only polymerises within the temperature range for optimal growth of *T. maritime.* MreB assembles without nucleation (or nucleation is highly favourable and fast) and with little or no contribution from filament end-to-end annealing (both are important for actin assembly). The rates of ATP hydrolysis and phosphate release of MreB are similar to that of F-actin. The critical concentration for MreB polymerisation is ~3 nM, which is ~100 times lower than the critical concentration for actin polymerisation. A lower critical concentration for MreB assembly suggests a higher affinity both between MreB monomers and between MreB monomer and protofilament than for actin, and this may explain the lack of a nucleation phase. This is also consistent with the smaller longitudinal spacing (51 Å) between MreB monomers in a protofilament. The much lower intracellular concentration of MreB in bacteria (estimated ~5.6 μM) (Jones et al., 2001) compared with actin in eukaryotes (≤550 μM) (Pollard et al., 2000) may indeed require stronger interactions among MreB proteins. Without accessory proteins, polymerised MreB forms predominantly filamentous bundles. Besides filamentous bundles, MreB spontaneously forms ring-like structures with a relatively narrow distribution of diameters (~160 nm) (Esue et al., 2005), which are smaller than

observed *in vivo* (Carballido-López, 2006). Therefore, it is likely that bacteria use accessory proteins that cross-link MreB filamentous bundles to form larger spirals. Their findings suggest that despite high structural homology, MreB and actin display significantly different assembly properties. However, Bean and Amann (2008) used the native form of *T. maritima* MreB without a His-tag and found two phases of polymerisation, which might correspond to the nucleation and elongation phases of polymer growth. ATP hydrolysis of *T. maritima* MreB is fast, suggesting that *in vivo* most polymerised MreB proteins are in an ADP-bound state. Importantly, the critical concentrations for the polymerisation of ATP- and ADP-bound forms are close, indicating MreB might be able to display treadmilling (Bean and Amann, 2008). Nevertheless, new studies based on purified *B. subtilis* and *E. coli* MreBs showed significant interspecies differences in the *in vitro* behaviours of MreB homologues (Mayer and Amann, 2009; Nurse and Marians, 2013), highlighting the importance of studying MreB from different species.

Bean and Amann (2008) used fluorescence imaging to examine fluorescently-labelled MreB and observed thick, rigid bundles of ~3 μm long *in vitro*. Bulk measurements of the rheological properties of MreB gels showed that MreB forms a very stiff gel *in vitro* (Esue et al., 2006). However, the relationship between *in vitro* gel stiffness and *in vivo* MreB function remains to be explored. Nevertheless, Wang et al. (2010) have shown that MreB filaments contribute significantly to the overall stiffness of *E. coli* cells.

By quantitative immunoblotting, Jones et al. (2001) found that there are ~8,000 molecules of MreB and ~12,000 to 14,000 molecules of Mbl per *B. subtilis* cell. In *E. coli*, the amount of MreB was estimated as ~17,000 molecules per cell in slowly growing cells and ~40,000 molecules per cell in rapidly growing cells (Kruse et al., 2003). Assuming a longitudinal monomer spacing of 51 Å within both of MreB and Mbl protofilaments, this is enough to assemble 41 μm and 66 μm of MreB and Mbl protofilaments, respectively (Erickson, 2001). Since the helical filaments seen by fluorescent microscopy would have a length of 3-6 μm, and most of the MreB and Mbl proteins are in a polymerised form (Carballido-Lopez and Errington, 2003), the helical filaments probably correspond to bundles of about 10 protofilaments, which could provide significant mechanical rigidity. These structures have been called “cables” by analogy to the actin cables of yeast cells.

Dynamics of MreB assembly

The dynamic nature of MreB cytoskeleton is thought as a major feature of this system (Carballido-López, 2006; Pilhofer and Jensen, 2013). Indeed, an MreB mutant forming static filaments is not functional, showing that dynamics of MreB assemblies is essential for their function (Defeu Soufo and Graumann, 2006). Studies with the fluorescent protein-tagged versions of MreB, Mbl, and MreBH show that they form dynamic filamentous structures that are stable but not rigid. The filamentous structures elongate in parallel with cell growth and reconfigure continuously during the cell growth and division cycle (Carballido-Lopez and Errington, 2003; Defeu Soufo and Graumann, 2004). FRAP experiments also showed that Mbl "cables" continuously remodel, turning over in ~8 min, which is similar to the turnover rates measured for actin in various eukaryotic cells (Carballido-Lopez and Errington, 2003). The cables can be severed when the septum forms. Besides, a single Mbl cable is not a continuous structure, but most likely comprises a series of overlapping protofilaments. Although a single MreB/Mbl protofilaments would be expected to have a polarity, there is no overall polarity in the cables. Besides, most of the MreB/Mbl proteins are in a polymerised form at any one time (Carballido-Lopez and Errington, 2003). Taken together, these results indicate that the MreB/Mbl cables are composed of bundles, and turnover and growth occur by lateral association/dissociation of preformed protofilaments from a soluble pool. Consistently, Esue et al. (2005) have shown that MreB assembles with little or no contribution from filament end-to-end annealing *in vitro*. Strikingly, *in vivo* single-molecule imaging suggests that MreB molecules treadmill within short (~300 nm) filamentous structures (Kim et al., 2006).

Cellular localisation and structure of MreB assemblies

MreB homologues localise beneath the cytoplasmic membrane forming two major filamentous structures: helices along the cell length (Fig. 1.14 A) and midcell rings (Cabeen and Jacobs-Wagner, 2010; Carballido-López, 2006; Shaevitz and Gitai, 2010). In *C. crescentus* and *E. coli*, these two patterns interconvert according to the cell cycle stages, and this transition depends on the Z-ring (Figge et al., 2004; Gitai et al., 2004; Vats and Rothfield, 2007). However, helices are predominant for the three MreB isoforms in *B. subtilis* (Carballido-López, 2006; Defeu Soufo and Graumann, 2006), and a midcell MreB ring is dominant in *R. sphaeroides* (Slovak et al., 2005). These MreB structures are dynamic and flexible, and can grow with cell elongation, separate at cytokinetic sites, expand, compress, or rotate (Cabeen and Jacobs-Wagner, 2010; Carballido-López, 2006).

However, current high-resolution imaging studies have suggested a different view of the large-scale configurations of MreB structures (Fig. 1.14 B) (Domínguez-Escobar et al., 2011; Garner et al., 2011; van Teeffelen et al., 2011). Instead of continuous helical or circular filaments, recent discoveries indicate that MreB might form discrete "patches" that move perpendicular to the longitudinal axis. This discrepancy in the cellular structures of MreB is discussed in more details in Chapter 4.

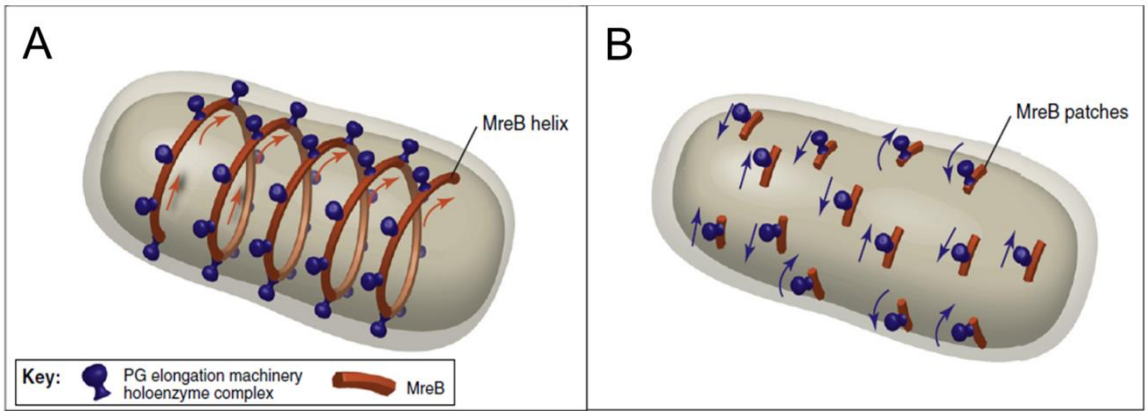

Figure 1.14. Schematics illustrating a simplified comparison of two models for *in vivo* MreB structure and movement. Both models depict MreB (brown) couples with the peptidoglycan (PG) elongation machinery (purple), which collectively represents the cylindrical wall synthesis machinery. **(A)** Filamentous MreB helix which is a scaffold for other cell-wall synthesis proteins. **(B)** Short MreB patches that move bidirectionally with PG elongation proteins. Adapted from White and Gober (2012).

Functions of MreB

Morphogenesis

Although various shapes are encountered in bacteria, they can be simply classified as spherical (cocci), cylindrical (rod), curved (vibrioid), and helical (spiral). Since the coccus is the simplest of possible cell shapes, it can be viewed as the "default". The vibrioid can be viewed as a curved rod, and a spiral is an elongated vibrioid (Margolin, 2004; Margolin, 2009; Young, 2010). Thus, the puzzle of bacterial morphogenesis can be first simplified as how a rod gets its shape. The morphological phenotypes of cells with defects in MreB functions (Cabeen and Jacobs-Wagner, 2010; Carballido-López, 2006; Shaevitz and Gitai, 2010), as well as the phylogenetic distribution of MreB homologues in

nonspherical bacteria (Daniel and Errington, 2003), strongly argue that MreB plays a critical role in the establishment of a rod shape.

Jones et al. (2001) first suggested that the MreB and Mbl cytoskeletal structures may act as a structural brace and control cell shape. Or alternatively, by analogy with the postulated role of actin in yeast (Pruyne and Bretscher, 2000), they may operate by exerting spatial control over the cell-wall-synthesizing machinery. Subsequent studies provided evidences supporting both mechanisms. By using a fluorescent derivative of the antibiotic vancomycin to detect the localisation of nascent cell-wall synthesis, Daniel and Errington (2003) demonstrated that synthesis of the sidewall in *B. subtilis* occurs in a helical manner which depends on Mbl helices, suggesting that MreB filaments might direct cell-wall synthesis activity to produce a rod-shape bacterium. Consistent with this, penicillin-binding protein 2 (PBP2), which has a critical role in synthesizing cylindrical peptidoglycan and maintaining a rod shape, locates in a spiral pattern that depends on MreB (den Blaauwen et al., 2003; Figge et al., 2004). It is proposed that MreB cytoskeleton serves as an organizer or tracking device for PBP2 (and thus the peptidoglycan synthesis activity). MreB has also been implicated in directing the localisation of many other components of the cell-wall synthesis machinery (Margolin, 2009; Shaevitz and Gitai, 2010; White and Gober, 2012). Collectively, these results suggest that MreB exerts spatial and temporal control over peptidoglycan synthesis to affect bacterial morphogenesis.

The dynamic helical or circular MreB structures were thought to form the track for the cell-wall synthesis machinery. Besides, treadmilling of MreB may contribute to the movement/redistribution of cell-wall synthesis machinery. However, recent studies have shown a different view. As mentioned above, high-resolution imaging shows that MreB might form short patches rather than long filamentous structures in bacteria (Fig. 1.14 B) (Domínguez-Escobar et al., 2011; Garner et al., 2011; van Teeffelen et al., 2011). These MreB patches move circumferentially with other cell-wall synthesis proteins. Intriguingly, the movement of MreB patches is powered by peptidoglycan synthesis activity, not the opposite. It is suggested that short MreB patches might respond to the tracks made by the newly synthesized peptidoglycan strands and reinforce their circumferential directionality. MreB patches could also constrain the mobility of cell-wall synthesis machinery to achieve defined cell wall geometry (Domínguez-Escobar et al., 2011; Garner et al., 2011; van Teeffelen et al., 2011). A current study further shows that MreB assemblies preferentially localise to negatively curved regions of the cell envelope, which this localisation targets cell-wall growth in these regions (Ursell et al., 2014). Then, surface deformations

caused by new peptidoglycan insertion could direct circumferential movement of MreB. This feedback on the localisation of MreB and cell wall growth could result in MreB-mediated robust, uniform cell-wall synthesis at the cellular scale without requiring global organisation (Ursell et al., 2014). Another study shows that PBP2 moves much faster and more erratically than MreB (Lee et al., 2014). PBP2 interacts with the rest of the cell-wall synthesis machinery/MreB patches through a dynamic cycle of transient association. This dynamic association of PBP2 buffers spatially distributed growth against fluctuations in component concentrations (Lee et al., 2014).

MreB cytoskeleton may also fulfil its morphological function by applying a physical force to maintain cell width and reinforce the stability of the cell wall (Sun and Jiang, 2011; Typas et al., 2012). Indeed, micromanipulation of cells shows that MreB cytoskeleton contributes to the bending stiffness of *E. coli* (Wang et al., 2010).

In addition to the overall cell shape, Wagner et al. (2005) demonstrated that MreB might coordinate with RodA and PBP2 to play a role in *C. crescentus* stalk formation. MreB may also participate in the morphological adaptations of *V. parahaemolyticus* under environmental stresses (Chiu et al., 2008).

Chromosome segregation

MreB might be involved in bacterial chromosome dynamics. Expression of a dominant-negative ATPase-defective form of MreB in merodiploid *E. coli* produced filamentous cells with altered MreB cytoskeletal structure. These cells have severe localisation defects of the nucleoid and of the *oriC* and *ter* regions, indicating that MreB cytoskeleton is important for directional segregation of chromosomes (Kruse et al., 2003). Consistently, depletion of *B. subtilis* MreB leads to a strong chromosome segregation defect (Defeu Soufo and Graumann, 2003). Importantly, the chromosome segregation defects in both organisms arise prior to significant changes in cell shape. However, controversial conclusions have been derived from other studies of *B. subtilis* and *E. coli* (Bendezú and de Boer, 2008; Formstone and Errington, 2005; Karczmarek et al., 2007). Nevertheless, studies on *V. cholerae* and *Helicobacter pylori* support the role of MreB in chromosome segregation (Srivastava et al., 2007; Waidner et al., 2009).

In *C. crescentus*, MreB depletion or overexpression also disrupts the polar localisation of *oriC* (Gitai et al., 2004). Gitai et al. (2005) took the advantages of A22, which causes a rapid and reversible disintegration of the MreB assemblies (see below). A22 treatment of *C. crescentus* cells completely inhibits the segregation of *oriC* or an *oriC*-distal locus. Importantly, this effect was reversible.

In addition, chromosome was successfully segregated when A22 was administered to cells with A22-resistant *mreB* alleles. Their results also suggested that there is a two-step mechanism for chromosome segregation in *C. crescentus*: first the *oriC* is segregated in an MreB-dependent manner, and then the rest of the chromosome follows through an MreB-independent mechanism. However, Shebelut et al. (2009) showed that the effects of A22 are growth condition-dependent. Whether MreB directly or indirectly affects chromosome segregation remains to be determined.

In addition to chromosome segregation, MreB might participate in other aspects of chromosome dynamics: MreB affects chromosome decatenation in *E. coli* (Madabhushi and Marians, 2009) and chromosome condensation in *V. cholerae* (Srivastava et al., 2007). MreB could also regulate DNA replication. Defeu Soufo and Graumann (2005) reported that MreB is important for the midcell localisation of the replication machinery, and A22-treatment slows DNA replication in *C. crescentus* (Shebelut et al., 2009). Interestingly, MreB is used by a *B. subtilis* phage for efficient DNA replication (Muñoz-Espín et al., 2009).

Protein localisation

MreB's localisation to a "track-like" structure suggests a role of MreB in macromolecule positioning or trafficking. In addition to proteins participate in chromosome dynamics and cell wall synthesis (see above), evidences of MreB-dependent localisation have come from proteins belonging to diverse functional categories.

Gitai et al. (2004) showed that MreB is necessary for the localisation of multiple polar protein markers in *C. crescentus*. Wagner et al. (2005) also found that *C. crescentus* cells depleted of MreB are unable to recover proper polarity when MreB is restored: they exhibit branching and stalk synthesis at abnormal places along the cell cylinder. Intriguingly, MreB is involved in the initiation, rather than the maintenance, of the localisation of the polar marker PopZ in *C. crescentus* (Bowman et al., 2008). To date, MreB has been implicated in the localisation of carboxysome (Savage et al., 2010), gliding motility proteins (Mauriello et al., 2010), inclusion bodies (Rokney et al., 2009), and pilus-associated proteins (Cowles and Gitai, 2010).

Chemical modulators of MreB

Unlike FtsZ, only a few chemicals have been identified as MreB inhibitors. *S*-(3,4-dichlorobenzyl)isothiourea (A22) was originally identified in a screen for inhibitors of chromosome partitioning in *E. coli* (Iwai et al., 2002). A22 induces

spherical, anucleate cells in *E. coli*, phenotypes that reminiscent *mreB* mutants. Iwai et al. (2002) thus suggested that the target of A22 might be MreB, and this idea has been confirmed by Gitai et al. (2005). Since MreB is essential in most bacteria, earlier studies usually use depletion to perturb MreB function. However, this method is slow, requiring several generation times before MreB protein levels are significantly reduced. For a rapid method of disrupting MreB function, Gitai et al. (2005) explored the use of small molecules. They treated *C. crescentus* cells with actin inhibitors like cytochalasin D, latrunculin, jasplakinolide, and phalloidin. All of these compounds failed to affect MreB *in vivo*. A22, however, mimics the effects of MreB depletion and causes a rapid and reversible disassembly of the MreB filaments. They also showed that A22 is highly specific for MreB. The specificity and rapid and reversible effect of A22 on MreB make it particularly useful for the temporal analysis of MreB function. A22 binds MreB and perturbs its ATP-binding region (Bean et al., 2009; Gitai et al., 2005). A22 has now been widely used to dissect the functions of MreB (Foss et al., 2011). However, A22 causes MreB-independent growth inhibition that varies with A22 concentration, culture medium conditions, and bacterial species. MP265, a synthesized A22 structural analogue, is less toxic than A22 for growth but equally efficient for disrupting MreB assemblies (Takacs et al., 2010).

Other known MreB inhibitors including sceptrin, which might bind to or perturb the ATP-binding pocket of MreB (like A22) (Rodríguez et al., 2008), and CBR-4830 is an indole that binds to MreB and inhibits its ATP-dependent polymerisation (Robertson et al., 2007).

ParA-like proteins

Proteins in the Walker A Cytoskeletal ATPases (WACAs) family are found in most bacterial species and represent a group of prokaryote-specific cytoskeletal proteins (Michie and Löwe, 2006). MinD and ParA are the two best-studied members in this family. It is now clear that ParA proteins form a group of general partitioning machinery capable of performing multitudes of tasks (Lutkenhaus, 2012; Szardenings et al., 2011). ParA proteins perform their DNA segregation function in concert with a DNA-binding protein (normally termed ParB) and a *cis*-acting, centromere-like DNA sequence (*parS*). The "motor" ParA contains a conserved deviant Walker A motif (GXXXGKT; where X is any amino acid) which is involved in the nucleotide binding (Michie and Löwe, 2006). Despite being classified as plasmid-encoded Ia/Ib and chromosome-encoded subfamilies, ParAs

can be categorized into two subtypes: “large” ParAs possessing an N-terminal DNA-binding helix-turn-helix motif and “small” ParAs that lack this motif (Gerdes et al., 2010). Large and small ParAs have respectively large and small cognate adaptor ParBs (Livny et al., 2007). Recently, additional subfamilies within the MinD/ParA family have been identified. These proteins are involved in the positioning of different proteins, and have been referred to as “orphan” ParAs (i.e. not associated with the “usual” ParB partner). They include PpfA (section 1.2), ParC (section 1.2), carboxysome-segregating ParA (Savage et al., 2010), TadZ/CpaE (involved in the polar positioning of type IV pili) (Perez-Cheeks et al., 2012), VirC1 (involved in the polar localisation of conjugation machinery) (Atmakuri et al., 2007), YjhQ/BcsQ (involved in the polar synthesis of cellulose) (Le Quéré and Ghigo, 2009), and MipZ.

Emerging evidences indicate that ParA-like systems employs different mechanisms to position their cargos (Gerdes et al., 2010; Lutkenhaus, 2012; Ptacin et al., 2010; Szardenings et al., 2011). Nevertheless, some shared features of chromosome- and plasmid-segregating ParAs are: (1) dynamic movement over the nucleoid; (2) ATP-dependent non-specific binding to DNA; (3) interaction with the ParB–*parS* complex (Gerdes et al., 2010; Ptacin et al., 2010; Salje, 2010). Despite these shared features, the actual molecular mechanisms linking ParA dynamics with DNA partitioning is still mysterious (Gerdes et al., 2010; Howard and Gerdes, 2010). Basically, two types of models are proposed: filament-pulling model and diffusion-ratchet model (Fig. 1.15) (Howard and Gerdes, 2010; Szardenings et al., 2011). Both models employ a “time-delay ratchet” (Howard and Gerdes, 2010; Ptacin et al., 2010; Vecchiarelli et al., 2010; Vecchiarelli et al., 2012) which may be originated from the slow multi-step conformational transition of ParA upon ATP binding (Vecchiarelli et al., 2010). The primary difference between these models is whether ParA polymerises into filaments, and whether depolymerisation of filaments can provide the pulling force for DNA segregation (Howard and Gerdes, 2010).

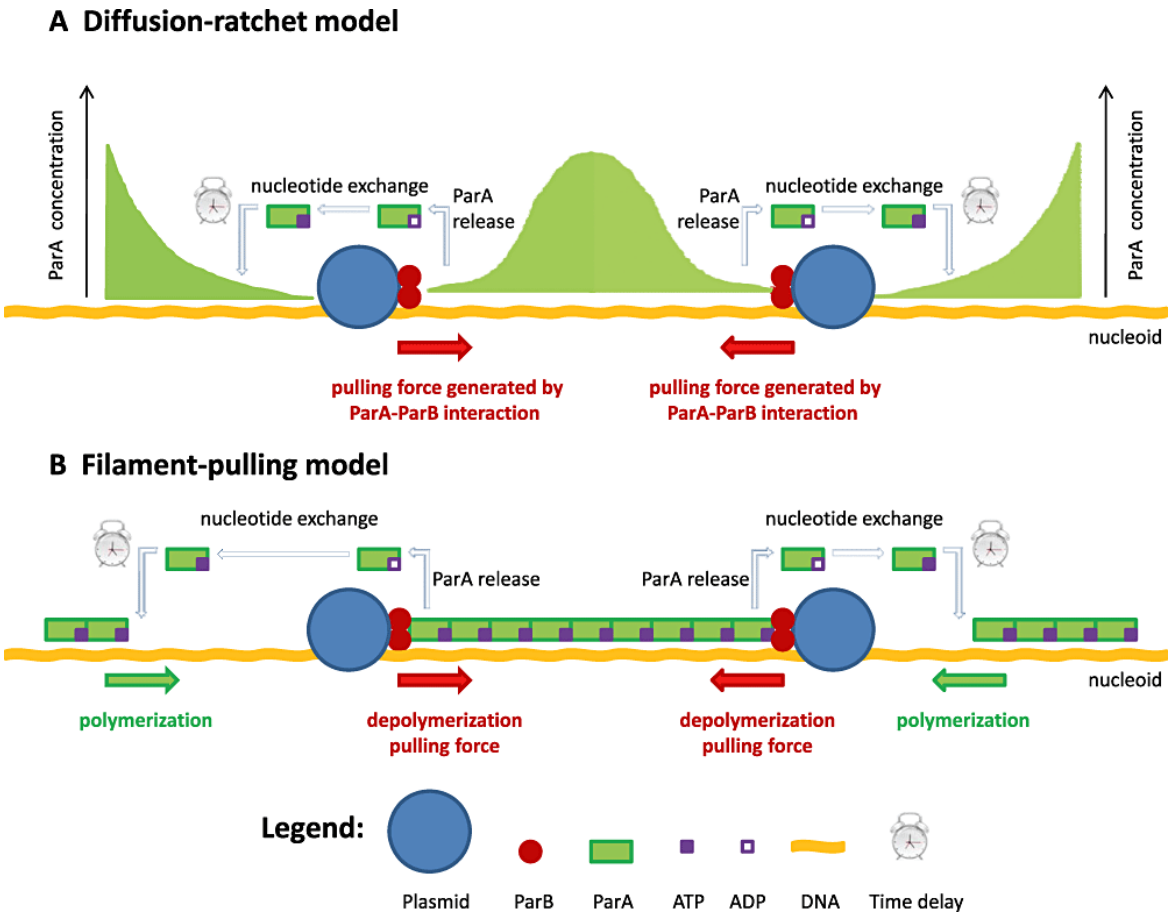

Figure 1.15. Schematic representations of the "diffusion-ratchet" model (A) and the "filament-pulling" model (B). The figure illustrates two plasmids being pulled towards each other across the nucleoid surface. In **(A)**, the pulling force is directed towards regions of higher ParA concentration where a greater number of ParA–ParB bonds can be formed. The clock symbol represents a time delay induced by a slow conformational change of ParA to its DNA-binding form. In **(B)**, the pulling force is generated by ParA filament depolymerisation. The same time delay as in (A) is shown. From Howard and Gerdes (2010).

Numerous studies have shown that chromosome- and plasmid-segregating ParAs form filamentous structures *in vivo* and *in vitro*. Initial observations suggest that ParA of pB171 oscillates in helical structures between the two ends of the nucleoid (Ebersbach and Gerdes, 2004) and form ATP-dependent filaments *in vitro* (Ebersbach et al., 2006). The ParA homologue SopA of F plasmid also polymerises into filaments in an ATP-dependent manner *in vitro*, with a filament elongation rate similar to that of plasmid movement *in vivo*. SopA undergoes cycles of polymerisation and depolymerisation, and oscillating between ParB–*parS* complexes (SopB–*sopC*). The dynamic behaviour of SopA is critical for plasmid segregation, since static filaments formed by SopA mutants are defective

in plasmid segregation (Lim et al., 2005). *In vivo*, SopA forms a large focus that oscillates between the two ends of the nucleoid (Hatano et al., 2007). Simultaneously, SopA also forms a filamentous structure that spans the entire length of the nucleoid without being shortened as the plasmid migrates. Although the SopA filament as a whole remains constant in length, the intensity distribution of SopA does change. ATP-dependent polymerisation of different ParA homologs into filamentous structures was further observed *in vitro* (Barilla et al., 2005; Bouet et al., 2007; Ditkowski et al., 2010; Dunham et al., 2009; Hui et al., 2010; Leonard et al., 2005; Pratto et al., 2008; Ptacin et al., 2010) and *in vivo* (Adachi et al., 2006; Hatano et al., 2007; Jakimowicz et al., 2007; Pratto et al., 2008; Ptacin et al., 2010; Ringgaard et al., 2009). Currently, Vecchiarelli et al. (2010) found no evidence for *in vitro* polymerisation of P1 plasmid ParA even at high concentrations. They propose that the observed *in vivo* helical structures are the results of an underlying helical structure of the nucleoid (Berlatzky et al., 2008; Fisher et al., 2013). However, this notion cannot explain the slightly curved filamentous structures formed by *C. crescentus* ParA *in vivo* (Ptacin et al., 2010). It is critical to clarify whether ParA really polymerises into filaments.

In the filament-pulling model (Fig. 1.15 B), a pulling force is generated by depolymerisation of ParA filament stimulated by the ParB–*parS* complex (Gerdes et al., 2010; Howard and Gerdes, 2010; Szardenings et al., 2011). In general, Apo-ParA binds ATP, changes its conformation, and dimerizes. ParA-ATP dimmers bind cooperatively to nucleoid DNA, leading to polymerisation. Subsequently, a growing ParA filamentous structure (bundles of ParA polymers) contacts a ParB–*parS* complex. ParB stimulates the ATPase activity of ParA at the end of the filamentous structure, resulting in the release of ParA from the nucleoid. New ParA-ATP filament ends accessible for ParB are left. For each depolymerisation event, the ParB–*parS* complex can either detach or remain attached to the end of the depolymerising ParA filamentous structure. The moving ParB–*parS* complex "ratchets" along the end of a retracting ParA filamentous structure and leaves behind it a ParA-free nucleoid zone. Eventually, the recycling ParA-ATP subunits assemble into a new filamentous structure in this zone that grows toward the ParB–*parS* complex from the opposite side. Upon contact formation, this new filamentous structure will move the plasmid in the opposite direction. In this way, a ParB–*parS* complex will wiggle between other ParB–*parS* complexes and the nucleoid ends.

In the diffusion-ratchet model (Fig. 1.15 A), since *parS*-bound ParB directly interacts with ParA, the plasmid cargo will have a higher affinity for high-density ParA regions (Gerdes et al., 2010; Howard and Gerdes, 2010; Szardenings et al.,

2011; Vecchiarelli et al., 2012). Binding of ParB stimulates the ATPase activity of ParA causing ParA to release from the nucleoid, and depletes ParA in the vicinity of the ParB–*parS* complex. The plasmid will therefore experience an attractive force towards regions of higher ParA concentration. The disassociated ParA re-bind ATP and go through a slow multi-step conformational transition before regaining the DNA-binding state. This "time-delay ratchet" allows an even redistribution of DNA-binding-competent ParA. Combining the activity of ParB, the system generates a dynamic instability in the local concentrations of nucleoid-bound ParA, which in turn drives the oscillation/uneven distribution of nucleoid-associated ParA. The steady-state non-equilibrium spatial distribution of ParA and ParB provides the force for long-ranged plasmid movement. Multiple plasmids will develop a trend to position themselves equidistant to each other along the nucleoid (Gerdes et al., 2010; Howard and Gerdes, 2010; Szardenings et al., 2011; Vecchiarelli et al., 2012). Intriguingly, although SopA forms filaments *in vivo* and *in vitro*, a current *in vitro* reconstitution study provides strong evidence that SopA segregates plasmid DNA via a diffusion-ratchet mechanism (Vecchiarelli et al., 2014). Besides, the *in vivo* ParA filaments might be artefacts of the imaging methods (Margolin, 2012; Vecchiarelli et al., 2012).

Dynamic oscillation might be a general feature of diffusion-ratchet mechanisms. This feature uses cyclic activity that iteratively explores the positions of plasmids and constantly adjusts the interplasmid distance according to the number of plasmids present (Gerdes et al., 2010; Salje, 2010; Szardenings et al., 2011). A minimal self-organized oscillatory system can be built on a self-assembling protein and a surface. For the best studied MinCDE system, the surface is the cytoplasmic membrane. Alternatively, ParA systems use the surface of the nucleoid (Gerdes et al., 2010; Lutkenhaus, 2012; Salje, 2010; Szardenings et al., 2011; Vecchiarelli et al., 2012). Both systems use the ATPase activity of a WACA (i.e. MinD and ParA) as a switch, which is stimulated by a protein partner (MinE and ParB). This results in perpetual cycles of ParA polymerisation/ depolymerisation that continuously equi-partition plasmids. A prediction of this behaviour is that a non-oscillatory ParA/MinD system will require a tethering mechanism cooperates with it. Strikingly, the non-oscillatory *B. subtilis* MinD and *C. crescentus* MipZ cooperate with the polar anchor DivIVA and ParB, respectively (Lutkenhaus, 2012). Besides, ParC also attaches to HubP to position chemosensory clusters (section 1.2). The oscillatory behaviour of the carboxysome-segregating ParA system (Savage et al., 2010) suggests a diffusion-ratchet mechanism is used. Whether similar mechanism is used by

PpfA to partition the cytoplasmic chemosensory cluster is unclear at this moment. Nevertheless, the nucleoid is important for PpfA's function and a ParB analogue TlpT is present.

It should be emphasized that the entire process of ParA-mediated plasmid partitioning is thought to take place on the surface of the nucleoid (Howard and Gerdes, 2010; Lutkenhaus, 2012; Szardenings et al., 2011; Vecchiarelli et al., 2012). The nucleoid is also vital for ParABS-mediated chromosome segregation (Ptacin et al., 2010). ParA can localise and function on several nucleoids independently at the same time and can pull plasmids between well-segregated, adjacent nucleoids (Ringgaard et al., 2009). The regular plasmid distribution over the nucleoid leads to ordered plasmid partitioning from the mother cell to the daughter cells. Plasmids lacking *par* loci are randomly distributed in spaces not occupied by nucleoids (Niki and Hiraga, 1997; Ringgaard et al., 2009; Yao et al., 2007). Thus, ParA-mediated recruitment of plasmids to the nucleoid is a specialized mechanism that ensures equi-partitioning. This mechanism is advantageous since chromosome segregation is paramount to the host cell. It is plausible to coordinate plasmid partitioning with nucleoid dynamics. By linking to the nucleoid, plasmid partitioning could couple with the host's cell cycle. However, it is not necessary that plasmids hitch a ride on the chromosome.

Interactions between different bacterial cytoskeletal proteins

Currently, areas of active investigation in bacterial cell biology are largely rooted in the bacterial cytoskeleton (Cabeen and Jacobs-Wagner, 2010; Gitai, 2005; Goley, 2013; Ingerson-Mahar and Gitai, 2012). As the number of identified bacterial cytoskeletal proteins has expanded sharply (Ingerson-Mahar and Gitai, 2012; Pilhofer and Jensen, 2013), an emerging theme is the choreography of cytoskeletal networks. Classic examples are the interactions between MinCDE/MipZ–FtsZ and FtsA–FtsZ.

The Z-ring dependent reorganisation of MreB cytoskeleton into a midcell ring-like structure indicates that FtsZ and MreB might interact directly or indirectly (Figge et al., 2004; Gitai et al., 2004; Vats and Rothfield, 2007). This idea was currently confirmed in *E. coli*: MreB and FtsZ interact directly (Fenton and Gerdes, 2013). This interaction is required for Z-ring constriction, likely via a transfer of cell-wall synthesis enzymes from the lateral site to the mature divisome, which allows cells to synthesise the septum. Crescentin, a bacterial intermediate filament protein, controls *C. crescentus* cell curvature. This function

requires an interaction between crescentin and MreB (Charbon et al., 2009). CTP synthase, which forms a cytoplasmic filamentous structure, also colocalises with crescentin and exhibits an inhibitory effect on crescentin-mediated cell curvature (Ingerson-Mahar et al., 2010). It would be interesting to further explore undiscovered interactions between bacterial cytoskeletal systems in different levels.

1.5 Aims of this Study

The advances in prokaryotic cell biology clearly demonstrate that the spatiotemporal dynamics of a biological system is essential to understand its function in bacteria. Chemotaxis and cell division are very different cellular activities but both are accomplished by the concerted actions of several molecular complexes that localise at specific sites in the cell (de Boer, 2010; Sourjik and Armitage, 2010). At cell division each daughter cell must inherit a complement of chemosensory proteins to allow efficient chemotaxis. Hence, the positioning of chemosensory proteins must coordinate with cell division and it has been suggested that sophisticated mechanisms have evolved to orchestrate the spatial regulation of cell division and chemotaxis (Sourjik and Armitage, 2010). Previous studies have suggested that the FtsZ, MreB or ParA-like cytoskeletal systems may participate in this process. However, except for a number of controversial models, there is still no satisfactory mechanistic explanation for how bacteria establish the specific localisation of their chemosensory proteins. Besides, it is becoming clear that different bacteria may use different mechanisms to position their chemosensory proteins. Therefore, the aim of this study is to explore the role of FtsZ and MreB cytoskeleton in the partitioning of chemosensory clusters in *R. sphaeroides*. This goal is divided into the following objectives:

- Establish the spatiotemporal dynamics of FtsZ and MreB through the cell cycle of *R. sphaeroides* via live-cell fluorescence microscopy.
- Establish the spatiotemporal dynamics of membrane and cytoplasmic chemosensory clusters through the cell cycle of *R. sphaeroides* via live-cell fluorescence microscopy.
- Use quantitative fluorescence microscopy to obtain detailed understandings of the dynamic behaviours and assembling kinetics of the *R. sphaeroides* membrane chemosensory cluster. Inspect whether or not a stochastic self-assembly process might contribute to the formation and positioning of membrane chemosensory cluster in *R. sphaeroides*.
- Examine the possible roles of FtsZ and MreB in the partitioning of membrane and cytoplasmic chemosensory clusters via simultaneous monitoring of pairs of chemosensory and cytoskeletal proteins through the *R. sphaeroides* cell cycle.
- Explore the roles of other known protein localisation mechanisms in the positioning of *R. sphaeroides* chemosensory clusters.

Chapter 2. Materials and Methods

The gift of the great microscopist is the ability to think with the eyes and see with the brain. Deep revelations into the nature of living things continue to travel on beams of light.

— Daniel Mazia

2.1 Bacterial Strains and Growth Conditions

The strains and plasmids (Table 2.1) used in this study were constructed as described before (Porter et al., 2007). For strain storage, stationary-phase culture were mixed with glycerol (final concentration of 20%), frozen in liquid nitrogen, and immediately stored at –80 °C. *E. coli* strain XL1-Blue was used for cloning. *E. coli* strain S17-1*λpir* was used for conjugal DNA transfer into *R. sphaeroides.* All *R. sphaeroides* strains were derived from WS8N (Porter et al., 2011b) and grown in succinate medium or on Luria-Bertani (LB) agar plates (see Appendix) with antibiotics at 30°C. *E. coli* strains were grown in LB medium (with shaking) or on LB agar plates with antibiotics at 37°C. When appropriate, the antibiotics nalidixic acid and kanamycin were used at 25 μg ml^{-1}. All experiments were performed with log-phase aerobic (with shaking) or photoheterotrophic (1.5 ml culture in 1.7 ml Eppendorfs and illuminated with light at 10 W m^{-2}) cells. To inhibit protein synthesis, chloramphenicol was added to the bacterial culture at a final concentration of 50 μg ml^{-1} (Romagnoli et al., 2002). For time-lapse imaging, cells pre-treated with chloramphenicol for 90 min were laid on agarose pads pre-soaked in medium containing chloramphenicol.

Table 2.1. Bacterial strains and plasmids used in this study

Strains/plasmids	Relevant genotype/description	Reference or source
R. sphaeroides		
WS8N	Spontaneous nalidixic acid-resistant derivative of wild-type WS8	Porter et al. (2011b)
JPA187	WS8N containing a *gfp-mreB* fusion in place of the genomic *mreB*	Slovak et al. (2005)
JPA500	WS8N containing an *mcpG-gfp* fusion in place of the genomic *mcpG*	Wadhams et al. (2000)
JPA533	WS8N containing a deletion of $cheOp_2$ and an *mcpG-gfp* fusion in place of the genomic *mcpG*	Wadhams et al. (2000)
JPA1418	WS8N containing a *yfp–*$cheW_3$ fusion in place of the wild-type $cheW_3$ in the chromosome	Wadhams et al. (2003)
JPA1455	JPA1418 containing a *cfp–*$cheW_4$ fusion in place of the wild-type $cheW_4$ in the chromosome	Wadhams et al. (2003)
JPA1558	WS8N containing a *tlpT–yfp* fusion in place of the wild-type *tlpT* in the chromosome	Wadhams et al. (2003)
JPA2241	JPA1558 containing pIND4-*ftsZ–cfp*	This study
JPA2242	JPA1418 containing pIND4-*ftsZ–cfp*	This study
JPA2243	WS8N containing pIND4-*ftsZ–yfp*	This study
JPA2245	JPA1558 containing pIND4-*mreB–cfp*	This study
JPA2246	JPA1418 containing pIND4-*mreB–cfp*	This study
JPA2248	WS8N containing pIND4-*mreB–yfp*	This study
JPA2252	JPA1558 containing pIND4-*cfp–mreB*	This study

JPA2253	JPA1418 containing pIND4-*cfp–mreB*	This study
JPA2254	WS8N containing pIND4-*yfp–mreB*	This study
JPA2255	WS8N containing an *mcpB-rfp* fusion in place of the genomic *mcpB*	This study
JPA2380	JPA187 containing pIND4-*ftsZ–rfp*	This study
JPA2381	JPA1455 containing pIND4-*ftsZ–rfp*	This study
JPA2382	JPA533 containing pIND4-*cheW*$_2$*cheW*$_3$	This study
E. coli		
XL1-Blue	General cloning host	Stratagene
S17-1*λpir*	A strain capable of mobilizing pIND4 and pK18*mobsacB* into *R. sphaeroides*	Penfold and Pemberton (1992)
Plasmids		
pIND4	IPTG-inducible expression vector for *R. sphaeroides*; $P_{A1/04/03}$, *lacI*^{q}, Km^R	Ind et al. (2009)
pK18*mobsacB*	Allelic exchange suicide vector mobilized by *E. coli* S17-1*λpir*; Km^R	Schafer et al. (1994)
pIND4-*ftsZ–cfp*	pIND4 containing *ftsZ–cfp*	This study
pIND4-*ftsZ–rfp*	pIND4 containing *ftsZ–rfp*	This study
pIND4-*ftsZ–yfp*	pIND4 containing *ftsZ–yfp*	This study
pIND4-*mreB–cfp*	pIND4 containing *mreB–cfp*	This study
pIND4-*mreB–yfp*	pIND4 containing *mreB–yfp*	This study
pIND4-*cfp–mreB*	pIND4 containing *cfp–mreB*	This study
pIND4-*yfp–mreB*	pIND4 containing *yfp–mreB*	This study
pIND4-*cheW*$_2$*cheW*$_3$	pIND4 containing *cheW*$_2$*cheW*$_3$	This study

2.2 Molecular Genetic Techniques

DNA cloning

Plasmid purification: *E. coli* cultures containing the plasmids of interest were grown in LB broth with appropriate antibiotic(s) at 37°C for overnight. Plasmid DNA was then extracted using the QIAfilter plasmid Miniprep or Midiprep kit (Qiagen) according to the manufacturer's instructions.

Purification of *R. sphaeroides* chromosomal DNA:
R. sphaeroides cultures were grown to stationary phase and 1.5 ml of culture was centrifuged and the pellet was snap frozen in liquid nitrogen. The frozen pellet was then resuspended in 0.5 ml lysis buffer (10 mM Tris-HCl pH 8.0, 1 mM EDTA, 1% SDS) and heated to 65°C. Proteinase K (100 mg) was added and the mixture was incubated at 45°C for 2 h. The chromosomal DNA was then extracted twice with 0.5 ml phenol:chloroform:isoamylalcohol (25:24:1 v/v) solution, and precipitated with 100% ethanol and incubated at –20°C for 30 min. Following incubation the sample was centrifuged at 16000 × *g* for 15 min, the pellet was then washed with 70% ethanol and spun again as above. The pellet was then dried at 37°C for overnight and resuspended in 50 µl sterile water and stored at –20°C.

DNA manipulations:
Polymerase Chain Reaction (PCR), restriction enzyme digestion, de-phosphorylation of digested plasmid DNA, and DNA ligation were carried out according to standard protocols (Green and Sambrook, 2012). Overlap extension PCR was used to create constructs for generating deletion strains and genomic replacement strains, as described before (Porter et al., 2007).

For DNA electrophoresis, gels were made using 0.8%–2% multi-purpose agarose (Roche) in 0.5 × TBE buffer (see Appendix). DNA was electrophoresed at voltages between 80–140 V. Gels were visualised by staining in 1 ng/ml ethidium bromide for 15 min and viewing on a UV transiluminator. DNA fragments were purified from agarose gels using the Gel Extraction Kit (Qiagen) according to the manufacturer's instructions.

DNA Sequencing:
All constructs were checked by DNA sequencing before use. DNA sequencing was done by the Automated DNA Sequencing Service from Geneservice (Source BioScience). The BigDye termination method (PE Biosystems) was used on a 3730

DNA sequencer (Applied Biosystems). Contigs were generated using the Staden software package and analysed using Clone Manager (Sci Ed Central).

Preparation of *E. coli* competent cells:

One millilitre of *E. coli* stationary-phase culture was inoculated into 50 ml of LB broth and then incubated at 37°C until reached an OD_{600} of 0.4. The culture was then transferred to a 50 ml falcon tube and incubated on ice for 30 min, before being centrifuged at 1000 × *g* for 10 min at 4°C. The pellet was resuspended in 16 ml ice cold TFB-I (see Appendix), and incubated on ice for 1 h, before being centrifuged at 750 × *g* for 10 min at 4°C. The pellet was then resuspended in 4 ml ice cold TFB-II (see Appendix). Resuspended cells were frozen in liquid nitrogen and stored at –80°C as 100-µl aliquots.

Transformation:

One hundred microlitre of *E. coli* competent cells were defrosted on ice, and then incubated on ice with plasmid DNA (25 µl for ligation products or 1 µl for purified plasmid) for 45 min. The cells were then heat shocked by incubating them at 42°C for 45 s and then immediately placed on ice for 45 s. One millilitre of LB medium was then added to the cells and incubated at 37°C for 1 h before being plated on LB agar plates with the appropriate antibiotic.

Conjugation of plasmids into *R. sphaeroides*

Transformation is not working for *R. sphaeroides* so plasmids were introduced via conjugation from *E. coli* S17-1*λpir* cells. One millilitre of mid-log phase *E. coli* cells carrying the plasmid of interest and 1 ml of stationary-phase *R. sphaeroides* cells were centrifuged at 3500 × *g*. Pellets of both *E. coli* and *R. sphaeroides* cells were washed in 1 ml LB broth (without antibiotics), and then resuspended in 100 µl LB broth. *E. coli* S17-1*λpir* cells were gently resuspended to avoid shearing the pili. Then 10 µl of *E. coli* cells were gently mixed with 100 µl of *R. sphaeroides* cells, and the mixture was pipetted onto a sterile nitrocellulose filter on an LB agar plate without antibiotic. The plate was incubated on 30°C for overnight, and then the cells were washed off the filter in LB broth and spread onto LB agar plates containing nalidixic acid and the appropriate selective antibiotic for the plasmid.

Genomic replacement for constructing mutants and fluorescent-protein fusions of *R. sphaeroides*

DNA recombination was used to introduce mutations or fluorescently-labelled versions of genes into the *R. sphaeroides* genome (Porter et al., 2007). This was achieved by using the suicide vector pK18*mobsacB*. For genomic deletions, plasmid constructs were created to contain the 500-bp upstream and downstream regions flanking the gene of interest, but not the gene itself. For N-terminally tagged genomic replacements, plasmid constructs were created to contain the upstream 500-bp region, the tag, and the first 500 bp of the gene. For C-terminally tagged genomic replacements, plasmid constructs were created to contain the final 500 bp of the gene, the tag and the downstream 500-bp region.

Plasmid constructs were transferred into the parent *R. sphaeroides* strains by conjugation, and spread onto LB agar plates containing kanamycin and naladixic acid. Colonies grown were regrown in succinate media with naladixic acid for 48 h. The absence of kanamycin allows the second recombination event to occur as this excises the vector backbone, including the Km^R and *sacB* genes, from the genome. This event was selected for by further plating cells onto M22 (see Appendix) 10% sucrose plates. Since the second recombination event can result in the excision of either the parental gene or the desire construct, PCR was used for screening.

2.3 Microscopy and Image Analysis

Preparation of cells for microscopy

Cells were grown as described above and immobilized on agarose pads. Agarose pad slides were made by adding a thin layer of 0.8% agarose in succinate medium to a slide and then applying 3 μl of cells to the agarose pad before adding a cover slip. For long-term or multi-sample time-lapse imaging, cells were added to each well of a 4-well Lab-Tek-chambered coverglass (Thermo Fisher Scientific), then an agarose pad was placed on the top of each sample. For inducing filamentation, cells were (1) treated with 2.5 μg ml^{-1} cephalexin for 3.5 h or (2) induced with 250 μM IPTG for overnight for FtsZ–YFP overexpression before imaging.

Image acquisition

Cells were mostly imaged at 25°C using a DeltaVision platform (Applied Precision) with an Olympus IX70 wide-field microscope equipped with a 100 × 1.4 NA Plan-Apochromat objective and a Coolsnap HQ camera. The UltimateFocus™ function was used to continually monitor the position of the stage to eliminate z-drift during time-lapse imaging. The live-cell filter set was used: CFP (Ex: 436/10; Em: 465/30), GFP (Ex: 470/40; Em: 525/50), mCherry (Ex: 580/20; Em: 630/60), and YFP (Ex: 492/18; Em: 535/30). Imaging settings were carefully selected to avoid saturation of the camera, and were kept constant for similar samples. To optimize the accuracy of protein colocalisation, each z-stack was acquired with one channel immediately followed by another. Cells were optically sectioned into multiple slices spacing 80–120 nm.

Two other systems were also used: (1) Nikon Eclipse Ti confocal microscope (Nikon). The microscope was controlled using NIS Elements software (Nikon). The Perfect Focus System (PFS) was used in time-lapse imaging to maintain focus. Images were captured using a photon multiplier tube. (2) Nikon Eclipse TE200 epifluorescence microscope. Samples were illuminated with a mercury lamp with the appropriate excitation and emission filters (Chroma) for fluorescence imaging, or a halogen lamp for brightfield imaging. Images were captured using a Hamamatsu ORCA-ER CCD camera. The microscope was controlled using the Simple PCI 6 software package.

Image processing and analysis

Fluorescence images are, unless specified, maximal projections of z-stacks deconvolved using the DeltaVision softWoRx 4.0.0 restoration system (Applied Precision). However, for quantification of intensity, sum projections were used. Background intensity was determined by imaging wild-type WS8N cells and was subtracted. Quantification and analysis were performed in ImageJ (http://rsbweb.nih.gov/ij) or DeltaVision softWoRx 4.0.0. Brightness and contrast adjustment, when performed, was applied uniformly to whole images. For single-particle tracking, distance measurement and colocalisation categorizing, the centroid (for spherical chemosensory clusters), centre of mass (for irregular-shaped chemosensory clusters) and edges (for FtsZ assemblies) were used. For quantifying colocalisaion, JACoP (Bolte and Cordelieres, 2006) was used as a plug-in for ImageJ. The Cell Counter plug-in for ImageJ

(http://rsbweb.nih.gov/ij/plugins/cell-counter.html) was used to count and categorize assemblies and cells.

Fluorescence recovery after photobleaching (FRAP)

FRAP was performed on a Nikon Eclipse Ti confocal microscope (Nikon) using a 100 × objective with the pinhole open. Cells were excited (514.5 nm for YFP) using a 40-m Wargon laser and imaged prebleach every 250 ms for 10 s. A small region of the cell was then bleached for 100–300 ms and then observed every 750 ms to 2 s for 2–30 min depending on the protein of interest. To determine FRAP times, circular regions of interest of equal size were defined around bleached and unbleached areas using the NIS elements software (Nikon). The effect of photobleaching caused by image acquisition was corrected for by measuring the percentage loss of total cell fluorescence at each time point in unbleached cells. The time taken for the fluorescence intensity in the bleached region to reach half the plateau level was calculated by using the easyFRAP software package (Rapsomaniki et al., 2012).

2.4 Sphaeroplasting

A sphaeroplasting protocol that preserves inner and outer membrane integrity (Ranjit and Young, 2013) was adapted. *R. sphaeroides* cultures were grown to an OD_{700} of 0.2 and 1 ml was centrifuged. Cells were then washed with phosphate-buffered saline (PBS; 137 mM NaCl, 2.7 mM KCl, 10 mM Na_2HPO_4, 2 mM KH_2PO_4, pH 8.0) for once and resuspended in 1 ml PBS, and 5 μl was transferred into 500 μl of PBS containing 0.5 M sucrose and lysozyme (20 μg/ml) and incubated at 25 °C for 20 min. Then, 500 μl of PBS containing lysozyme (20 μg/ml) was added to this suspension, which was incubated at 25 °C for an additional 20 min. Sphaeroplasts were then harvested by centrifugation at 500 × *g* for 15 min and washed with 1 ml of sucrose recovery medium (succinate medium containing 0.25 M sucrose), and the resulting pellet was gently resuspended in 10 μl of sucrose recovery medium. Sphaeroplasts were placed onto a sucrose recovery soft agarose pad (sucrose recovery medium plus 0.7% agarose) for imaging.

Chapter 3. Spatiotemporal Dynamics of FtsZ during the Cell Cycle of *R. sphaeroides*

One ring to rule them all, one ring to find them,

One ring to bring them all and in the darkness bind them.

— *The Lord of the Rings*, John R. R. Tolkien

3.1 Aims

The spatiotemporal dynamics of FtsZ in *R. sphaeroides* have not been previously reported. I therefore characterised localisation patterns of FtsZ through the *R. sphaeroides* cell cycle before examining its roles in the positioning of chemosensory clusters.

3.2 Cell Cycle Stage-Specific Localisation of FtsZ

Since fluorescent protein fusions of FtsZ homologues are not fully functional in any bacterial species studied so far (Erickson et al., 2010), FtsZ was examined in a derivative of wild-type strain containing a low-copy inducible plasmid expressing *ftsZ–yfp* (yellow fluorescent protein). Leaky expression or induction with IPTG (isopropyl-β-d-thiogalactopyranoside) up to 10 μM did not affect cell growth and morphology. Nevertheless, I sought to estimate the ratios between native FtsZ and FtsZ–YFP. We do not have an antibody for *R. sphaeroides* FtsZ. An antibody recognized *E. coli* FtsZ has been tested but failed to detect *R. sphaeroides* FtsZ. However, quantitative microscopy suggests that when induced with 5 μM IPTG, there are ~2,500 FtsZ–YFP molecules per cell. The reported native expression levels of FtsZ in different bacteria are 4,000–30,000 per cell (Erickson et al., 2010). *C. crescentus*, the closest relative of *R. sphaeroides* among these bacteria, has 9,500 FtsZ molecules per cell. Therefore, FtsZ–YFP will probably account for ~20% of total cellular FtsZ in *R. sphaeroides*. Previous studies have

shown that the amount of FtsZ–fluorescent protein fusions can up to 50% of the total cellular FtsZ without any detectable defects (Fu et al., 2010). Hence, unless specified, cells were treated with 5 μM IPTG for the results mentioned in this chapter.

The typical ring-like structures (Erickson et al., 2010) (Fig. 3.1) were seen in ~36% of cells in snapshots (Table 3.1). The observed patterns suggest a cell cycle-specific localisation of FtsZ–YFP: a faint band (a ring in 3D) appeared at midcell first (Fig. 3.1, cell 1), which constricted into a brighter band with smaller radius (Fig. 3.1, cell 2). Further invagination produced a pair of daughter cells sharing an FtsZ spot (Fig. 3.1, cell 3). The completion of septation splits the shared spot into two independent spots localised at the new poles of the two sibling cells (Fig. 3.1, cell 4). This model was confirmed by time-lapse imaging (Fig. 3.2). The midcell Z-ring constricted and further invagination produced a pair of daughter cells sharing an FtsZ assembly. The completion of septation split the shared assembly into two independent spots localised at the new poles of the two cells (Fig. 3.2, 30′ to 90′), similar to the cell cycle-specific pattern seen in the model α-proteobacterium *C. crescentus* (Aaron et al., 2007; Thanbichler and Shapiro, 2006). Recent studies with another α-proteobacterium, *Agrobacterium tumefaciens*, revealed a similar localisation pattern of FtsZ (Brown et al., 2012; Zupan et al., 2013), suggesting that the cell cycle-specific localisation pattern of FtsZ (Fig. 3.1 and 3.2) might be conserved in α-proteobacteria. Nevertheless, FtsZ forms polar spots after cell division in the ε-proteobacterium *H. pylori* (Specht et al., 2013) and the Gram-positive bacterium *Corynebacterium glutamicum* (Ramos et al., 2005). Intriguingly, all these bacteria show certain degrees of asymmetric cell division (Fig. 3.1, cells 1 and 2; Fig. 3.4 A) (Brown et al., 2012; Daniel and Errington, 2003; Hallez et al., 2004; Specht et al., 2013).

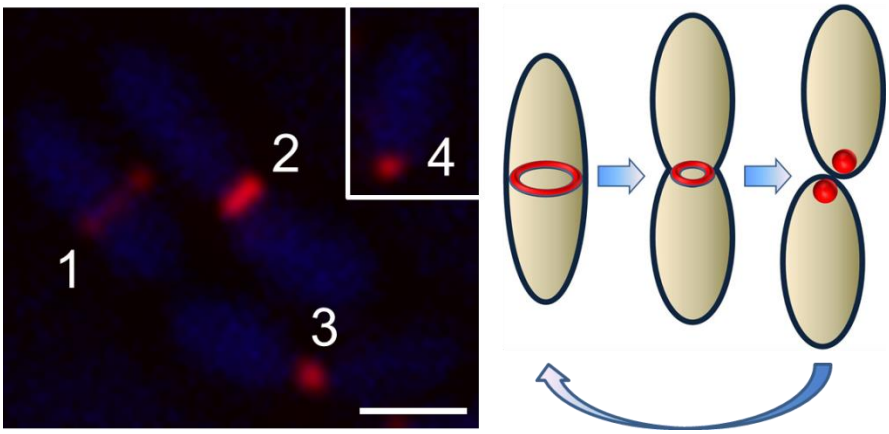

Figure 3.1. Snapshots show different configurations of FtsZ cytoskeletal structures in *R. sphaeroides*. Numbers indicate the possible timing for the

appearance of different configurations during the cell cycle. Initiated at its formation at the midcell (1), the Z-ring constricts into a spot (2 to 3) that is further split by the separation of daughter cells (4). Later, the polar spot of FtsZ reorganizes into a midcell Z-ring and the whole cycle repeats. Cells were treated with 5 μM IPTG. Red: FtsZ–YFP; blue: differential interference contrast (DIC). Scale bar: 1 μm. Right panel: a schematic shows this process.

Table 3.1. The proportion of FtsZ–YFP within different FtsZ assemblies in *R. sphaeroides* cell populations

FtsZ assemblies	% of cells (n=848)	% of FtsZ–YFP molecules present in the assemblies[a]
Polar spot	12.2±5.5 (16.8±1.7)[b]	54.2±13.7 (n=17)
Midcell node/Z-ring precursor	51.6±14.8 (50.9±3.8)[b]	66.0±8.0 (n=47)
Mature Z-ring[c]	36.2±11.6 (32.3±3.2)[b]	66.1±6.9 (n=44)

[a] $\text{Intensity}_{\text{assembly}}/\text{Intensity}_{\text{total cellular}} \times 100\%$.

[b] For cells treated with chloramphenicol.

[c] Including constricting Z-rings.

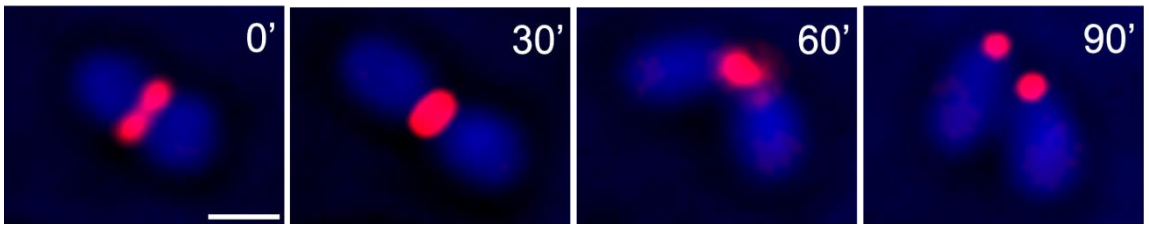

Figure 3.2. Time-lapse images of the cell cycle stage-specific localisation of FtsZ in *R. sphaeroides*. A midcell band (a ring in 3D) constricts into a denser band with smaller radius. The completion of septation results in two FtsZ spots at the new poles. Red: FtsZ–YFP; blue: DIC. Numbers: minutes of observation. Scale bar: 1 μm.

Depending on the cell-cycle stage, the Z-ring was not always a continuous, uniform structure, but frequently showed gaps (Fig. 3.3 A) and heterogeneous

distributions (Fig. 3.3 B), consistent with current super-resolution imaging studies (Buss et al., 2013; Fu et al., 2010; Holden et al., 2014; Strauss et al., 2012). This uneven distribution of FtsZ may reflect the development process of the Z-ring (section 3.3) (Buss et al., 2013) or the constriction of the Z-ring during cytokinesis (Buss et al., 2013; Strauss et al., 2012).

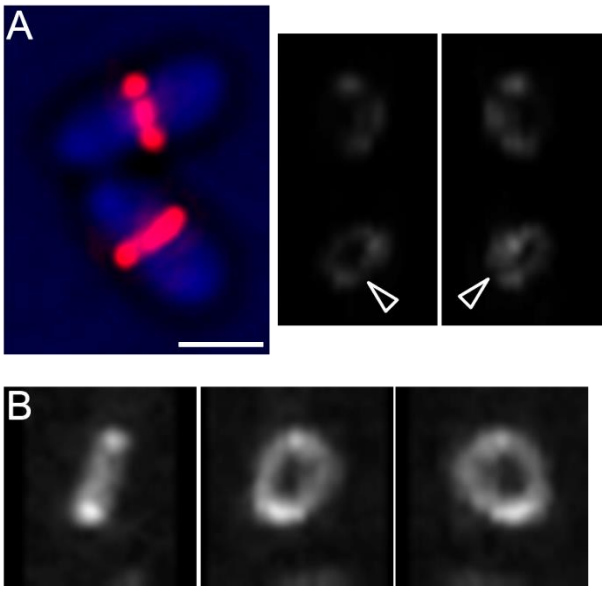

Figure 3.3. Distribution of FtsZ–YFP in the Z-ring. **(A)** Cells containing Z-ring precursors (upper) or a mature Z-ring (lower). The FtsZ structures are viewed from different angles for their 3D reconstructions. Red: FtsZ–YFP; blue: DIC. Arrowheads: gaps in the Z-ring. Scale bar: 1 μm. **(B)** A Z-ring in a cephalexin-treated cell viewed from different angles for its 3D reconstruction.

A controversial aspect of current models of Z-ring constriction is whether or not FtsZ disassembles extensively and delocalises from the Z-ring (Erickson et al., 2010; Lan et al., 2009; Strauss et al., 2012). Quantifying time-lapse images of dividing *R. sphaeroides* cells (n=12) showed constant total intensity (0.98±0.05 fold-change [mean, with standard deviation used throughout this thesis]) of the Z-ring during constriction (from 0 to ~40% decrease in the Z-ring radius), while the Z-ring density increased (12.8±0.8% per 10% decrease in the Z-ring radius), suggesting the protein content remaining constant. The condensation of the Z-ring may provide contractile force for cytokinesis (Lan et al., 2009; Strauss et al., 2012).

I frequently observed noticeable differences in the intensities of FtsZ polar spots in sibling cells (Fig. 3.2, 90′ and 3.7, 30′). The relative intensities of polar chemosensory clusters can be used to distinguish between old and young poles (Ping et al., 2008). I followed the intensities of both FtsZ assemblies and polar chemosensory clusters through cell division (n=20 cell pairs) and found that in 70% (*p*-value=0.0184) the sibling cells with smaller polar chemosensory clusters (i.e. younger poles) received more FtsZ molecules after cytokinesis (1.89±0.56 fold, $p<0.00003$). This result suggests that although FtsZ content does not link to the

"absolute age" of cell poles, FtsZ may have asymmetric inheritance correlated to cellular asymmetry/polarity (Hallez et al., 2004; Kysela et al., 2013; Macara and Mili, 2008).

3.3 The Development of the Z-ring

The appearance of the Z-ring at the midcell initiates the assembly of the divisome, a process that has been extensively studied. However, how the Z-ring forms in the first place is a largely unanswered question (Adams and Errington, 2009; de Boer, 2010; Erickson et al., 2010; Meier and Goley, 2014). The localisation pattern of FtsZ in snapshots of *R. sphaeroides* provides intriguing clues to this puzzle (Fig. 3.4). Cells in the later stages of septation (i.e. a cell-pair with a high degree of invagination and an FtsZ spot between the two daughter-cell compartments; Fig. 3.4, A and C) frequently have faint FtsZ spots and short fragments at the future cytokinetic sites of the daughter cells (white and blue arrowheads, respectively; Fig. 3.4, A and C). A transverse gradient of FtsZ extending from a spot was also present in many cells (Fig. 3.4 A, yellow arrowheads). Similar structures also existed in new-born cells (Fig. 3.4 B). These midcell structures can be grouped into three categories according to their 2D-projection images: (1) asymmetric or symmetric distributions of spots/fragments at the midcell periphery (2) peripheral spot/fragment-pairs with other spots/fragments in-between (3) a large spot with a filamentous structure extended from it (Fig. 3.5). The localisation pattern of these midcell FtsZ spots and short fragments in late-septation and new-born cells (Table 3.1) suggests they are Z-ring precursors.

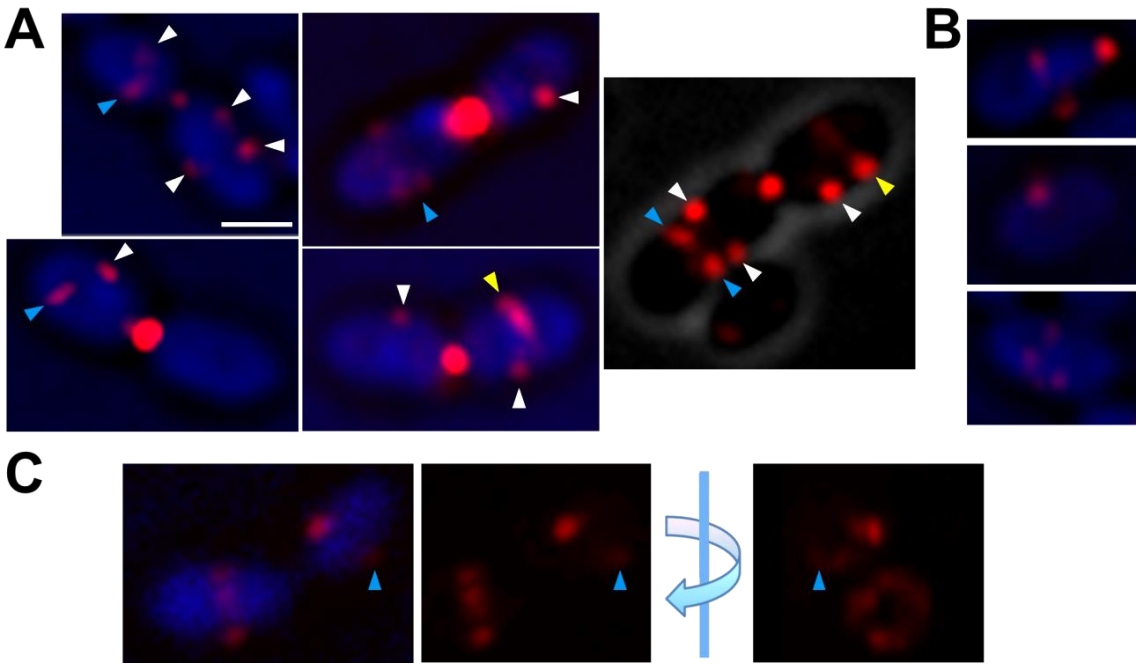

Figure 3.4. Putative Z-ring precursors seen in snapshots. Red: FtsZ–YFP; blue: DIC. Scale bar: 1 μm. **(A)** Cells in late stages of septation. The bright spots between two sibling daughter cell compartments are constricting Z-rings. The DIC image was inverted to provide a better contrast for the right image. Arrowheads: white, spots; blue, short fragments; yellow, spots with extending gradients. **(B)** New-born cells. Upper: a cell with a polar spot and two midcell patches. Middle: a cell with a midcell spot. Bottom: a cell with midcell patches. **(C)** A pair of sibling cells. The left cell had a midcell Z-ring precursor and the right cell had a midcell spot and a faint filament (blue arrowheads). The image for YFP channel was rotated for a better view of the ring and spot/filament.

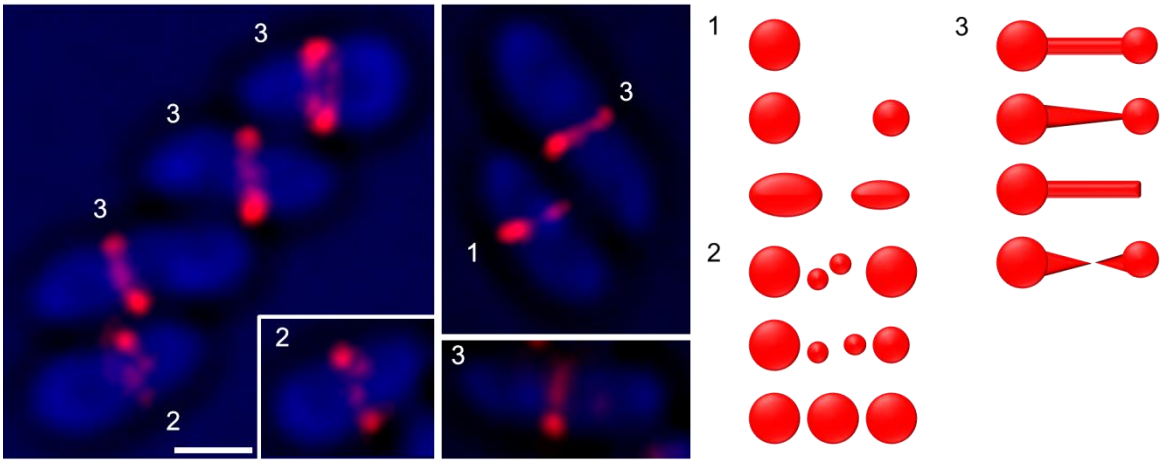

Fig. 3.5. Different patterns of Z-ring precursors. These putative precursor structures can roughly be grouped into three categories according to their 2D-projection images: (1) asymmetric or symmetric distributions of

spots/fragments at the midcell periphery (2) peripheral spot/fragment pairs with other spots/fragments in-between (3) spots with FtsZ spatial gradients extending from them. Left panel: images of typical structures. Right panel: schematics for different patterns as indicated in the actual images. Red: FtsZ–YFP; blue: DIC. Scale bar: 1 μm.

A model is proposed to explain the relationship between these structures and their implications in the development of Z-ring (Fig. 3.6). In this model, the Z-ring initiates as a midcell precursor "node". Cells normally have one dominant node at cell periphery, and a minor node might also present at an approximately opposite position. Later, an FtsZ gradient emanates from the node (presumably the major node) and extends circumferentially. Initially, an asymmetric distribution of FtsZ exists in the precursor structure. The gradient eventually encircles the midcell-plane and a more uniform distribution of FtsZ is reached.

Time-lapse imaging provides direct evidence that the Z-ring developed from the node precursors (Fig. 3.7). After cytokinesis, the polar FtsZ spots redistributed to the midcell and transverse FtsZ spatial gradients extended from the midcell nodes (Fig. 3.7, 60′ to 90′ and 3.8). The transverse FtsZ spatial gradients gradually encircled the midcell plane (Fig. 3.8). The contact/attachment of the growing end to another node (or another side of the original node), or the connection of two nodes, may trigger a reorganisation of FtsZ distribution.

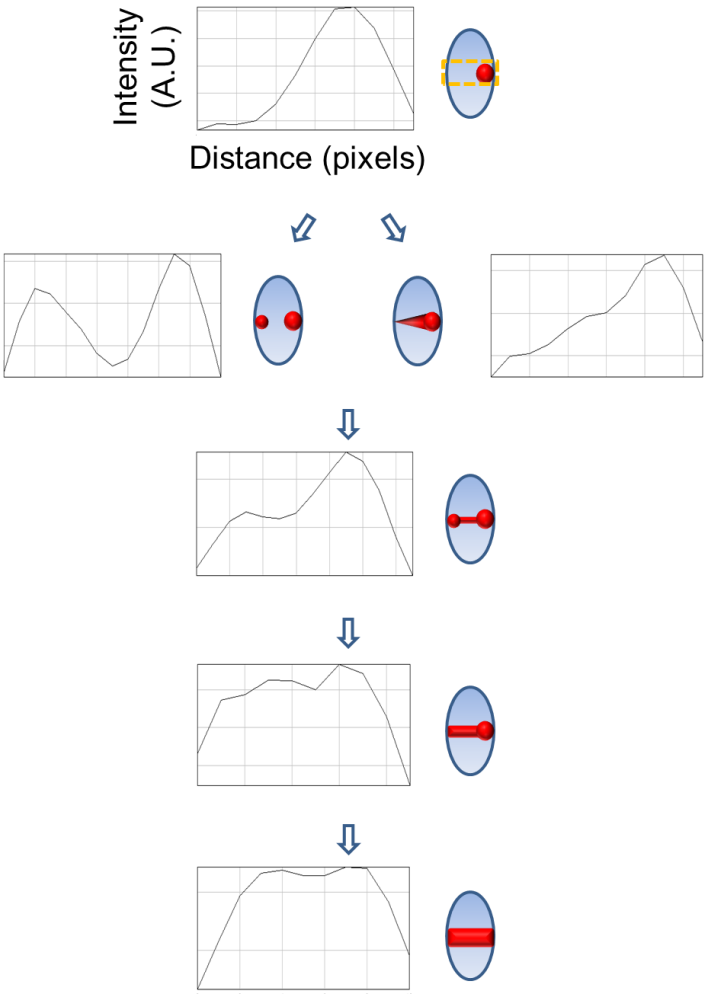

Fig. 3.6. A pathway for Z-ring formation. Schematics depict the typical patterns in this pathway. The fluorescence intensity profiles across the midcell sections (yellow dashed box) for actual fluorescence images with the corresponding patterns are shown. After moving from the new poles, the midcell nodes reorganize and FtsZ spatial gradients extend and encircle the midcell plane. A cell could have more than one midcell node. A.U.: arbitrary units.

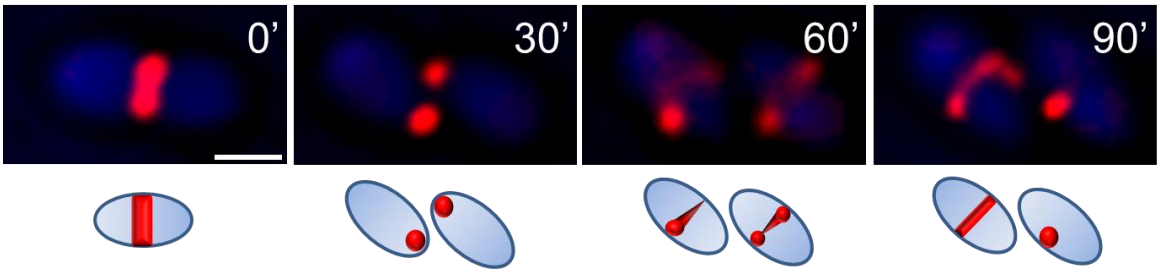

Fig. 3.7. The Z-ring is developed from precursor nodes. Polar FtsZ–YFP spots move to the future cytokinetic sites and fluorescence signals extend from the midcell nodes. Schematics are shown for each image frame. Red: FtsZ–YFP; blue: DIC. Numbers: minutes of observation. Scale bar: 1 μm.

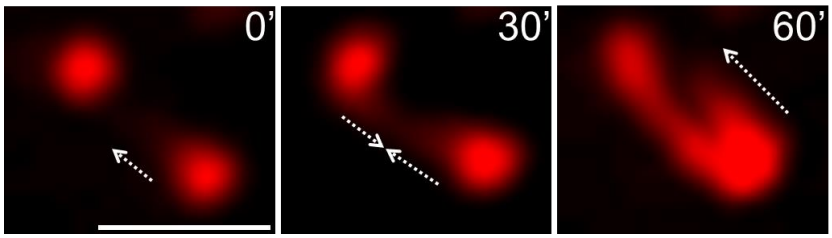

Fig. 3.8. Time-lapse images of the midcell showing the FtsZ spatial gradients (dashed arrows) extend from one midcell node toward the other. The longitudinal axis of the cell is perpendicular to the dashed arrows. Red: FtsZ–YFP. Numbers: minutes of observation. Scale bar: 1 μm.

The distribution of FtsZ along the precursor fluctuated before reaching a more symmetric arrangement (Fig. 3.9 and 3.10). Newly formed Z-rings had uneven FtsZ distributions, which were uniformized before constriction (Fig. 3.10), suggesting either this symmetric distribution is a prerequisite for Z-ring constriction, or the fluctuation of FtsZ is difficult to be resolved since constricting Z-rings have smaller radii.

Intriguingly, the development process reversed in 15.85% cells (Fig. 3.7, 60'–90', right cell; 3.11; 3.13 C). This reverse was not seen for extensively constricted Z-rings, suggesting the development process cannot reverse once the Z-ring matures or constriction has started. The translation inhibitor chloramphenicol has no apparent effect on Z-ring development (Table 3.1), suggests the redistribution of FtsZ molecules between the precursor nodes is sufficient for Z-ring formation.

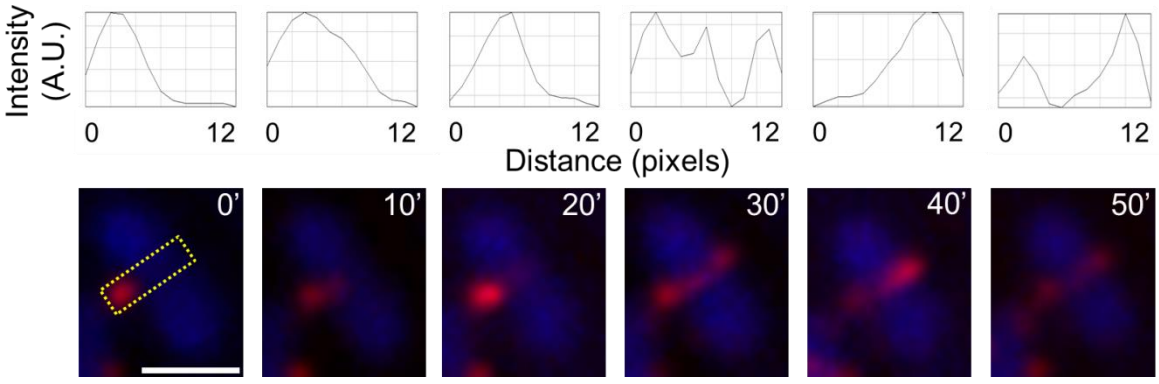

Fig. 3.9. Fluctuations of FtsZ–YFP distribution along the precursor and early Z-ring. The fluorescence intensity profiles (upper panel) across the Z-ring precursors (yellow dashed box) are shown along with their corresponding time-lapse frames. Scale bar: 1 μm.

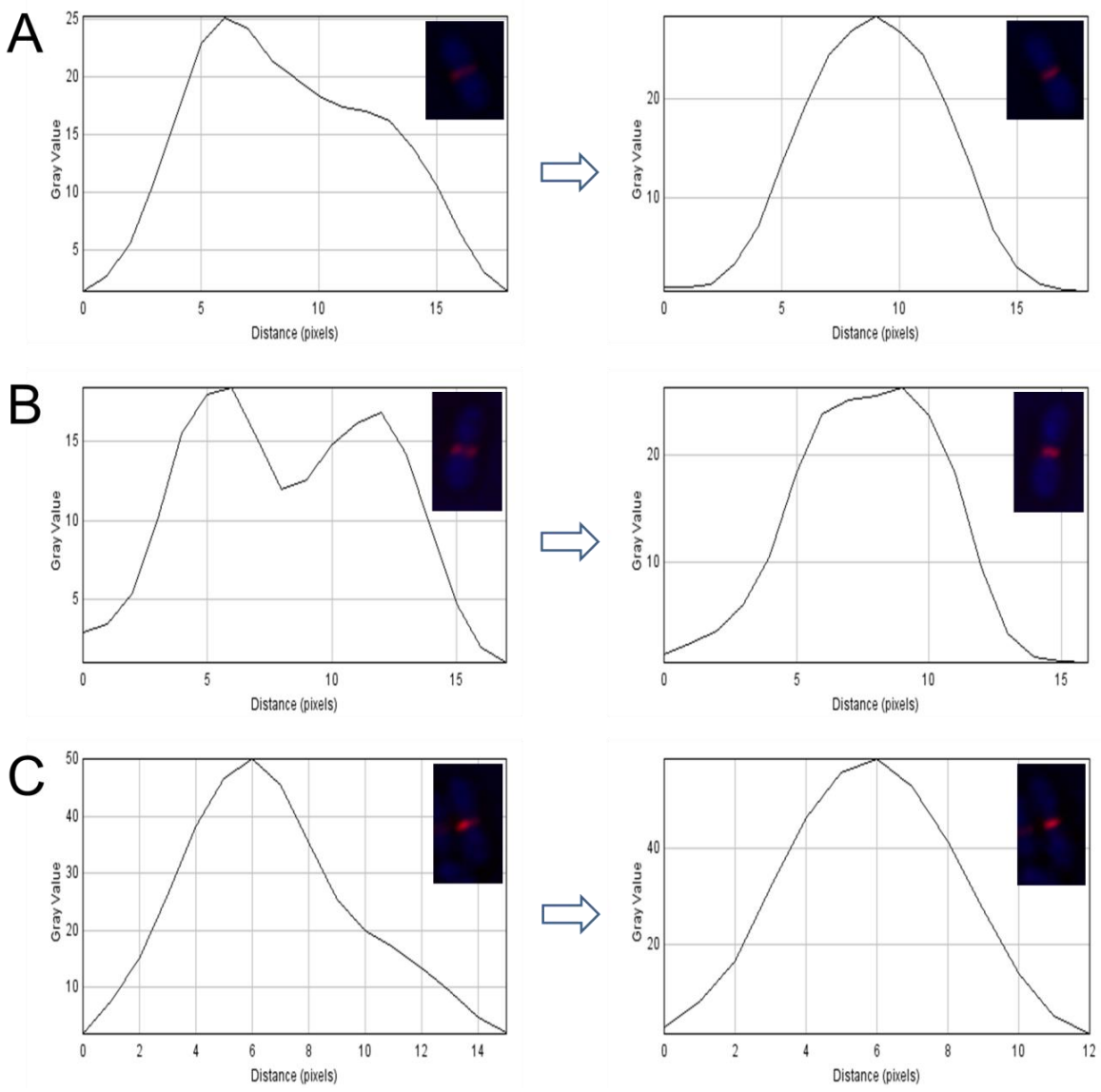

Fig. 3.10. The distribution of FtsZ along the Z-ring become more even/symmetric in later septation stages. The fluorescence profiles across the midcell sections containing FtsZ structures are shown. Inserts: the corresponding successive frames in the time-lapse series. A, B, and C show the results from three different dividing cells which all show constrictions at the second time frames.

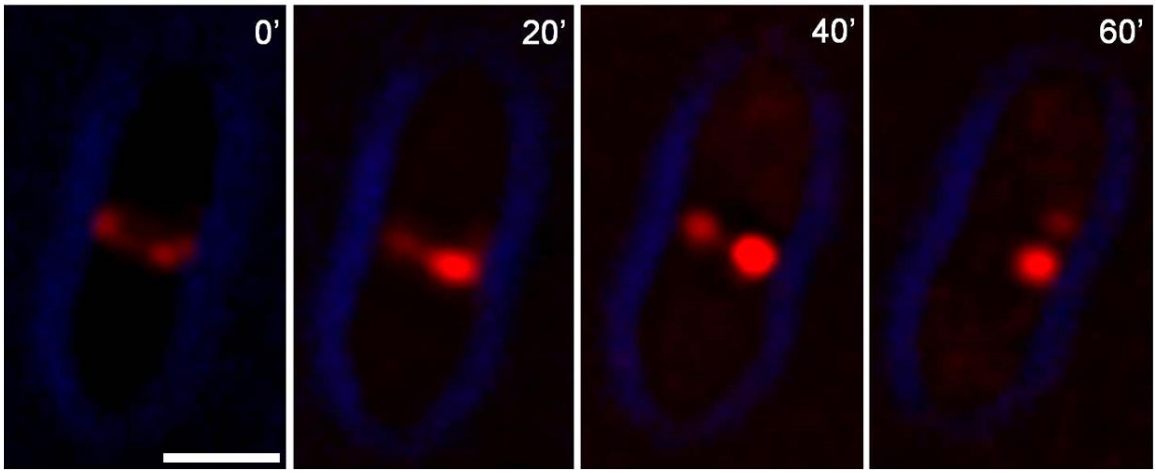

Fig. 3.11. Reversion of Z-ring development. Numbers: minutes of observation. Scale bar: 1 μm.

3.4 FtsZ Forms Different Macromolecular Assemblies

FtsZ forms at least two kinds of subcellular structures through the *R. sphaeroides* cell cycle: spots and ring-like assemblies. Right after cytokinesis, FtsZ assembles into polar spots which then gradually redistribute to the midcell and may have dynamic localisation before Z-ring formation. The Z-ring appears to initiate at midcell precursor nodes, from which an FtsZ spatial gradient extends circumferentially. Initially, an asymmetric distribution of FtsZ exists but it eventually encircles the midcell plane with a more symmetric distribution.

Does FtsZ form similar structures in different assemblies (polar spot and midcell Z-ring)? A correlation was found between the density of Z-ring/ring-precursors and total cellular intensity, but not for polar spots (Fig. 3.12). These results suggest that the Z-ring becomes more dense with increasing FtsZ content, in agreement with a loose bundle model (Fu et al., 2010; Piro et al., 2013), while the polar spot has a more constant packing density. Hence, polar spots and Z-ring/ring-precursors may have different molecular architectures.

By quantifying YFP intensity, I also found that midcell nodes/Z-ring precursors and mature Z-rings contained a larger percentage of the total FtsZ–YFP molecules than polar spots (Table 1). However, there is a significant pool of FtsZ–YFP molecules that are not localised to visible assemblies at any given time in the cell.

Taken together, these results suggest that the Z-ring is a loose structure that can accommodate a wide range of FtsZ subunits to perform mechanical functions

(Fu et al., 2010; Lan et al., 2009; Strauss et al., 2012). On the other hand, the polar FtsZ spots are passive structures for depositing FtsZ, spatially constrained by negative regulators like MipZ. Besides, the presence of different Z-ring precursor structures suggests that reorganizations of the ultrastructure of FtsZ cytoskeleton might also occur during the formation of Z-rings.

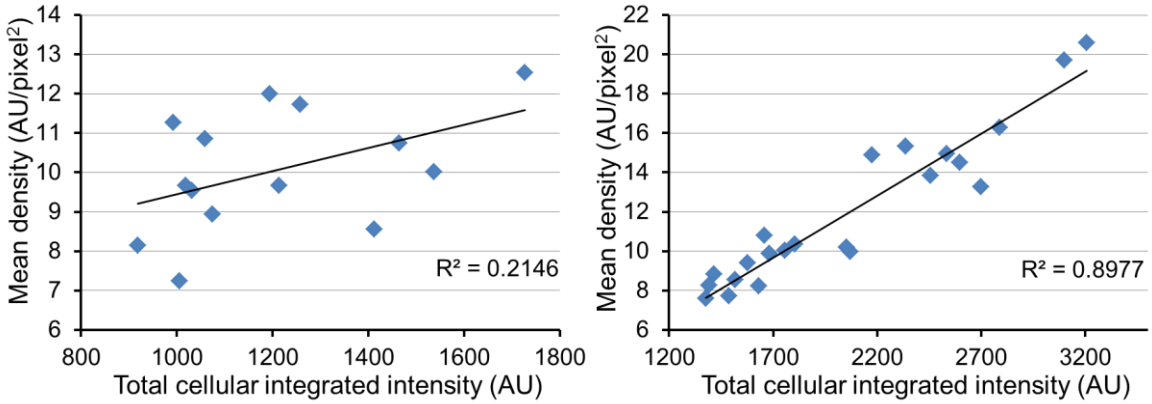

Figure 3.12. Correlation plots show the relationships between FtsZ–YFP densities in different assemblies and total cellular FtsZ–YFP intensity. Left: polar FtsZ spots (n=14); right: Z-rings or precursors (n=23).

Prior to the formation of mature Z-rings, FtsZ spots are mobile and dynamic over our observation time scale of tens of minutes (Fig. 3.13). FtsZ spots were able to localise at both cell poles in the same cell (Fig. 3.13 A, yellow arrowheads), raising the question of how FtsZ is positioned in *R. sphaeroides*. FtsZ spots appeared to integrate/separate and adjust positions (Fig. 3.13 B), resulting in changes in spot intensity (Fig. 3.13). Due to the resolution limit we could not exclude the possibility that two spots came too close to be distinguished (Fig. 3.13 B, 20'). However, the change in relative intensity (Fig. 3.13 B, 10' to 30') suggests they integrated and reformed. This observation indicates that in *R. sphaeroides* FtsZ is repositioned to future cytokinetic sites via dynamic clusters rather than spiral structures proposed for other bacteria (Ben-Yehuda and Losick, 2002; Peters et al., 2007; Specht et al., 2013; Thanbichler and Shapiro, 2006; Thanedar and Margolin, 2004). The proposed helix-like intermediate of FtsZ might merely be a reflection of the oscillatory behaviour of FtsZ assemblies (Bisicchia et al., 2013). However, we cannot exclude the possibility that other configurations of FtsZ assemblies may contribute to Z-ring formation in *R. sphaeroides*.

Before the formation of a proto-Z-ring, the reorganisation of midcell nodes (i.e. extension of FtsZ gradients that eventually encircle the midcell plane) could

occur more than once (Fig. 3.13 C). In the example given in Fig. 3.13 C, the FtsZ gradient was wrongly extended in the direction of the longitudinal axis (white arrowhead in Fig. 3.13 C, 0′). Then a new midcell node formed (Fig. 3.13 C, 10′) and an FtsZ gradient extended later (white arrowhead in Fig. 3.13 C, 20′). The proto-ring only formed after the third round of reorganization. It is also possible that reversion of Z-ring development occurred in this cell. These results clearly showed that Z-ring precursors are very dynamic structures.

Strikingly, FtsZ has similar behaviours in photoheterotrophic cells (Fig. 3.14), suggesting that the dramatic rearrangement of the cytoplasmic membrane and the change in cell shape which occur during photoheterotrophic growth have no effect on the positioning of FtsZ and the cell division machinery.

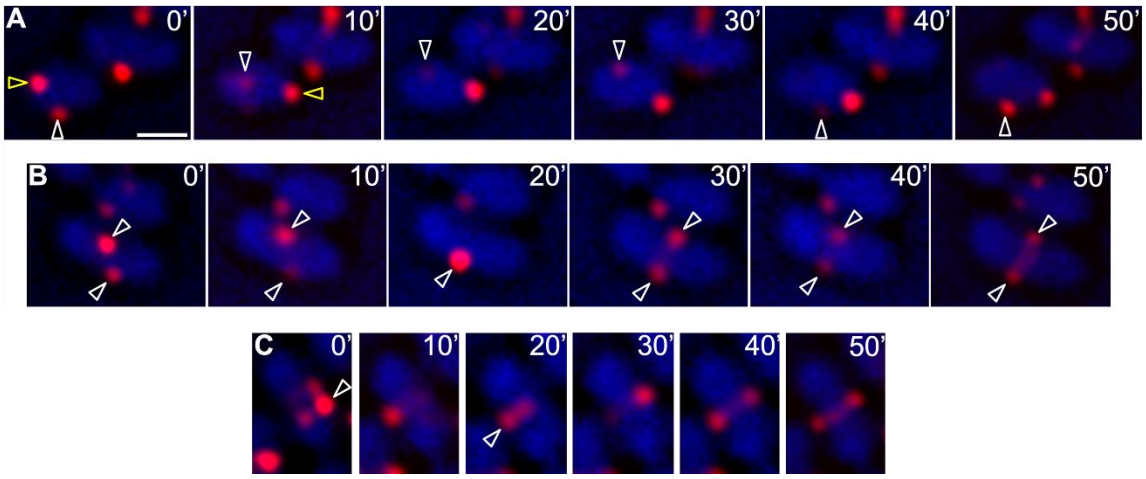

Figure 3.13. Time-lapse images showing the spatiotemporal dynamics of FtsZ spots and Z-ring precursors. Red: FtsZ–YFP; blue: DIC. Numbers: minutes. Scale bars: 1 μm. **(A)** FtsZ spots change positions. Yellow arrowheads: polar spots. White arrowheads: midcell spots. **(B)** FtsZ spots are gradually positioned at the midcell. Two spots integrate into a single midcell node (10′ to 20′) which then separate into two nodes (30′). These two nodes are properly positioned at a plane perpendicular to the longitudinal axis of the cell, results in a perpendicular Z-ring (50′). **(C)** A cell with two rounds of unsuccessful FtsZ-gradient extension (white arrowheads) before the development of a proto-ring. Numbers: minutes.

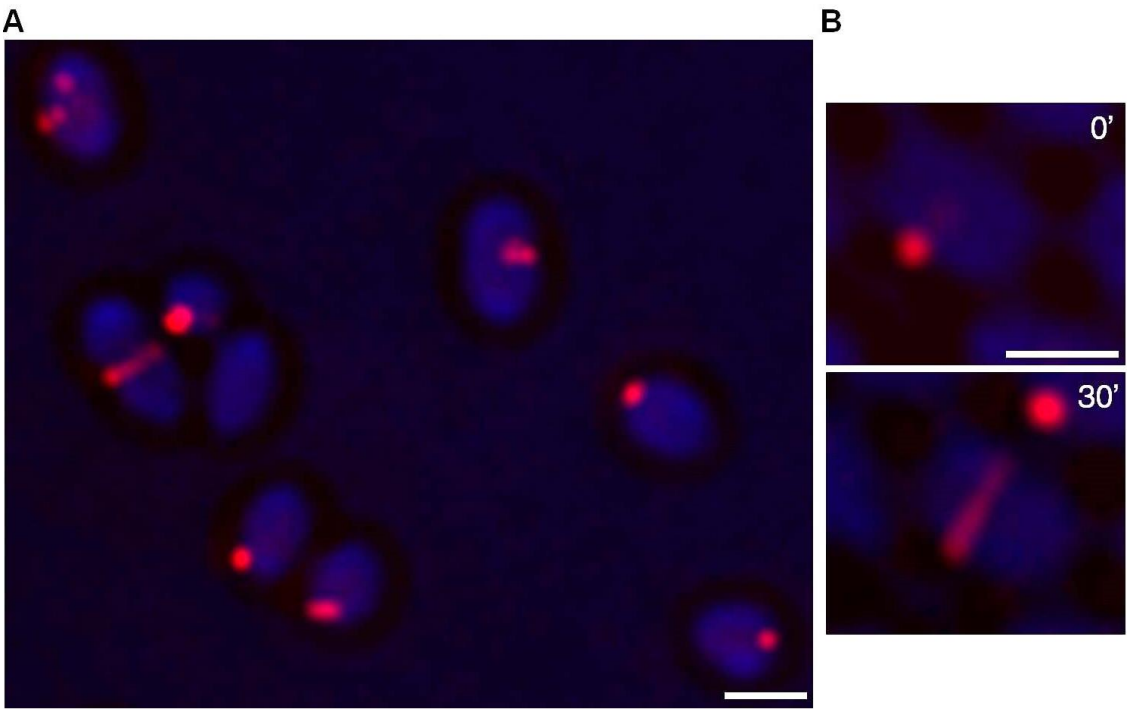

Figure 3.14. Spatiotemporal dynamics of FtsZ in photoheterotrophic *R. sphaeroides* cells. Red: FtsZ–YFP; blue: DIC. Scale bars: 1 μm. **(A)** An image shows the typical polar spots, Z-ring precursors and a Z-ring. **(B)** Time-lapse images show Z-ring development. Numbers: minutes of observation. These results are similar to aerobic cells.

Mild overexpression (20 μM IPTG) of FtsZ–YFP in *R. sphaeroides* resulted in multiple Z-rings/ring-precursors (Fig. 3.15, A and B). Some cells became filamentous (Fig. 3.15 B). Higher overexpression (50 μM IPTG) led to multiple FtsZ spots and short filaments and severe cell filamentation (Fig. 3.15 C). Strong overexpression of FtsZ–YFP resulted in two distinct FtsZ assemblies: randomly distributed spots and long filamentous structures (Fig. 3.16). In this scenario, most cells had only one type of FtsZ assembly, but in ~5% of cells FtsZ spots and curved filaments could co-exist, albeit each structure occupied distinct cellular compartments (Fig. 3.17). Intriguingly, "hybrid" structures (i.e. filaments with nodes) could be seen at the interfaces of the two compartments (Fig. 3.17, inset). The patterns of FtsZ assemblies in FtsZ–YFP-overexpressing cells (Figs 3.15 C and 3.17) suggest that the FtsZ spots might form first, and then reorganize into long filaments, presumably by the protrusion of FtsZ gradients from the spots (Fig. 3.18, yellow arrowheads). Multiple spots could be linked in this manner and resulted in long filaments with several nodes (Fig. 3.18, white arrowheads).

Overexpression has been used to dissect the biochemical and structural properties of FtsZ assemblies (Li et al., 2007; Specht et al., 2013; Srinivasan et al.,

2008). The morphological similarity of the FtsZ assemblies in overexpressing cells and the Z-ring precursors in normal cells prompted me to further explore the formation of these structures. Time-lapse imaging clearly showed that filamentous structures extended from FtsZ precursor nodes and eventually formed long filaments (Fig. 3.19, upper panel). Filamentous structures also extended from (constricting) Z-rings to form long filaments that encircled the periphery of the cell (Fig. 3.19, middle and bottom panels). Since the Z-ring is more likely to be an arc rather than a closed ring (Fu et al., 2010), it is possible that excess FtsZ molecules were added at the ends of the arc, and the growing filaments no longer constrained by the normal spatial regulation and extended in the direction that is more parallel to the longitudinal axis. Intriguingly, FtsZ fluctuated along the filamentous structures (Fig. 3.19), resulted in growth/shrinkage of filaments, as well as large scale movements of FtsZ assemblies around the cell periphery (Fig. 3.19, middle panel). This fluctuation may be similar to that occurs in normal Z-rings/ring precursors, albeit in a different geometric scenario.

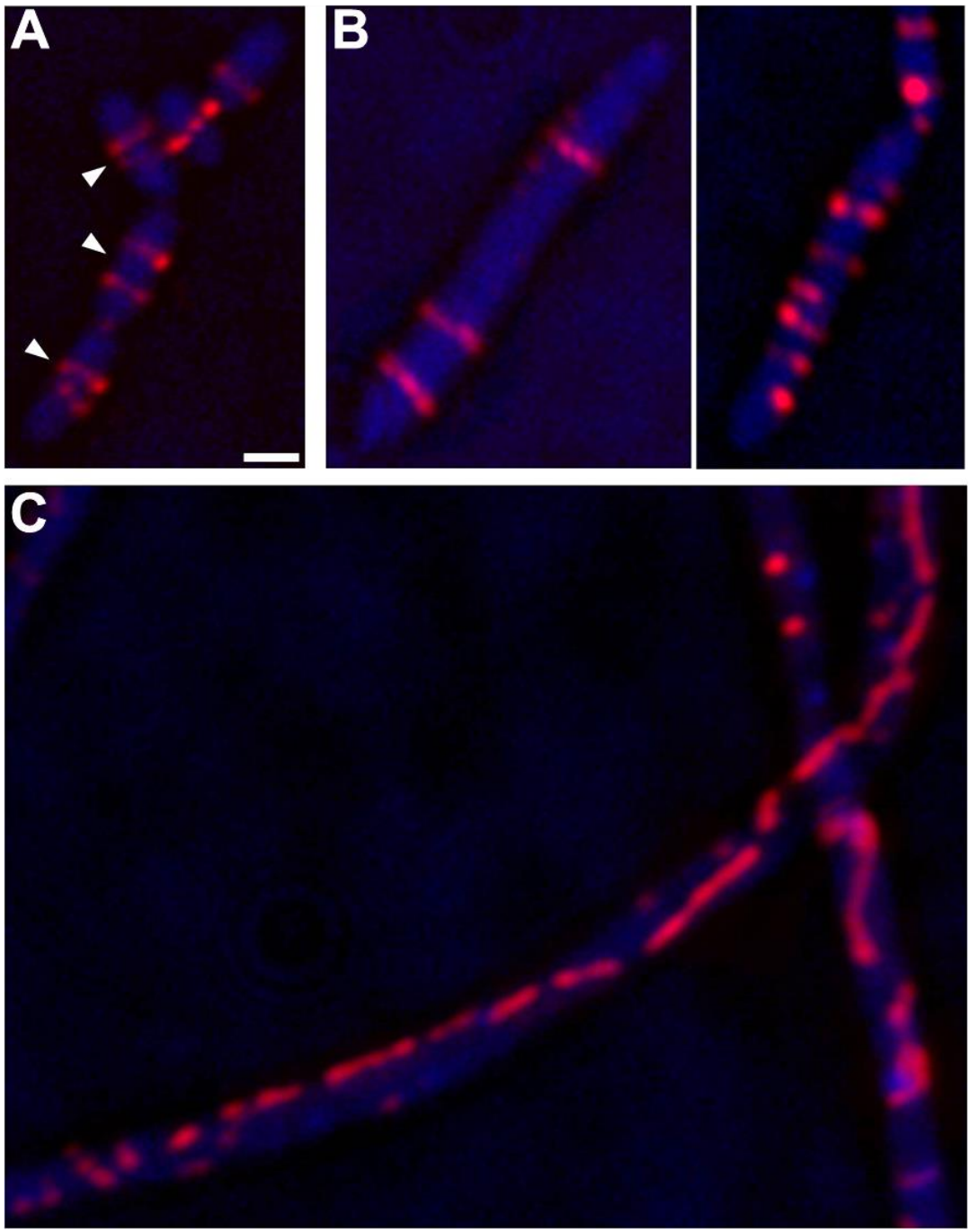

Figure 3.15. *R. sphaeroides* cells mildly overexpressing FtsZ–YFP. Cells were treated with 20 (A and B) or 50 μM IPTG (C) for 18 h. **(A)** Normal-length cells with multiple Z-rings/ring-precursors (arrowheads). **(B)** Filamentous cells with multiple Z-rings/ring-precursors. **(C)** Filamentous cells with FtsZ spots and short filaments. Red: FtsZ–YFP; blue: DIC. Scale bar: 1 μm.

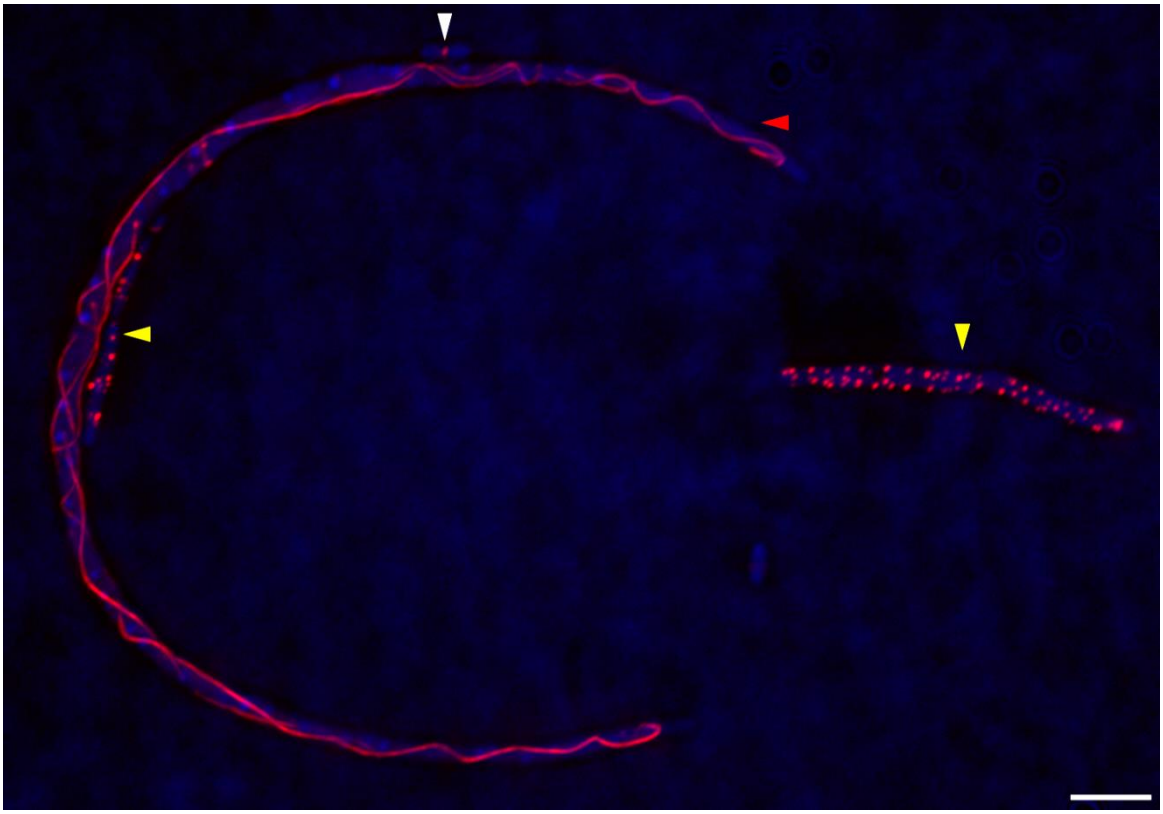

Figure 3.16. *R. sphaeroides* cells overexpressing FtsZ–YFP (treated with 100 μM IPTG for 18 h). Red: FtsZ–YFP; blue: DIC. Arrowheads: white, a normal-length cell with a constricting Z-ring; yellow, cells with FtsZ spots; red, a cell with long FtsZ filaments. Scale bar: 5 μm.

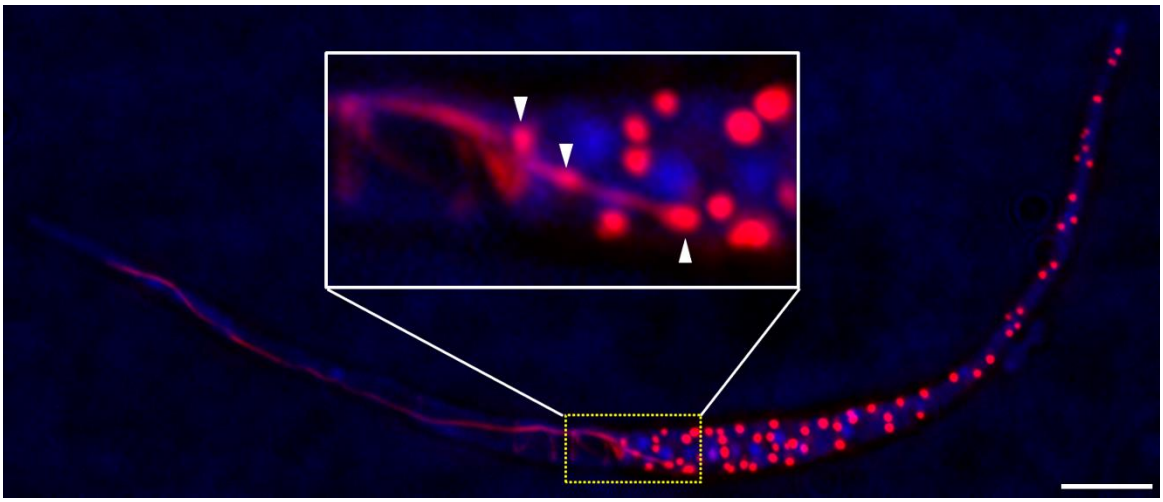

Figure 3.17. *R. sphaeroides* cells overexpressing FtsZ–YFP (treated with 100 μM IPTG for 18 h). Red: FtsZ–YFP; blue: DIC. Arrowheads: nodes with connecting FtsZ filaments. Scale bar: 5 μm.

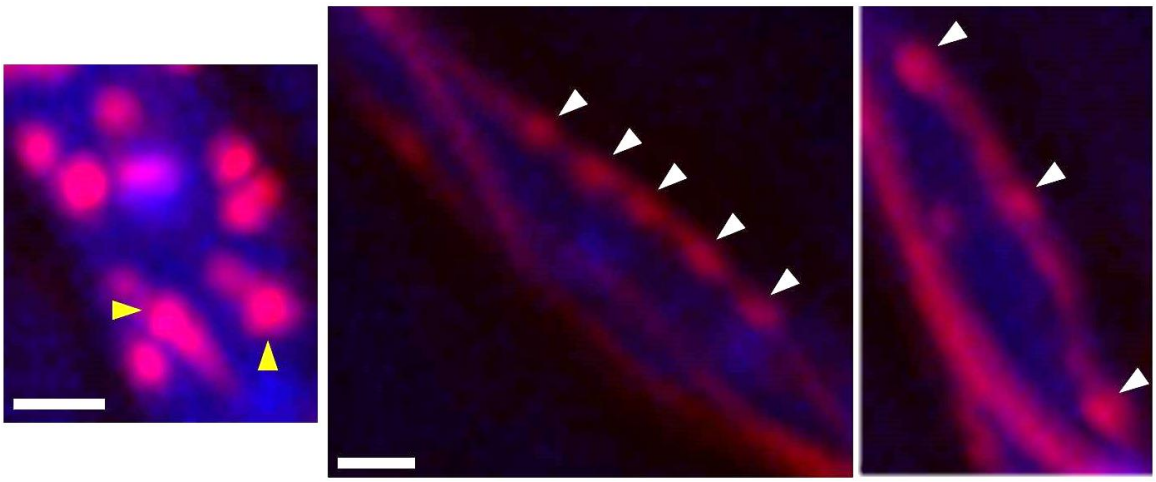

Figure 3.18. *R. sphaeroides* cells overexpressing FtsZ–YFP (treated with 100 μM IPTG for 18 h). Red: FtsZ–YFP; blue: DIC. Arrowheads: white, long FtsZ filaments with nodes; yellow, FtsZ spots with protruding gradients. Scale bars: 1 μm.

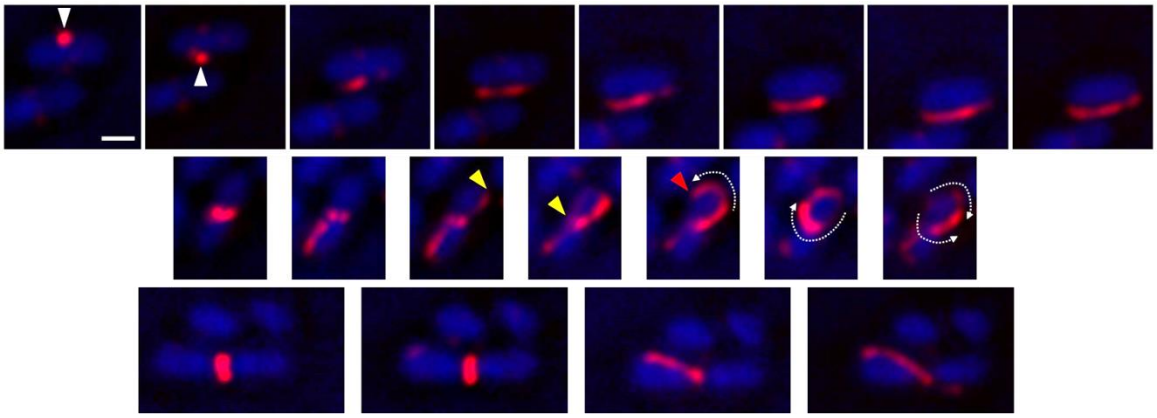

Figure 3.19. Time-lapse images showing the reorganisation of FtsZ assemblies during FtsZ–YFP overexpression. Cells were incubated with 50 μM IPTG. Red: FtsZ–YFP; blue: DIC. Arrowheads: white, FtsZ precursor nodes; yellow, growth of FtsZ filaments; red, shrinkage of FtsZ filaments. Dashed arrows: putative directions of FtsZ redistributions. Scale bar: 1 μm.

I performed fluorescence recovery after photobleaching (FRAP) (Lippincott-Schwartz et al., 2003) on different FtsZ assemblies to investigate their dynamics. FRAP uses a focused laser beam to photobleach a portion of a fluorescent structure and measures the recovery of fluorescent signal in the photobleached area caused by exchange of subunits between the photobleached and surrounding areas (Lippincott-Schwartz et al., 2003). Fig. 3.20 shows a typical

FRAP curve for the Z-ring in normal cells (induced with 5 μM IPTG). In agreement with previous studies, I found that the Z-ring is highly dynamic (Fig. 3.20 and Table 3.2), with a half time of recovery comparable to those in *B. subtilis* (Adams et al., 2011; Anderson et al., 2004), *E. coli* (Anderson et al., 2004; Charbon et al., 2011; Geissler et al., 2007), *H. pylori* (Specht et al., 2013), and *Streptomyces coelicolor* (Willemse et al., 2011). Intriguingly, Z-ring precursors were slightly less dynamic than the Z-ring (Table 3.2). The spatial resolution of the confocal microscopy used to perform the FRAP experiments is not sufficient to clearly distinguish between midcell nodes with/without extended FtsZ gradients. Further experiments with better resolution will be required to explore whether FtsZ nodes undergoing/not undergoing reorganisation may have different dynamics. It is also desirable to compare the dynamics of the node part to the gradient part of a developing Z-ring precursor. The polar FtsZ spot was also very dynamic, albeit less than the Z-ring/ring-precursor (Table 3.2). Because of the small size of these FtsZ assemblies and the difficulty in precisely control the dimension of the photobleaching area, a significant portion of the FtsZ–YFP is bleached in many cells. Thus, I could not obtain conclusive results for the mobile vs. immobile fractions. The average mobile fraction for all FtsZ assemblies is 52.2 ± 24.5%.

The striking behaviours of FtsZ assemblies in overexpressing cells (Figs 3.18 and 3.19) prompted me to further study their dynamics by FRAP. Remarkably, FtsZ spots and filaments resulted from FtsZ–YFP overexpression were almost as dynamic as normal FtsZ assemblies (Table 3.2). This result showed that the FtsZ spots and filaments in overexpressing cells were not merely inactive aggregates. Interestingly, the Z-rings in mild-overexpression cells (induced with 50 μM IPTG) were last dynamic (Table 3.2). It is unclear whether this minor difference has any correlation with the inability of the Z-ring to constrict under the mild overexpression condition.

To summarise, the above results show that FtsZ forms distinct assemblies during the cell division cycle of aerobic and photoheterotrophic *R. sphaeroides*, as well as under FtsZ–YFP overexpression conditions.

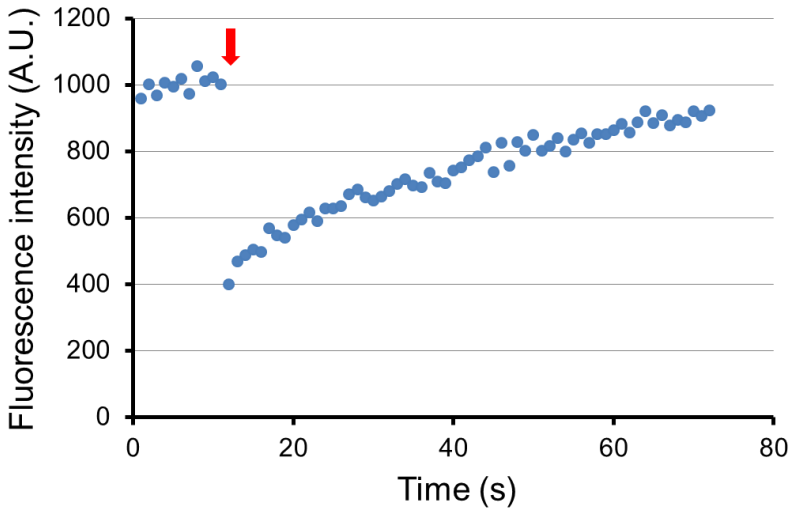

Figure 3.20. A typical FRAP curve of the *R. sphaeroides* Z-ring. The points represent the fluorescence intensity within the photobleached region. The data points have been corrected for background and fluorescence loss during the observation period. Red arrow: the time point of photobleaching.

Table 3.2. Summary of FRAP measurements of different FtsZ assemblies

FtsZ assemblies	Recovery half time±SD (sec)
Normal cells[a]	
Polar spot	7.8±1.6 (n=3)
Midcell node/Z-ring precursor	6.7±2.9 (n=8)
Mature Z-ring	6.1±2.3 (n=13)
Overexpressing cells	
Mature Z-ring[b]	8.7±3.1 (n=20)
Spot[c]	7.7±2.9 (n=21)
Filament[c]	7.5±2.7 (n=6)

[a] Induced with 5 μM IPTG.
[b] Induced with 50 μM IPTG for 4 h.
[c] Induced with 100 μM IPTG for 18 h.

3.5 Different FtsZ Structures in Sphaeroplasts

FtsZ affects bacterial morphogenesis via a spatial regulation of peptidoglycan synthesis (Cava et al., 2013; Margolin, 2009). Does peptidoglycan conversely affect FtsZ? Previous studies showed that FtsZ forms aberrant assemblies in cell-wall synthesis mutants (Addinall and Lutkenhaus, 1996; Bendezú and de Boer, 2008; Corbin et al., 2002; Potluri et al., 2012; Shih et al., 2005). The aberrant assemblies include short and long arcs, rings with branches, slanted rings, spirals, patches, and more-complex patterns like extended structures that failed to span the circumference of the cell but branched or folded back on themselves (Addinall and Lutkenhaus, 1996; Bendezú and de Boer, 2008; Corbin et al., 2002; Potluri et al., 2012; Shih et al., 2005). Since FtsZ arcs have been observed in nonmutant cells acquired abnormal cell shapes as a result of mechanical stress (Männik et al., 2012), it is unclear whether the effects on FtsZ is geometrical or biochemical (Potluri et al., 2012). In an effort to establish sphaeroplasts as useful systems to study FtsZ and chemosensory protein clusters, I found some interesting effects of sphaeroplasting on FtsZ.

After sphaeroplasting, a portion of rod-shaped cells still existed (presumably retaining at least partially intact peptidoglycan sacculi). Normal Z-rings were easily observed in these rod-shaped cells (Fig. 3.21). However, Z-rings were only present in <1% of spherical cells (Fig. 3.21, inset). Spots/fragments (Fig. 3.23 A and B; 73±12% of cells) and arcs (Figs 3.22 and 3.23 C, white arrowheads; 25±9% of cells) were the dominant FtsZ structures in sphaeroplasts (Fig. 3.22), which were morphologically similar to FtsZ polar spots and precursors under diffraction-limited microscopy (Figs 3.4 and 3.7). Structures similar to nodes with extended gradients could be seen in single sphaeroplasts (Fig. 3.23 C, yellow arrowhead) or between two un-separated sphaeroplasts (Fig. 3.23 E). Filament-like structures encircled the full circumference of cognate sphaeroplasts were occasionally observed (Fig. 3.23 D). It is possible that the loss of peptidoglycan disturbs the development of Z-rings or prevents Z-rings from constricting, both may result in the reversion of Z-rings/ring-precursors into spots (Fig. 3.11). Arcs, on the other hand, could be the residues of Z-rings unable to constrict, or they could be resulted from spots that reentered reorganization.

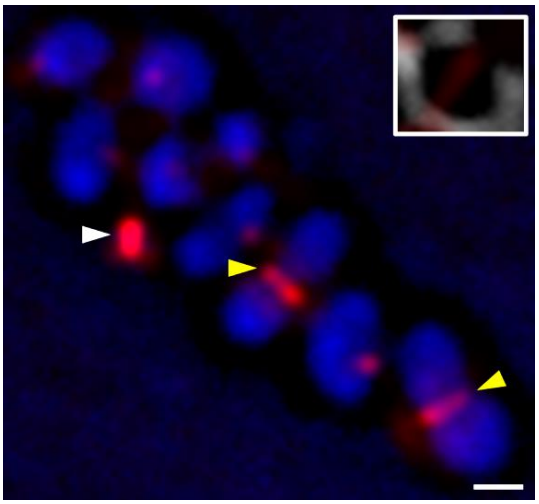

Figure 3.21. Normal Z-rings in rod-shaped cells (yellow arrowheads) and a sphaeroplast (inset). White arrowhead: an FtsZ fragment in the extracellular environment. Scale bar: 1 μm.

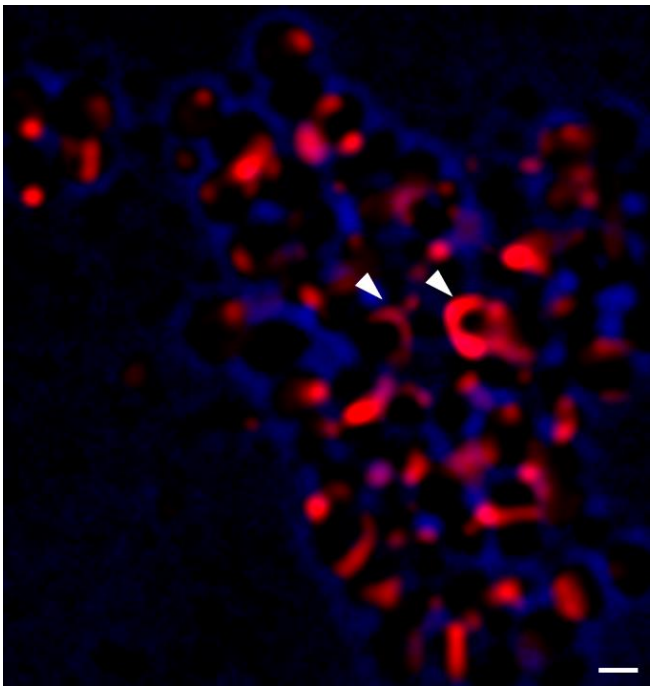

Figure 3.22. A representative image showing the FtsZ structures in *R. sphaeroides* sphaeroplasts. White arrowheads: FtsZ arcs. Red: FtsZ–YFP; blue: inverted DIC. Scale bar: 1 μm.

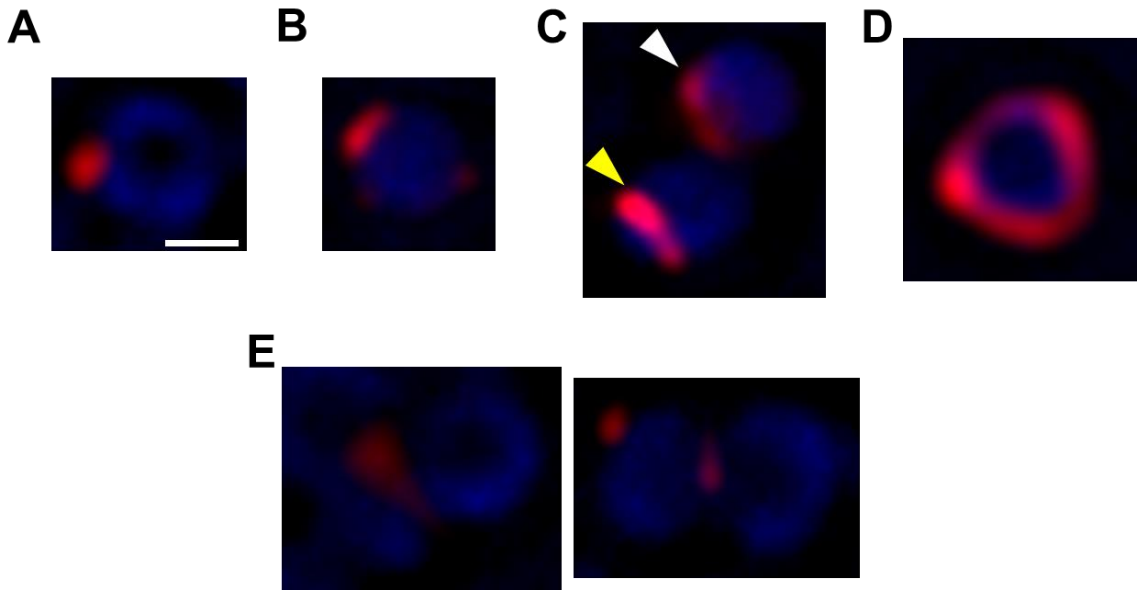

Figure 3.23. Different FtsZ structures in *R. sphaeroides* sphaeroplasts. **(A)** A spot. **(B)** Spots and a short fragment. **(C)** An arc (white arrowhead) and a node with an extended gradient (yellow arrowhead). **(D)** A filament-like structure encircled the cell periphery. **(E)** Two pairs of un-separated sphaeroplasts with arcs in-between. Red: FtsZ–YFP; blue: DIC. Scale bar: 1 μm.

Gentle lysis of sphaeroplasts could be a promising strategy for establishing *in vitro* systems to study native FtsZ structures, including biochemical analysis (Mishra et al., 2013), single-molecule quantification (Jain et al., 2011), and ultrastructure dissection (Brandt et al., 2009). Ghost cells and cell debris containing different FtsZ assemblies could be seen for the sphaeroplasting preparations (Fig. 3.24 A, white arrowhead). Intriguingly, there were some extracellular FtsZ assemblies morphologically similar to *in vivo* FtsZ structures (Fig. 3.24). Further studies will be required to examine how close these extracellular assemblies were to the *in vivo* structures.

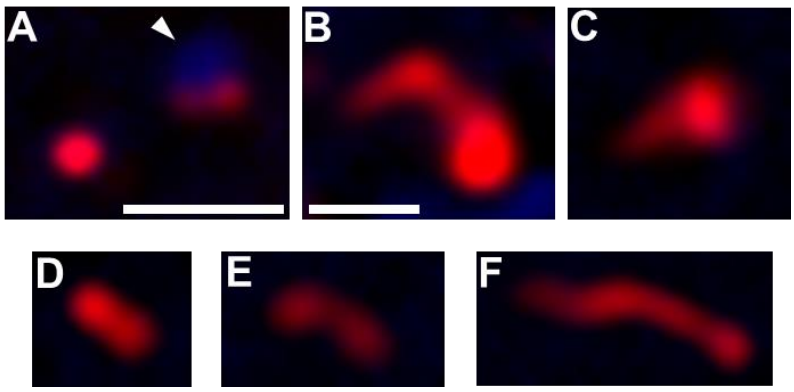

Figure 3.24. Different extracellular FtsZ assemblies in *R. sphaeroides* sphaeroplast preparations. **(A)** A spot and a short fragment within small cell debris (white arrowhead). **(B and C)** Nodes with extended gradients. **(D and E)** Short fragments. **(F)** A long filament. Red: FtsZ–YFP; blue: DIC. Scale bars: 1 μm; A and all other images have the same scale, except B.

3.6 Discussion & Conclusions

The data in this chapter show that FtsZ forms dynamic, cell cycle-dependent assemblies in *R. sphaeroides*, which can exhibit substantial reorganisation during the formation of the Z-ring. The polar spots localised to the new poles immediately after cytokinesis redistribute to the midcell to initiate the formation of the Z-ring (Figs 3.6 and 3.7). These polar spots could move as single or multiple independent entities (Fig. 3.13). FtsZ spots change in their intensities, numbers, and positions (Fig. 3.13). Redistribution of FtsZ spots to the midcell allows the formation of Z-rings. FtsZ spatial gradients stretch out from nodes and eventually encircle the midcell plane (Fig. 3.8), undergoing rearrangements and a more symmetric allocation is reached (Figs 3.9 and 3.10).

Z-ring formation

Structures similar to FtsZ nodes have been seen for FtsZ homologues in *A. tumefaciens* (Zupan et al., 2013), *B. subtilis* (Gregory et al., 2008; Jensen et al., 2005), *C. crescentus* (Quardokus et al., 2001), *E. coli* (Buss et al., 2013; Sun and Margolin, 1998), *Magnetospirillum gryphiswaldense* (Müller et al., 2014), sporulating *S. coelicolor* (Willemse et al., 2011), an ectosymbiotic γ-proteobacterium divides longitudinally (Leisch et al., 2012) and cyanelles (cyanobacteria-like endosymbionts) (Sato et al., 2009), suggesting a common mechanism for the formation of Z-rings.

Fission yeast *S. pombe*, an important eukaryotic model organism that possesses septation-type cytokinesis similar to rod-shaped bacteria, uses an analogous node/aster mechanism to form the contractile ring (Roberts-Galbraith and Gould, 2008; Yonetani et al., 2008). Thus, the node-precursor mechanism may have certain advantages for establishing a midcell contractile ring for septation. By comparing the similarity and difference between the prokaryotic and eukaryotic apparatuses, we may be able to discover the design principles for the formation of cytokinetic rings.

One current model for Z-ring formation suggests that the Z-ring forms by the collapse of a helical structure (Ben-Yehuda and Losick, 2002; Gregory et al., 2008; Peters et al., 2007; Thanbichler and Shapiro, 2006; Thanedar and Margolin, 2004). However, less than 1% of *R. sphaeroides* cells showed the extended spiral-like structures under medium induction (up to 7.5 μM IPTG). Instead, more than 50% of *R. sphaeroides* cells had clear Z-ring precursors (Table 3.1). One possibility is that similar Z-ring precursors are only transiently present in other bacteria, and the helical structures may represent a relaxed Z-ring or adjacent structures. The longer cell cycle of *R. sphaeroides* increases the chance of seeing the Z-ring precursors and serves as a good model to study Z-ring development.

Another nucleation site model (Addinall and Lutkenhaus, 1996; Pichoff and Lutkenhaus, 2005) suggests the formation of Z-ring initiates at single (Addinall and Lutkenhaus, 1996) or multiple (Pichoff and Lutkenhaus, 2005) midcell sites. Bidirectional polymerisations emerging from nucleation sites produce long FtsZ polymers that associate laterally to form Z-rings. For the nucleation model to be true, the Z-ring must be composed of a few long protofilaments that grow from the nucleation sites and encircle the midcell plane. However, *in vitro* and *in vivo* data suggest that FtsZ protofilaments from diverse species are only 50–200 nm long (Erickson et al., 2010; Hou et al., 2012; Katzmann et al., 2011; Li et al., 2007), much shorter than the circumference of a typical bacterium. Since the midcell node in *R. sphaeroides* contains the majority of total cellular FtsZ molecules (Table 3.1), further protein synthesis is not required for Z-ring formation (i.e. the relocation of polar spots and the reorganisation of midcell nodes into mature Z-rings), and the Z-ring development process is reversible (Fig. 3.11), I believe that the main function of midcell nodes is probably to allow reorganization/redistribution of FtsZ rather than *de novo* nucleation. Nevertheless, it is possible that the reorganization/redistribution of FtsZ may include nucleation–polymerisation processes taking place at the edges of the FtsZ nodes/gradients.

Two current studies proposed other mechanisms which could be jointly

described as "cluster coalescence". Buss et al. (2013) used super-resolution imaging to study the functions of ZapA/B in Z-ring assembly in *E. coli*. They found FtsZ structures similar to the single midcell nodes (Fig. 3.7) and midcell clusters (Figs 3.4 and 3.5) described in this thesis. These "FtsZ clusters" exist in wild-type, *ΔzapA*, and *ΔzapB* cells (Buss et al., 2013), but the clusters are widely dispersed in the absence of ZapA and ZapB. They thus proposed that ZapA/B bring the dynamic FtsZ clusters into close proximity at midcell and corral these clusters to form a larger continuous structure (i.e. the Z-ring). The node model and this cluster corralling model are not mutually exclusive. However, the lack of time-lapse imaging data in their work, as well as the fact that the patterns they observed are more consistent with the node model rather than many FtsZ foci aligned together, suggest that the corralling process might represent a later stage of Z-ring formation (discussed below). Wezel and collogues found that during sporulation of *S. coelicolor*, the divisome component SsgB recruits FtsZ into foci at the pre-cytokinetic sites (Willemse et al., 2011). The foci somehow form Z-rings later. Wezel and collogues suggested that FtsZ foci are sequentially formed at the pre-cytokinetic site, eventually forming the complete Z ring, rather than that the Z-ring is produced from two gradually expanding spots (Willemse and van Wezel, 2009). However, apart from observing that three FtsZ foci can localise at the pre-cytokinetic site together (Willemse and van Wezel, 2009), there is no evidence for step-wise alignment of FtsZ foci into the Z-ring.

Based on the reasons discussed above, I believe the node model could be applicable to Z-ring formation in different bacteria. However, how does the Z-ring develop from the precursor node? In the simplest scenario, the FtsZ node, once positioned at the pre-cytokinetic site, can spontaneously reorganize: FtsZ gradients stretch out from the node and encircle the pre-cytokinetic plane. Intriguingly, an *in vitro* reconstituted system containing FtsZ and FtsA self-organizes into dynamic cytoskeletal patterns like travelling streams and rotating swirls (Loose and Mitchison, 2014). Since FtsA also colocalises with FtsZ in node-like structures (Zupan et al., 2013), it is likely that FtsA can trigger the reorganisation of FtsZ nodes *in vivo*. However, a ring-like FtsZ structure appears at midcell much earlier, before FtsA forms any detectable structures in *C. crescentus* (Goley et al., 2011), suggesting the involvement of other FtsZ-interacting proteins in the reorganisation (if any). For example, FzlA, an early FtsZ-interacting protein that alters FtsZ structures *in vitro* (Goley et al., 2010), may participate in Z-ring formation by triggering structural transitions. Besides, components of the cell-wall synthesis machinery (e.g. MreB) also colocalise with FtsZ ring-like structures early in the *C. crescentus* cell cycle (Goley

et al., 2011) and in *R. sphaeroides* (Chapter 4) (Slovak et al., 2006; Slovak et al., 2005). The circumferential movement of the cell-wall synthesis machinery (Domínguez-Escobar et al., 2011; Garner et al., 2011; van Teeffelen et al., 2011) may assist in reorganizing FtsZ assemblies at the pre-cytokinetic site. However, it is also possible that FtsZ nodes can spontaneously reorganize without an absolute requirement for other FtsZ-interacting proteins, since an FtsZ ring-like structure forms at the midcell earlier than any other known *C. crescentus* FtsZ-interacting proteins (Goley et al., 2011). Besides, FtsZ by itself can form ring-like structures *in vitro* (Osawa et al., 2008). It is also possible that different bacterial species may utilize different mechanisms to reorganize the FtsZ node.

In biology, a sophisticated spatiotemporal regulation can create a "positive" role for a "negative" regulator. In *B. subtilis* high concentrations of MinC are found primarily at the septum as double rings that flank the Z-ring (Eswaramoorthy et al., 2011). MinC shows dynamic circumferential movements within the double rings (Gregory et al., 2008). The double-ring organisation is believed to prevent disruptions of the Z-ring (Eswaramoorthy et al., 2011). However, the close proximity raises the possibility that MinC could interact with the adjacent Z-ring. Since MinC inhibits lateral interactions between FtsZ protofilaments (Dajkovic et al., 2008), the dynamic circumferential movement of MinC is capable of promoting reorganisation of FtsZ assemblies. Similarly, the colocalisation of MipZ spots/arcs with midcell FtsZ assemblies (Nelly Dubarry, unpublished data) provides a putative means to regulate the dynamics of FtsZ assemblies. For example, by promoting the partial disassembly of the FtsZ node, MipZ can trigger the reorganisation of the FtsZ node and the formation of proto-Z-rings.

What happens after a proto-Z-ring has formed by the reorganisation of midcell FtsZ nodes? I found that the distribution of FtsZ subunits along the proto-Z-ring fluctuates before constriction. The fluctuating pattern (Fig. 3.9) is in accord with a shuttling/oscillatory behaviour. The *in vitro* dynamic FtsZ–FtsA cytoskeletal travelling streams and rotating swirls persist for tens of minutes during which their diameter does not change (Loose and Mitchison, 2014). It is plausible to assume that the behaviours of the *in vitro* system reflect certain aspects of the fluctuation of FtsZ described in section 3.3.

Previous studies suggested that a maturation period takes place before the proto-Z-ring becomes a mature Z-ring/divisome (Aarsman et al., 2005; Rico et al., 2010). During maturation, the proto-Z-ring is not stable (Rico et al., 2010), which is consistent with the reversion of proto-Z-rings back to nodes (Fig. 3.11). In *C. crescentus* and *E. coli*, a significant time-delay exists (15–35% of total cell cycle

depending on the growth rate) before the recruitment of the rest of the divisome components to the proto-Z-ring (Aarsman et al., 2005; Goley et al., 2011). This period may be responsible for the relocation of FtsZ along the proto-Z-ring (Fig. 3.9) for a more even distribution. ZapA and ZapB may promote this process by stabilizing/aligning FtsZ assemblies (Fig. 3.5) that appear during this period (Buss et al., 2013). This can explain why Z-ring assembly still occurs in *ΔzapA* or *ΔzapB* cells, albeit that the precursor-like FtsZ clusters have a more dispersed localisation (Buss et al., 2013). Furthermore, *C. crescentus* FtsZ also forms dynamic arc- or spiral-like structures that erratically shuttle around the pre-cytokinetic site, and these structures condense into a stable Z-ring just before indentation of the cell envelope (Thanbichler and Shapiro, 2006).

Distinct FtsZ assemblies

How the cytoskeleton forms different structures to drive diverse cellular processes is a fundamental question in eukaryotic cell biology. With the fast growth of researches in bacterial cytoskeletal systems, we know face this challenge in prokaryotic cell biology. Different *in vivo* configurations of the FtsZ cytoskeleton have been identified before, mainly by genetic approaches (Erickson et al., 2010). Diverse *in vitro* structures of FtsZ assemblies have also been observed under different conditions, including the effects of different FtsZ-interacting proteins (Erickson et al., 2010; Kirkpatrick and Viollier, 2011). However, a clear understanding of the architecture, dynamics, and mechanisms of formation is still lacking for many of these diverse structures, even for the prominent Z-ring (Erickson et al., 2010; Meier and Goley, 2014).

Here I discovered that in a single bacterial species, *R. sphaeroides*, distinct FtsZ structures exist according to the cell-cycle stages. These structures have their specific functions in the cell: the polar FtsZ spot is a reservoir of FtsZ molecules after cell division, and can redistribute FtsZ to the future cytokinetic site; the midcell node is the embryo for Z-ring development, from which different Z-ring precursor structures are generated; and the Z-ring for cytokinesis. In yeast, a single actin isoform (which perform the analogous cytokinetic role as FtsZ) functions in three distinct structures (patches, cables, and rings) that have different architectures (Berepiki et al., 2011; Kovar et al., 2011; Moseley and Goode, 2006). Quantitative image analysis (Fig. 3.12) suggested that the Z-ring/ring-precursors have an architecture that is in consistent with the loose bundle model (Biteen et al., 2012; Fu et al., 2010; Piro et al., 2013; Strauss et al., 2012), while the polar spot might have a more constant packing density. This

difference may reflect the different functions of the two types of assemblies. The loose bundle architecture of the Z-ring can accommodate a wide range of FtsZ subunits to produce mechanical force and a huge amount of divisome proteins to accomplish diverse functions. The polar spot, as a reservoir to redistribute FtsZ molecules, probably not requires such a high flexibility.

Under super-resolution microscopy, the polar FtsZ spot in *C. crescentus* appears as a highly dense spheroid with surrounding heterogeneous clouds (Biteen et al., 2012; Holden et al., 2014). However, the small size (92×72–133 nm) and high density of the polar spot prohibit obtaining ultrastructural details. FRAP experiments showed that FtsZ polar spots in *H. pylori* are two-fold less dynamic than the Z-ring, with a halftime of recovery of ~18 s (Specht et al., 2013). These results are consistent with the idea that FtsZ polar spot and the Z-ring may have distinct molecular organizations. Interestingly, the polar spot in *R. sphaeroides* is also less dynamic than the Z-ring and ring-precursors (Table 3.2). In *S. coelicolor*, SsgB and FtsZ foci (i.e. Z-ring precursors) are both ~8-fold less dynamic than the mature Z-ring as shown by FRAP (Willemse et al., 2011). Since the Z-ring in *S. coelicolor* has a recovery halftime comparable to most bacteria studied, it is likely that the specific SsgB-mediated sequestration of FtsZ contributes to the decreased dynamics of FtsZ in pre-divisional cells (Willemse et al., 2011). It will be interesting to compare the molecular architecture of the FtsZ node in *R. sphaeroides* to that of the FtsZ focus in *S. coelicolor*.

In eukaryotes, a large set of accessory proteins participate in the global regulation of different cytoskeletal structures (Berepiki et al., 2011; Howard and Hyman, 2007; Kovar et al., 2011; Maiato et al., 2004; Moseley and Goode, 2006). Given the expanding network of FtsZ regulators (Kirkpatrick and Viollier, 2011), it is interesting to study how these proteins control the assembly and function of distinct FtsZ structures. Indeed, the observation that different FtsZ-associated proteins colocalise at FtsZ assemblies (Z-ring or polar spot) with distinct spatiotemporal dynamics (Goley et al., 2011) suggests an unexplored network composed of different FtsZ assemblies and their cognate components. To coordinate the proper combination of accessory proteins, different FtsZ assemblies must separate themselves from one another to maintain specificity within a crowded cell.

Dynamic positioning of FtsZ spots

In this subsection, the term "FtsZ spots" will be used for the polar spots and nodes that are not undergoing visible reorganisation (i.e. no extended FtsZ

gradients). Since a verity of regulating mechanisms are used by different bacteria to position FtsZ, here I will only focused on *R. sphaeroides* and the other two α-proteobacteria (*A. tumefaciens* and *C. crescentus*) with similar cell cycle-dependent FtsZ localisation patterns. This and previous studies (Thanbichler and Shapiro, 2006; Zupan et al., 2013) showed an overall pattern as following: FtsZ forms a polar spot at the new pole of each sibling cell after cell division, this polar spot disappears later and a Z-ring forms at the cytokinetic site. However, from the low-resolution images (Costa et al., 2008; Schofield et al., 2010; Thanbichler and Shapiro, 2006; Zupan et al., 2013), it is difficult to tell whether the polar spot dissembles while FtsZ molecules reassemble at the midcell, or the polar spot can actually move to the midcell. Here, I showed that the polar spot can move toward the midcell as a whole entity (see Fig. 6.7) or multiple individual clusters (Fig. 3.13). The spots integrate/separate continuously, and they can shift positions even from one pole to another (Fig. 3.13). Massive disassembly and reassembly may also happen (Fig. 3.13). Besides, small spots/clusters can appear at the future cytokinetic site while the Z-ring or the polar spot is still present (Fig. 3.4). Similarly, patterns like bipolar foci, multiple polar foci, unipolar focus with single midcell focus, and unipolar focus with paired foci at midcell have been observed in *A. tumefaciens* (Zupan et al., 2013) and *C. crescentus* (Costa et al., 2008; Thanbichler and Shapiro, 2006). All these results show that FtsZ spots have complex spatiotemporal dynamics in these three bacteria.

In wild-type *C. crescentus* populations, a small number of cells show deviant chromosome segregation patterns, and concomitant behaviours of FtsZ spots (e.g. shifting positions from one pole to the other) have been seen (Thanbichler and Shapiro, 2006). Since the chromosome segregation-coordinated movement of MipZ clusters is relatively slow (comparing to MinCDE waves) and produces heterogeneous patterns of FtsZ-depolymerising zones (Thanbichler and Shapiro, 2006), the corresponding behaviours of FtsZ spots would be complex. The presence of a second chromosome (Porter et al., 2011b) with a putative MipZ-recruiting ParB homologue may further increase the complexity in *R. sphaeroides*.

In vitro results suggest that MipZ might alter the conformation of FtsZ protofilaments to prevent their assembly into higher-order macromolecular complexes (Thanbichler and Shapiro, 2006). Therefore, a moving MipZ gradient may disassemble the polar spot and biases its reassembly toward the midcell. Imagining if the disassembly/assembly cycle mainly occurs at the surface of the FtsZ spot, a Brownian ratchet-like process could "push/pull" a quasi-stable FtsZ spot toward the midcell. In other words, a pattern of an FtsZ polar spot keeps

moving toward the midcell (Fig. 6.7).

Rise and break: overexpression and sphaeroplasting as experimental systems to study FtsZ

Overexpression has been used to obtain useful insights of FtsZ (Dziadek et al., 2002; Gamba et al., 2009; Latch and Margolin, 1997; Li et al., 2007; Ma et al., 1996; Potluri et al., 2012; Quardokus et al., 2001; Ramos et al., 2005; Specht et al., 2013; Srinivasan et al., 2008; Ward and Lutkenhaus, 1985). In many cases, overexpression of wild-type or fluorescent protein-tagged FtsZs has similar phenotypes, including the configuration changes of FtsZ cytoskeleton. Presumably due to the imbalance between the stoichiometries of FtsZ to other divisome components, overexpression of FtsZ blocks cell division and produces filamentous cells containing multiple FtsZ patches, rings, spirals, or arcs (Li et al., 2007; Ma et al., 1996; Potluri et al., 2012). Mild overexpression (including native up-regulation) normally produces short helical structures or regularly positioned ring-like structures (Fig. 3.15 A and B) (Ben-Yehuda and Losick, 2002; Ma et al., 1996; Potluri et al., 2012). Higher/longer overexpression, however, produces spots or very long filaments (Figs 3.16 and 3.17) (Ma et al., 1996).

The observation that strong overexpression of FtsZ–YFP in *R. sphaeroides* results in two distinct FtsZ assemblies (spots and long filamentous structures) is interesting, because most cells have only one type of these FtsZ assemblies. When they occasionally co-exist, each structure occupies distinct cellular compartments (Fig. 3.17). These patterns suggest there are distinct phases/mechanisms governing their formation (e.g. cell cycle-specific factors). Intriguingly, when *H. pylori* FtsZ is overexpressed in an ectopic eukaryotic host, there are two distinct structures that do not co-exist (Specht et al., 2013). FRAP experiments indicated that these structures are just slightly less dynamic than the native Z-ring (Specht et al., 2013). Table 3.3 also shows that in *R. sphaeroides* the overexpression-induced structures are as dynamic as native FtsZ structures.

Previous studies have shown that spot-like and filamentous structures, as well as filamentous networks interconnecting dots, can be seen when *E. coli* FtsZ is overexpressed in yeast or mammalian cells (Srinivasan et al., 2008; Yu et al., 1999). FRAP experiments revealed that these structures are as dynamic as the native Z-ring (Srinivasan et al., 2008). Since long filaments, spots, and hybrid structures (Fig. 3.17) also exist in FtsZ-overexpressing *E. coli* cells (Ma et al., 1996), they may represent intrinsic properties of FtsZ. Consistently, the two *M.*

gryphiswaldense FtsZ homologues also form spots in their native host or long filaments and spots in *E. coli* when overexpressed (Müller et al., 2014).

Based on the conserved configurations in different host cells, the comparable turnover dynamics, and similar behaviours (e.g. gradient extension from a spot) (Figs 3.18 and 3.19), I suggest FtsZ–YFP overexpression could be a useful system to study the native FtsZ assemblies. For instance, by co-overexpressing other FtsZ regulators or unknown genes with specific localisations (Werner et al., 2009), proteins promote reorganisation of FtsZ nodes could be identified.

The severe loss of Z-rings in sphaeroplasts (Figs 3.22 and 3.23) indicates that either cell morphology or the peptidoglycan (or associated systems) affects the formation/stability of the Z-ring. However, as those cell-wall mutants used in previous studies (Addinall and Lutkenhaus, 1996; Bendezú and de Boer, 2008; Corbin et al., 2002; Potluri et al., 2012; Shih et al., 2005), the sphaeroplast system cannot provide a conclusive answer by itself. Further experiments like combining sphaeroplasts with microchambers to control the cell shape (Renner and Weibel, 2011) are required to clarify the two possibilities. Nevertheless, the presence of structures (both in the sphaeroplasts and the extracellular environment) which are morphologically similar to FtsZ polar spots and precursors makes the sphaeroplast system an attracting attempt toward *in vitro* systems for biochemical studies (Mishra et al., 2013), single-molecule imaging (Jain et al., 2011), and ultrastructure visualization (Brandt et al., 2009) of FtsZ assemblies.

Conclusions

The detailed spatiotemporal dynamics of FtsZ through the *R. sphaeroides* cell cycle was described for the first time in this chapter. FtsZ forms distinct structures in *R. sphaeroides*, with polar spots moving from the new pole to the midcell to produce nodes from which the Z-ring develops. This information provides new perspectives on the complete life cycle of the Z-ring. I also propose a model for Z-ring formation which may be applicable to other FtsZ homologues.

Chapter 4. Spatiotemporal Dynamics of MreB during the Cell Cycle of *R. sphaeroides*

The human mind always makes progress, but it is a progress in spirals.

— Madame de Stael

4.1 Aims

In this chapter I sought to characterise the localisation patterns of MreB through the *R. sphaeroides* cell cycle before examining its role in the positioning of chemosensory clusters. A previous study from our group has shown that MreB localises to the midcell in elongating *R. sphaeroides* cells (Slovak et al., 2005). MreB remains at the midcell as septation begins but relocalises to future cytokinetic sites before the completion of septation (Slovak et al., 2005). However, the work was performed with immunofluorescence microscopy and a non-fully functional *gfp–mreB* (***g***reen ***f***luorescent ***p***rotein) replacement of the native *mreB* gene (Slovak et al., 2005). Here, I used a dual-tagged strain for colocalisation study with FtsZ, as well as a merodiploid *yfp–mreB* strain that shows normal phenotypes, to better reveal the spatiotemporal dynamics of MreB during the cell cycle in living *R. sphaeroides* cells.

4.2 Cell Cycle Stage-specific Localisation of MreB

A *R. sphaeroides* strain with its genomic *mreB* replaced by a *gfp–mreB* fusion was constructed before (Slovak et al., 2005). Slower growth rate and abnormal morphology suggest the *gfp–mreB* gene is only partially functional (Slovak et al., 2005). However, 49% of the cells show normal cell shape and localisation patterns similar to those obtained by immunofluorescence microscopy of native MreB (Slovak et al., 2005). Time-lapse imaging suggested that MreB has dynamic localisation during the *R. sphaeroides* cell cycle: GFP–MreB localises to the cytokinetic site as a ring-like structure during septation, and relocalises to the

midcells of sibling cell compartments before the completion of septation (Slovak et al., 2005). This localisation pattern suggests a role for MreB in *R. sphaeroides* septation. To examine this possibility, I tried to observe the localisation of MreB and FtsZ simultaneously. I constructed a dual-tagged *R. sphaeroides* strain in which the expression of *gfp–mreB* and *ftsZ–rfp* (***r***ed ***f***luorescent ***p***rotein) are under the control of native and *lac* promoters, respectively.

Cells of this dual-tagged strain had similar morphology as that of single-tagged (*gfp–mreB*) strain when induced with low IPTG concentrations (<10 μM) (Fig. 4.1). Initial observations showed that GFP–MreB formed foci or ring-like structures at the midcell, while FtsZ–RFP formed either midcell foci/rings or polar spots (Fig. 4.2). The localisation patterns of GFP–MreB and FtsZ–RFP are consistent with those seen in single-tagged strains (Chapter 3) (Slovak et al., 2005). Thus, MreB and FtsZ might have a cell cycle stage-dependent colocalisation in *R. sphaeroides* (Fig. 4.2).

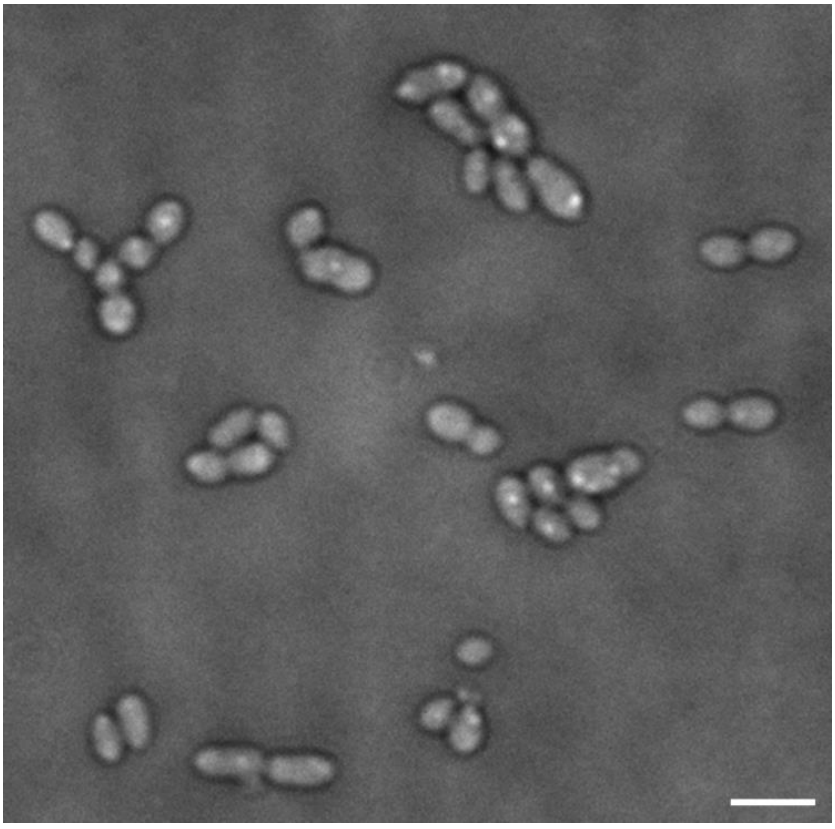

Figure 4.1. Cell morphology of the dual-tagged (*ftsZ–rfp* and *gfp–mreB*) *R. sphaeroides* strain. Shown here is a DIC image of cells treated with 5 μM IPTG. Scale bar: 3 μm.

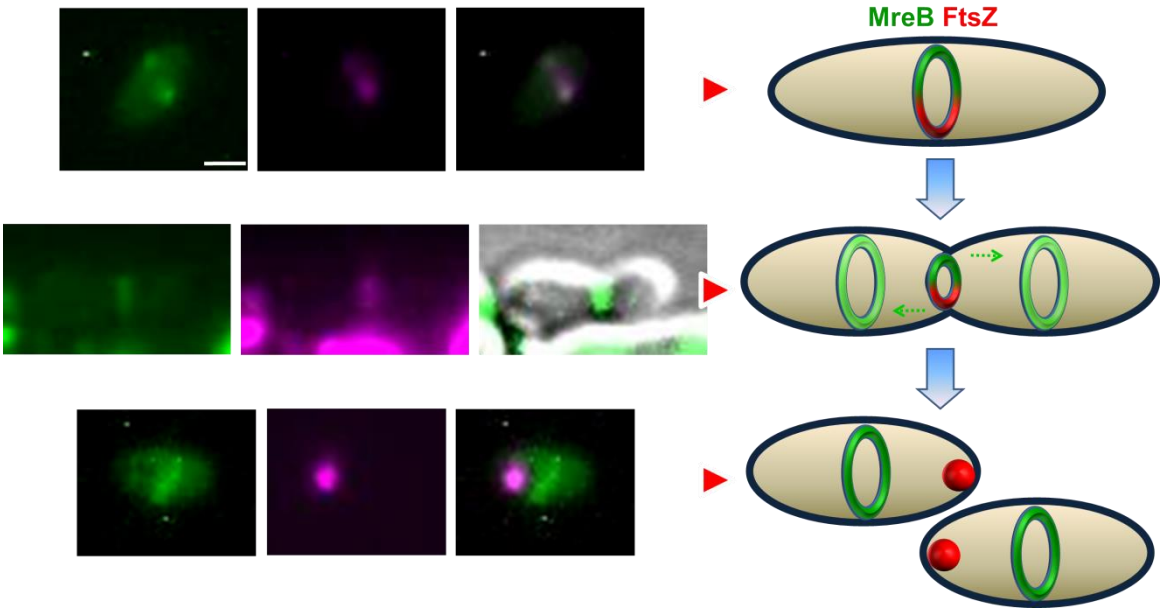

Figure 4.2. Snapshots showing the putative cell cycle stage-specific colocalisation between FtsZ–RFP and GFP–MreB in *R. sphaeroides*. Left: localisation of FtsZ–RFP (purple) and GFP–MreB (green) in cells treated with 5 μM IPTG. Single channels and merged images are shown for early-septation (upper), late-septation (middle), and new-born (bottom) cells. Right: simplified schematics for each cell cycle stage are given. In this model, FtsZ and MreB colocalise at the midcell after the formation of the Z-ring. MreB might form a ring-like structure. FtsZ and MreB could form a single ring or two adjacent rings. After the initiation of constriction, MreB gradually forms two new ring-like structures at the midcells in the two daughter-cell compartments. After septation, FtsZ stays at new poles before the formation of new Z-rings. Scale bar: 1 μm.

To further examine the cell cycle stage-dependent colocalisation of FtsZ and MreB, optical sectioning by deconvolution microscopy was performed. The dominant models for the *in vivo* configurations of MreB cytoskeleton during the past decade are filamentous helices or rings (Shaevitz and Gitai, 2010). However, I observed a patchy pattern for GFP–MreB in most cells (Fig. 4.3). These GFP–MreB spots were circumferentially arranged into a ring-like configuration (Fig. 4.3) (Slovak et al., 2005). This observation is consistent with current super-resolution imaging studies (Domínguez-Escobar et al., 2011; Garner et al., 2011; Swulius and Jensen, 2012; van Teeffelen et al., 2011). In certain cells, GFP–MreB patches might localise in a helical pattern (Fig. 4.4). In addition, GFP–MreB formed filamentous arcs, rings and helices in a small portion of cells (Fig. 4.5). FtsZ–RFP formed either midcell nodes/rings or polar spots (Fig. 4.3 A,

arrowheads). Most of the midcell nodes (71±20%) and Z-rings (87±12%) were at least partially colocalised with MreB (Fig. 4.3 A, blue and red arrowheads). The pattern suggests FtsZ nodes/rings and MreB colocalise at the midcell until constriction, after which MreB relocalises at future midcell before FtsZ (Figs 4.3 A and 4.5 C). These results confirmed that MreB has a cell cycle stage-specific localisation in *R. sphaeroides* (Slovak et al., 2005).

Figure 4.3. (Next page) GFP–MreB forms circumferentially arranged patches in *R. sphaeroides*. **(A)** Merged images for cells treated with 5 μM IPTG. Green: GFP–MreB; red: FtsZ–RFP; blue: DIC. Arrowheads: yellow, polar FtsZ spots; white, FtsZ spots presumably moving towards the midcell; blue, a midcell FtsZ node; red, Z-ring/ring-precursor. **(B)** 3D reconstruction of subcellular localisation of GFP–MreB viewed from different angles for the left image in (A). Scale bar: 1 μm.

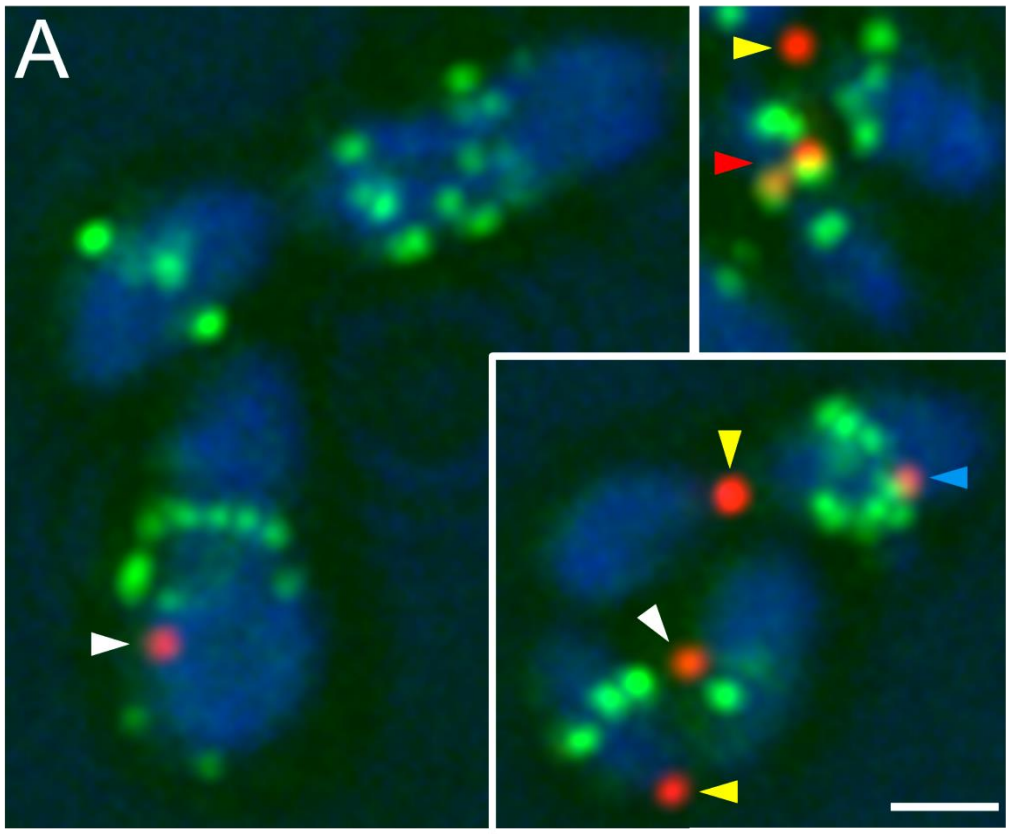
A

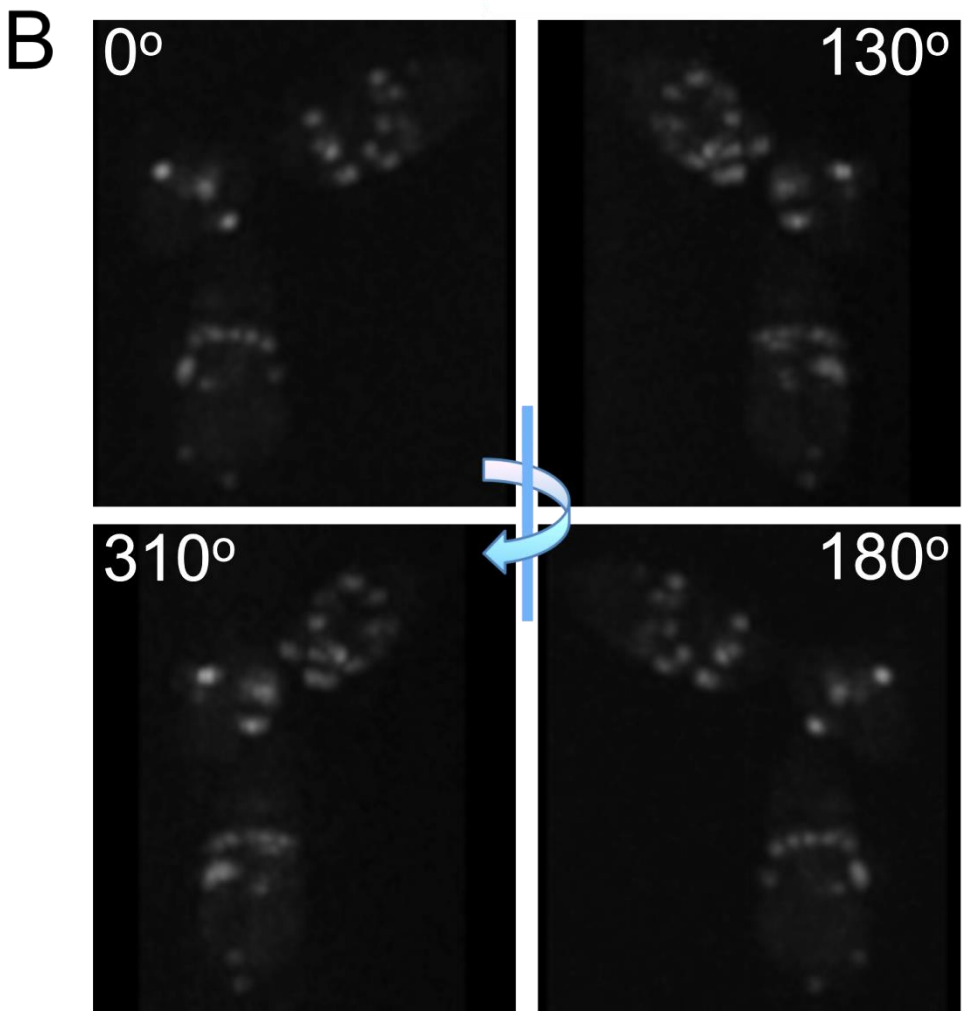
B
0°
130°
310°
180°

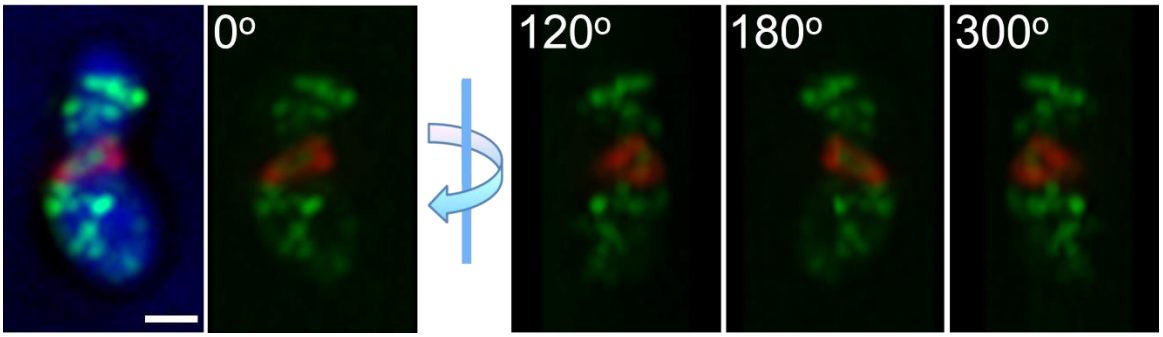

Figure 4.4. GFP–MreB patches could arrange in a helical pattern in *R. sphaeroides* cells. Shown are merged images of projections. Cells were treated with 5 μM IPTG. The right three images were viewed in different angles. Green: GFP–MreB; red: FtsZ–RFP; blue: DIC. Scale bar: 1 μm.

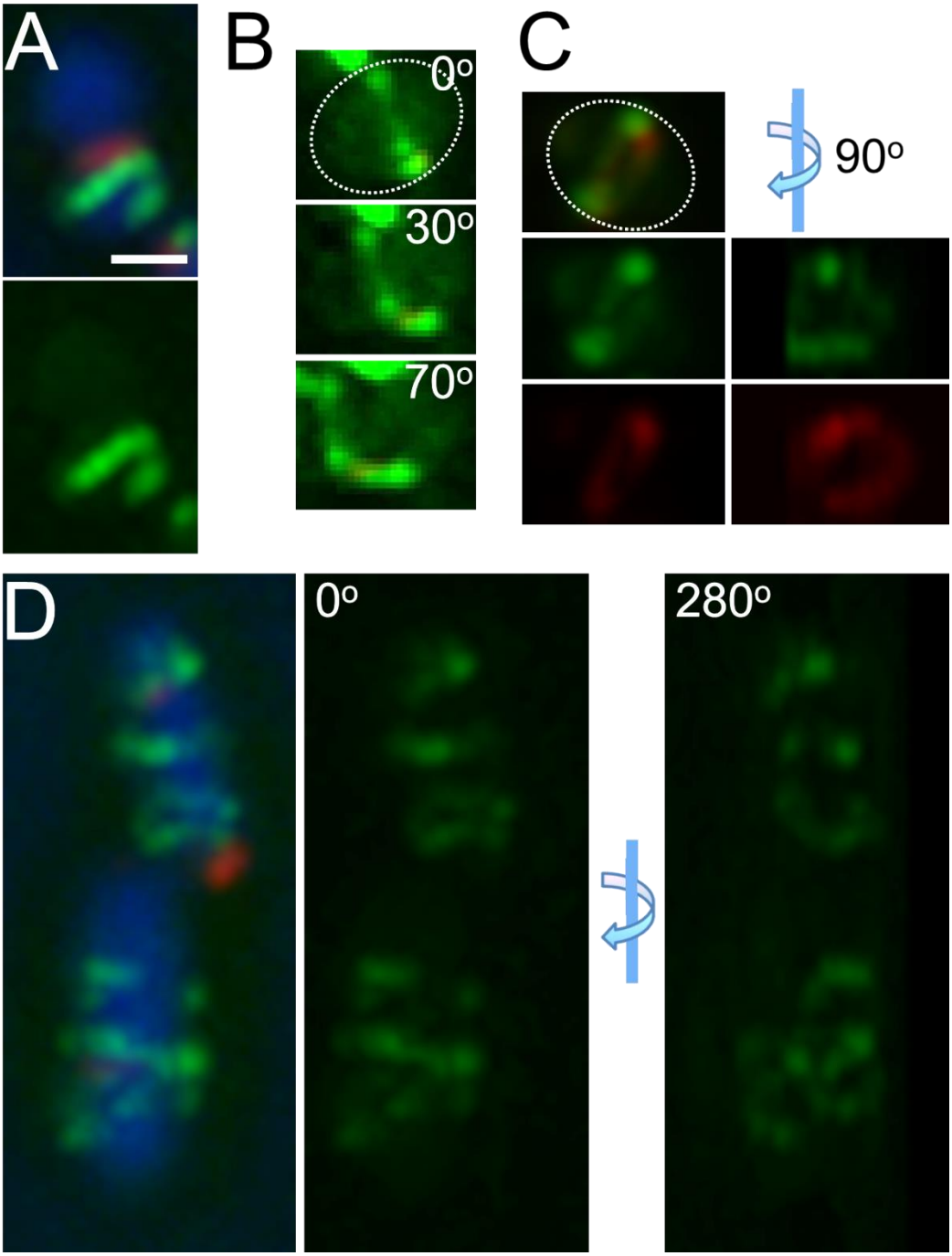

Figure 4.5. GFP–MreB forms filamentous structures in some cells. Cells were treated with 5 μM IPTG. **(A)** and **(B)**, arcs. **(C)** A ring-like structure (the two images in the right column were rotated 90°). **(D)** Helices or multiple arcs. Dashed lines demarcate cell outlines. Green: GFP–MreB; red: FtsZ–RFP; blue: DIC. Scale bar: 1 μm.

4.3 Dynamic Colocalisation between FtsZ and MreB

The cell cycle stage-specific colocalisation between MreB and FtsZ described in the previous section shows the colocalisation is dynamic. In most cells, only partial colocalisation was seen (Figs 4.5 C, 4.6, and 4.7). Furthermore, the colocalisation pattern of the MreB ring-like arrangement and the Z-ring suggest two adjacent, independent structures (Figs 4.6, lower panel and 4.7). Intriguingly, MreB assemblies were highly dynamic, moving around the cell (or disassembling/reassembling) with an average midcell localisation (Fig. 4.6, upper panel). The partial colocalisation of MreB and FtsZ is true for both patchy (Fig. 4.7 A) and filamentous (Figs 4.5 C, 4.6 lower panel, and 4.7 B) MreB structures.

Overexpression of FtsZ–RFP in the dual-tagged strain resulted in wider, filamentous cells (Figs 4.8, red arrowhead). The degree of colocalisation between MreB and FtsZ increased significantly in these cells (Figs 4.8). Intriguingly, the enhanced colocalisation only occurred in filamentous cells (Figs 4.8, red arrowhead), for both filamentous and spot-like structures. These results suggest that excess polymerised FtsZ may recruit MreB, resulting in the abnormal cell morphology.

Overall, the above results suggest that the colocalisation between MreB and FtsZ in *R. sphaeroides* is very dynamic.

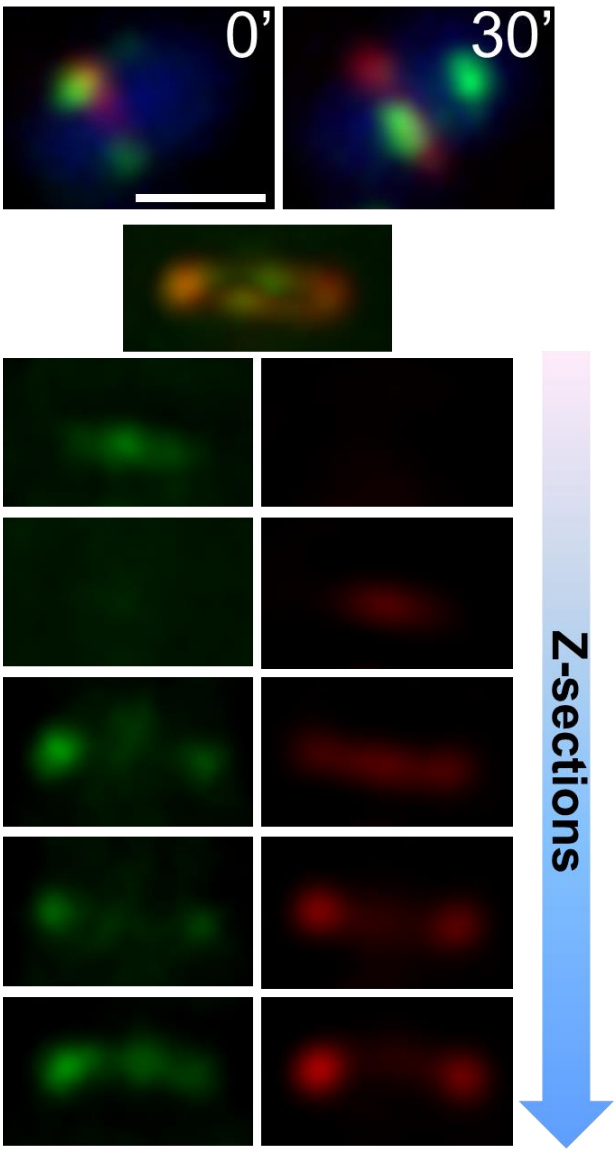

Figure 4.6. MreB and FtsZ form independent structures that partially colocalise at the midcell. Upper panel: MreB assemblies are highly dynamic, moving around the cell (or assembling/ disassembling) with an average mid- cell localization. The Z-ring (30’) matured from a precursor (0’). Lower panel: individual z-sections for FtsZ and MreB structures. The first image is a maximum projection. Green: GFP–MreB; red: FtsZ–RFP; blue: DIC. Numbers: minutes. Scale bar: 1 μm.

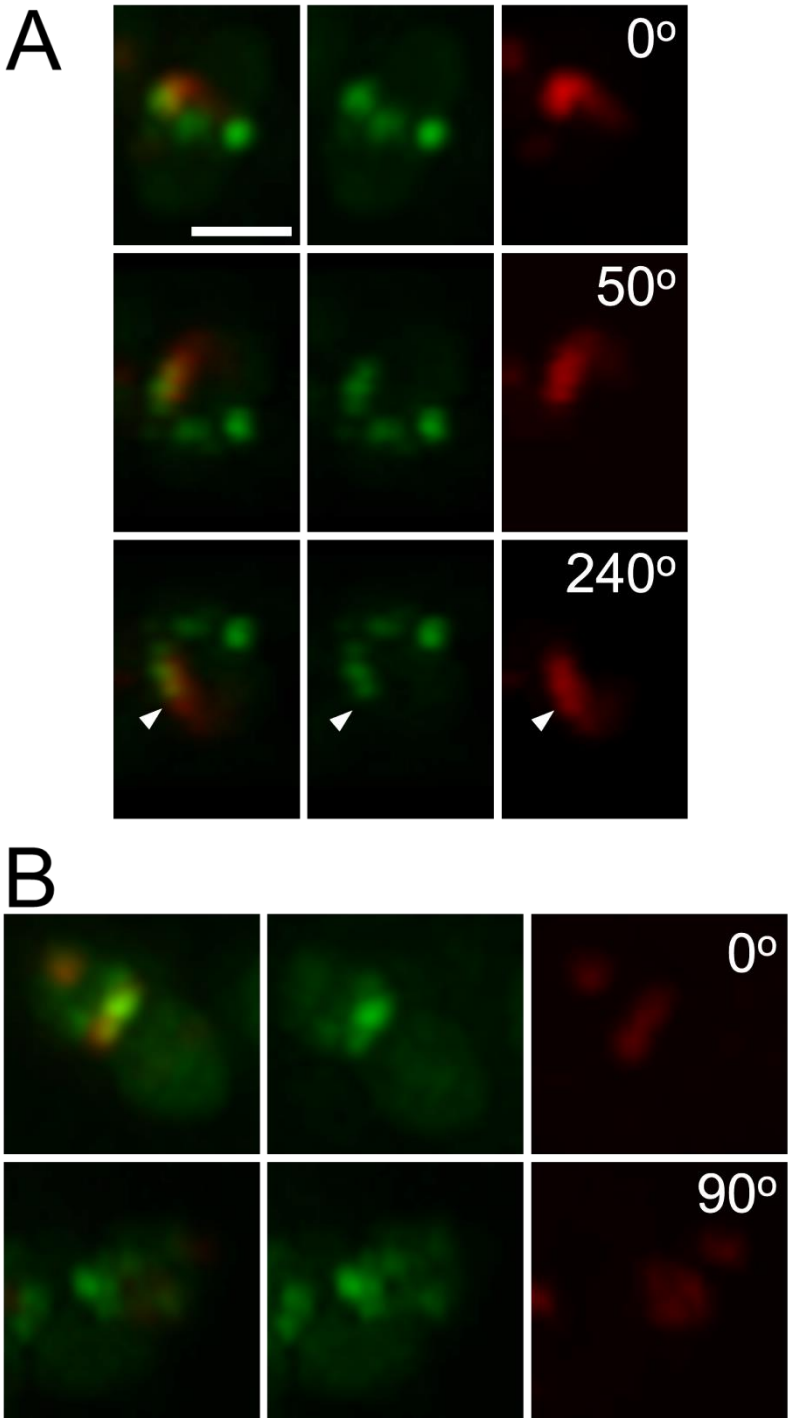

Figure 4.7. MreB and FtsZ partially colocalise in *R. sphaeroides*. **(A)** A cell with midcell FtsZ arc and MreB patches arranged in a circular manner. White arrowheads indicate the edge of the colocalised region. Different panels are images viewed in different angles. **(B)** As in (A), despites that the FtsZ arc was more similar to a ring. Cells were treated with 5 μM IPTG. Green: GFP–MreB; red: FtsZ–RFP; blue: DIC. Scale bar: 1 μm.

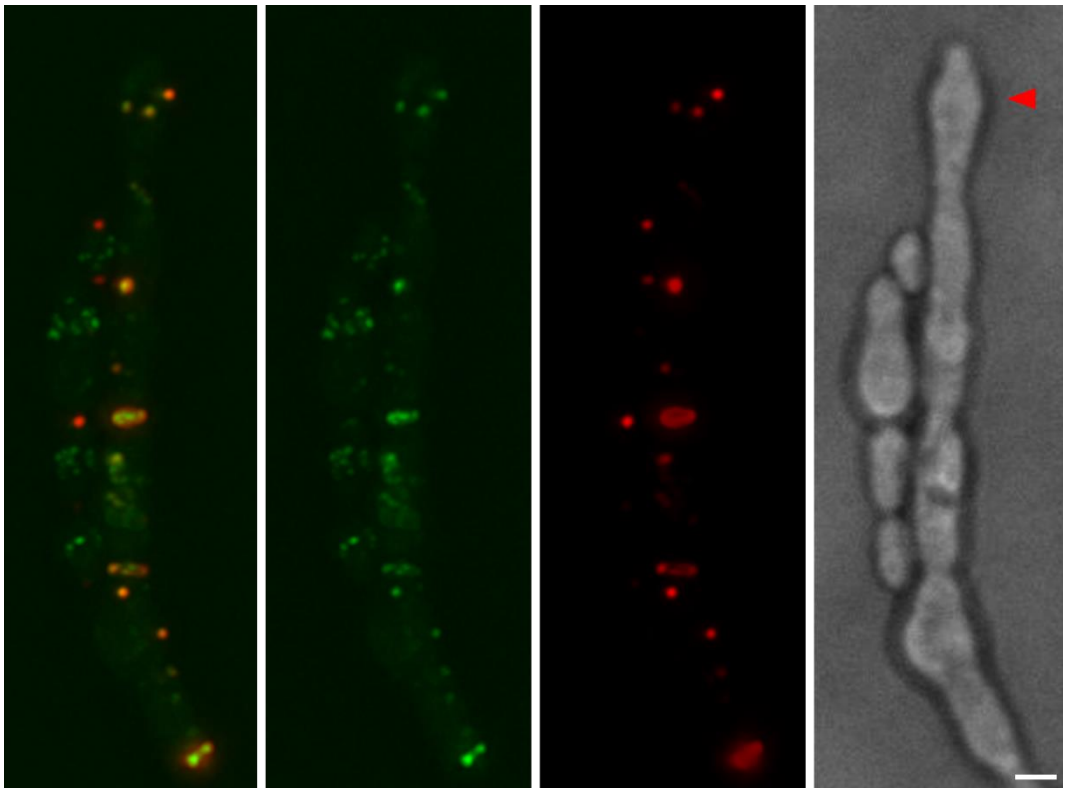

Figure 4.8. Extensive colocalisation of GFP–MreB and FtsZ–RFP in FtsZ–RFP -overexpressing cells (induced with 200 μM IPTG). Red arrowhead: a filamentous cell. Green: GFP–MreB; red: FtsZ–RFP. Left-most image is a merged image for GFP and RFP channels. A DIC image is shown on the right. Scale bar: 1 μm.

4.4 Different Configurations of the MreB Cytoskeleton

Since the GFP–MreB fusion is not fully functional (Slovak et al., 2005), I examined the localisation of *R. sphaeroides* MreB in a merodiploid strain containing an IPTG-inducible copy of *yfp–mreB* in addition to the native genomic *mreB* copy. Leaky expression resulted in a similar patchy pattern of MreB localisation (Fig. 4.9) (Slovak et al., 2005). However, MreB formed filamentous ring-like or helical structures in cells induced with 10 μM IPTG (Figs 4.9 B and 4.10). These filamentous structures are similar to those observed in many other bacteria (Carballido-López, 2006; Shaevitz and Gitai, 2010). Some ring-like structures also had adjacent "tails" (Fig. 4.10 A, arrowheads). These results suggest that higher levels of YFP–MreB promote the formation of filamentous structures.

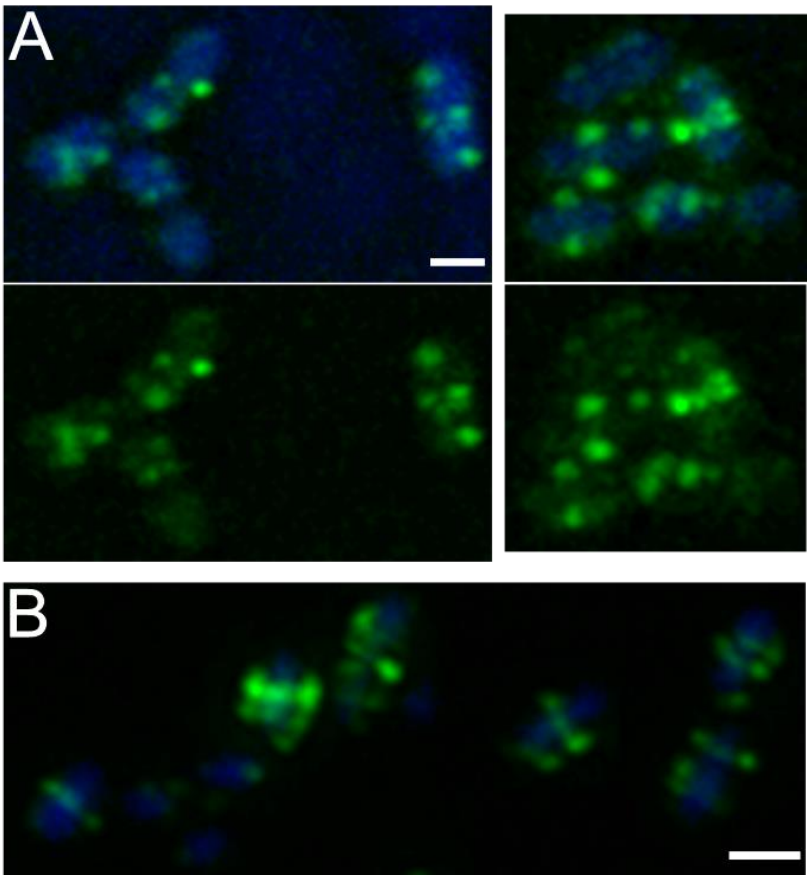

Figure 4.9. Effects of YFP–MreB expression levels on the structures of MreB cytoskeleton. Cells were grown in the presence (B) or absence (A) of 10 μM IPTG. Green: YFP–MreB; blue: DIC. Scale bar: 1 μm.

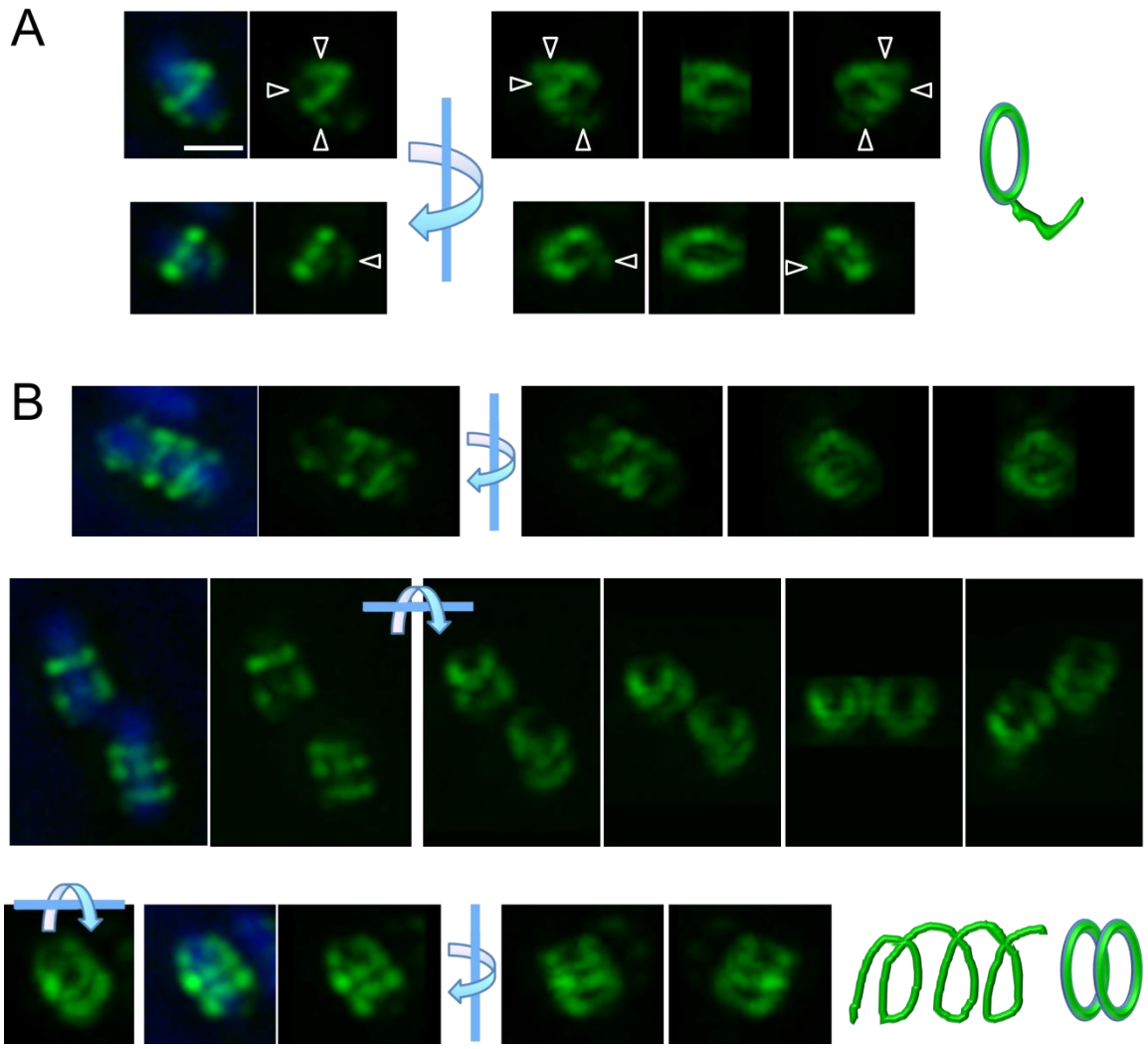

Figure 4.10. YFP–MreB forms filamentous structures when expressed at higher levels. Images are projections for cells treated with 10 μM IPTG. The images for YFP channel were rotated in different angels for better appreciation of the 3D nature of filamentous structures. **(A)** Ring-like structures with adjacent tails (arrowheads). **(B)** Helices or multiple ring-like structures. Schematics for each configuration are given. Green: YFP–MreB; blue: DIC. Scale bar: 1 μm.

To clarify the correlation between YFP–MreB concentration and cytoskeletal configurations, I tried to quantify the patchness of MreB structures. In an ideal circumstance, the fluorescence profiles across the longitudinal axes of cells with fluorescent patchy or filamentous structures will look like those in Fig. 4.11 A. Filamentous structures give a more smooth profile with smaller differences between peaks and troughs (Fig. 4.11 A, right), whereas patchy structures give a fluctuated profile with more dramatic changes between peaks and troughs (Fig.

4.11 A, left). To test this notion, cells with patchy or filamentous FtsZ–YFP structures (Chapter 3) were analysed. The fluorescence profiles were indeed similar to the ideal models (Fig. 4.11 B). A cell with a half compartment dominated by patchy structures and the other with both kinds of structures showed a combination of the two fluorescence profile patterns (Fig. 4.11 C), and it is easy to discriminate between the two compartments by the fluorescence profile. These results demonstrate the applicability of longitudinal fluorescence profiles in quantify the patchness of cytoskeletal structures. The differences between peak and trough values were used, expressed as fold-changes ("patchness index") (Fig. 4.11 D). The calculated patchness indexes for cells shown in Fig. 4.11 B are 3.81 (patchy) and 1.21 (filamentous).

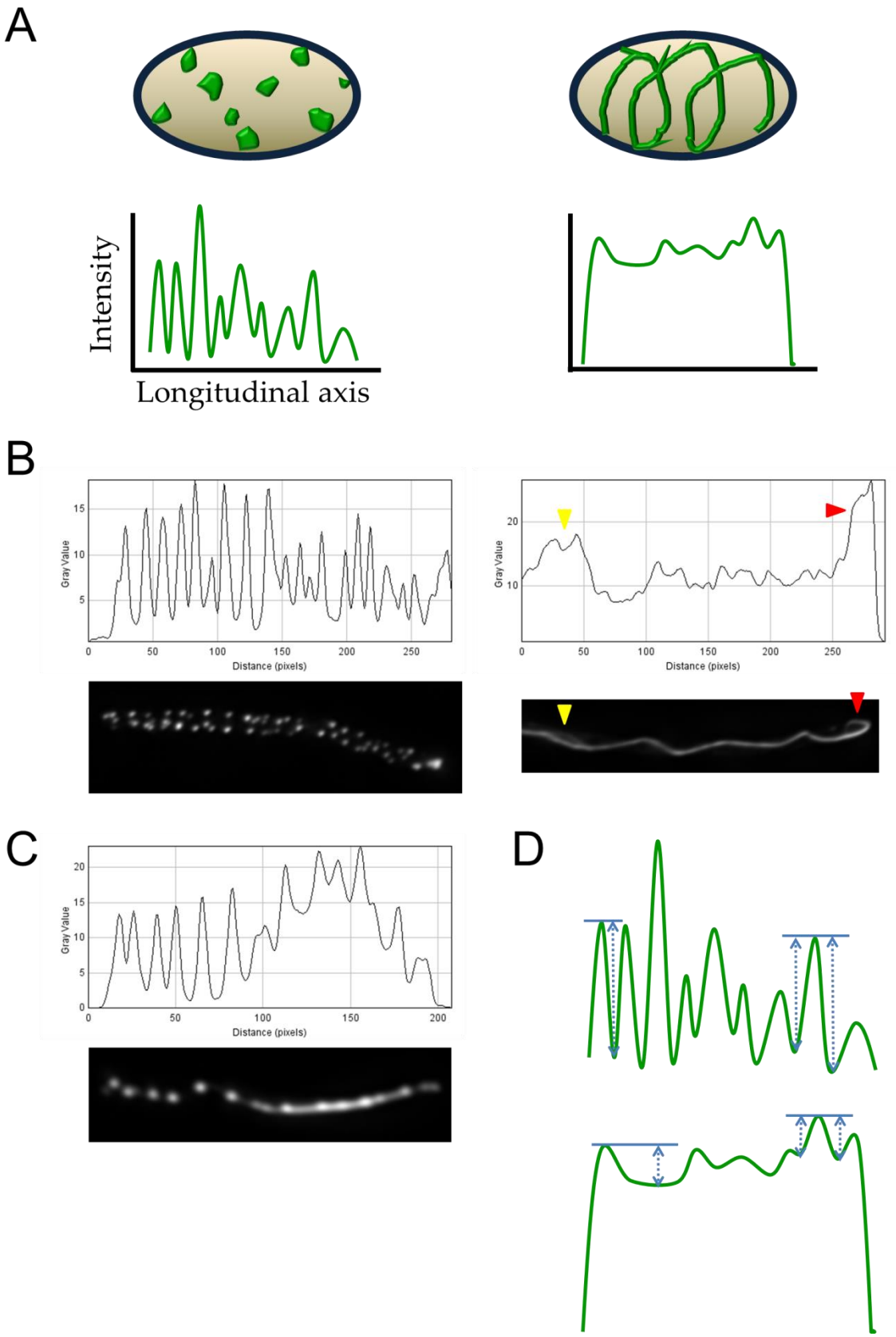

Figure 4.11. Quantification of the patchness of bacterial cytoskeletal structures. **(A)** Rationale for the usage of longitudinal fluorescence profile for quantifying patchness. The schematics for cells with patchy or filamentous structures and

their ideal fluorescence profiles are shown. **(B)** Applications of longitudinal fluorescence profiling for analysing patchness of FtsZ cytoskeletal structures. FtsZ–YFP-overexpressing cells show either patchy (left) or filamentous (right) patterns of FtsZ structures. The presence of double filaments (yellow arrowheads) and a hairpin-like structure (red arrowheads) resulted in higher peaks. **(C)** A cell with scattered patches along the whole cell and a filament extended in the right half. **(D)** The calculation of patchness index. The values of peaks were divided by the values of adjacent troughs. The mean fold-change value of all peak-trough pairs was defined as patchness index for each cell. The values of the outermost peaks were divided by the values of adjacent inner troughs.

When applying this approach to YFP–MreB-expressing cells, the shorter cell length (comparing to filamentous FtsZ–YFP-overexpressing cells) resulted in lower peak resolutions (Fig. 4.12 A and B). Nevertheless, a negative correlation between YFP–MreB intensity and patchness index was found (Fig. 4.12 C). According to these results, it is possible that *R. sphaeroides* MreB displays a concentration-dependence of the cytoskeletal configurations. Under lower expression levels (e.g. native expression of GFP–MreB or leaky expression of YFP–MreB), MreB mainly forms patches, but forms filamentous structures more frequently under higher expression levels (e.g. YFP–MreB induced by 10 μM IPTG). However, both MreB patches and filaments might arrange in a similar helical or circular pattern.

Two scenarios might exist: (1) there are certain helical/circular "tracks" for MreB. Increased expression of MreB fills up these tracks and the subcellular structures appear filamentous (2) higher MreB concentration favors the integration of patchy assemblies into filaments, or directly enhances the formation of longer MreB assemblies. The first notion is supported by two current findings: (1) time-lapse super-resolution imaging of YFP–MreB in *C. crescentus* cells showed that discrete spots are "linked" in a filamentous helix in the merged image of all time frames, indicates a helical track travelled by MreB spots (Biteen et al., 2008) (2) MreB molecules move processively along peripheral tracks roughly perpendicular to the longitudinal axis in *B. subtilis*, *C. crescentus*, and *E. coli* (Domínguez-Escobar et al., 2011; Garner et al., 2011; Kim et al., 2006; Reimold et al., 2013; van Teeffelen et al., 2011). However, the two scenarios are not mutually exclusive. Besides, close proximity of individual MreB assemblies may create pseudo filamentous structures.

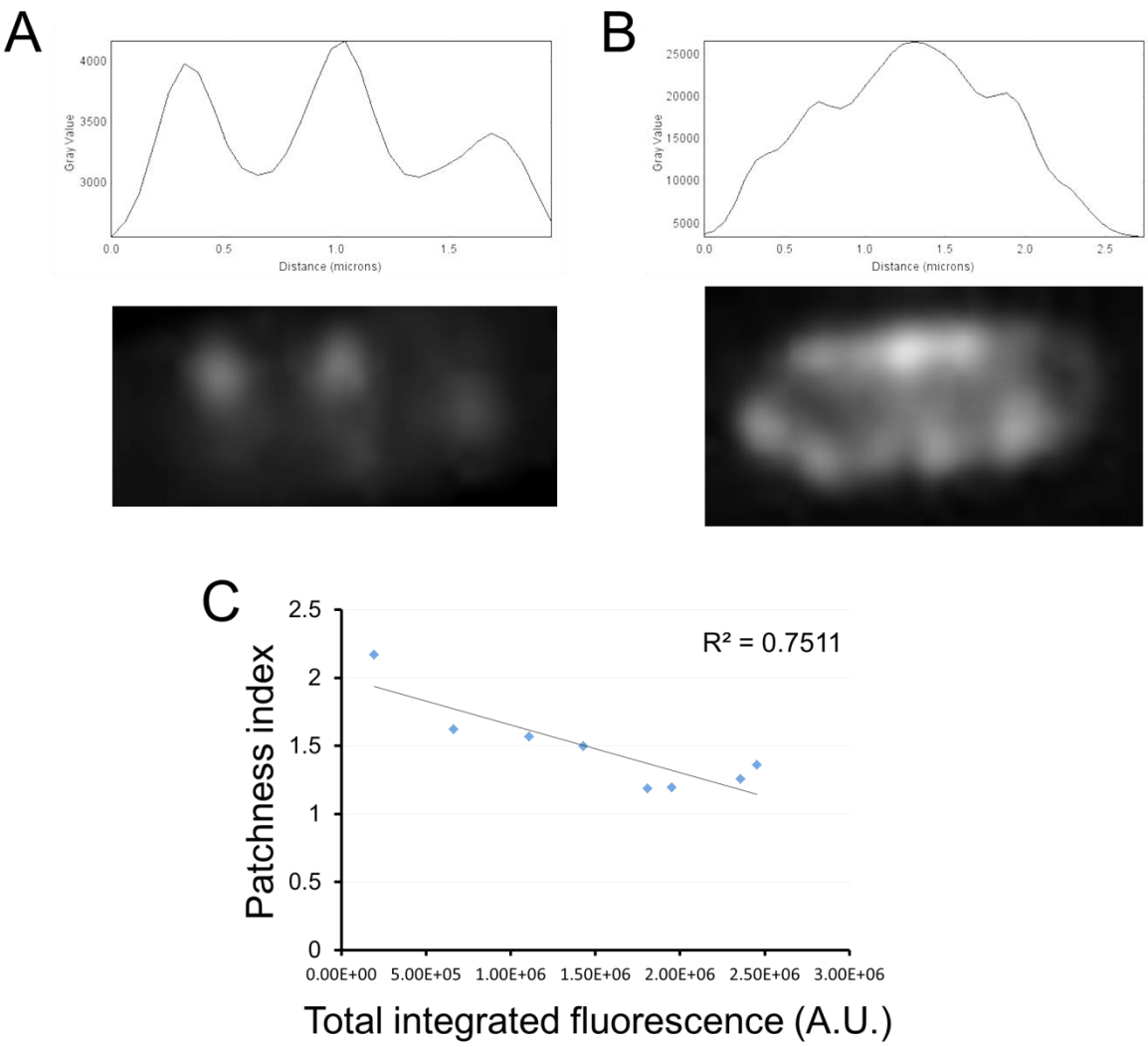

Figure 4.12. Patchness of the MreB cytoskeleton in YFP–MreB-expressing cells. Grey-scale images of the YFP channel and the corresponding intensity profiles are shown for cells with patchy **(A)** or filamentous **(B)** MreB structures. **(C)** Correlation plot showing the negative relationship between the YFP–MreB expression levels (total cellular integrated intensity) and the corresponding patchness indexes.

The above results and the dramatic localisation change of MreB assemblies (Fig. 4.6 upper panel) suggest that MreB continuously reorganizes its cytoskeletal configurations in *R. sphaeroides*, in addition to the cell cycle-specific localisation changes (Slovak et al., 2005). Time-lapse imaging with short intervals (~5% of total cell cycle length) confirmed this idea. The reorganizations of the MreB cytoskeleton can be roughly divided as: (1) from filamentous to patchy (Fig. 4.13); (2) from patchy to filamentous (Fig. 4.14); (3) between filamentous structures (Fig. 4.15). MreB assemblies frequently moved in/out the cell pole (arrowheads in Figs

4.13–4.15). In *B. subtilis*, the MreB paralogue Mbl forms foci close to or at the cell poles, and filamentous structures seem to nucleate from these foci and move towards the cell centre (Defeu Soufo and Graumann, 2004). Although higher expression levels of YFP–MreB may enhance the formation of filamentous structures, the reorganisation of MreB cytoskeletal configurations is not apparently affected (for [IPTG] ≤ 10 μM).

To summarise, the MreB cytoskeleton in *R. sphaeroides* was flexible and highly dynamic which kept changing its configurations. Therefore, even *R. sphaeroides* has a much longer cell-cycle length, its MreB cytoskeleton was as dynamic as other homologous systems (Carballido-López and Errington, 2003; Defeu Soufo and Graumann, 2004).

Strikingly, MreB has similar behaviours in photoheterotrophic cells (Fig. 4.16), suggesting that the intense rearrangement of the cytoplasmic membrane which occurs during photoheterotrophic growth have no effect on the positioning of MreB and probably also the cell-wall synthesis machinery.

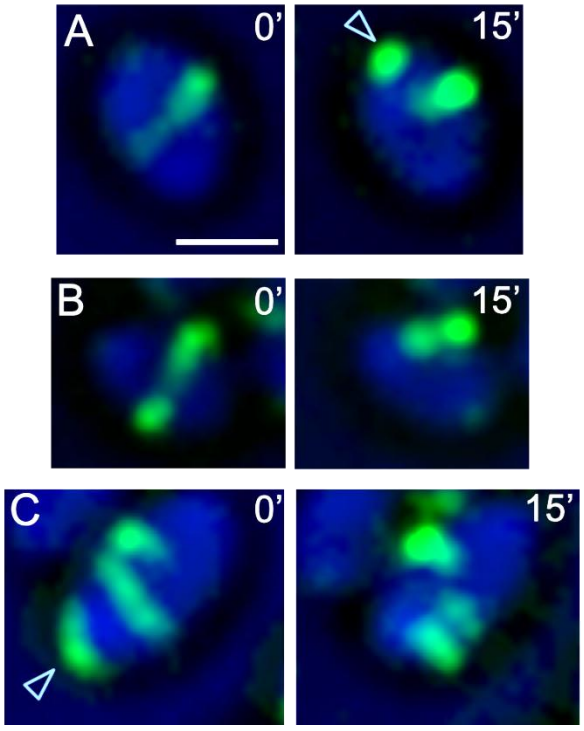

Figure 4.13. Dynamic reorganisation of MreB filamentous structures into more patchy structures. **(A)** and **(B)**: from arcs/rings to patches. **(C)**: from multiple arcs to patches/short fragments. Arrowheads: MreB assemblies at the cell pole. Green: YFP–MreB; blue: DIC. Numbers: minutes. Scale bar: 1 μm.

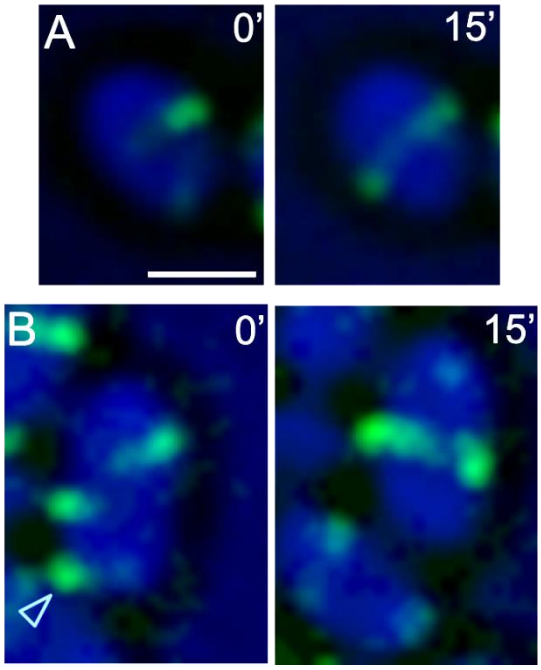

Figure 4.14. Dynamic reorganisation of MreB patchy structures into filamentous structures. Arrowhead: MreB assemblies near the cell pole. Green: YFP–MreB; blue: DIC. Numbers: minutes. Scale bar: 1 μm.

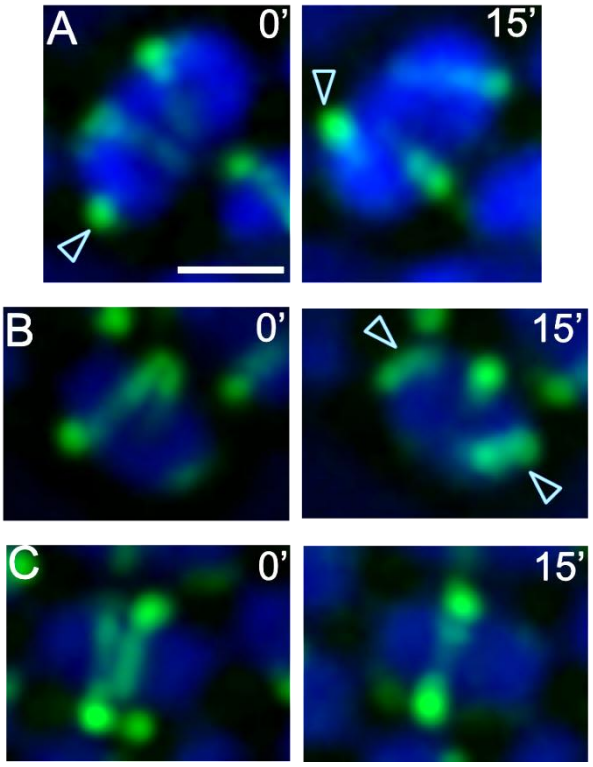

Figure 4.15. Dynamic reorganisation between MreB filamentous structures. **(A)** Two arcs change their orientations and locations. A patch also moves from the tip to the edge of the cell pole (arrowheads). **(B)** From an arc/spiral to midcell patch and short fragments at the cell poles (arrowheads). **(C)** From a spiral or two arcs to a ring/arc. Green: YFP–MreB; blue: DIC. Numbers: minutes. Scale bar: 1 μm.

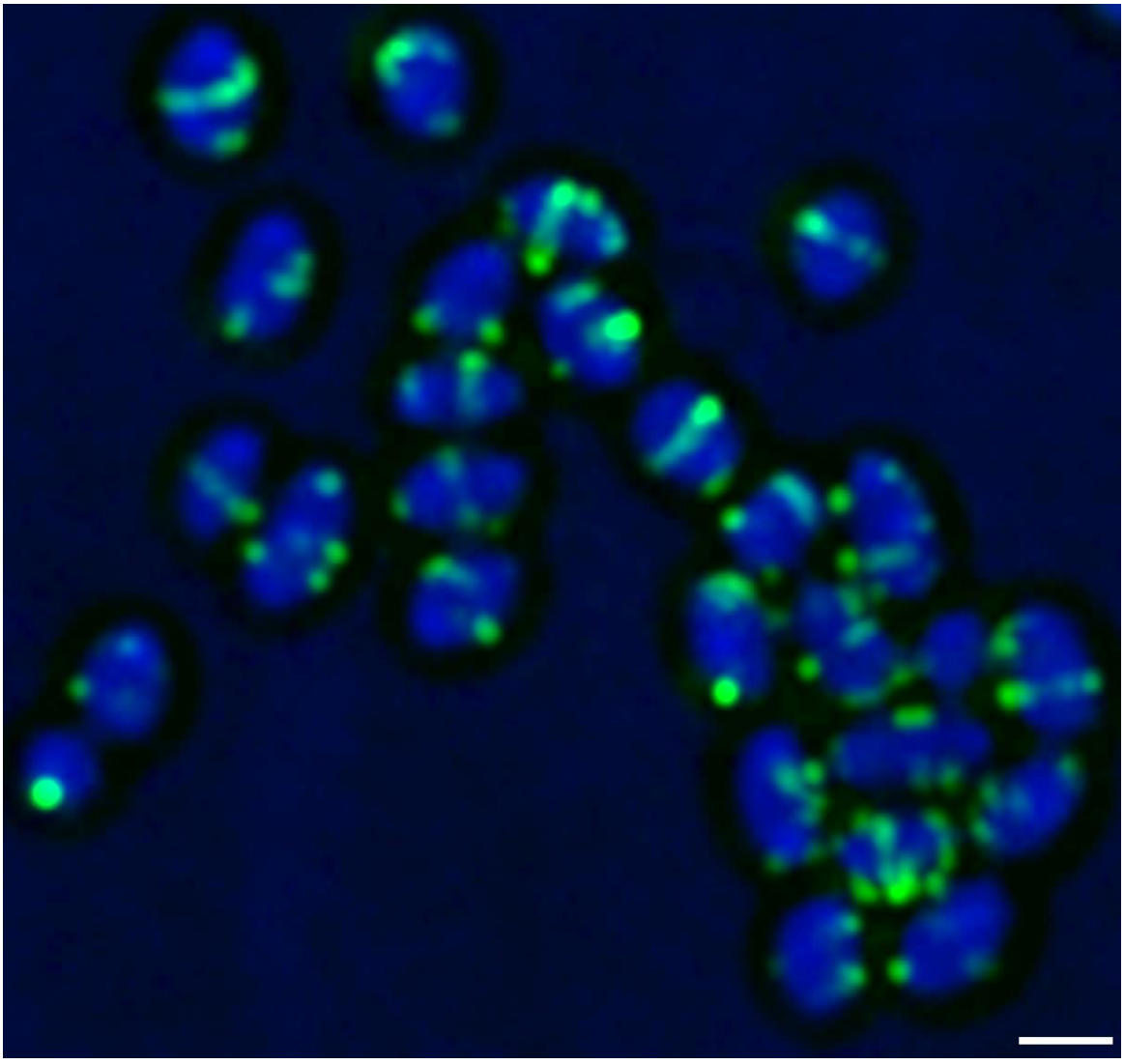

Figure 4.16. MreB cytoskeletal structures in photoheterotrophic *R. sphaeroides* cells. Green: YFP–MreB; blue: DIC. Scale bars: 1 μm.

4.5 Discussion and Conclusions

The proposed cell cycle stage-specific localisation of *R. sphaeroides* MreB (Slovak et al., 2005) was confirmed by simultaneous observations with FtsZ—FtsZ nodes/rings and MreB colocalise at the midcell until constriction, after which MreB relocalises at future midcells before FtsZ (Fig. 4.3 A). A merodiploid strain expressing YFP–MreB provides further details about the spatiotemporal dynamics of MreB in *R. sphaeroides*. The MreB cytoskeleton continuously reorganizes between patchy and filamentous structures, and MreB assemblies can quickly change their cellular locations (Figs 4.13–4.15). The local availability of peptidoglycan template/precursors (Eraso and Margolin, 2011) or changes in membrane curvature (Ursell et al., 2014) may contribute to these dynamic behaviours.

The presence of discrete MreB assemblies at *R. sphaeroides* cell poles is interesting (Figs 4.13–4.15). In other bacteria MreB assemblies either localise at cell poles as extended parts of the major helices, or only as small portions of the patchy structures. In *R. sphaeroides*, significant portions of MreB could be found as filamentous/patchy assemblies at cell poles. PBP2 and MreC, proteins of the cell-wall synthesis machinery, also have a similar polar localisation (Slovak et al., 2006). Whether this polar localisation of MreB/C and PBP2 contributes to polar peptidoglycan synthesis remains to be tested. Nevertheless, the polar localisation of MreB assemblies might be a reflection of MreB's preference for negatively curved regions of the cell envelope (Ursell et al., 2014).

A spiral yarn: the *in vivo* configurations of MreB assemblies

The story about the configurations of MreB cytoskeleton is a tale of spirals that progresses in spirals. The discovery of bacterial actin homologues forming helical filamentous structures (Jones et al., 2001) is so alluring—it stirred up an upheaval of hunts for helical patterns in diverse prokaryotes. The MreB helix is believed to participate in the spatial regulation of many other biomolecules (Carballido-López, 2006; Shaevitz and Gitai, 2010), and helical localisations were reported for many of them.

Patchy MreB assemblies have been observed since the publication of Errington and colleagues' landmark paper (Jones et al., 2001). Before, these patchy assemblies were usually interpreted as parts of filamentous helices, which were difficult to be resolved by conventional fluorescence microscopy. However, no long (>80 nm) MreB filaments were detected in a current cryo-tomography

study of *B. subtilis*, *C. crescentus*, *E. coli* and *V. cholerae* (for which MreB has been reported to form long helices in these bacteria) (Swulius et al., 2011). A series of super-resolution fluorescence microscopy studies later suggest that MreB homologues do not form extended helical structures. Instead, they assemble into discrete patches which move circumferentially around the cell in *B. subtilis*, *C. crescentus*, and *E. coli* (Domínguez-Escobar et al., 2011; Garner et al., 2011; van Teeffelen et al., 2011). Swulius and Jensen (2012) further suggested that long MreB helices is an artefact caused by the N-terminal YFP tag, at least for *E. coli* MreB. These current reports already triggered a set of discussions on the reasons for the controversial conclusions in the past and current studies (Chastanet and Carballido-Lopez, 2012; Eraso and Margolin, 2011; Margolin, 2012; White and Gober, 2012). Intriguingly, a present article addressed some of the proposed causes and showed that under super-resolution microscopy, MreB forms long filamentous structures in *B. subtilis* and *E. coli*, which run at angles diverging up to 40° relative to the cell circumference. Suboptimal growth conditions lead to formation of patch-like structures rather than extended filaments (Reimold et al., 2013).

In the light of my observations of MreB's behaviours in *R. sphaeroides*, I would like to provide some possible explanations. The debate on the *in vivo* configuration of MreB assemblies can be divided into two parts: does MreB form patches or long filaments, and are they helically arranged? For *R. sphaeroides*, the answer to the first question seems to be both. Indeed, MreB assemblies seem to continuously reorganize between the two configurations. It has been proposed that MreB expression level and growth conditions affect the appearances of MreB assemblies (Chastanet and Carballido-Lopez, 2012; Reimold et al., 2013). However, the results are controversial. In *R. sphaeroides* the two configurations could be seen in the same population, suggesting they are dynamically interchanging. Nevertheless, I cannot exclude the possibility that higher expression levels of MreB may enhance the chance to observe more filamentous structures. Since MreB patches/filaments also fuse and split in other bacteria (Defeu Soufo and Graumann, 2004; Domínguez-Escobar et al., 2011; Reimold et al., 2013), it is plausible to suggest that assemblies of MreB homologues reorganize between filamentous and patchy configurations.

The second question, whether MreB assemblies are helically arranged, is more complicated. As a very basic pattern seen in the nature (Galloway, 2010), it is difficult to argue about whether something is really helical or not. The circumferential movement of MreB patches is roughly perpendicular to the longitudinal axis, with frequently observed slanted tracks (Biteen et al., 2008;

Domínguez-Escobar et al., 2011; Garner et al., 2011; Kim et al., 2006; Reimold et al., 2013; van Teeffelen et al., 2011). Even only exists transiently, a filamentous structure longer than one turn of the cell circumference, could be described as helical. Besides, the spacing of discrete MreB patches is compatible with a helical pattern. However, the question is somehow similar to an argument about whether a cloud is more like a dog or a dragon. Therefore, a more appropriate question would be: is there any cell-wide, coherent helical arrangement of MreB? In *R. sphaeroides* the answer seems to be no, and a helical arrangement might be a pseudo-state created by dynamically reorganising patches and filaments.

To summarise, I suggest that MreB assemblies possess interchangeable patchy and filamentous configurations. The dynamic behaviours of these assemblies create a helical-like pattern. This idea can provide a putative solution for the current debate of the configuration of MreB assemblies (Domínguez-Escobar et al., 2011; Garner et al., 2011; Reimold et al., 2013; van Teeffelen et al., 2011). To have an ultimate answer, systematic, parallel investigations of all used bacterial strains and culture conditions on different imaging platforms might be necessary.

Colocalisation of MreB and FtsZ

As the number of identified bacterial cytoskeletal proteins has expanded sharply, an emerging theme is the choreography of cytoskeletal networks (Cabeen and Jacobs-Wagner, 2010). The cell cycle stage-dependent colocalisation of MreB and FtsZ implies that a complex, interacting cytoskeletal network exists in *R. sphaeroides*. MreB forms ring-like structures which colocalise with and are dependent on the Z-ring in *C. crescentus* and *E. coli* (Aaron et al., 2007; Figge et al., 2004; Gitai et al., 2004; Vats and Rothfield, 2007). This Z-ring dependence could be resulted from a direct MreB–FtsZ interaction (Fenton and Gerdes, 2013) or coordination via the conserved RodZ protein (Alyahya et al., 2009; Bendezu et al., 2009; Muchová et al., 2013; Shiomi et al., 2008; van den Ent et al., 2010). However, the establishment of medial ring-like arrangement of MreB seems to be independent of the Z-ring in *R. sphaeroides* (Figs 4.2 and 4.3) (Slovak et al., 2005), suggesting a different mechanism to position MreB assemblies in this bacterium. Intriguingly, PBP2 and MreC, components of the cell-wall synthesis machinery, form midcell ring-like structures in new-born *R. sphaeroides* cells, and in septating cells, these proteins may redistribute to future midcells before MreB (Slovak et al., 2006). It is likely that PBP2 and MreC rather than FtsZ recruit MreB to the midcell in *R. sphaeroides*. Nevertheless, FtsZ assemblies resulted from FtsZ-overexpression

may recruit MreB (Fig. 4.8), suggesting the Z-ring could maintain the septal localisation of MreB before it is further recruited by PBP2/MreC to future midcells. Further experiments are needed to explore the role of Z-ring in the midcell localisation of MreB in *R. sphaeroides*. To this end, I used a commercially available FtsZ-depolymerising chemical berberine (Boberek et al., 2010) for dissecting the function of FtsZ assemblies. Unfortunately, the strong intrinsic autofluorescence (Keffer et al., 2013) and slow effect of berberine made the results inclusive.

Conclusions

The MreB cytoskeleton continuously reorganizes between patchy and filamentous structures in *R. sphaeroides*. The reorganisation also occurs at larger length-scale and longer time-scale: MreB changes its main localisation according to cell-cycle stages, and colocalises with FtsZ at the midcell until constriction. MreB localises at pre-cytokinetic sites before FtsZ, which is different compared with *C. crescentus* and *E. coli*. This observation suggests that there are diverse interacting modes in the homologous cytoskeletal networks in different bacteria, and there is a unique mechanism to position MreB at the midcell/septum in *R. sphaeroides*.

Chapter 5. Relative Positioning between MreB and Chemosensory Clusters

*To **B**e, or not to **B**e, that is the question.*

— *Hamlet*, William Shakespeare

5.1 Aims

The actin homologue MreB participates in a broad range of spatial organisation in bacteria, including cell polarity and protein localisation (Carballido-López, 2006; Shaevitz and Gitai, 2010). Having established the spatiotemporal dynamics of MreB in *R. sphaeroides* (Chapter 4), I examined the possible role MreB plays in the positioning of membrane and cytoplasmic chemosensory clusters in this chapter.

5.2 The Relative Positioning between MreB and Membrane Chemosensory Clusters

To explore the possible role of MreB plays in the positioning of membrane chemosensory clusters, I monitored the localisation of membrane chemosensory proteins together with MreB.

The functional YFP fusion of $CheW_3$, expressed as a genomic replacement, was used as a marker for membrane chemosensory clusters (Wadhams et al., 2003). The localisation pattern of membrane chemosensory clusters in *R. sphaeroides* can be roughly divided into four categories: (1) unipolar (2) unipolar with lateral clusters (3) bipolar (4) bipolar with lateral clusters (see Chapters 6–8 for more details). A *yfp–cheW*$_3$-expressing strain containing an IPTG-inducible copy of *cfp–mreB* (***c***yan ***f***luorescent ***p***rotein) was used for monitoring the colocalisation pattern of MreB and membrane chemosensory clusters. The localisations of MreB or membrane chemosensory clusters are similar to those in

single-tagged strains (Fig. 5.1). The presence of discrete MreB assemblies at cell poles (Figs 4.13–4.15 and 5.1, arrowheads) indicates a putative role of MreB for anchoring membrane chemosensory clusters there. However, despite occasional close proximity/colocalisation, no specific correlation was found between the polar localisations of MreB and membrane chemosensory clusters (Fig. 5.1, arrowheads). To rule out the possibility that MreB may leave a location after positioning membrane chemosensory clusters there, time-lapse images were analysed. No clues were found for any active roles of MreB in the positioning of membrane chemosensory clusters (data not shown). As for polar chemosensory clusters, lateral clusters only showed random colocalisation with MreB (Fig. 5.1).

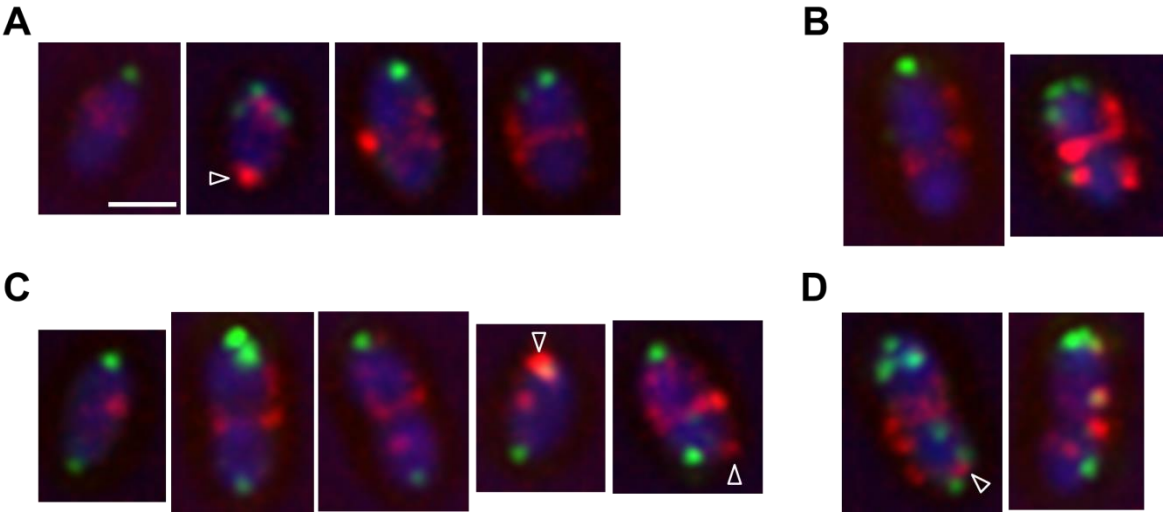

Figure 5.1. The relative positioning of MreB and membrane chemosensory clusters in cells with different localisation patterns of chemosensory proteins: **(A)** unipolar; **(B)** unipolar with lateral clusters; **(C)** bipolar; **(D)** bipolar with lateral clusters. Cells were not induced with IPTG. Green: YFP–$CheW_3$; red: CFP–MreB; blue: DIC. Arrowheads: polar MreB assemblies. Scale bar: 1 μm.

5.3 The Relative Positioning between MreB and Cytoplasmic Chemosensory Clusters

The functional YFP fusion of TlpT, expressed as a genomic replacement, was used as a marker for cytoplasmic chemosensory clusters (Wadhams et al., 2003). The localisation pattern of cytoplasmic chemosensory clusters in *R. sphaeroides* can be roughly divided into three categories: (1) single midcell cluster (2) single polar cluster (3) two clusters (see Chapter 9 for more details). An *yfp–tlpT*-expressing strain containing an IPTG-inducible copy of *cfp–mreB* was used for monitoring the colocalisation pattern of MreB and cytoplasmic chemosensory clusters. The localisations of MreB or cytoplasmic chemosensory clusters were similar to those in single-tagged strains (Fig. 5.2). As membrane clusters, no specific correlation was found between the positioning of MreB and cytoplasmic chemosensory clusters in snapshots (Fig. 5.2) or time-lapse series (data not shown).

The cytoplasmic chemosensory cluster roughly localises around (pre)cytokinetic sites (Fig. 5.2 and Chapter 9) (Roberts et al., 2012; Thompson et al., 2006). To further characterise its positioning relative to MreB, filamentous *R. sphaeroides* cells were used. Again, no specific correlation was found (Fig. 5.3).

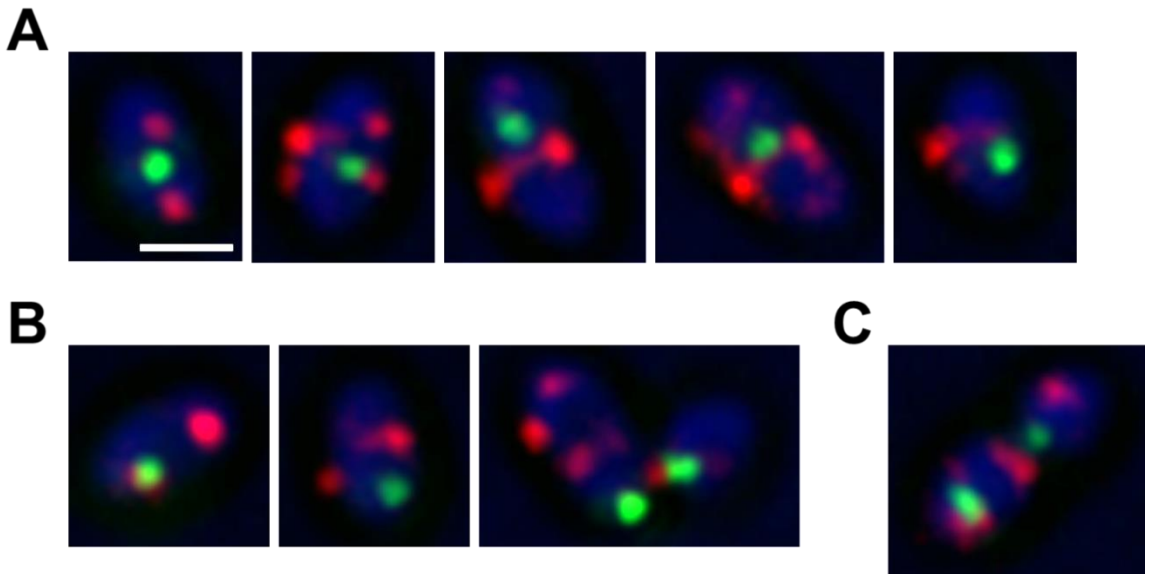

Figure 5.2. The relative positioning of MreB and cytoplasmic chemosensory clusters in cells with different localisation patterns of chemosensory proteins. **(A)** Single midcell cluster. **(B)** Single polar cluster. **(C)** Two clusters. Cells were not induced with IPTG. Green: YFP–TlpT; red: CFP–MreB; blue: DIC. Scale bar: 1 μm.

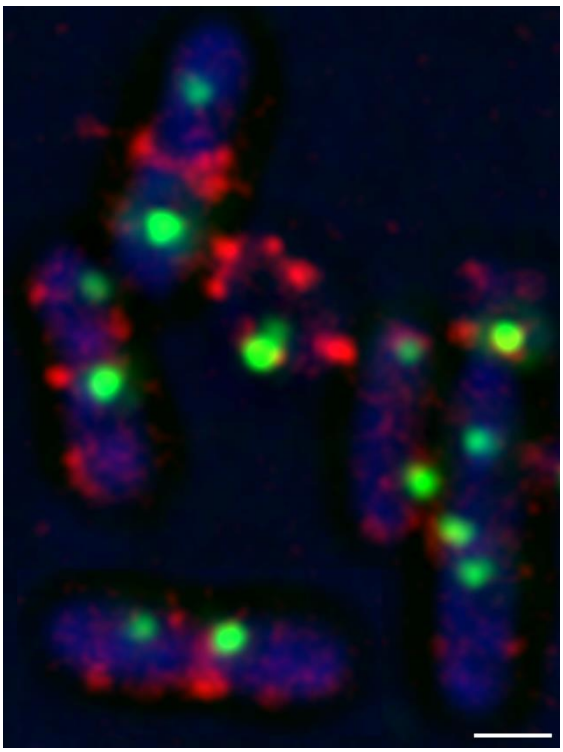

Figure 5.3. The relative positioning of MreB and cytoplasmic chemosensory clusters in filamentous cells. Cells were treated with cephalexin for 3 h before imaging and not induced with IPTG. Green: YFP–TlpT; red: CFP–MreB; blue: DIC. Scale bar: 1 μm.

5.4 Discussion and Conclusions

The MreB cytoskeleton can potentially provide positioning information or anchorage for chemosensory clusters. To test this possibility, I performed simultaneous observations of MreB with membrane/cytoplasmic chemosensory clusters. No correlation was found between the localisation/dynamics of MreB and those of the two chemosensory systems.

MreB and the positioning of membrane chemosensory clusters

In addition to the components of cell-wall synthesis machinery, MreB has been implicated in the localisation of many proteins, including *C. crescentus* polar histidine kinases/response regulator (Gitai et al., 2004), *E. coli* chemoreceptor Tar (Shih et al., 2005), *M. xanthus* gliding motility proteins (Mauriello et al., 2010), and *P. aeruginosa* pilus-associated proteins (Cowles and Gitai, 2010). In *E. coli*, Tar mainly localises at cell poles with some helical distributions along lateral sites (Shiomi et al., 2006). Shiomi et al. (2006) proposed that the helical localisation is resulted from the transient association of Tar with the general protein translocation machinery (Sec). However, the Tar/Sec helices are different from the MreB helical structures, suggesting MreB is not responsible for the positioning of

lateral Tar clusters (Shiomi et al., 2006). In another study with *ΔmreB* cells, Tar is randomly positioned around the cell periphery of *E. coli* (Shih et al., 2005). The authors therefore concluded that MreB is required for the polar localisation of Tar. However, MreB is a pleiotropic protein, makes it difficult to unravel the direct effects of MreB on protein localisation from indirect effects caused by growth defects or abnormal cell morphology (Shaevitz and Gitai, 2010). I believe that MreB's effects on the localisation of Tar (and presumably other associated chemosensory proteins) can be attributed to the disruption of cell morphology/cell envelope rather than a specific function of MreB (see Chapter 8 for more details). Consistent with this idea, a short treatment with the MreB-depolymerising chemical A22 does not affect the positioning of *E. coli* and *P. aeruginosa* membrane chemosensory clusters (O'Connor et al., 2012; Oh et al., 2014; Thiem et al., 2007). Abnormal localisation of chemosensory clusters only appears after cell morphology is disturbed (Oh et al., 2014; Thiem et al., 2007). Taken together, the results described in this chapter and previous studies (Shiomi et al., 2006; Thiem et al., 2007) suggest that MreB does not have a direct role in the positioning of membrane chemosensory clusters in *R. sphaeroides* and *E. coli*.

MreB and the positioning of cytoplasmic chemosensory clusters

As an assembly containing thousands of proteins, the cytoplasmic cluster may have some similarities to bacterial intracellular proteinaceous organelles (Murat et al., 2010; Shively et al., 2009; Yeates et al., 2008).

MreB influences the polar localisation of inclusion bodies in *E. coli* (Rokney et al., 2009), and carboxysome localisation/organisation in *Synechococcus elongatus* (Savage et al., 2010). The effect on inclusion bodies is probably due to the loss of normal rod-shape in *E. coli*, not a specific role plays by MreB (Winkler et al., 2010). Strikingly, the localisation/organisation of the carboxysome seems to be disrupted in *ΔmreB S. elongatus* cells which still retain their rod-shape (Savage et al., 2010). Savage et al. (2010) proposed that MreB defines a structure that is used to organize carboxysomes, likely the chromosome (Jain et al., 2012). Although the positioning of MreB and cytoplasmic chemosensory clusters does not have any clear correlation, I cannot exclude the possibility that MreB participates in the spatial regulation of cytoplasmic chemosensory clusters via an indirect action. However, the essentiality of *mreB* and inefficiency of A22 in *R. sphaeroides* make this possibility difficult to test.

Conclusions

The distinct localisation pattern of MreB and its crucial functions in bacterial spatial organisation prompted me to investigate the role of MreB in the positioning of membrane and cytoplasmic chemosensory clusters in *R. sphaeroides*. However, no apparent correlation was found between the positioning of MreB and the two chemosensory systems.

Chapter 6. Spatiotemporal Dynamics of Membrane Chemosensory Clusters Relative to FtsZ in *R. sphaeroides*

To reach a port, we must sail—sail, not tie at anchor.

— *Fireside Chat 1938*, Franklin D. Roosevelt

6.1 Aims

A protein stably associated with the cytokinetic site will localise at the new poles after cell division. In *C. crescentus* (Goley et al., 2011) and *R. sphaeroides* (Chapter 3), components of the cytokinetic machinery (e.g. FtsZ) remain at the new poles after cell division. Proteins could therefore couple their localisation to the cytokinetic site/divisome to establish a polar localisation. This mechanism is utilized by the *C. crescentus* membrane-bound polar landmark TipN (Huitema et al., 2006; Lam et al., 2006). In predivisional cells, TipN is targeted to midcell via an association with the divisome, and localises at the new poles after cell division (Huitema et al., 2006; Lam et al., 2006; Yeh et al., 2010). A similar cytokinetic site-association mechanism has been proposed for the polar localisation of membrane chemosensory clusters (Greenfield et al., 2009; Thiem et al., 2007; Thiem and Sourjik, 2008; Wang et al., 2008a), but was not directly examined before. Having established the spatiotemporal dynamics of FtsZ in *R. sphaeroides* (Chapter 3), I investigated whether or not this cytokinetic site- association mechanism is responsible for the polar localisation of membrane chemosensory clusters in *R. sphaeroides*.

6.2 Membrane Chemosensory Clusters Do Not Localise at Cytokinetic Sites

To test the cytokinetic site-association mechanism in *R. sphaeroides*, I observed the positioning of membrane chemosensory clusters in cephalexin-induced

filamentous cells. Cephalexin treatment blocks septation/constriction but does not affect the formation of cytokinetic rings. The resultant filamentous cells are therefore widely used as a system to study protein localisation, including the putative association with the divisome. The functional YFP fusion of $CheW_3$, expressed as a genomic replacement, was used as a marker for membrane chemosensory clusters (Wadhams et al., 2003).

The cytokinetic site-association mechanism predicts a localisation pattern as depicted in Fig. 6.1 A. Unlike what the mechanism predicts, membrane chemosensory clusters in filamentous *R. sphaeroides* cells did not colocalise with cytokinetic sites (marked by FtsZ–CFP) (Figs 6.1 B, 6.2, and 6.3 A). Strikingly, no detectable membrane clusters were found in the vicinities of Z-rings (Figs 6.2 and 6.3 A; also see section 6.3). The relative positioning of Z-rings and membrane chemosensory clusters was consistent with a pattern: chemosensory clusters not only keep farthest to each other, but also to Z-rings. Occasionally (21% of cells), Z-rings were not positioned at the mid- or quarter-cells, and concomitant exclusions of membrane chemosensory clusters were seen (Fig. 6.2, lower panel). These results suggest that although stochastic self-assembly may participate in the positioning of membrane chemosensory clusters in *R. sphaeroides*, the final positions are not correlated with future cytokinetic sites. Indeed, the membrane clusters appear unable to localise to the cytokinetic sites.

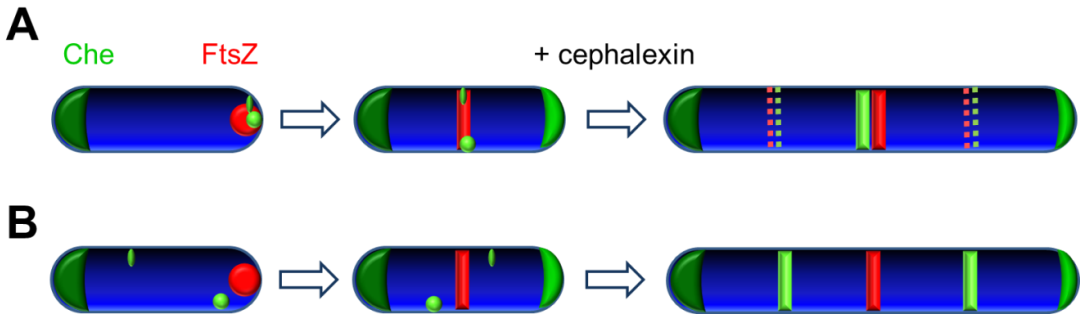

Figure 6.1. Simplified schematics for the relative positioning between FtsZ (red) and membrane chemosensory clusters (green). **(A)** Predicted patterns for membrane cluster localisation via stochastic self-assembly/cytokinetic site-association before and after filamentation. The left and middle cells represent newborn and elongating cells, respectively. **(B)** The observed patterns.

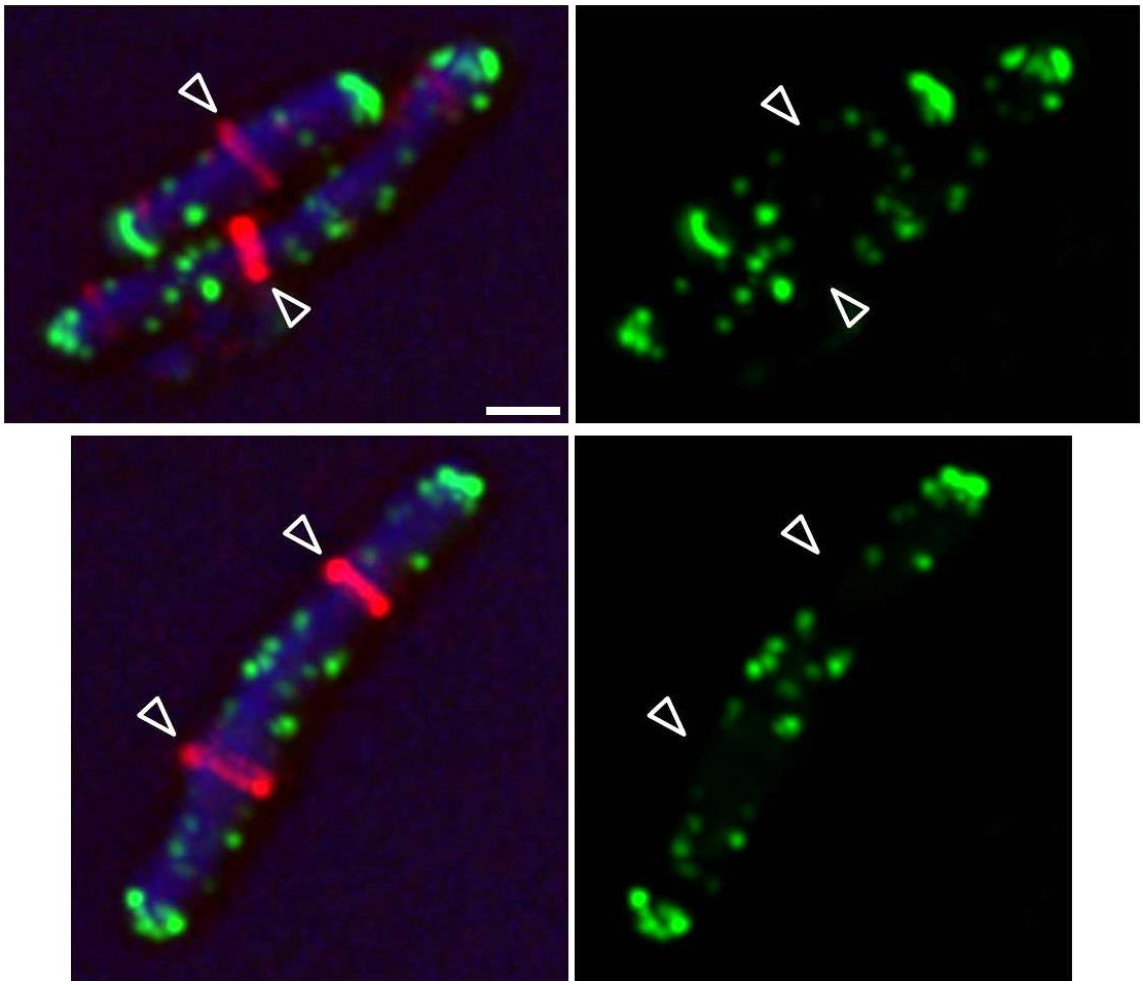

Figure 6.2. Localisations of the Z-ring and membrane chemosensory clusters in cephalexin-treated cells. Images show that the Z-ring and lateral membrane chemosensory clusters do not colocalise. Arrowheads: positions of Z-rings. Green: YFP–CheW$_3$; red: FtsZ–CFP; blue: DIC. Scale bar: 1 μm.

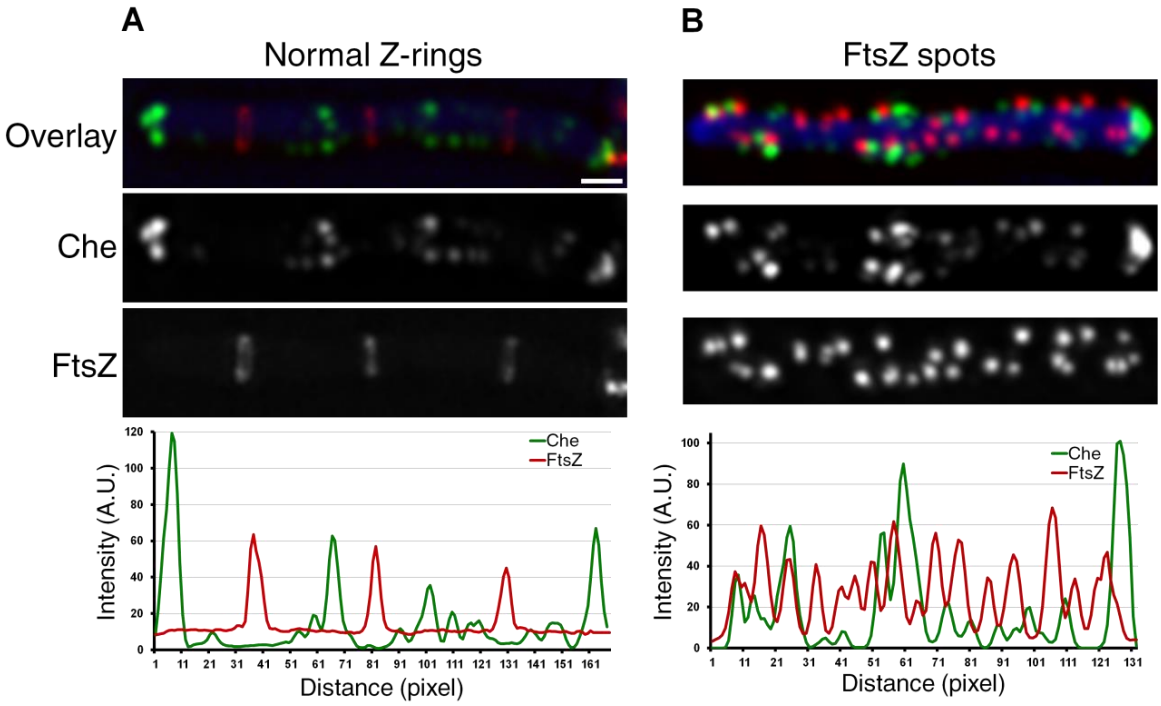

Figure. 6.3. Relative positions between different FtsZ assemblies and membrane chemosensory clusters in filamentous cells. Intensity profiles along the long cell axes are shown for YFP–CheW$_3$ and FtsZ–CFP. **(A)** A cephalexin-treated cell with normal Z-rings. **(B)** FtsZ-overexpressing cells (induced with 250 μM IPTG for overnight) showing FtsZ spots and no Z-rings. Membrane chemosensory clusters and FtsZ spots are close but do not colocalise when examined in 3D. One pixel is equal to 0.065 μm.

6.3 Membrane Chemosensory Clusters and FtsZ Do Not Colocalise

The relative positioning between Z-rings and membrane chemosensory clusters in filamentous cells showed that they do not colocalise. I next examined their relative positioning in normal cells. Consistently, Z-rings and membrane chemosensory clusters did not colocalise in normal cells (Figs 6.1 B and 6.4), even for the extensively constricted Z-rings (Fig. 6.4, yellow arrowheads). Surprisingly, membrane chemosensory clusters also did not colocalise with FtsZ polar spots (Fig. 6.4, white arrowheads). Moreover, this unipolar localisation could be seen for some newborn cells which already had midcell Z-rings/ring precursors (Fig. 6.4, blue arrowheads). These observations have two important implications: (1) the bipolar localisation of *R. sphaeroides* membrane chemosensory clusters is

established after cell division (examined in Chapter 8) (2) FtsZ assemblies may somehow prohibit membrane chemosensory clusters from localizing in their vicinities (because otherwise a simple stochastic self-assembly process will result in midcell and bipolar localisations disregarding the presence of FtsZ assemblies). For the second implication, it is still possible that a certain concentration of chemosensory proteins is required before a new-pole or midcell cluster can form. However, there was no obvious correlation between the amount of chemosensory proteins in the cell and the appearance of new-pole clusters (Fig. 6.5). Besides, the ± 10% of cell length region around the midcell did not contain any detectable membrane chemosensory clusters (Fig. 6.5), consistent with the results for filamentous cells: membrane chemosensory clusters did not colocalise with the Z-ring/cytokinetic site. These results also argues against a purely stochastic self-assembly process in the positioning of membrane chemosensory clusters in *R. sphaeroides*. Similar relative localisation patterns were seen for FtsZ and membrane clusters chemosensory in photoheterotrophic cells (Fig. 6.6).

Time-lapse imaging was used to further investigate these phenomena. Intriguingly, membrane chemosensory clusters moved into the very tip of the new pole once FtsZ polar spots were no longer present (Fig. 6.7). Although diffraction-limited images occasionally show them to be close (Fig. 6.7, 20′), FtsZ polar spots never colocalised with new-pole clusters when examined in 3D. I sought to explore whether this is just a coincidence of the timing of two independent processes.

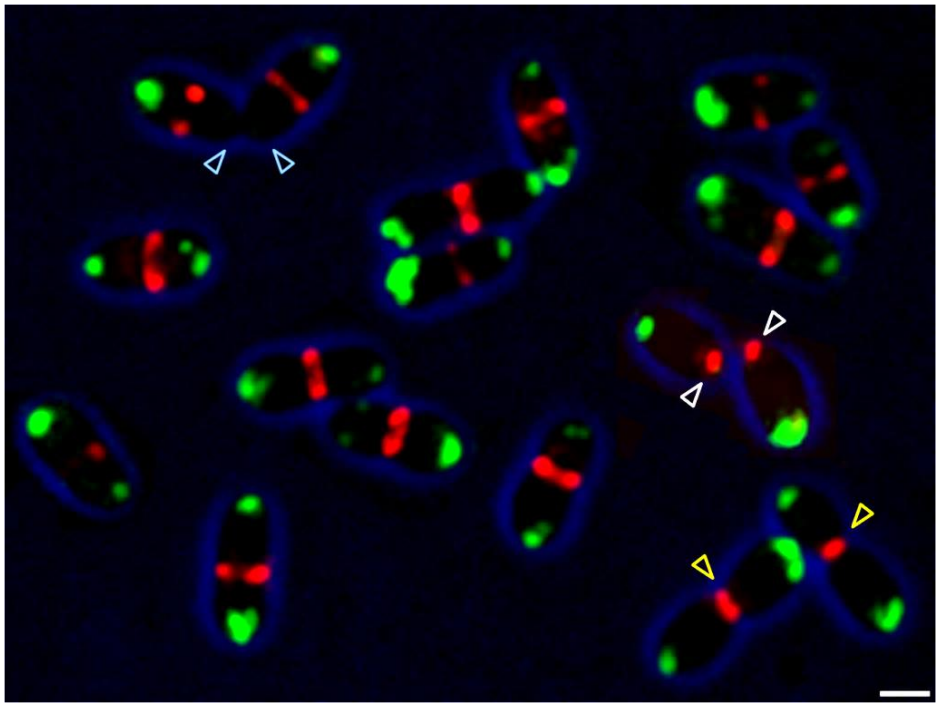

Figure 6.4. Localisations of FtsZ and membrane chemosensory clusters in normal cells. Arrowheads: blue, newborn cells with midcell Z-ring/ring-precursor but no new-pole chemosensory clusters; white, newborn cells with FtsZ polar spots but no new-pole chemosensory clusters; yellow, cells with extensively constricted Z-rings. Green: YFP–CheW$_3$; red: FtsZ–CFP; blue: inverted DIC. Scale bar: 1 μm.

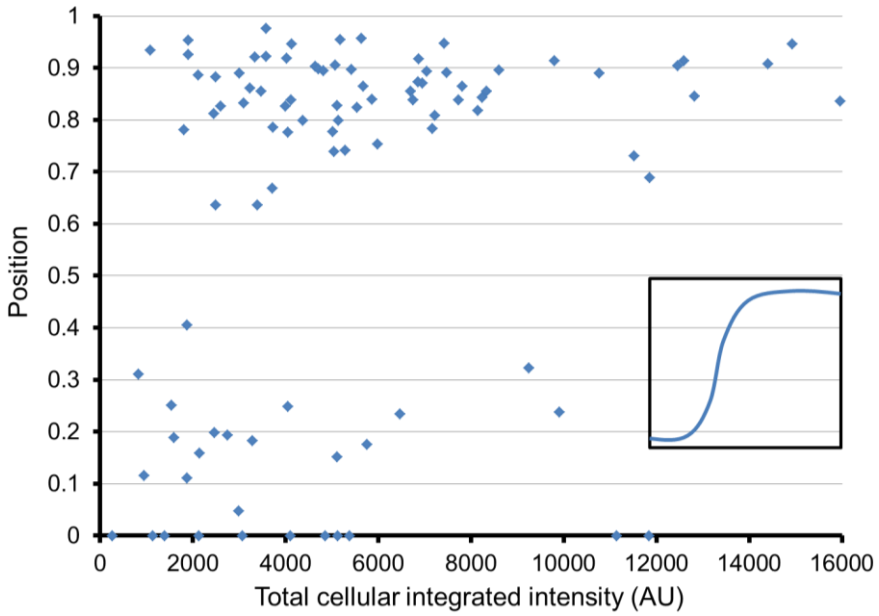

Figure 6.5. The relationship between the amount of YFP–CheW$_3$ and the formation of new-pole clusters. Position: normalized distance of any given clusters to the tip of the old pole. Inset: a simplified theoretical pattern showing if there had been a positive correlation. N=95.

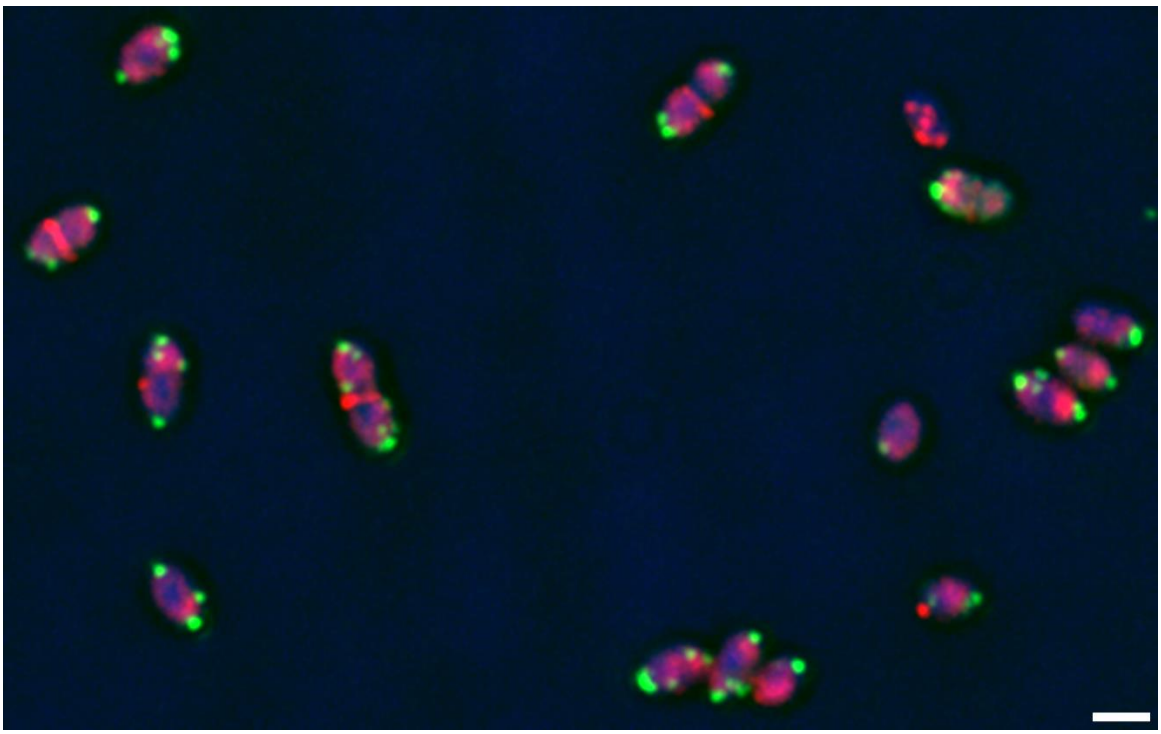

Figure 6.6. Localisation patterns of FtsZ and membrane chemosensory clusters in photoheterotrophic cells. Note that the cells have strong peripheral cyan fluorescence signals (shown in red channel here) from the photosynthetic pigments. Green: YFP–CheW$_3$; red: FtsZ–CFP; blue: DIC. Scale bar: 1 μm.

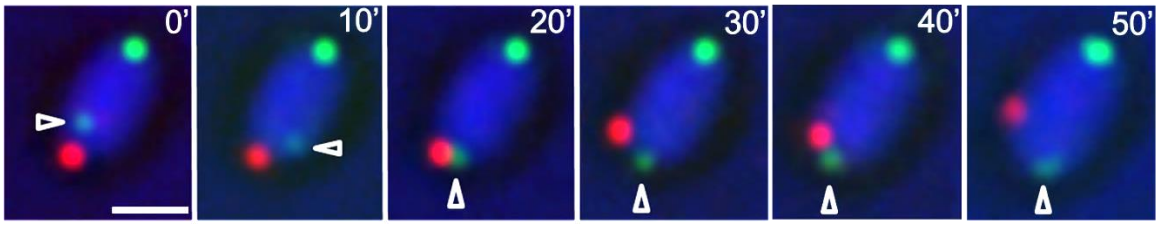

Figure 6.7. FtsZ and membrane clusters do not colocalise at the new pole. Arrowheads: a membrane cluster moves into the new pole. Green: YFP–CheW$_3$; red: FtsZ–CFP; blue: DIC. Numbers: minutes. Scale bar: 1 μm.

Blocking cytokinesis, which consequently delays the redistribution of FtsZ and formation of new-poles, should accelerate the relative timing of new-pole cluster formation if there is merely a coincidence of timing (Fig. 6.8, left part of the schematics). If the membrane curvature of the cell pole is the main determinant for polar chemosensory cluster localisation (Endres, 2009), releasing cells from cephalexin treatment should also accelerate the formation of new-pole

clusters. If however the presence of Z-rings/FtsZ polar spots at the forming new pole affects the establishment of new-pole clusters, we should see a time delay (Fig. 6.8, right part of the schematics). Small membrane chemosensory clusters gradually moved into the new pole only after FtsZ started leaving (Fig. 6.8; seen in 88.6% of cells, n = 88). The simplest explanation is that chemosensory clusters move from the old poles or lateral sites, diffuse around the cell, but are excluded from the developing new poles by constricting Z-rings. The completion of cytokinesis allows the laterally accumulated clusters to diffuse into the new poles. Moreover, the data support the notion that new-pole clusters are formed after cell division.

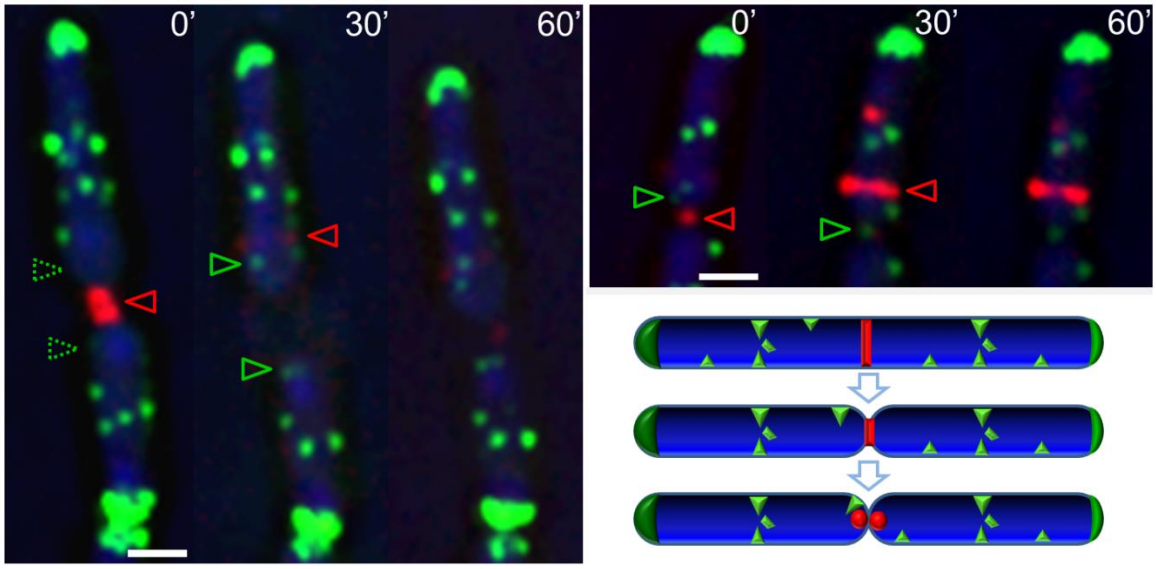

Figure 6.8. The positions of the membrane chemosensory cluster relative to FtsZ in cells released from cephalexin treatment. Green: YFP–CheW$_3$; red: FtsZ–CFP; blue: DIC. Red arrowheads: FtsZ assemblies. Dashed and solid green arrowheads: zones without and with detectable membrane clusters respectively. Numbers: minutes. Schematic: possible scenarios of membrane cluster formation at the new pole. Left compartment: If membrane curvature is the ultimate cue for new-pole targeting of the membrane cluster, releasing the cells from cephalexin treatment should result in colocalisation of FtsZ and membrane clusters at the new pole once the typical membrane curvature has formed for a stochastic process (i.e. the membrane cluster will move into and stay at the polar region in the presence of FtsZ). Right compartment: In another scenario, the presence of FtsZ at the new pole affects the polar localisation of membrane clusters. Scale bars: 1 μm.

From the above data, it seems that the Z-ring inhibits/constrains membrane chemosensory clusters from accumulating at cytokinetic sites, while FtsZ polar spots might have a different effect (e.g. steric hindrance) at cell poles. Overexpression of FtsZ in *R. sphaeroides* resulted in randomly distributed spots (Fig. 6.3 B and Chapter 3). Close proximity of FtsZ and membrane chemosensory clusters was only observed for FtsZ spots, not for Z-rings (Fig. 6.3). Accordingly, membrane chemosensory clusters localised as proposed for a stochastic self-assembly pattern (i.e. the "default" pattern) in FtsZ-overexpressing cells lacking Z-rings (Fig. 6.3 B). This observation indicates that the Z-ring (or associated factors) modifies the localisation pattern of membrane chemosensory clusters in *R. sphaeroides*, while the FtsZ polar spot only has steric hindrance effects. Intriguingly, when FtsZ polar spots occasionally moved back to the very tips of cell poles, it appears they may displace chemosensory clusters localised there (Fig. 6.9).

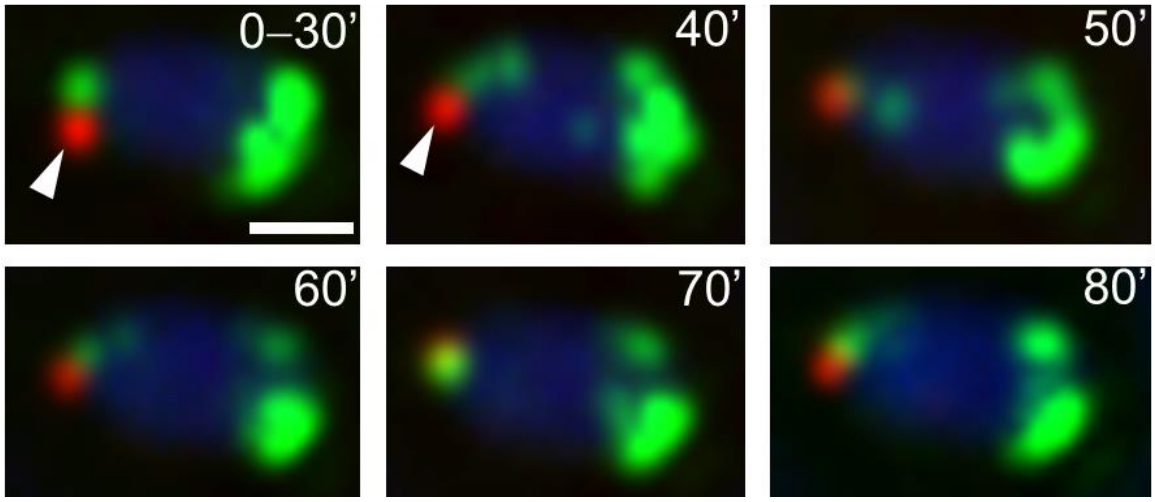

Figure 6.9. FtsZ polar spots displace membrane chemosensory cluster at the cell pole. Arrowheads: an FtsZ polar spot shifts back to the cell tip. The FtsZ polar spot and membrane chemosensory cluster are static for the first 30 min, then the FtsZ spot moves back to the very tip. The chemosensory cluster concomitantly changes its localisation and dynamically moves around the cell pole. Green: YFP–$CheW_3$; red: FtsZ–CFP; blue: DIC. Numbers: minutes. Scale bars: 1 μm.

As a huge macromolecular assembly that alters the cell envelope, the Z-ring/divisome may exclude other proteins from its vicinity. I sought to further explore this by following the dynamics of lateral chemosensory clusters relative to the Z-ring in cephalexin-treated cells. The average distance between Z-rings

and their nearest lateral clusters is 324±100 nm (n = 92) (Fig. 6.10 C). This result suggests a region covering ~300 nm at both sides of the Z-ring is unfavourable for the localisation of membrane chemosensory clusters in *R. sphaeroides* (Fig. 6.10). Interestingly, although membrane chemosensory clusters could stay close to the Z-ring transiently, they would eventually leave the Z-ring vicinity (Fig. 6.10 A, arrowheads). This result also shows that unlike *E. coli* (Thiem et al., 2007), lateral chemosensory clusters were dynamic rather than static in *R. sphaeroides*.

To summarise, the Z-ring/divisome could prohibit membrane chemosensory clusters from localising at its vicinity, but the FtsZ polar spot only showed steric hindrance effect (Fig 6.11).

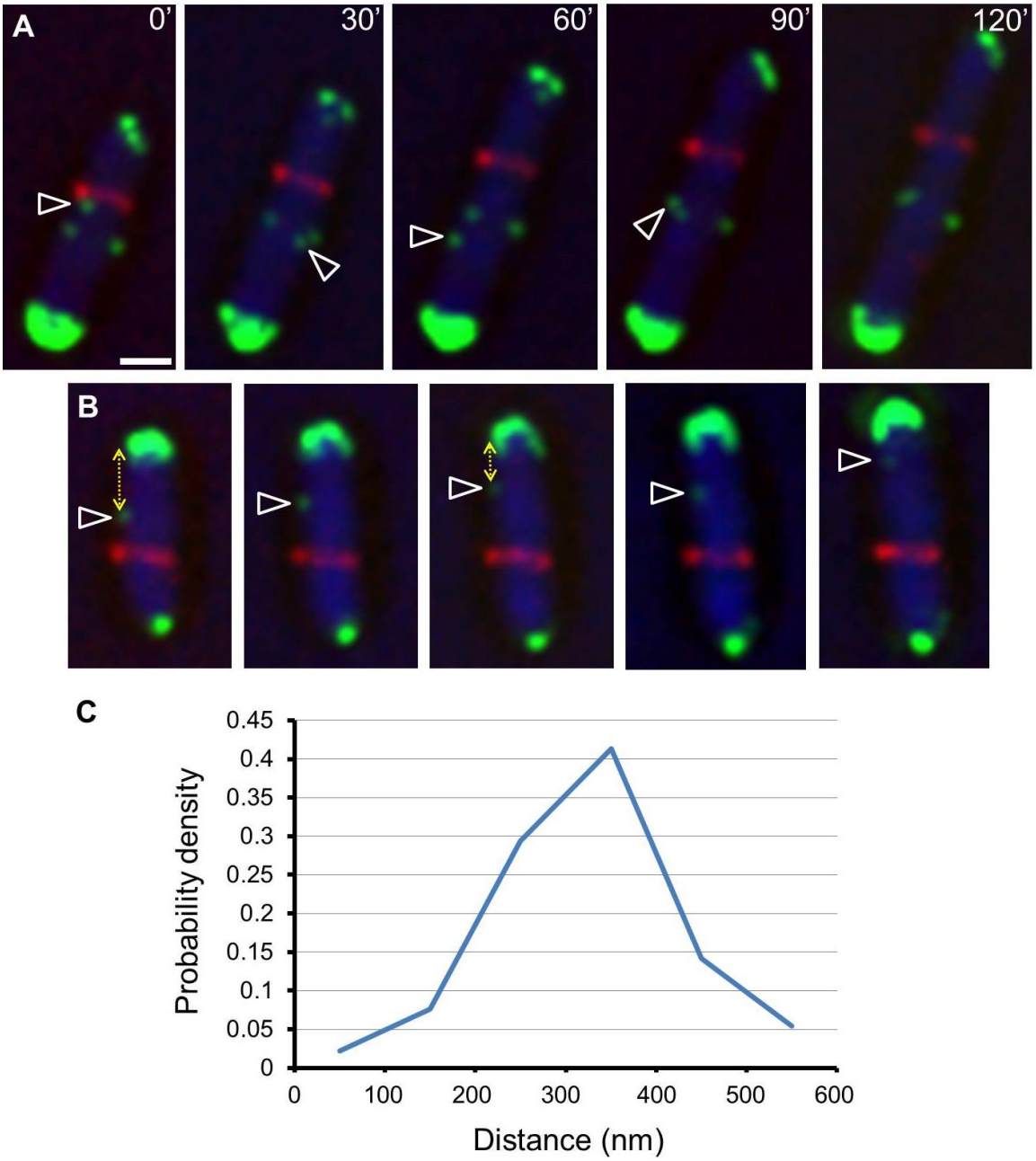

Figure 6.10. Dynamics of lateral chemosensory clusters relative to the Z-ring in cephalexin-treated cells. Green: YFP–CheW$_3$; red: FtsZ–CFP; blue: DIC. Numbers: minutes of observation. Scale bar: 1 μm. **(A)** A membrane cluster initially localises close to the Z-ring, but soon moves away (arrowheads). Overall, the cluster stays outside the Z-ring vicinity. **(B)** The movement of lateral chemosensory clusters is discontinuous. The distance between the moving cluster and the cell pole becomes shorter (yellow arrows), suggesting the cluster is not passively pushed (e.g. by the cell elongation process). **(C)** The probability density function plot for finding a membrane cluster within the vicinity of the Z-ring. X-axis is the distance from the cluster to the Z-ring.

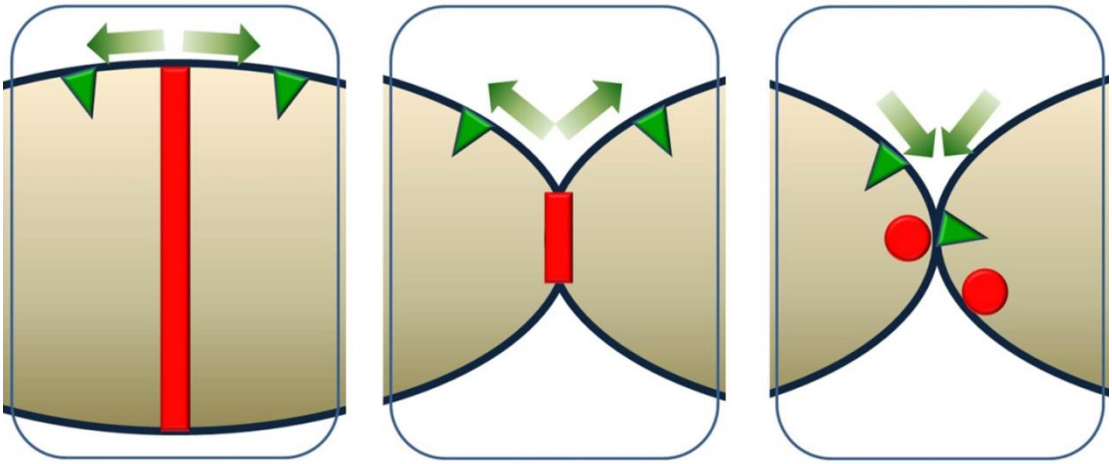

Figure 6.11. The effects of FtsZ assemblies (red) or associated factors on the localisation of membrane chemosensory clusters (green). Chemosensory clusters are unable to stay in the vicinity of unconstricted (left) and constricting (middle) Z-rings, and show an overall away-from-the-Z-ring behaviour (green arrows). FtsZ polar spots only have a steric hindrance effect (right), so chemosensory clusters can move into the cell pole (green arrows) but only set at the regions not occupied by FtsZ spots.

6.4 Discussion and Conclusions

The current model for membrane chemosensory cluster positioning in most bacteria is a mechanism combining stochastic self-assembly and cytokinetic site-anchoring (Greenfield et al., 2009; Thiem et al., 2007; Thiem and Sourjik, 2008; Wang et al., 2008a). The stochastic self-assembly process can explain how the formation of lateral clusters could **initiate** at the periodic midcell, quartercells, etc. positions. However, it cannot explain why lateral clusters could statically stay there (i.e. **maintenance**). An anchor is required, and the Z-ring/divisome is a promising candidate (Dworkin, 2009; Laloux and Jacobs-Wagner, 2014). In this chapter I directly tested this possibility. Surprisingly, *R. sphaeroides* lateral chemosensory clusters show very different characteristics comparing to those in *E. coli*: they are dynamic and do not localise at cytokinetic sites. Moreover, the "common" bipolar localisation of *R. sphaeroides* membrane chemosensory clusters is established after cell division. These interesting behaviours are further explored in Chapter 7.

Another striking observation is the "exclusive" effects of FtsZ assemblies on the positioning of membrane chemosensory clusters. Although FtsZ spots seem to only have a steric-hindrance effect on the localisation of membrane

chemosensory clusters, the Z-ring shows a striking exclusive effect around it. There are three possibilities. Firstly, the Z-ring/divisome may create an environment with different physicochemical properties in its vicinity (Lopez-Montero et al., 2012). These differences may prevent membrane chemosensory clusters to localise in the Z-ring/divisome vicinity. Secondly, cell elongation taking place around the Z-ring (Aaron et al., 2007; Slovak et al., 2006; Slovak et al., 2005) may passively push membrane chemosensory clusters away. However, the behaviours of membrane chemosensory clusters (Fig. 6.10 A and B) do not support this notion. But I cannot exclude the possibility that cell elongation aids in the exclusion process. Thirdly, it may be a result of different dynamics of the membrane chemosensory clusters in *E. coli* and *R. sphaeroides*. Unlike the static clusters in *E. coli* (Thiem et al., 2007), membrane chemosensory clusters are dynamic in *R. sphaeroides*. The huge Z-ring/divisome may act as a barrier to the movement of membrane chemosensory clusters in *R. sphaeroides*. Thus, the movement of membrane chemosensory clusters is restricted between the cell poles and the Z-ring/divisome. Then, random movements of membrane clusters between the Z-ring/divisome and cell poles will produce a time-averaged position roughly at the centre (away from the Z-ring). However, this scenario cannot explain the delayed accumulation of membrane clusters at forming new poles (Fig. 6.8).

The striking differences between the positioning of membrane chemosensory clusters in *R. sphaeroides* and *E. coli* could be resulted from the putative differences in their Z-rings/divisomes or septa/constrictions (Cava et al., 2013; Judd et al., 2005). It is also possible that their membrane chemosensory clusters have differences that render them interact differently with the otherwise similar Z-rings/divisomes.

For *E. coli* chemosensory clusters, the identity of the anchor at the cytokinetic site remains unknown. Nevertheless, the applicability of the stochastic self-assembly/cytokinetic site-anchoring mechanism is unclear, since it is developed solely based on the studies of one specific bacterium. In addition to *R. sphaeroides*, high proportions of *P. aeruginosa* (Bardy and Maddock, 2005; Güvener et al., 2006; O'Connor et al., 2012) and *S. meliloti* (Meier and Scharf, 2009) cells show unipolar localisation of membrane chemosensory clusters. This is also true for *E. coli* (Maddock and Shapiro, 1993; Ping et al., 2008). The presence of a high-proportion of unipolar cells is not directly against the stochastic self-assembly/cytokinetic site-anchoring mechanism, but does hint at the probable existence of different mechanisms (Ringgaard et al., 2011). Moreover,

the localisation pattern of membrane chemosensory clusters in *P. aeruginosa* suggests a mechanism closer to that proposed for *R. sphaeroides* here (Chapter 8).

In conclusion, FtsZ and membrane chemosensory clusters do not colocalise in *R. sphaeroides*, and the Z-ring is not a cytoskeletal anchor for lateral clusters. However, the exclusive effect associated (directly or indirectly) with the Z-ring and a stochastic self-assembly process may synergistically determine the positioning of membrane chemosensory clusters in *R. sphaeroides*.

Chapter 7. Membrane Chemosensory Proteins Form Dynamic Unit-clusters

Coming together is a beginning; keeping together is progress; working together is success.

— Henry Ford

7.1 Aims

In contrast to other bacteria (Güvener et al., 2006; Thiem et al., 2007) , time-lapse imaging shows a very dynamic behaviour of membrane chemosensory clusters in *R. sphaeroides* (Figs 6.7—6.10). In this chapter, I conducted further investigations on this dynamic behaviour to have a better understanding of its biological implications.

7.2 Membrane Chemosensory Clusters Are Dynamic

The polar "caps" formed by membrane chemosensory proteins have been viewed as single large, static entities (Greenfield et al., 2009; Ping et al., 2008; Schulmeister et al., 2008; Zhang et al., 2007). However, my observations suggest that in *R. sphaeroides*, the polar caps are composed of smaller, dynamic clusters. The polar caps changed their shapes continuously (e.g. Fig. 6.9 and 6.10) as these small clusters congregate and segregate (Figs 7.1 and 7.2). Polar and lateral chemosensory clusters are both dynamic (Figs 7.1 and 6.10 A and B). In contrast, only polar clusters are mobile in *E. coli* (Thiem et al., 2007).

Tracking the membrane chemosensory clusters showed they were dynamic and moved randomly in the membrane. Small clusters could move within the cell pole (Figs 7.1 and 7.2) or along the lateral site (Fig, 6.10), move from the lateral site into the cell pole (Fig. 6.7), or vice versa (Chapter 8). Single-particle tracking showed that lateral chemosensory clusters have a diffusion coefficient *D* of

$4.1 \times 10^{-3} \pm 3.0 \times 10^{-3}$ $\mu m^2\ min^{-1}$, with an average velocity of 17±6 nm min^{-1}, and a maximum of ~80 nm min^{-1}. The velocity is comparable to the mobile polar clusters in *E. coli* (Thiem et al., 2007). Individual lateral clusters frequently showed pauses with varied time length (mean = 41.5±28.1 min, n = 34 clusters; Fig. 6.10 A and B). However, the mean square displacement (MSD) versus time interval plots of most trajectories (74%) can be fitted with a straight line ($R^2 = 0.97 \pm 0.03$), indicating normal Brownian diffusion. The other 26% showed sub-diffusion-like patterns. The pauses and constrains could be caused by transient encounters with membrane obstacles like cell-wall synthesis machinery. Interestingly, *E. coli* polar clusters also show discontinuous movements (Thiem et al., 2007).

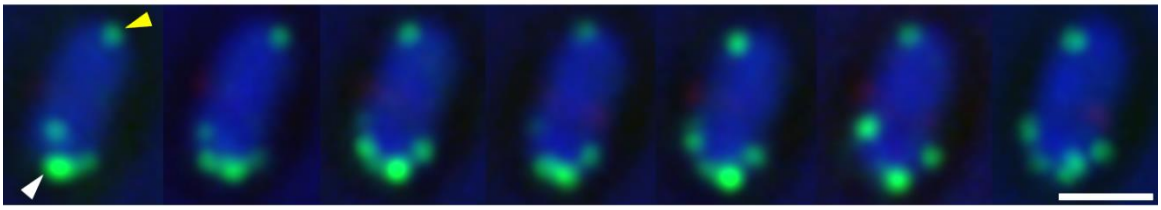

Figure 7.1. Time-lapse images of YFP–$CheW_3$ demonstrating that the polar "cap" (white arrowhead) is composed of several smaller clusters which congregate and segregate continuously. The single new-pole cluster (yellow arrowhead) is also dynamically moving around the cell pole. Green: YFP–$CheW_3$; red: FtsZ–CFP; blue: DIC. The interval between time frames is 10 min. Scale bar: 1 μm.

7.3 Membrane Chemosensory Clusters Have a Unit-size

The dynamic behaviour of polar chemosensory clusters (Fig. 7.1) shows that the "polar cap" was composed of smaller, dynamic clusters. It also suggests that there may be a basic unit of membrane chemosensory proteins, and the polar caps or bigger clusters are formed from dynamic congregation–segregation of these "unit-clusters" (Fig. 7.2 B, schematics). This idea is supported by quantifying the intensities of small clusters over time (Fig. 7.2 A and B). The mean autocorrelation value is 0.9960 ± 0.0664 (n=17 cluster pairs). It should be noted that these unit-clusters were not rigid, they could change shapes, and congregation-segregation processes could result in contaminant intensity gain/loss of participating clusters. Despite this flexibility, chemosensory proteins seem to form independent unit-clusters.

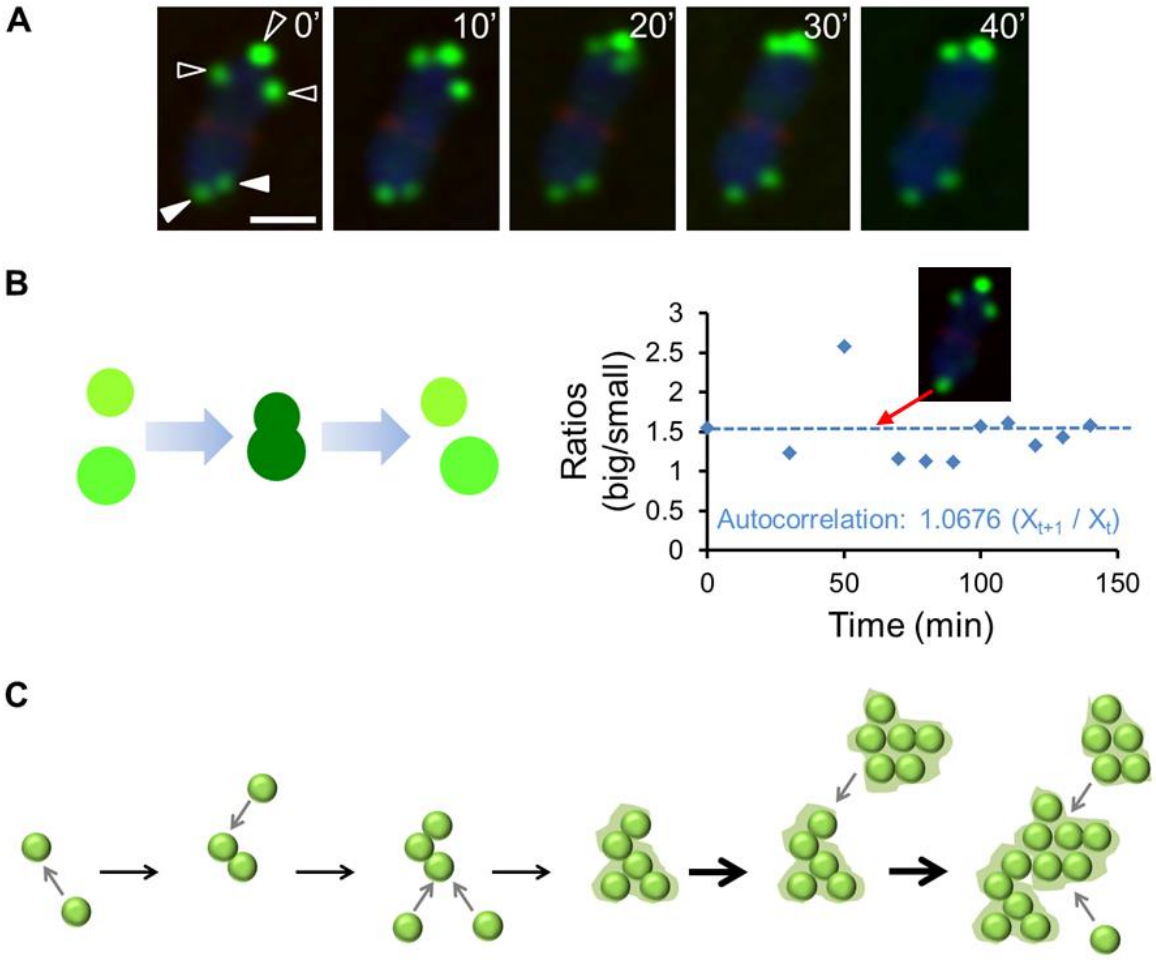

Figure 7.2. The membrane chemosensory clusters might operate as unit-clusters. **(A)** Time-lapse images of YFP–CheW$_3$ demonstrating that the polar "cap" is composed of several smaller clusters (arrowheads) which congregate and segregate continuously. Green: YFP–CheW$_3$; red: FtsZ–CFP; blue: DIC. Numbers: minutes. Scale bar: 1 μm. **(B)** The intensities of two YFP–CheW$_3$ clusters (filled arrowheads in (A) were monitored over time and the ratios between them are shown. The mean autocorrelation value (x_{t+1}/x_t) is given. If membrane clusters operate as unit-clusters, the intensity ratios should keep constant after congregation–segregation (schematic). The time points without values represent congregations of the two clusters (e.g. red arrow and inset). **(C)** A model for the formation of unit-clusters (shaded) (corresponding to the first phase in Fig. 7.5; black thin arrows) and congregation of unit-clusters (second phase in Fig. 7.5; black thick arrows). Each sphere represents an oligomer of chemosensory proteins.

I observed similar localisation patterns for chemosensory receptors McpB and McpG (Fig. 7.3), suggesting this is not specifically connected to the chemosensory protein fusion (YFP–CheW$_3$) used. Therefore, membrane chemosensory proteins formed independently moving dynamic unit-clusters which may have a maximum size. Strikingly, although the cellular distributions of McpB and McpG were close, they were not identical (Fig. 7.4). In some cells, a cellular region may have only one type of receptors (Fig. 7.4, arrowheads). Further studies are required for clarifying the molecular architecture of these chemosensory clusters (e.g. whether they form mixed clusters in colocalised areas). Nevertheless, this observation reinforces the idea that the polar cap is not a single huge entity, it is composed of teams of chemosensory proteins.

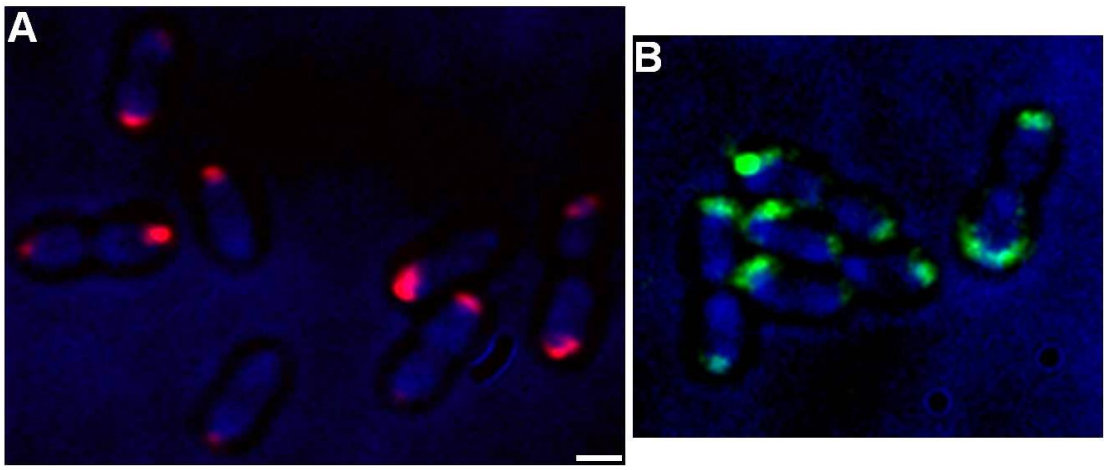

Fig. 7.3. Localisation patterns of chemosensory receptors in *R. sphaeroides* cells. **(A)** McpB–RFP (red). **(B)** McpG–GFP (green). Blue: DIC. Scale bar: 1 μm.

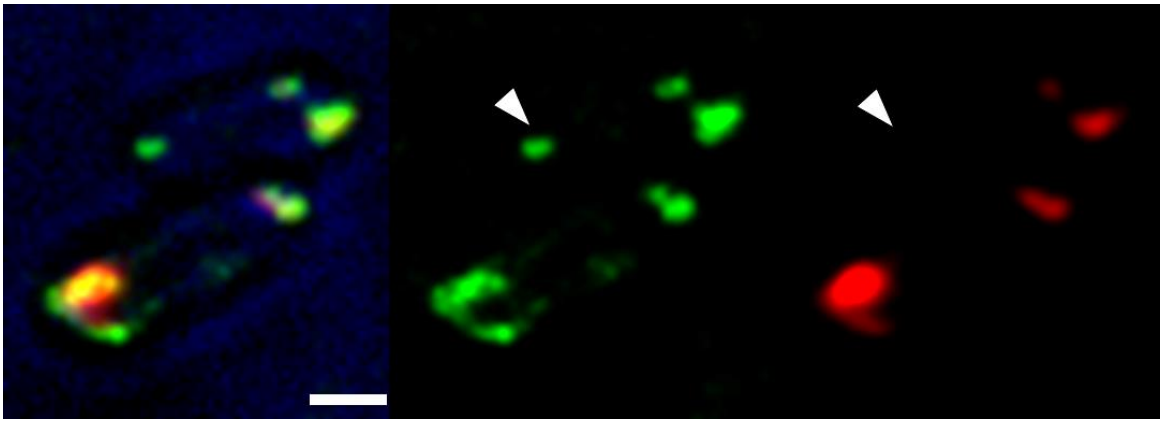

Fig. 7.4. Chemosensory receptors probably form distinct clusters in *R. sphaeroides*. Left: merged image; middle: McpG–GFP; right: McpB–RFP. Blue: DIC. Arrowheads: a region only with detectable McpG–GFP cluster but no McpB–RFP cluster. Scale bar: 1 μm.

To estimate the size of unit-clusters, I ranked membrane chemosensory clusters in snapshots according to their intensities. In a snapshot of asynchronous samples, ranking the intensity of clusters could provide the temporal information about cluster formation similar to what could be obtained from time-lapse images. The distribution of cluster intensity shows a two-phase pattern (Fig. 7.5) which can be explained by a unit-cluster model (Fig. 7.2 C), with unit-clusters growing by assembling processes (first linear phase in Fig. 7.5), with end of the linear phase representing the average size of unit-clusters. The second exponential phase represents the combination (congregation) of growing and mature unit-clusters (Fig. 7.2 C). It should be noted that the first linear phase does not imply that the unit-clusters grow linearly, since exponential growth with a small increase rate could also result in a good linear fit. Instead, the two-phase pattern indicates the nature of dominant assembling components (e.g. oligomers or unit-clusters).

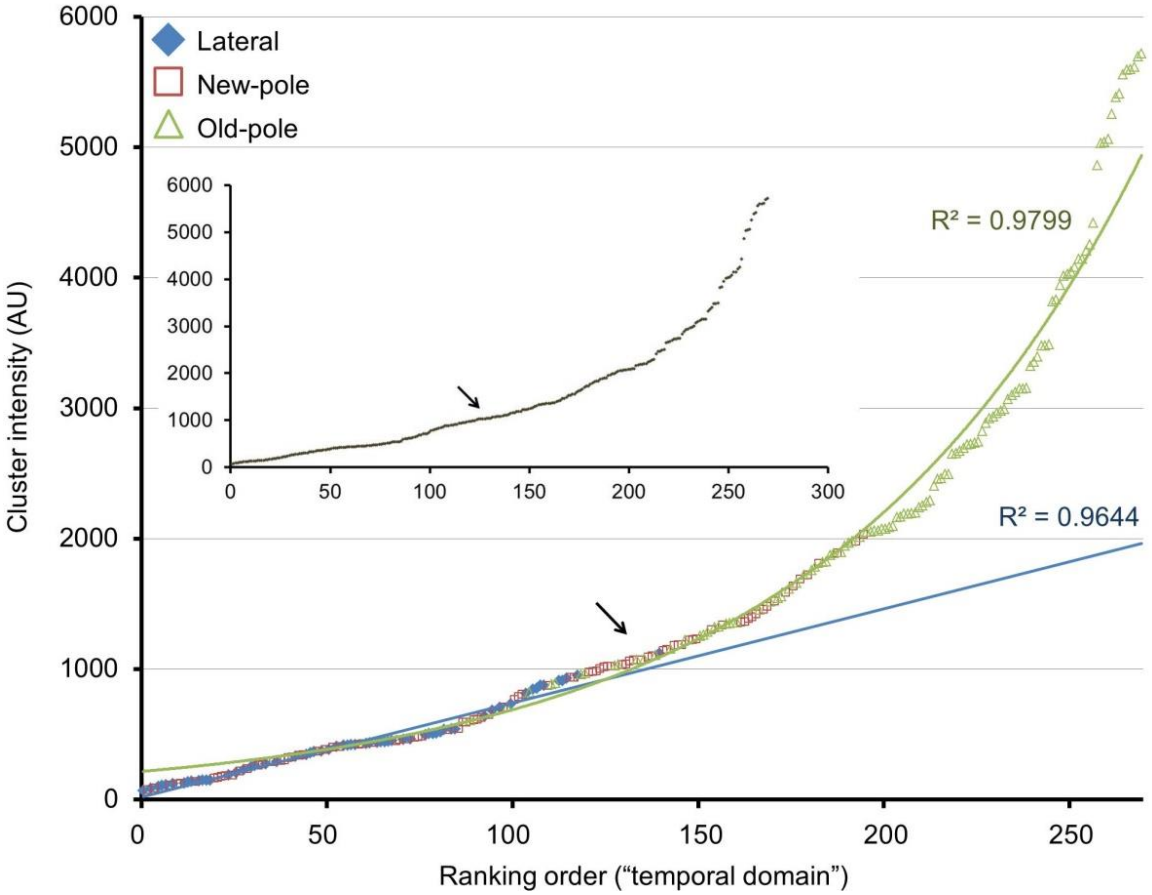

Fig. 7.5. Intensity-ranking analyses of membrane chemosensory clusters. Membrane clusters are ranked by their intensities from snapshots of normal cells. A two-phase distribution can be seen (1st linear and 2nd exponential). The transition point (arrow) may represent the average size of unit-clusters. Distinct

distributions of lateral, new-pole, and old-pole clusters are observed in the intensity-ranking curve (inset: pool of all clusters). Lateral clusters are within the linear phase, and most old-pole clusters are within the exponential phase. New-pole clusters are within the linear phase and about the first 1/3 portion of the exponential phase. Regression lines and their R^2 are shown for lateral and new-pole clusters. Here, one arbitrary unit (AU; count on our camera detector) roughly equal to 1.95 proteins.

Since membrane chemosensory clusters are better separated in filamentous FtsZ-overexpressing cells, I performed intensity-ranking analyses on these cells for the average size of unit-clusters by correlating fluorescence intensity to quantitative fluorimetry data (Wilkinson et al., 2011). The data suggest an average of ~1,100 $CheW_3$ proteins per unit-cluster. Mapping each cluster to the intensity-ranking curve by its localisation reveals striking patterns (Fig. 7.5). The first linear phase is mainly composed of lateral and new-pole clusters, while the second exponential phase is composed of new-pole and old-pole clusters (Fig. 7.5). The distribution patterns suggest lateral clusters are basically growing unit-clusters, old-pole clusters are essentially congregations of multiple unit-clusters, and new-pole clusters can be made of either one or more unit-clusters. The average intensity of lateral clusters is ~470 counts on our imaging setup (corresponding to ~920 $CheW_3$ molecules), coinciding with the plateau-like region of intensity-ranking curve (Fig. 7.6, dashed circle). The intensities of larger lateral clusters bunch together around a value (Fig. 7.6, solid circle) about twice of that of the plateau-like region, suggesting these larger lateral clusters are composed of two unit-clusters. The intensity-ranking curve of new-pole clusters also shows a first linear phase (Fig. 7.7). The intensity value at the transition point is ~500 counts (corresponding to ~970 $CheW_3$ molecules). Taken together, the estimations of unit-cluster size from the intensity distributions of lateral and new-pole clusters in normal cells, as well as clusters in filamentous cells, suggest a value of ~920–1,100 $CheW_3$ proteins per unit-cluster.

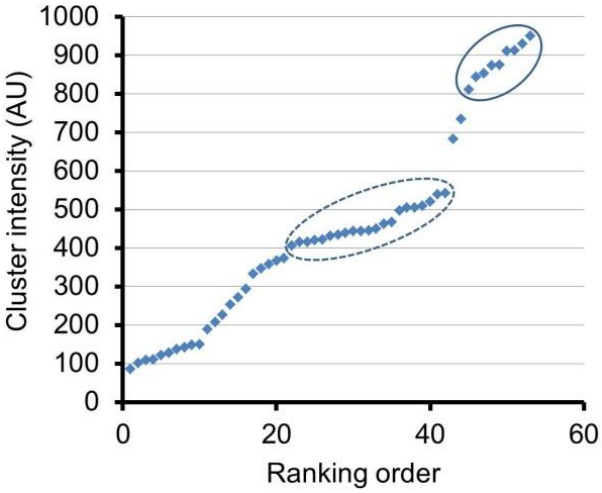

Fig. 7.6. Intensity-ranking for lateral clusters. The curve agrees with the clusters grow and reach the unit-size (plateau-like region, dashed circle), and two unit-clusters congregate (solid circle).

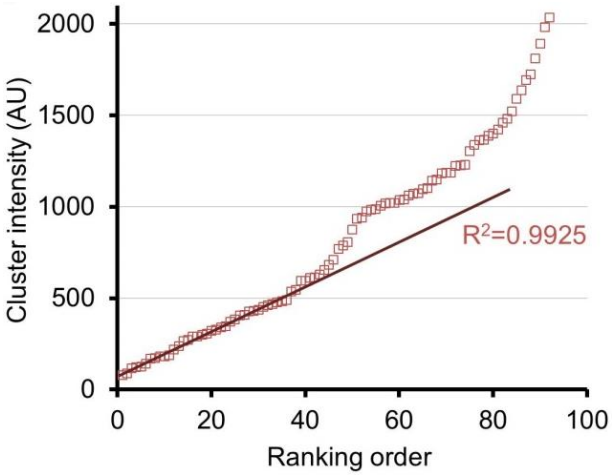

Fig. 7.7. Intensity-ranking for new-pole clusters. Regression line and its R^2 are shown for the linear phase.

7.4 Discussion and Conclusions

While many of the previous fluorescence and cryo-electron microscopy data have suggested that membrane chemosensory proteins form massive polar clusters, my data suggest that in *R. sphaeroides* there is an optimum cluster size and these smaller dynamic clusters are free to diffuse, but tend to accumulate at the poles (see Chapter 8 for more details). Similar congregation–segregation process of polar clusters (Thiem et al., 2007) and pattern of intensity-ranking plots (Ping et al., 2008) have been reported for *E. coli*. Thus, it is possible that the unit-cluster idea could be applied to other bacteria.

Individuality in the crowd: unit-clusters of membrane chemosensory proteins

Quantification of fluorescence intensities from lateral clusters in normal and filamentous *R. sphaeroides* cells suggests an average size for unit-cluster of about 1,000 $CheW_3$ molecules. As quantitative fluorimetry data suggest an average of 8,700±260 $CheW_3$ molecules per cell (with the majority present in membrane clusters) (Wilkinson et al., 2011), this suggests six to eight clusters per unit cell, which correlates well with the numbers seen in normal and filamentous cells when clusters were segregated (e.g. Figs 6.2 and 7.1).

Fission and fusion of polar chemosensory clusters occur in *E. coli* (Thiem et al., 2007). However, since polar clusters were viewed as single entities (Thiem and Sourjik, 2008), the significance of these behaviours was underestimated before. Intriguingly, the growth rate of *E. coli* clusters correlates negatively with cluster size: smaller clusters show an average positive growth rate, whereas larger clusters shrunk over time (Thiem and Sourjik, 2008). The unit-cluster idea (Fig. 7.2 B and C) can explain this phenomenon, as well as the size-distribution of chemosensory clusters in *E. coli* (Greenfield et al., 2009; Ping et al., 2008). Intriguingly, a current report shows that 93% of chemoreceptor Tsr molecules are confined within small areas (170–290 nm) near the cell pole (Oh et al., 2014). Whether similar unit-clusters exist for other bacterial membrane chemosensory systems remains as an interesting unanswered question. However, it is worthy to mention that in *V. cholerae*, which utilizes polar anchorage to position membrane chemosensory clusters, CheW only forms a single cluster at each pole and does not form lateral clusters in normal cells (Ringgaard et al., 2011; Ringgaard et al., 2014; Yamaichi et al., 2012). Cryo-electron tomography revealed that polar chemosensory clusters in *V. cholerae* are about six fold lager than those in *R. sphaeroides* (Briegel et al., 2009). It is possible that in *V. cholerae* the polar anchor ParP constrains the distribution of CheA (Ringgaard et al., 2014), which forces chemoreceptors, CheA, and CheW to form a huge polar cluster or multiple closely positioned small clusters.

The exact size of the whole unit-cluster is difficult to estimate at this moment, since the stoichiometry of $CheW_3$ to other components is unclear in *R. sphaeroides*. Even for the extensively studied *E. coli* system, the ratio between chemoreceptors and CheW is highly variable (1.5–7) among different studies (Briegel et al., 2012; Li and Hazelbauer, 2004, 2011; Liu et al., 2012). Electron cryo-tomography suggests an average of ~2,200 receptors per cluster in *R. sphaeroides* cultured in

rich medium (i.e. probably has less chemosensory protein levels) (Briegel et al., 2009). However, it is difficult to correlate this observation with the fluorescence microscopy data described in this chapter. Indeed, the estimated sizes of *E. coli* membrane chemosensory clusters from different electron cryo-tomography studies are wide (500–5,200 receptors per cluster) (Briegel et al., 2009; Khursigara et al., 2011; Zhang et al., 2007). However, this variance is unsurprised because electron cryo-tomography is unable to distinguish between growing clusters from mature ones, as well as transiently congregated unit-clusters. A current single-molecule tracking study shows that chemoreceptor Tsr is confined in areas ranging 170–290 nm in diameter (Oh et al., 2014), which might contain 2,300–6,600 receptors (Briegel et al., 2009). Quantitative time-lapse super-resolution fluorescence imaging might be the ideal approach to further determine the size of unit-clusters, since unit-clusters dynamically congregate-segregate.

Clustering is a widespread organizing principle of membrane proteins (Mueller et al., 2012), including signalling molecules (Cebecauer et al., 2010). The question is if cells have sufficient amount of constituting molecules, will clusters keep growing till the interacting force and surrounding environment no longer allow? Is there any optimal size-range/upper limit of a specific cluster? The size (upper limit) of membrane chemosensory clusters could be jointly determined by intracluster forces that hold constituting subunits and the nature of surrounding environments (Endres, 2009). It is likely that intercluster interactions create transient, unstable couplings between unit-clusters. Exchange of components via congregation–segregation process is also possible. However, the clusters function in a unitary manner over time.

In the simplest scenario, protein-protein interactions alone can cluster proteins (Douglass and Vale, 2005) and determine the assembly size (Sieber et al., 2007). The eukaryotic syntaxin forms membrane clusters composed of ~75 molecules via self-assembly (Sieber et al., 2007). The bulky N-terminal domain causes syntaxins to adopt a bunch-like structure, in which syntaxins are conformationally constrained. The resulting steric hindrance prevents further attachments of more molecules, thus sets an upper limit for the cluster (Sieber et al., 2007). Similar steric constraint, i.e. the conical geometry of receptor trimer-of-dimers that will produce a curved protein array, may limit the dimension of bacterial membrane chemosensory clusters, with a theoretically optimum size of 1200–3200 receptors (Duke and Graham, 2009; Endres, 2009). Intriguingly, based on predicted responsiveness, Khursigara et al. (2011) showed that >1,400 receptors per cluster might be optimal. However, the conformation of receptor trimer-of-dimers seems to be flexible (Hall et al., 2012) or not that

bended (Briegel et al., 2012; Francis et al., 2004), making this simple geometric explanation uncertain. Nonetheless, even if the chemosensory array is flat, a crowded protein layer can bend the cytoplasmic membrane due to collisions between bound proteins (Stachowiak et al., 2012). The force generated by membrane elasticity to resist bending would limit the size of chemosensory clusters (Lefman et al., 2004; Stachowiak et al., 2012). Other putative limiting factors include the balance between the rates of assembly and disassembly (Rafelski and Marshall, 2008), receptor activity (Endres et al., 2008; Khursigara et al., 2011; Lamanna et al., 2005; Slivka and Falke, 2012; Wu et al., 2011), lipid domains (Govindarajan et al., 2012; Kusumi et al., 2012; Matsumoto et al., 2006), and protein/lipid dynamics (Fan et al., 2010; Mueller et al., 2012; Spira et al., 2012). How these factors might contribute to the size-determination of unit-clusters is of great interests. Noteworthy, the slow diffusion of chemoreceptors within bacterial membranes (Kumar et al., 2010; Oh et al., 2014) may allow the formation of huge clusters (i.e. comparing to the <50 nm-diameter nanoclusters normally found in mammalian cells) (Mueller et al., 2012).

The clustering of chemosensory proteins into large quaternary complexes may be important for the high level of sensitivity, gain, and robustness in the bacterial chemosensory pathway (Bray et al., 1998; Gestwicki and Kiessling, 2002; Hazelbauer et al., 2008; Pontius et al., 2013), but recent data suggest that signalling works through signalling teams that are smaller in size (Endres et al., 2008; Hansen et al., 2010). Additionally, modelling demonstrates that cluster size might be determined by functionality, and hence be "optimal" for signalling (Aquino et al., 2011). The suggested size is 5–30 receptors per cluster under the theoretical extrinsic and intrinsic noise used (Aquino et al., 2011). The difference between the predicted size and the observed unit-size could result from simplifications made during the modelling, or indicate different levels in the hierarchy of chemosensory organization. Nevertheless, multiple unit-clusters (comparing to a huge polar cap) could possess the benefit of clustering but also optimize the detection sensitivity by dynamically dispersing receptor arrays over the cell surface (Berg and Purcell, 1977). Moreover, with the same number of constituting proteins, several unit-clusters may generate better digital signals than a single huge cluster, hence improved signalling fidelity (Suzuki, 2012).

Wandering clouds: the dynamic behaviours of membrane chemosensory clusters

In contrast to *E. coli*, both polar and lateral chemosensory clusters are very dynamic in *R. sphaeroides*. However, the dynamics of mobile *E. coli* polar clusters (Thiem et al., 2007) and *P. aeruginosa* polar Che2-protein clusters (Güvener et al., 2006) are similar to that of *R. sphaeroides*. Supposing that lateral and polar clusters are similar assemblies, the most likely cause of the above distinct behaviours would lie in different cellular processes occurring at lateral sites. Since the stochastic self-assembly model cannot explain the static behaviour of *E. coli* lateral clusters (Greenfield et al., 2009; Thiem et al., 2007; Thiem and Sourjik, 2008), an anchor exists in *E. coli* to position lateral clusters remains as the simplest scenario. The identity of this anchor is still unknown.

As for many other large protein complexes which move in the cytoplasmic membrane (Mika and Poolman, 2011), the unit-clusters display both Brownian and anomalous diffusions. The anomalous diffusion is likely caused by obstructions like the cell-wall synthesis machinery that move circumferentially or membrane domains which may trap unit-clusters (Mika and Poolman, 2011). On the other hand, given the slightly longer cell cycle and shorter cell length of *R. sphaeroides*, the slow diffusion of unit-clusters is still sufficient for pole-to-pole traveling that may contribute to bipolar localisation and cluster inherence (Chapter 8).

The congregation-segregation of unit-clusters could be simply caused by random movements of unit-clusters, or further affected by receptor activity: receptor activity can alter the clustering or architecture of chemosensory arrays (Endres et al., 2008; Frank and Vaknin, 2013; Khursigara et al., 2011; Lamanna et al., 2005; Wu et al., 2011). These alterations could potentially modify the interactions between unit-clusters, enhancing or reducing their strengths (Khursigara et al., 2011; Slivka and Falke, 2012).

Conclusions

In *R. sphaeroides* membrane chemosensory proteins form unit-clusters which dynamically congregate-segregate and move around the cell. This observation challenges the *E. coli* paradigm and raises the question of what is the "general" behaviour of membrane chemosensory clusters. The unit-cluster idea has valuable implications for studying cell signalling (Cebecauer et al., 2010) and

hierarchical organisation of membrane proteins (Kusumi et al., 2012) beyond bacterial chemotaxis.

Chapter 8. How to Position Membrane Chemosensory Clusters in *R. sphaeroides*?

It takes all the running you can do to keep in the same place.

— *Through the Looking-Glass,* Lewis Carroll

8.1 Aims

Cell snapshots show that membrane chemosensory clusters have similar localisation patterns in *R. sphaeroides* and *E. coli*. However, the stochastic self-assembly/cytokinetic site-anchoring mechanism is not utilized by *R. sphaeroides* to position the chemosensory clusters (Chapter 6). In this chapter, I sought to discover the mechanism(s) used by *R. sphaeroides* to localise its membrane chemosensory proteins at the cell pole.

8.2 The Establishment of New-pole Membrane Chemosensory Clusters: Diffusion-and-trapping

How does *R. sphaeroides* establish the bipolar localisation of membrane chemosensory clusters if the clusters are not targeted to pre-cytokinetic sites? Unipolar localisation of membrane chemosensory clusters could be seen in newborn cells (Figs 6.4 and 8.1), suggesting new-pole clusters form after cell division and cells eventually reach a bipolar pattern. Two possible scenarios are: (i) new-pole clusters are formed via *de novo* nucleation and assembly, and (ii) new-pole clusters are derived from elsewhere in the cell, with these clusters moving to the new pole.

Inhibition of protein synthesis should impede the formation of new-pole clusters if they are formed *de novo*, while new-pole clusters derived from the diffusion of existing lateral/old-pole clusters should be unaffected. Control and chloramphenicol-treated cells had similar ratios of unipolar cells, 32±6% (n = 424)

and 30±3% (n = 653) respectively. By following the fate of unipolar cells using time-lapse imaging, I found that within 100 min, 55±2% (n = 197) became bipolar in the presence of chloramphenicol, comparing to 62±4% (n = 82) of control cells. This difference should be much greater if new-pole clusters formed *de novo*, because there would not be sufficient mature fluorescent chemosensory proteins to form new clusters at the onset of imaging.

The second scenario, new-pole clusters are derived from elsewhere in the cell, with these clusters moving to the new pole, is consistent with observations described in Chapters 6 and 7. The formation of dynamic unit-clusters allows individual membrane chemosensory clusters to move around in the cell (Chapter 7). If cells in snapshots were arranged by the localisation pattern of FtsZ, which could be an indication of cell cycle stages, the localisation pattern of membrane chemosensory clusters is consistent with unit-clusters move from the old pole or lateral sites into the new pole (Fig. 8.1). Indeed, time-lapse imaging showed that unit-clusters left old poles and moved along the length of the cell (Fig. 8.2). The lateral movement of clusters suggests new-pole clusters can derive from lateral or even old-pole clusters, to become trapped by the curvature at the new pole (Figs 6.7, 6.8, 8.2 B) (Endres, 2009; Thiem et al., 2007).

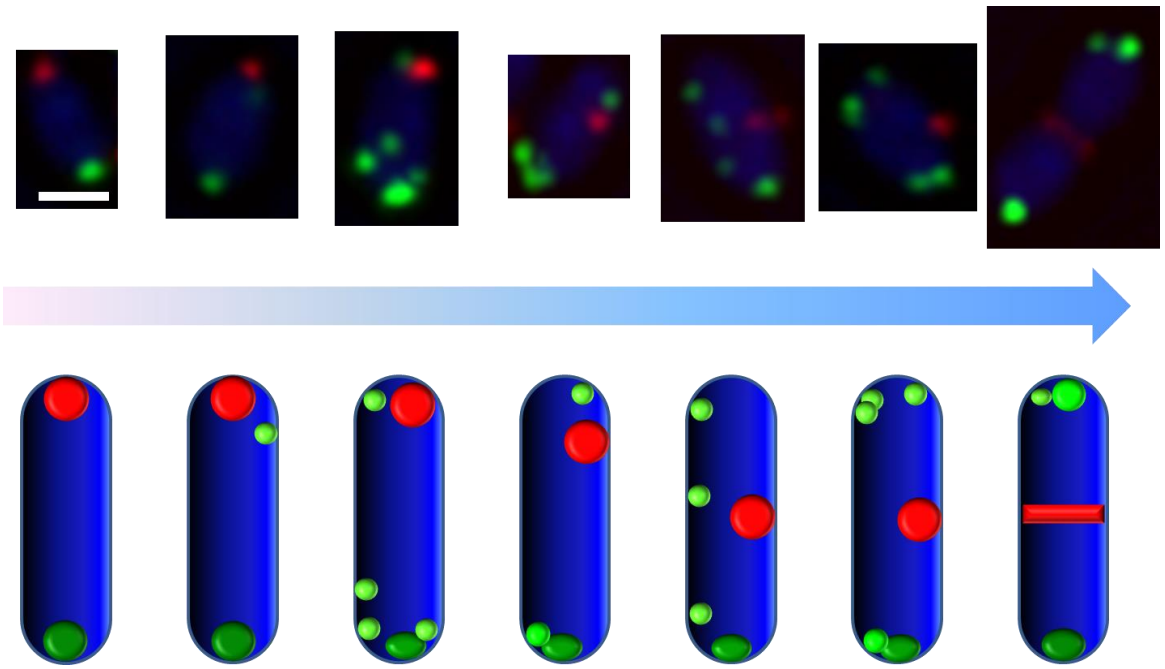

Figure 8.1. Typical localisation patterns of FtsZ and membrane chemosensory clusters in normal cells. Cell snapshots and corresponding schematics are arranged by the progress of FtsZ (i.e. from polar spot to Z-ring). Arrow: progression through cell cycle. Green: YFP–CheW$_3$; red: FtsZ–CFP; blue: DIC. Scale bars: 1 μm.

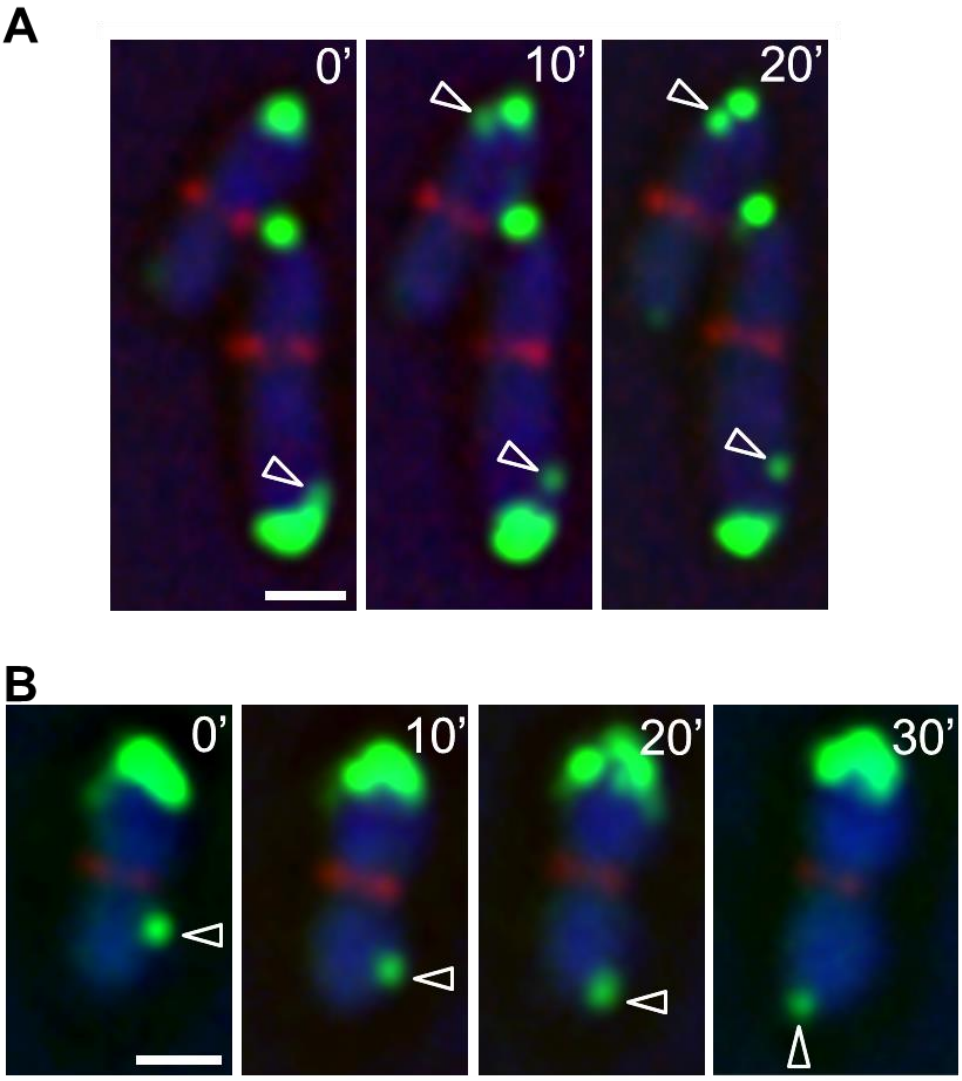

Figure 8.2. Unit-clusters can move away from the old pole towards the new pole (arrowheads). Green: YFP–CheW$_3$; red: FtsZ–CFP; blue: DIC. Numbers: minutes. Scale bars: 1 μm.

This idea was tested by using a different approach. I followed the behaviour of a chemoreceptor (McpG–GFP) in a *ΔcheW$_2$cheW$_3$* strain. In both *E. coli* and *R. sphaeroides* deletion of *cheW* results in diffuse chemoreceptors, somewhat more concentrated towards the curved polar regions but without cluster formation, with clusters reforming when *cheW$_2$cheW$_3$* are re-expressed (Wadhams et al., 2000 and this study). I followed the cluster formation when the expression of *cheW$_2$cheW$_3$* was induced by IPTG. Chemosensory clusters first formed dispersed around the cell and then gradually moved to and accumulated at cell poles (Fig. 8.3). Therefore, clustering of membrane chemosensory proteins can take

place all around the cell membrane, and the resultant chemosensory clusters have a propensity to move towards and accumulate at cell poles.

These results indicate new-pole clusters are derived from existing old-pole or lateral clusters. Directional movements would not be required for the proposed old-pole/lateral clusters-derived mechanism, since random movements coupled with polar trapping will eventually redistribute clusters to the new pole.

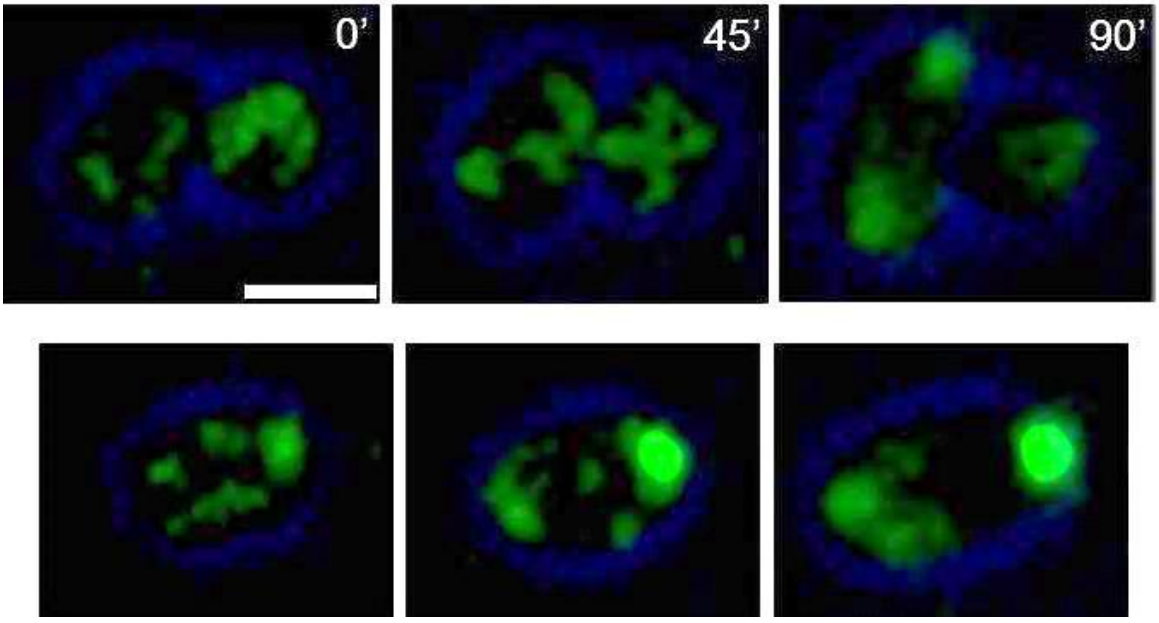

Figure 8.3. Reformation of polar membrane chemosensory clusters in *ΔcheW2cheW3* cells after induction of *cheW2cheW3*. Green: McpG–GFP; blue: cell outlines. McpG–GFP is initially delocalised, after induction clusters form and localisation at cell poles increases. Numbers: minutes. Scale bar: 1 μm.

8.3 Cell Geometry Affects the Positioning of Membrane Chemosensory Clusters

As described in section 8.2, cell-pole trapping might contribute to the polar localisation of dynamically moving unit-clusters. Mathematical modelling suggests that the conformation of receptor trimers-of-dimers fits better to the specific curvature at the cell pole, while the geometric mismatch at the lateral site disfavours chemoreceptors to localise there (Fig. 8.4 A) (Endres, 2009). Sphaeroplasting was therefore used to explore the roles of cell geometry in the positioning of membrane chemosensory clusters (Fig. 8.4 B). If membrane chemosensory clusters preferentially localise to regions with higher curvature (i.e.

the cell pole), they should become more evenly distributed if membrane curvature were made more uniform by sphaeroplasting. A sphaeroplasting protocol developed by Ranjit and Young (2013) was adapted for *R. sphaeroides*. The resulting sphaeroplasts lack peptidoglycan but have intact inner and outer membranes and periplasm (Ranjit and Young, 2013).

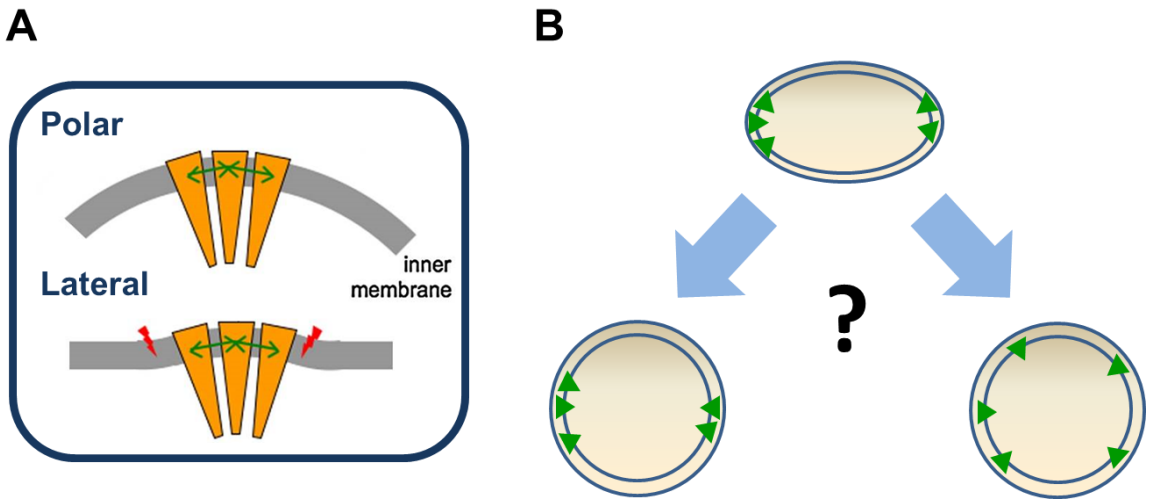

Figure 8.4. Putative effects of cell geometry on the localisation of membrane chemosensory clusters. **(A)** An ideal cluster composed of three trimers-of-dimers at the cell pole or lateral site. The interacting strength between trimers is indicated by green arrows. The inner membrane (grey) has different curvatures at polar or lateral regions. The cluster-membrane curvature mismatch causes energetically unfavourable membrane deformations (red streaks) at lateral regions. Adapted from Endres (2009). **(B)** Possible effects of sphaeroplasting on chemosensory clusters (green) localisation. Chemosensory clusters will either retain a clustering pattern (left) or become dispersed (right).

The distinct polar localisation of membrane chemosensory clusters was lost in lysozyme-induced sphaeroplasts (Fig. 8.5). Membrane chemosensory clusters dispersed all over the cell periphery of these spherical cells (Fig. 8.5). Pairs of linked sphaeroplasts could be seen, presumably derived from constricting cells (Fig. 8.6 A). Two patterns existed for these cell-pairs: two sibling spherical cells or one spherical cell coupled with a coccobacillus (Fig. 8.6 A). Intriguingly, chemosensory clusters shifted from the original polar regions to the new poles in the coccobacilli (Fig. 8.6 B).

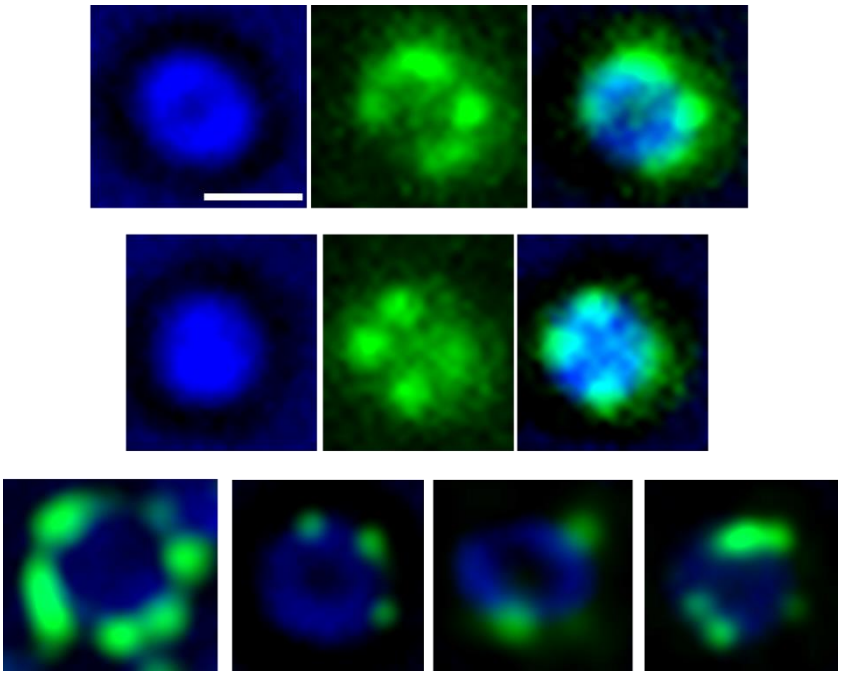

Figure 8.5. Localisation of membrane chemosensory clusters in sphaeroplasts. Individual channels are also shown for the upper and middle panels. Green: YFP–CheW$_3$; blue: DIC. Scale bars: 1 μm.

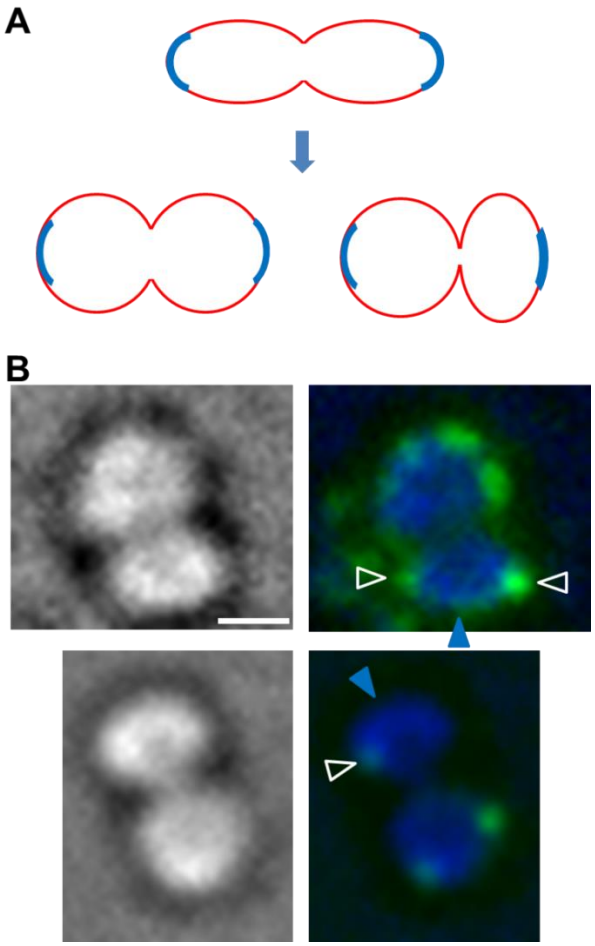

Figure 8.6. Localisation of membrane chemosensory clusters in sphaeroplast pairs. **(A)** Pairs of linked sphaeroplasts (bottom) are presumably derived from constricting cells (top). Two patterns exist: two spherical cells (bottom left) or one spherical cell coupled with a coccobacillus (bottom right). The regions corresponding to the original cell poles are shown in blue. **(B)** Chemosensory clusters (white arrowheads) localise to the new poles in the coccobacilli rather than the regions corresponding to the original polar regions (blue arrowheads). Green: YFP–CheW$_3$; blue: DIC. Scale bars: 1 μm.

The distributions of membrane chemosensory clusters were quantified in normal cells and sphaeroplasts. In normal cells, two major peak-areas corresponding to the polar localisation of chemosensory clusters were seen in most cells (Fig. 8.7). These peak-areas covered relatively small proportions of the cell periphery. In contrast, multiple peaks randomly covering high proportions of the cell membrane were found in sphaeroplasts (Fig. 8.8). The heterogeneous size and shape of sphaeroplasts, as well as the resolution limit of conventional fluorescence microscopy, make it difficult to perform a direct quantitative analysis of the correlations between cell curvature and cluster localisation. Nevertheless, the degree of dispersion was quantified by measuring the proportions of cell periphery covered by chemosensory clusters. The areas with fluorescence signals above the cellular background in the intensity profiles were considered as covered by chemosensory proteins (e.g. peak-areas in Fig. 8.7). A significant difference was found for the degree of dispersion between normal cells and sphaeroplasts: the average coverage of the cell periphery was 42.0±9.9% in normal cells (n=30), and 82.3±5.30% in sphaeroplasts (n=40). As a reference, the

membrane curvature is ~0.67 μm^{-1} for sphaeroplasts and ~2.08 μm^{-1} for normal cells (higher the curvature, smaller the value) (Renner and Weibel, 2011; Zimmerberg and Kozlov, 2006).

Taken together, the above results (Figs 8.3 and 8.5—8.8) suggest that chemosensory clusters preferentially localise to membrane regions with higher curvature.

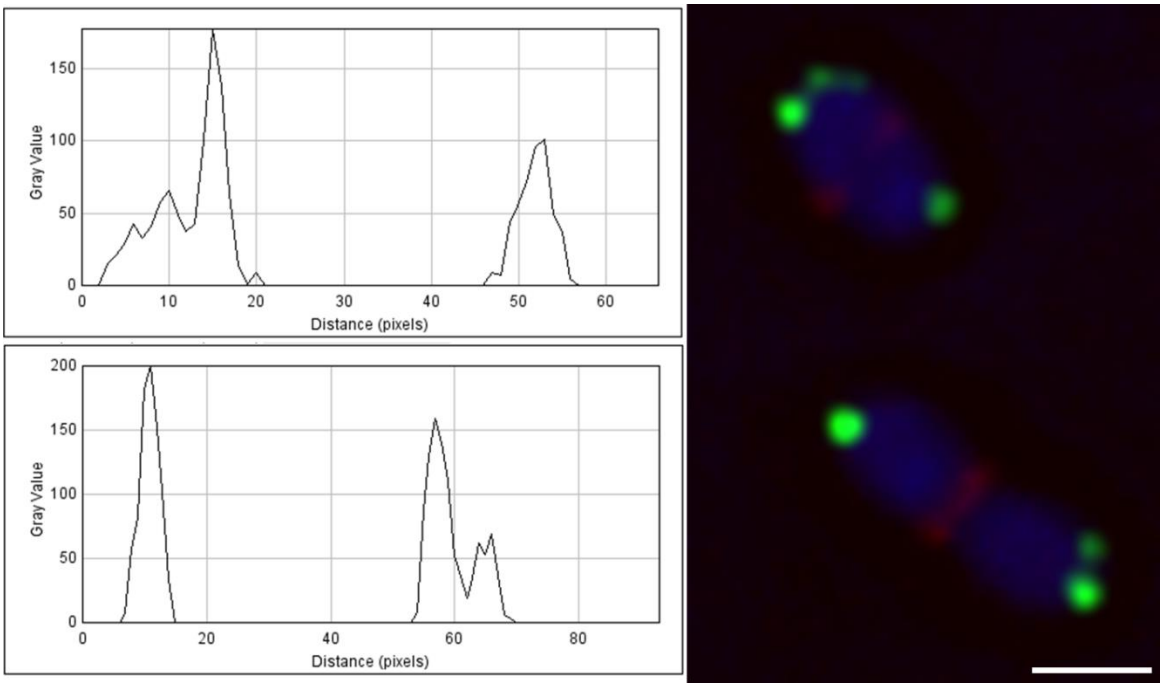

Figure 8.7. The distribution of membrane chemosensory clusters in normal cells. Histograms show the intensity profiles along the cell periphery for the two cells in the right panel. Green: YFP–CheW$_3$; red: FtsZ–CFP; blue: DIC. Scale bars: 1 μm. One pixel is equal to 0.065 μm in the histograms.

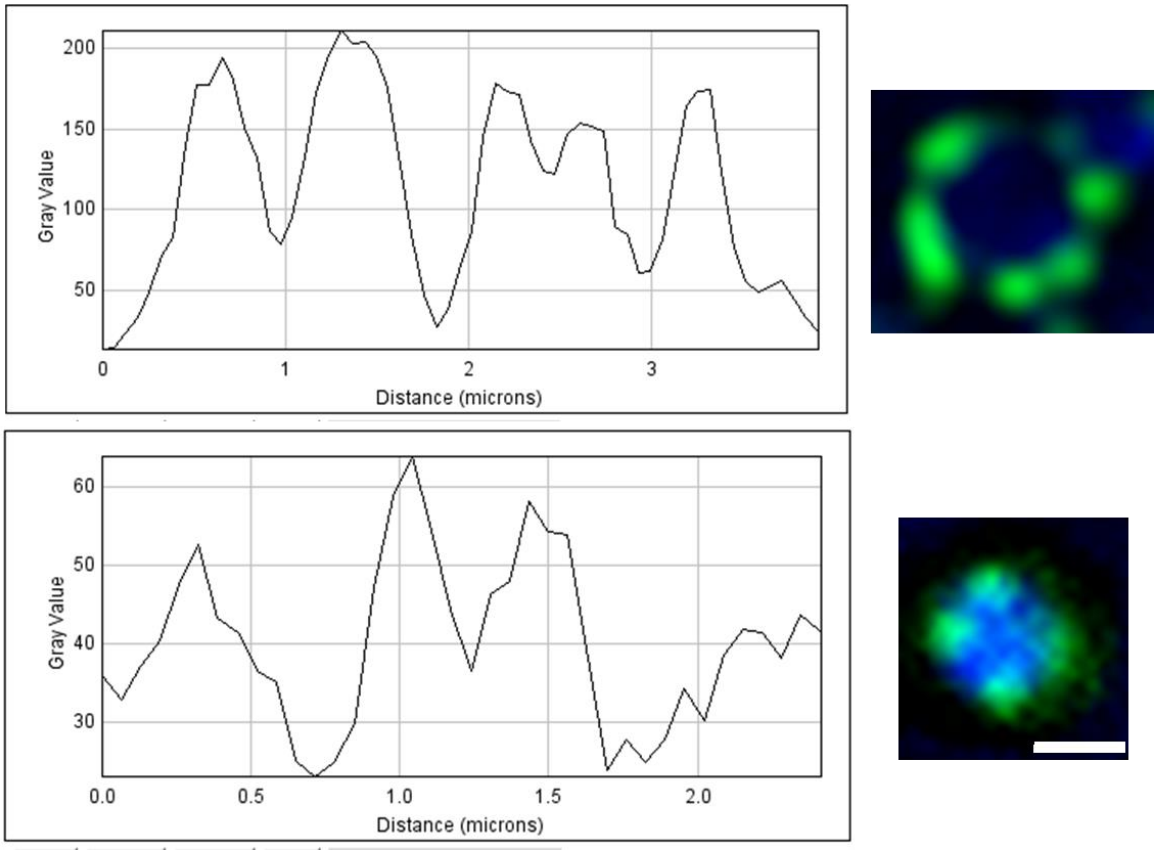

Figure 8.8. The distribution of membrane chemosensory clusters in sphaeroplasts. Histograms show the intensity profiles along the cell periphery for the two cells in the right panel. Green: YFP–$CheW_3$; blue: DIC. Scale bars: 1 μm.

8.4 Discussion and Conclusions

In many bacterial species, membrane chemosensory clusters accumulate at both poles, with one obvious old pole and one new pole (Gestwicki et al., 2000). A group of polar-flagellated γ-proteobacteria show a modified, cell cycle-dependent bipolar pattern: new-born cells have a unipolar distribution of chemosensory clusters at the old pole, and becomes bipolar as the new pole matures (Ringgaard et al., 2011). Stochastic self-assembly/cytokinetic site-anchoring (Greenfield et al., 2009; Thiem et al., 2007; Thiem and Sourjik, 2008; Wang et al., 2008a) and ParC–ParP-mediated diffusion-and-capture (Ringgaard et al., 2011; Ringgaard et al., 2014; Yamaichi et al., 2012) mechanisms have been proposed for the two patterns respectively. *C. crescentus* represents an extreme with a sole unipolar localisation programmed by its intrinsic asymmetry (Alley et al., 1992). In *E. coli* polar clusters seem relatively dynamic, but remain at the cell poles, while new clusters localised laterally at pre-cytokinetic sites, appearing

tightly localised (Fig. 8.9) (Thiem et al., 2007). The situation in *R. sphaeroides* seems very different (Fig. 8.9).

From the results described in this and two previous chapters, a clear picture of the dynamics and positioning of *R. sphaeroides* membrane chemosensory proteins emerged (Fig. 8.9): the "polar caps" appear to be formed from a number of smaller unit-clusters, which appear to freely diffuse in the membrane with some polar retention. The lateral clusters are not static, and there is no accumulation at pre-cytokinetic sites. Indeed, the clusters appear to be excluded from the vicinities of Z-rings. A periodic pattern seen in cephalexin-treated filamentous cells is probably determined by a synergistic action of stochastic self-assembly and an exclusive effect associated (directly or indirectly) with the Z-ring. Taken together, stochastic self-assembly, diffusion-and-trapping, and FtsZ-assemblies-associated exclusive/steric hindrance effects may co-ordinate to generate the spatiotemporal dynamics of membrane chemosensory proteins in *R. sphaeroides* (Fig. 8.9).

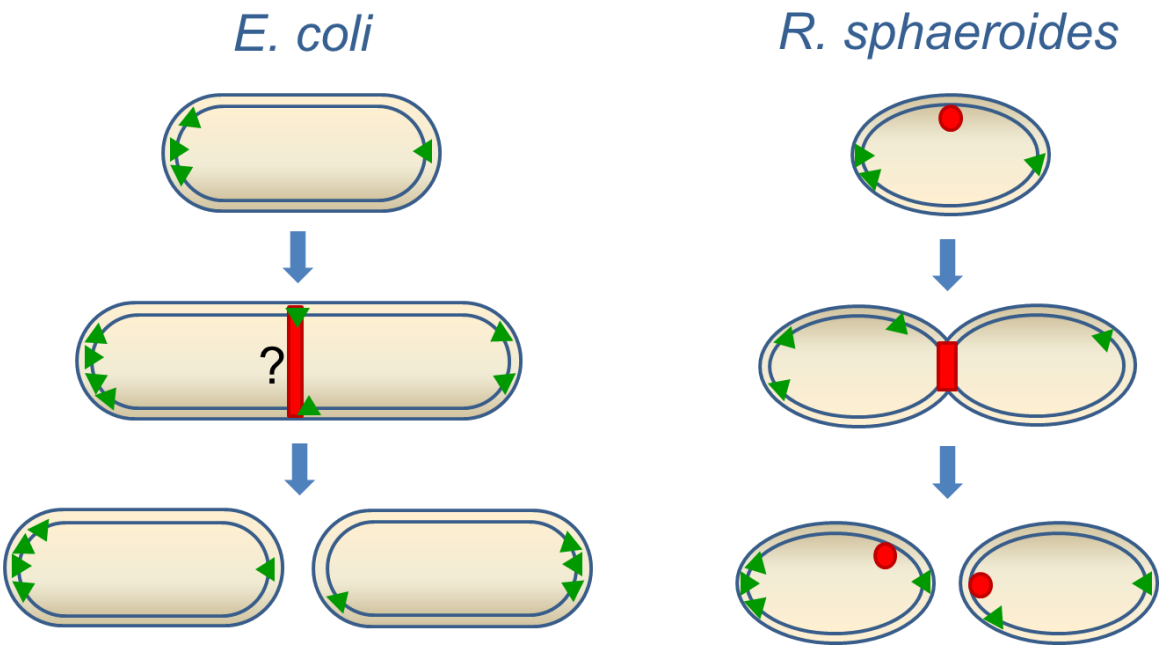

Figure 8.9. Simplified schematics for the dynamics and positioning of membrane chemosensory clusters in *E. coli* and *R. sphaeroides*. Membrane chemosensory clusters localise at (or close to) cytokinetic sites in *E. coli*, and anchors (e.g. the Z-ring) might exist to hold clusters static. These lateral clusters become new-pole clusters right after cytokinesis. In *R. sphaeroides*, membrane chemosensory proteins form dynamic unit-clusters which wander in the membrane but transiently trapped by the cell pole. Chemosensory clusters cannot stay in the

Z-ring/divisome vicinity, while FtsZ polar spots show steric hindrance effect. New-pole clusters are derived from lateral/old-pole clusters which move into the new-pole after cytokinesis. Green: membrane chemosensory clusters; red FtsZ assemblies.

Membrane geometry affects the localisation of *R. sphaeroides* membrane chemosensory clusters, in consistent with the observations on *E. coli* (Oh et al., 2014; Shih et al., 2005; Thiem et al., 2007). The consensus is that chemosensory clusters preferentially localise to membrane regions with higher curvature (i.e. cell poles) (Endres, 2009), and in the absence of curvature difference, chemosensory clusters localise indiscriminately. Cell rounding causes a fourfold reduction in the mobility of mobile (i.e. not clustered) chemoreceptor Tsr in *E. coli* (Oh et al., 2014), suggesting higher membrane curvature can retard movements of chemoreceptors, thus facilitating clustering or polar localisation. Intriguingly, Tsr is confined in domains of similar sizes in normal and spherical cells (Oh et al., 2014), consistent with the observation of unit-clusters in *R. sphaeroides* sphaeroplasts (e.g. Fig. 8.5, second cell from the left, bottom panel).

Protein localisation via "recognizing" membrane curvature has been well documented for two proteins, DivIVA and SpoVM, which are targetted to concave and convex sites, respectively (Huang and Ramamurthi, 2010; Ramamurthi, 2010; Strahl and Hamoen, 2012). How they recognize the specific geometric cues is yet unclear, but it is likely that individual DivIVA/SpoVM molecule would need to assemble into large structures to achieve cooperative sensing of membrane curvature (Huang and Ramamurthi, 2010; Lenarcic et al., 2009; Oliva et al., 2010; Ramamurthi et al., 2009; Strahl and Hamoen, 2012). Similarly, even the intrinsic conformation of receptor trimer-of-dimers might be distinct from the membrane curvature at the pole (Briegel et al., 2012; Francis et al., 2004; Hall et al., 2012), the clustering of membrane chemosensory proteins is probably favoured at more-curved regions (Endres, 2009; Zimmerberg and Kozlov, 2006). Indeed, molecular modelling shows that clustering of transmembrane proteins is increased by higher membrane curvature (Parton et al., 2011). It should be noted that chemoreceptors are still more concentrated at cell poles even without extensive clustering (Shiomi et al., 2005; Wadhams et al., 2000), indicating trimer-of-dimers or their unstable oligomers do have high propensity towards the cell pole. However, as huge transmembrane proteins with > 20 nm-long cytoplasmic domains, a sensing of overall membrane curvature rather than convex/concave might be more likely for chemoreceptors. For a clearer understanding of how chemosensory proteins use geometric cues to

position, the newly developed *in vivo* and *in vitro* systems that allow for the manipulation of membrane geometry may be very useful (Cabeen et al., 2009; Fenz and Sengupta, 2012; Jiménez et al., 2013; Männik et al., 2012; Renner et al., 2013; Renner and Weibel, 2011; Takeuchi et al., 2005). A systematic examination of native localisation of membrane chemosensory proteins in bacteria with diverse shapes may also yield interesting insights.

The general phosphotransferase system (PTS) proteins, enzyme I (EI) and HPr, which control carbon uptake and metabolism in bacteria, localise at the *E. coli* cell poles (Lopian et al., 2010) and interact with chemosensory proteins (Lux et al., 1995; Neumann et al., 2012). The spatial proximity may facilitate the interactions of PTS and chemosensory pathways to generate an optimal metabolic response to environmental cues (Amster-Choder, 2011). Strikingly, EI localises to the cell pole due to the higher membrane curvature (Govindarajan et al., 2013), suggesting similar mechanisms or cues are used by two interacting systems to enhance their functional coupling.

In conclusion, the positioning of *R. sphaeroides* membrane chemosensory clusters relies on cell geometry and simple diffusion rather than cytoskeletal anchoring: individual dynamic unit-clusters are not actively positioned at pre-cytokinetic sites, but rather randomly diffuse in the membrane, becoming trapped at the cell poles. The stochastic self-assembly/cytokinetic sites-anchoring mechanism was proposed to be the universal means for the positioning of membrane chemosensory clusters in most bacteria. However, the discovery of a polar anchor for targeting chemosensory clusters to the cell pole of certain polar-flagellated bacteria (Ringgaard et al., 2011) hints that the common bipolar localisation of membrane chemosensory proteins could be established by different ways. Here I found that a third mechanism exists in *R. sphaeroides*. It is intriguingly to see, then, how widely the stochastic self-assembly/cytokinetic sites-anchoring mechanism is actually utilized by different bacteria to position their chemosensory clusters. Nevertheless, the random walk coupling with geometric trapping mechanism may be utilized by other bacterial macromolecular assemblies for their spatial regulation.

Chapter 9. Spatiotemporal Dynamics of Cytoplasmic Chemosensory Clusters Relative to FtsZ in *R. sphaeroides*

Over earth and ocean, with gentle motion… This pilot is guiding me…

I pass through the pores of the ocean and shores; I change, but I cannot die.

— *The Cloud*, Percy Bysshe Shelley

9.1 Aims

The cytoplasmic chemosensory clusters are composed of homologues of the membrane clusters, and the daughter cells need to inherit both clusters on cell division to allow chemotaxis. Previous members in our group have shown that the cytoplasmic clusters move dynamically in *R. sphaeroides* with time-average positions at pre-cytokinetic sites (Roberts et al., 2012; Thompson et al., 2006). Here, I further investigated the role of FtsZ in the positioning of cytoplasmic chemosensory clusters.

9.2 Cytoplasmic Chemosensory Clusters Stay Close to FtsZ Assemblies during Most of the Cell Cycle

The protein TlpT is essential for chemotaxis and the integrity of the cytoplasmic chemosensory cluster (Wadhams et al., 2005). A functional YFP fusion of TlpT, expressed as a genomic replacement, was used as a marker for the cytoplasmic cluster (Thompson et al., 2006). The cytoplasmic chemosensory clusters roughly localise at the midcell of *R. sphaeroides* (Roberts et al., 2012; Thompson et al., 2006). Consistent with this, snapshots show that cytoplasmic chemosensory clusters were close to the Z-ring (Fig. 9.1 A). Using different FtsZ assemblies as indicators

of cell-cycle stages, I found that the colocalisation of cytoplasmic clusters and FtsZ was cell-cycle related: newborn cells had the lowest colocalisation, and the colocalisation increased as cell cycle proceeded (Fig. 9.2). The frequent proximity of cytoplasmic chemosensory clusters and constricting Z-rings or polar FtsZ spots was unexpected (Fig. 9.2 A, last and first cells respectively; Fig. 9.2 B), since it is believed that non-chromosome cytoplasmic cargos of ParA homologues move to future cytokinetic sites before cytokinesis (Gerdes et al., 2010; Lutkenhaus, 2012; Salje, 2010). Similar spatiotemporal dynamics of cytoplasmic chemosensory clusters was seen in photoheterotrophic cells (Fig. 9.3), indicating that the reorganisation of the cytoplasmic membrane does not interfere with cytoplasmic chemosensory cluster positioning.

At first glance, the high proximity of cytoplasmic chemosensory clusters and FtsZ assemblies suggests that FtsZ might participate in the positioning of the cytoplasmic clusters. Besides, for normal or filamentous cells with multiple cytoplasmic chemosensory clusters, most of them (86.0%, n=121) also have at least one cluster close to the Z-ring (Figs 9.1 B and 9.4). However, since there was only one Z-ring in each of the cells shown, it is unlikely that the Z-ring can position other clusters which were far away (Figs 9.1 B and 9.4). Therefore, it is more plausible to suggest that the cytoplasmic chemosensory cluster and FtsZ assemblies occupy similar regions over a large portion of the cell cycle, but they are positioned independently.

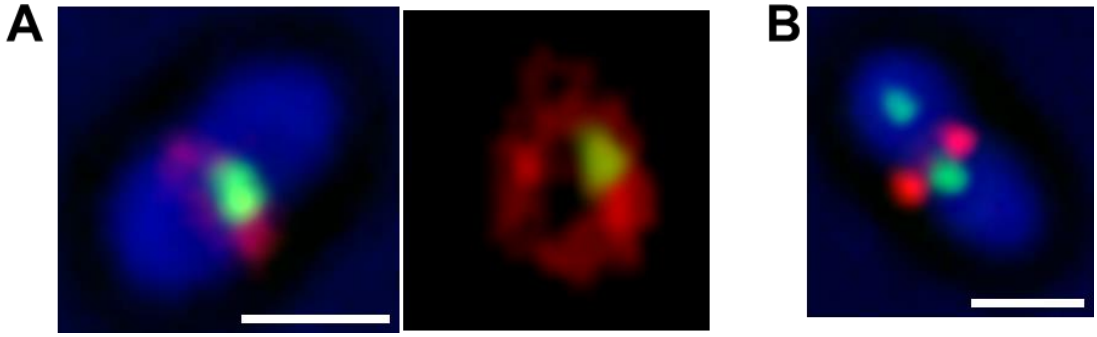

Figure 9.1. The positioning of the cytoplasmic chemosensory cluster relative to the Z-ring. **(A)** The position of the cytoplasmic cluster in a single-cluster cell. The cluster is in proximity of the cytoplasmic membrane and adjacent to the Z-ring. Right image: the 3D reconstruction viewed from a different angle (rotated 60°). **(B)** The positions of the cytoplasmic cluster in a two-cluster cell. Red, FtsZ–CFP; green, TlpT–YFP; blue: DIC. Scale bars: 1 μm.

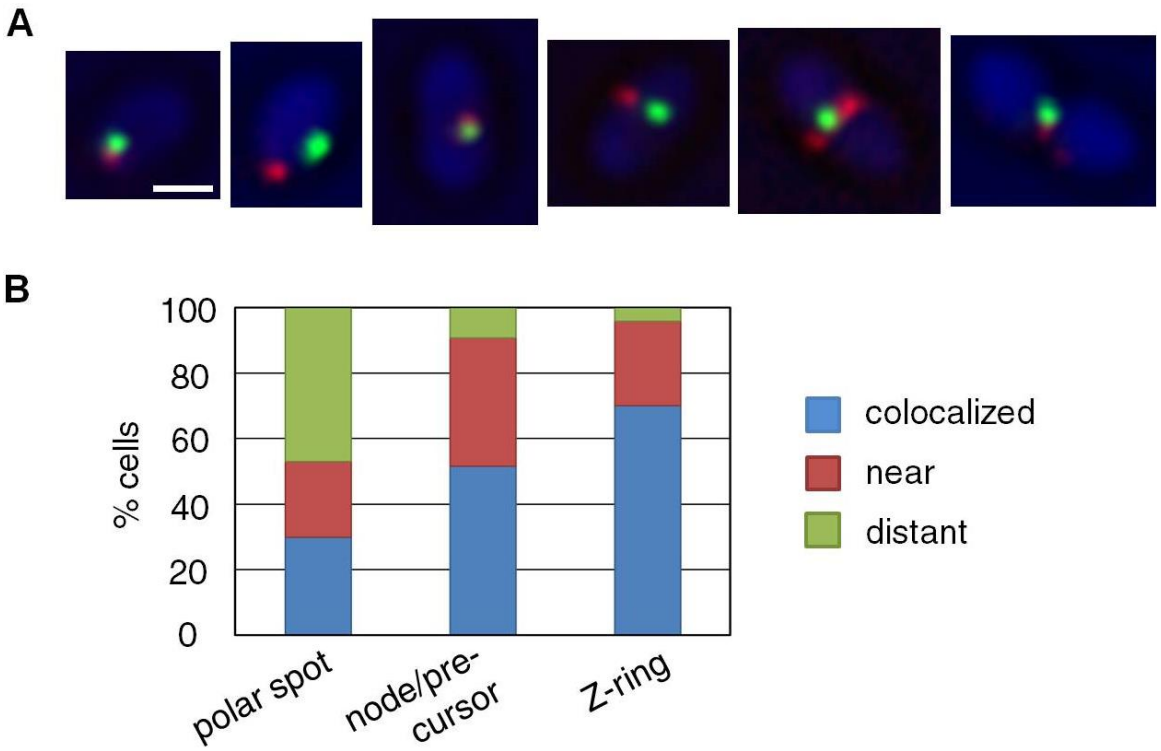

Figure 9.2. The positioning of the cytoplasmic chemosensory cluster and its relation to FtsZ. **(A)** Snapshots of cells at different cell-cycle stages. Red, FtsZ–CFP; green, TlpT–YFP; blue, DIC. Scale bars: 1 μm. **(B)** The quantification of relative positioning between cytoplasmic chemosensory clusters and FtsZ assemblies. Cells were grouped by their FtsZ assemblies and the relationships defined as: (1) colocalised: the two structures have overlaps in the diffraction-limited images; (2) near: the shortest distances between the cytoplasmic clusters' centroids and FtsZ assemblies' edges are less than the diameters of cognate cytoplasmic clusters; (3) distant: all remaining (n=521).

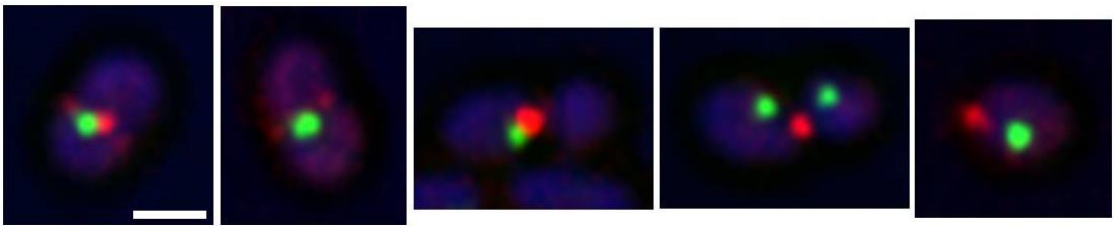

Figure 9.3. The relative positioning between FtsZ and cytoplasmic chemosensory clusters in photoheterotrophic *R. sphaeroides* cells. Red, FtsZ–CFP; green, TlpT–YFP; blue: DIC. Scale bars: 1 μm.

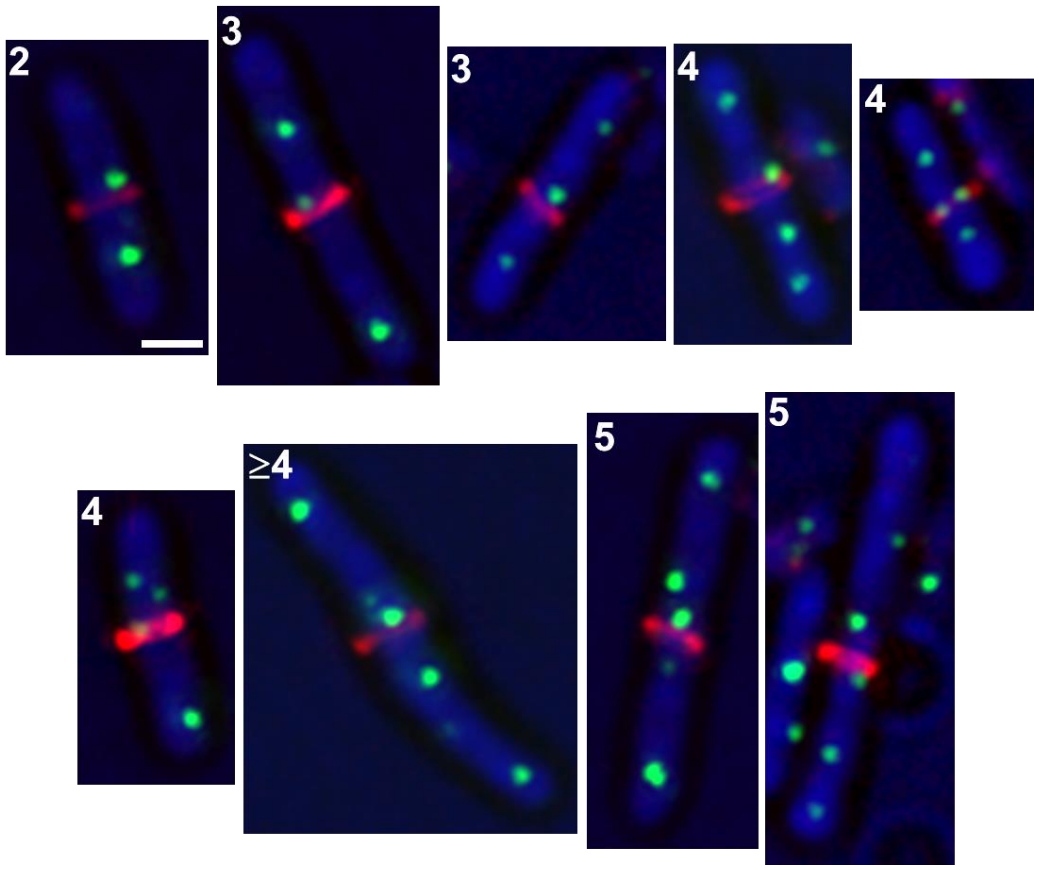

Figure 9.4. In filamentous cells with more than two cytoplasmic chemosensory clusters, at least one is colocalised with/very close to the Z-ring. Numbers: quantity of cytoplasmic clusters in each cell. Cells were treated with cephalexin for 3.5 h. Red, FtsZ–CFP; green, TlpT–YFP; blue: DIC. Scale bars: 1 μm.

9.3 Dynamics and Positioning of Cytoplasmic Chemosensory Clusters

To better understand the relationship between the positioning of FtsZ and the cytoplasmic chemosensory cluster, time-lapse imaging was used. Strikingly, in two-cluster cells, one cluster moved to a pre-cytokinetic site first (Fig. 9.5 A, white arrowhead), while another cluster stayed with the Z-ring and gradually moved to the other pre-cytokinetic site later (Fig. 9.5 A, green arrowheads). The proximity to the Z-ring was often seen even after extensive constriction of the Z-ring (Fig. 9.5 B, green and red arrowheads).

Together with the results shown in section 9.2, the relative positioning between FtsZ and cytoplasmic chemosensory clusters indicate two important things. Firstly, the cytoplasmic chemosensory clusters and FtsZ occupy similar subcellular locations, at least to within the optical resolution limit of our

microscope. However, the movement of cytoplasmic clusters to the pre-cytokinetic sites before FtsZ (Figs 9.1 B, 9.2 A, 9.3, 9.5) suggests cytoplasmic clusters do not use FtsZ assemblies as anchors for positioning. Secondly, the asymmetric partitioning of pairs of the cytoplasmic chemosensory clusters to future cytokinetic sites (Fig. 9.5) is different from other non-chromosome cytoplasmic cargos of ParA homologues, but is consistent with assemblies moving with chromosome segregation (Fig. 9.6) (Lutkenhaus, 2012), suggesting an important role for the chromosome in this process (Roberts et al., 2012).

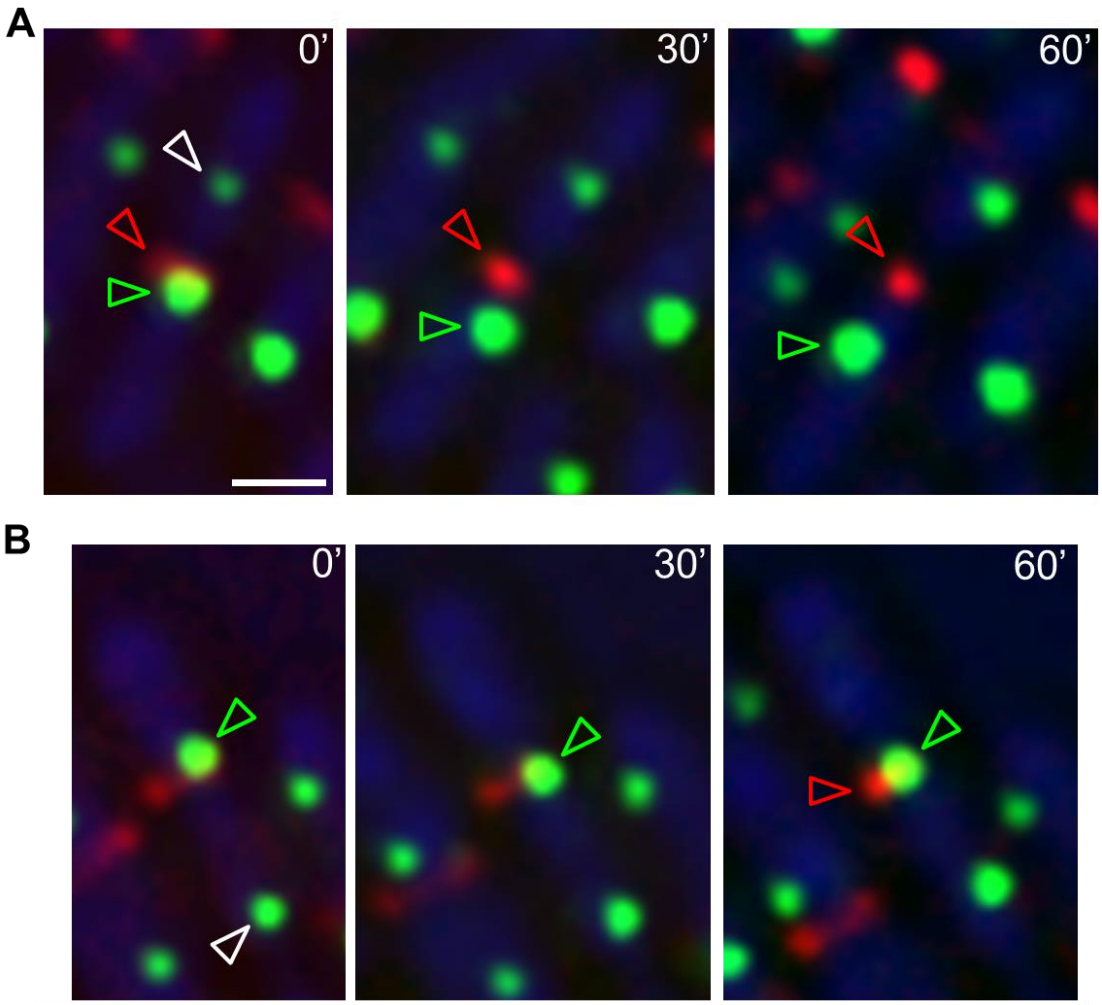

Figure 9.5. Asymmetric segregation of the cytoplasmic chemosensory clusters. **(A)** A two-cluster cell released from cephalexin treatment. Here, one cluster moves to future midcell first (white arrowhead), while another stays with the Z-ring at least till constriction (green arrowheads). Red arrowheads: Z-rings. **(B)** In a two-cluster cell released from cephalexin treatment, one cluster moves to future midcell first (white arrowhead), while another (green arrowheads) stays with the Z-ring even after intensive constriction (red arrowhead). Numbers: minutes of observation. Red, FtsZ–CFP; green, TlpT–YFP; blue: DIC. Scale bars: 1 μm.

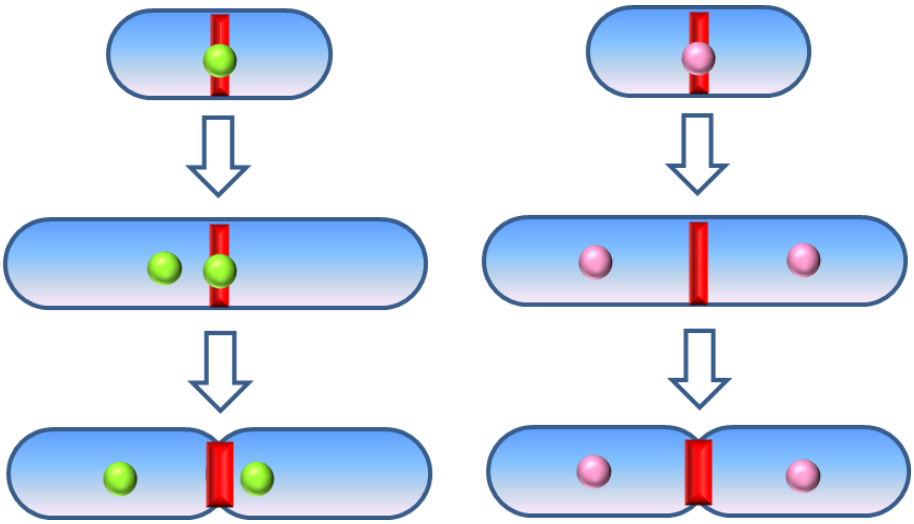

Figure 9.6. Simplified schematics for the partitioning patterns of the cytoplasmic chemosensory clusters (green, left). Also shown here is the general symmetric segregation model proposed for the partitioning of non-chromosome cytoplasmic cargos (purple, right) partitioned by ParA-like systems. Red: Z-rings. Arrows indicate progressions. For the cytoplasmic chemosensory clusters, one copy of the duplicated cluster moves toward one future cytokinetic site first. Another cluster stays around the divisome for longer, then moves to another cytokinetic site before the completion of cell division.

As mentioned in Chapter 6.2, the Z-ring was not always positioned precisely at the midcell (Fig. 6.2, lower panel). In some filamentous cells containing only one copy of the cytoplasmic chemosensory clusters, the cytoplasmic cluster was positioned far from the midcell (Fig. 9.7 A and B, green arrowheads). Intriguingly, the Z-ring also positioned very close to these cytoplasmic chemosensory clusters (i.e. shifted away from the "correct" midcell position) (Fig. 9.7 A and B, red arrowheads). The Z-ring seemed to arrive/form after cytoplasmic chemosensory clusters have already localised there. Consider the very long cell length (and thus numerous possible positioning sites), this coincidence of colocalisation is significant. In fewer cases, one copy of the cytoplasmic chemosensory clusters in two-cluster cells redistributed to a new location where the Z-ring was forming (Fig. 9.7 C, green arrowheads). These observations reinforce the idea that the cytoplasmic chemosensory clusters and FtsZ occupy similar subcellular locations.

Equi-partitioning is a central feature of non-chromosome cytoplasmic cargos positioned by ParA-like systems (Gerdes et al., 2010; Lutkenhaus, 2012; Salje, 2010; Vecchiarelli et al., 2012). A cargo has an average midcell position until the second cargo appears, which drives a shift in positions. Surprisingly, the

asymmetric segregation of cytoplasmic chemosensory clusters also occurred in one-cluster cells: the single cytoplasmic chemosensory cluster gradually left midcell for the new pole (Fig. 9.8, green arrowheads). This pattern might be compatible with chromosome segregation in *R. sphaeroides* (Nelly Dubarry, unpublished data).

Previous studies suggest that cytoplasmic chemosensory clusters are probably duplicated by the split of a cluster into two (Thompson et al., 2006). However, time-lapse imaging showed that only ~35% of dividing cells follow this route. In other ~65% of dividing cells, one daughter cell receives an existing cluster, while a new cluster becomes visible in another daughter cell shortly after cell division (Thompson et al., 2006). It is unclear whether a new cluster actually forms *de novo*, or an undetectable segregated cluster then grows. Using an imaging platform with better sensitivity and resolution, I found evidence supporting cytoplasmic chemosensory clusters could form *de novo*. Small clusters appeared in locations away from the original dominant clusters and grew in intensity (Figs 9.7 A, 9.8, 9.9; yellow arrowheads). Consider the slow movement and relative positioning of the small and big clusters, the simplest explanation is that the small clusters formed *de novo* and grew. Although rare, fusion of two clusters could be seen (Fig. 9.8, blue arrows).

The colocalisation of FtsZ and cytoplasmic chemosensory clusters was further examined in sphaeroplasts (Fig. 9.10). As mentioned in Chapter 3.5, sphaeroplasts were deficient in Z-ring formation, and it is difficult to distinguish between FtsZ polar spots and midcell nodes. Therefore, all FtsZ assemblies were viewed as the same group and their colocalisation with cytoplasmic chemosensory clusters was quantified (Table 9.1). The colocalisation of cytoplasmic chemosensory clusters and FtsZ was drastically reduced. However, if we consider "colocalised" and "near" (Table 9.1) as indications of close cellular locations, than cytoplasmic chemosensory clusters and FtsZ might still occupy similar regions in sphaeroplasts, if compare to the situation of FtsZ polar spots in normal cells. It is also possible that the close proximity of cytoplasmic clusters and FtsZ assemblies was a coincidence resulted from the random positioning of two structures.

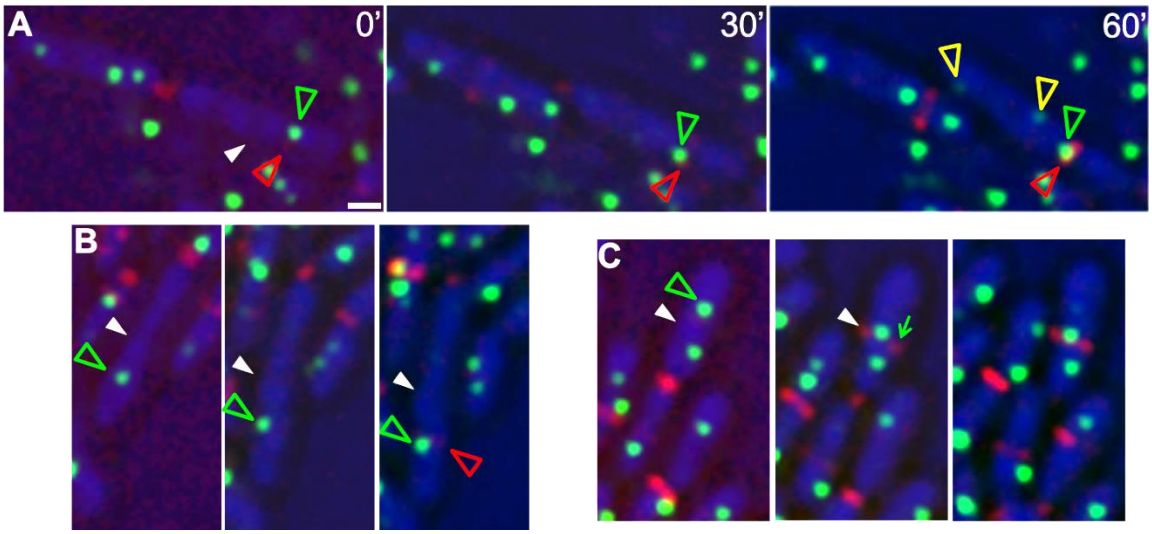

Figure 9.7. Cytoplasmic chemosensory clusters and FtsZ occupy similar subcellular locations. **(A and B)** The Z-ring (red arrowheads) is not positioned at the midcell (white arrowheads) but precisely at the positions with cytoplasmic clusters (green arrowheads). Yellow arrowheads: the appearance of two new clusters. **(C)** One of the cytoplasmic clusters (green arrowhead) localises outside of the midcell (white arrowheads) at the beginning, then moves (green arrow) to the midcell and colocalises with the Z-ring. Cells were released from cephalexin treatment. Numbers: minutes. Red, FtsZ–CFP; green, TlpT–YFP; blue: DIC. Scale bars: 1 μm.

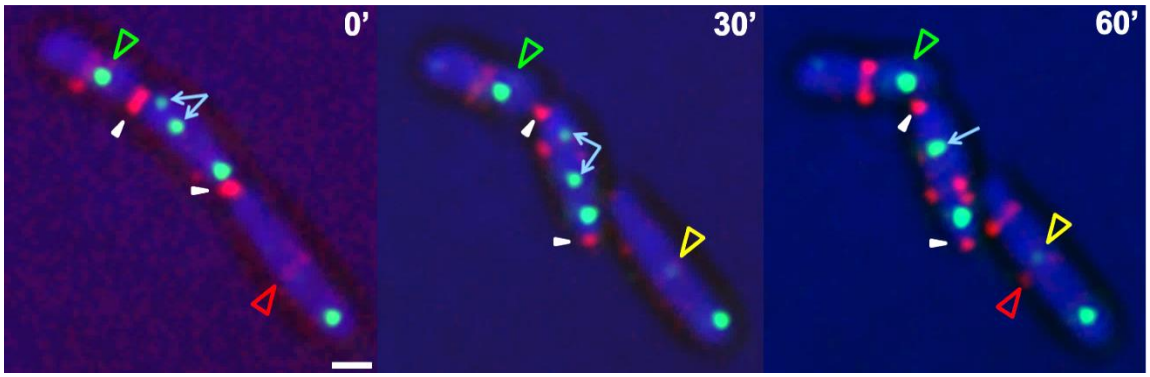

Figure 9.8. Dynamics of cytoplasmic chemosensory clusters in cells released from cephalexin treatment. Green arrowheads: a cluster is segregating without the presence of another cluster. Yellow arrowheads: the appearance of a new cluster, red arrowheads indicate the Z-ring or precursor that colocalises with the new cluster. Blue arrows: the fusion of two clusters. White arrowheads: the middle cell is derived from two cytokinetic events, which produce one FtsZ polar spot at each cell pole. Numbers: minutes. Red, FtsZ–CFP; green, TlpT–YFP; blue: DIC. Scale bars: 1 μm.

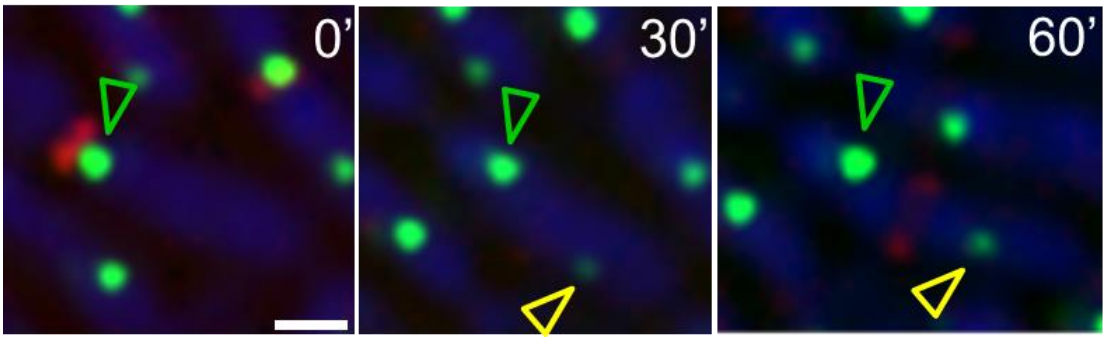

Figure 9.9. New cytoplasmic chemosensory clusters could form *de novo*. Yellow arrowheads: the appearance of a new cluster. Green arrowheads: an existing cluster. Cells were released from cephalexin treatment. Numbers: minutes. Red, FtsZ–CFP; green, TlpT–YFP; blue: DIC. Scale bars: 1 μm.

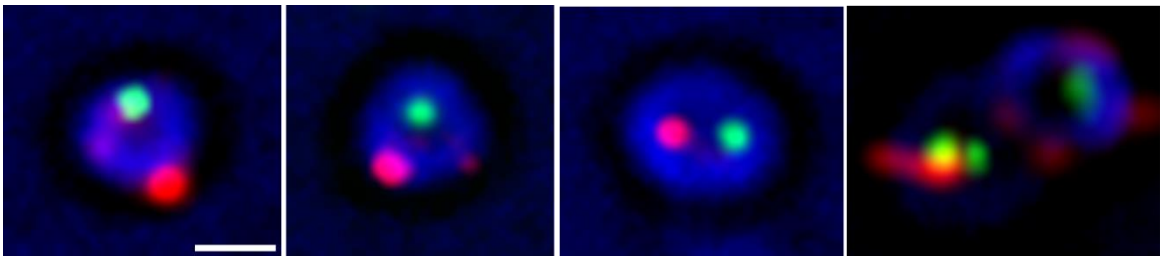

Figure 9.10. Relative positioning of cytoplasmic chemosensory clusters and FtsZ assemblies. Red, FtsZ–CFP; green, TlpT–YFP; blue: DIC. Scale bars: 1 μm.

Table 9.1. The relative positioning of cytoplasmic chemosensory clusters and FtsZ assemblies

FtsZ assemblies	Colocalization patterns		
	Colocalized[d]	Near[e]	Distant[f]
Spheroplast all[a]	17.9±9.9	38.6±10.6	43.5±17.5
Normal polar spot[b]	29.9±4.5	23.2±2.0	46.9±6.5
Normal midcell node/ Z-ring precursor[c]	51.7±15.4	39.2±9.5	9.1±6.1

[a] All FtsZ assemblies in spheroplasts were grouped together; n=296.
[b] For polar spots in normal cells; n=177.
[c] For midcell nodes/Z-ring precursors in normal cells; n=170.
[d] The two structures have overlaps in the diffraction-limited images.
[e] The shortest distances between the cytoplasmic clusters' centroids and FtsZ assemblies' edges are less than the diameters of cognate cytoplasmic clusters.
[f] All remaining (not d nor e).

9.4 Discussion and Conclusions

The cytoplasmic chemosensory cluster and FtsZ assemblies colocalise in a cell cycle-related manner (Fig. 9.2 B). The colocalisation mainly occurs at cytokinetic sites, but cytoplasmic chemosensory clusters leave for future cytokinetic sites before FtsZ. The cytoplasmic chemosensory cluster and FtsZ might occupy similar cellular locations, but FtsZ assemblies are probably not anchors for the positioning of cytoplasmic chemosensory clusters.

In *M. gryphiswaldense*, the magnetosomes undergo a dynamic pole-to-midcell translocation during the cell cycle, which is mediated by the actin-like protein MamK (Katzmann et al., 2011). A truncated *ftsZ* homologue (*ftsZm*) is located adjacent to genes controlling magnetosome chain formation. It has been proposed that midcell positioning of magnetosomes might be controlled by interactions with FtsZ or FtsZm (Müller et al., 2014). However, no evidence supports magnetosomes/MamK interact with the two FtsZ homologues (Müller

et al., 2014). But it is clear that the midcell localisation of magnetosome chains is critical for the segregation of magnetosomes into daughter cells (Katzmann et al., 2011). Therefore, localizing at the cytokinetic site might be a strategy utilized by different macromolecular assemblies for faithful partitioning.

The occupation of similar cellular regions could be resulted from the average midcell positioning of cytoplasmic chemosensory clusters. However, since colocalisation of FtsZ and cytoplasmic chemosensory clusters also exists for far-from-midcell positions (Fig. 9.7 A and B), there seems to have a deeper connections. One possibility is that cytoplasmic clusters and FtsZ localise to cellular regions with less nucleoid hindrance (Laloux and Jacobs-Wagner, 2014; Vecchiarelli et al., 2012). Although the nucleoid may contribute to the formation and partitioning of cytoplasmic chemosensory clusters (Roberts et al., 2012), how the nucleoid organisation may affect the architecture and localisation of cytoplasmic clusters is unclear. It is possible that a cellular region with a bigger DNA-free gap can provide a DNA surface for the cytoplasmic chemosensory cluster but still leave a room for it to assemble easier. Conventional fluorescence microscopy shows that chromosomes fill the entire *R. sphaeroides* cytoplasm (Thompson et al., 2006), similar to *C. crescentus* (Laloux and Jacobs-Wagner, 2014). It has been shown that the *C. crescentus* hub protein PopZ forms higher-order structures in regions of low DNA content (Laloux and Jacobs-Wagner, 2014). Thus, a cellular region with a bigger DNA-free gap may facilitate the colocalisation of cytoplasmic chemosensory clusters and FtsZ assemblies. Another possibility is that the cytoplasmic chemosensory cluster may recognize specific chromosomal loci or structures. Cells may evolve to have a specific chromosome architecture (Ptacin and Shapiro, 2013), so the relative positioning between these loci/structures and the *oriC* region is coordinated. Since the positioning of the *oriC* region affects the localisation of FtsZ via MipZ (Thanbichler and Shapiro, 2006), the proposed coordination may ensure that cytoplasmic chemosensory clusters can localise at (pre)cytokinetic sites.

Chromosome dynamics may also participate in the segregation of cytoplasmic chemosensory clusters. The asymmetric partitioning of cytoplasmic chemosensory clusters could be driven by the *C. crescentus*-like asymmetric chromosome segregation (Toro and Shapiro, 2010) in *R. sphaeroides* (Nelly Dubarry, unpublished data). This could be mediated by attaching the cytoplasmic chemosensory clusters to specific chromosomal loci/structures (e.g. via PpfA). Alternatively, chromosome segregation may cause a shift in "binding potency" and trigger the movement of cytoplasmic clusters. In this second scenario, DNA sequence-specificity is not required for PpfA. Chromosome segregation simply

changes the distribution of available non-specific binding sites, and PpfA will follow this shift, resulting in the segregation of cytoplasmic chemosensory clusters. The nucleoid itself, or chromosome dynamics, has critical roles in the spatial organisation of other cytoplasmic macromolecular assemblies, including carboxysomes (Jain et al., 2012), poly(3-hydroxybutyrate) (PHB) granules (Galán et al., 2011; Pfeiffer and Jendrossek, 2012; Pfeiffer et al., 2011; Wahl et al., 2012), plasmids (Gerdes et al., 2010; Lutkenhaus, 2012; Salje, 2010; Vecchiarelli et al., 2012), and polyphosphate (polyP) granules (Henry and Crosson, 2013). Nucleoid exclusion, association with a specific chromosomal locus, or nucleoid matrix (i.e. nonspecific DNA-binding of ParA-like proteins) have been proposed to explain the functions of the nucleoid in these cases. Except plasmid segregation, no strong evidence exists for any of them. Nevertheless, it is clear that the communications between the nucleoid and these macromolecular assemblies affect the spatial organisation of these diverse systems.

The exact mechanisms of the formation and duplication of cytoplasmic chemosensory clusters are under investigations (Jones, 2013). Conceivably, some similarities between membrane and cytoplasmic chemosensory clusters might exist. The emergence of new cytoplasmic chemosensory clusters (Figs 9.7—9.9, yellow arrowheads) is compatible to a stochastic self-assembly process (Thiem and Sourjik, 2008; Wang et al., 2008a). Besides, fusion (congregation-like) (Fig 9.8, blue arrows) and fission (segregation-like) (Thompson et al., 2006) of cytoplasmic chemosensory clusters can be seen. Thompson et al. (2006) showed that *de novo* formation of new cytoplasmic chemosensory clusters occurs in newborn cells not inheriting a cluster from the last cell division. Here I found that *de novo* cluster formation occurs in (filamentous) cells containing existing clusters (Figs 9.7—9.9, yellow arrowheads). It is possible that the shorter length/smaller volume of normal cells results in absorption of emerging clusters by the existing clusters, or a decrease in nucleation probability. Alternatively, newly formed clusters are quickly segregated to or directly nucleated at pre-cytokinetic sites (Figs 9.8 and 9.9, yellow arrowheads), therefore undistinguishable from new clusters "split" from existing clusters. In contrast to another ParA-like protein ParC (Ringgaard et al., 2011; Ringgaard et al., 2014), PpfA not only participates in the positioning of chemosensory clusters, but also their duplication (Thompson et al., 2006). The answer for how PpfA regulates the duplication of cytoplasmic chemosensory clusters may lie on the clarification of nucleation- vs. split-mode of new cluster formation.

In conclusion, the cytoplasmic chemosensory cluster and FtsZ assemblies occupy similar cellular locations, but FtsZ assemblies are not anchors for the

positioning of cytoplasmic chemosensory clusters. Comparing to other ParA-like proteins, the asymmetric segregation of cytoplasmic chemosensory clusters hints a different or modified mechanism employed by PpfA for cargo positioning.

Chapter 10. General Discussion

What we call the beginning is often the end. And to make an end is to make a beginning. The end is where we start from.

— *Little Gidding*, Thomas Stearns Eliot

10.1 Summary of Findings

The establishment and maintenance of the specific localisation of chemosensory proteins are pivotal for the survival of bacteria. Each round of cell division brings great challenges to these tasks. Based on the studies of *E. coli*, a stochastic self-assembly model has been proposed for the spatial regulation of membrane chemosensory clusters. This model, requires only simple physicochemical principles, is believed to be a common mechanism used by different bacteria. However, this model cannot explain the static behaviour of lateral membrane clusters in *E. coli*. Therefore, some forms of anchors are probably working in concert with the stochastic self-assembly process. The FtsZ and MreB cytoskeletons are the most likely known candidates. In this study, I tested whether these two bacterial cytoskeletons and the stochastic self-assembly process are responsible for the polar localisation of membrane chemosensory clusters in *R. sphaeroides*. As there have been no previous studies on FtsZ in *R. sphaeroides* I first investigated the spatiotemporal dynamics of FtsZ through the *R. sphaeroides* cell cycle. FtsZ has cell cycle-stage specific localisation similar to that observed in *C. crescentus* (Chapter 3). However, FtsZ polar spots move from the new pole to the midcell directly, not via the previously proposed helical intermediate. Besides, the Z-ring is developed from midcell nodes, suggesting a new mechanism for Z-ring formation. Surprisingly, the membrane chemosensory clusters in *R. sphaeroides* do not colocalise with FtsZ assemblies and show different behaviours comparing to those in *E. coli*. FtsZ does not act as an anchor for the membrane chemosensory clusters, but participates in their positioning probably by excluding them from localise in the Z-ring vicinity (Chapter 6).

The MreB cytoskeleton continuously reorganizes between patchy and

filamentous structures in *R. sphaeroides* (Chapter 4). MreB also changes its main localisation according to cell-cycle stages, and colocalises with FtsZ at the midcell until constriction. Intriguingly, MreB localises at pre-cytokinetic sites before FtsZ, which is different compared with *C. crescentus* and *E. coli*, suggesting a unique mechanism to position MreB at the midcell in *R. sphaeroides*. MreB shows no roles in the positioning of the membrane chemosensory clusters in *R. sphaeroides* (Chapter 5).

Previous studies have suggested that membrane chemosensory proteins in *E. coli* form huge polar caps and static small clusters at pre-cytokinetic sites. Using quantitative fluorescence imaging I found that membrane chemosensory proteins in *R. sphaeroides* behave very differently: they form individual dynamic unit-clusters with an optimal size which diffuse randomly and congregate–segregate continuously within the membrane (Chapter 7). The membrane chemosensory clusters show high propensity to curved regions (Chapter 8). The above results suggest that a diffusion-and-capture mechanism results in the polar localisation of membrane chemosensory clusters in *R. sphaeroides* (Chapter 8).

The time-averaged localisation and the involvement of a ParA homologue in the positioning suggest that the *R. sphaeroides* cytoplasmic chemosensory clusters may use a plasmid segregation-like mechanism for their partitioning. However, the distinct asymmetric segregation of cytoplasmic chemosensory clusters (Chapter 9) indicates a different mechanism. Although the cytoplasmic chemosensory clusters colocalise with FtsZ assemblies, they move to future cytokinetic sites before FtsZ, suggesting FtsZ is not an anchor for their positioning. MreB also shows no direct roles in the positioning of the cytoplasmic chemosensory clusters. Therefore, the FtsZ and MreB cytoskeletons are not anchors for the positioning of both membrane and cytoplasmic chemosensory clusters in *R. sphaeroides*.

10.2 The *In Vivo* Configurations of Bacterial Cytoskeletons

The relationship between form and function is the central aspect of cytoskeleton researches. This was illustrated by the diverse configurations and functions possess by different bacterial cytoskeletal proteins (Pilhofer and Jensen, 2013). However, two important questions remain to be answered. Firstly, what are the exact *in vivo* structures of the bacterial cytoskeletons? Secondly, are there multiple configurations existing for a given bacterial cytoskeletal protein? The conversion between patchy and filamentous MreB structures in *R. sphaeroides* (Chapter 4.4)

suggests a possibility that assemblies of MreB homologues can adopt both filamentous and patchy configurations. Which form is present in the cell at a given time is likely to be determined by the physiological and cell-cycle states. Further systematic investigations using different super-resolution imaging approaches will be necessary to explore this possibility.

In this study I also found that distinct FtsZ structures exist in *R. sphaeroides* according to the cell-cycle stages. These structures have their specific functions in the cell: the polar FtsZ spot is a reservoir of FtsZ molecules after cell division, and can redistribute FtsZ to the future cytokinetic site; the midcell node is the embryo for Z-ring development, from which different Z-ring precursor structures are generated; and the Z-ring for cytokinesis. In eukaryotes, cytoskeletal proteins also form distinct structures that perform different functions with the help of accessory proteins (Berepiki et al., 2011; Kovar et al., 2011; Moseley and Goode, 2006). Although previous super-resolution imaging studies have shown that the Z-ring is not a uniform, continuous structure (Biteen et al., 2012; Buss et al., 2013; Fu et al., 2010; Holden et al., 2014; Jennings et al., 2011; Li et al., 2007), the *in vivo* ultrastructures of different FtsZ assemblies remain obscure. Nevertheless, quantitative image analysis suggests that the Z-ring/ring-precursors have an architecture that is in consistent with a loose bundle model, while the polar spot might have a different organisation (Chapter 3.4). We have recently established collaboration with Jan Lowe's group (MRC Laboratory of Molecular Biology) to further investigate the ultrastructures of these different FtsZ assemblies via electron cryo-tomography. It would be interesting to see how the diverse *in vitro* FtsZ structures correlate to the formation of different *in vivo* higher-order structures.

With the quick growth in the studies of bacterial cytoskeletal systems, it is now clear that homologous bacterial cytoskeletal proteins can form distinct structures, and proteins belonging to different families can adopt similar configurations (Pilhofer and Jensen, 2013). To understand the designing principles underlying these different form-and-function combinations, clear pictures of the *in vivo* structures of bacterial cytoskeletons are certainly essential.

10.3 Spatial Organisation of Chemosensory Proteins

Clustering of chemosensory proteins

Clustering is a fundamental means for spatial organisation of chemosensory

proteins, which greatly improves the efficiency, fidelity and robustness of chemotaxis (Bray et al., 1998; Gestwicki and Kiessling, 2002; Hazelbauer et al., 2008; Pilhofer and Jensen, 2013; Pontius et al., 2013). Previous studies have suggested that a stochastic self-assembly process may be responsible for the clustering. Here, by using quantitative time-lapse imaging, I found that membrane chemosensory proteins form unit-clusters with an optimal size, therefore provides a missing organisation level between the molecular signalling teams and the huge cellular clusters. The unit-size behaviour of *R. sphaeroides* membrane chemosensory proteins probably applies to other bacterial species (Chapter 7.4). The use of more rod-shaped species (e.g. *E. coli*) where the escape of mobile unit-clusters from curved poles is probably less common than in *R. sphaeroides*, may render the unit-size behaviour difficult to be observed. Although mathematical modelling has suggested that there might be an optimal size for chemosensory clusters (Aquino et al., 2011), this study provides the first direct demonstration and quantification of such a cluster size.

In eukaryotes, intrinsic interactions between protein components, constrains of cytoskeletal networks, and effects of local membrane organisation all contribute to the size distribution of membrane protein clusters (Mueller et al., 2012). The currently identified bacterial membrane domains (López and Kolter, 2010) are hence promising organizers of these chemosensory unit-clusters. Therefore, in addition to a direct implication in chemotaxis, studying the size determination and dynamics of unit-clusters may also reveal a hidden organisation of bacterial membrane.

While the membrane chemosensory proteins form unit-size clusters, the *R. sphaeroides* cytoplasmic chemosensory proteins form clusters without any preference size (Chapter 9). FRAP experiments show that the cytoplasmic cluster is a relatively stable structure with limited turnover (Jones, 2013). In cells with defects in PpfA's functions, the cytoplasmic clusters keep growing and result in very huge clusters (Roberts et al., 2012; Thompson et al., 2006). These observations suggest that different mechanisms are used for size determination of two homologous chemosensory clusters. The nucleoid is supposed to play a matrix-like role for the cytoplasmic cluster (analogous to the the role of cytoplasmic membrane to the membrane cluster). It is possible that the differences in the cognate matrixes, or the presence of a ParA system for partitioning, may be responsible for the differences in size determination of membrane and cytoplasmic clusters.

Positioning of chemosensory clusters

It has been assumed that the stochastic self-assembly/cytokinetic-site anchoring model may reflect the positioning mechanism for the universal polar/subpolar localisation of membrane chemosensory clusters. However, the identity of the anchor for lateral clusters remains unclear. The localisation pattern, however, suggests that the FtsZ or MreB cytoskeletal systems are likely candidates. Here I showed that they are not involved in anchoring the membrane chemosensory clusters to the pre-cytokinetic sites in *R. sphaeroides* (Chapters 5 and 6). Nevertheless, current studies show that a ParA-like protein, ParC, does anchor the membrane chemosensory clusters to the cell pole in some polar-flagellated bacteria (Ringgaard et al., 2011; Ringgaard et al., 2014; Yamaichi et al., 2012).

So far, the positioning mechanisms for membrane chemosensory clusters are directly studied in only three bacterial models (*E. coli*, *R. sphaeroides*, and vibrios). Intriguingly, three bacterial models yielded three different mechanisms, raising the possibility that more mechanisms are waiting to be discovered. Nevertheless, a fundamental "diffusion-and-capture" principle is used by *R. sphaeroides* and vibrios, albeit differently via cell geometry and a ParA-like anchor, respectively. The limited appearance of ParC homologues, and the putative evolutionary path of the tripartite ParC–ParP–CheA system (Ringgaard et al., 2011; Ringgaard et al., 2014; Yamaichi et al., 2012), suggesting that a ParA homologue was acquired by an ancestor of a group of polarly flagellated γ-proteobacteria. This ParA homologue then developed a role in the positioning of membrane chemosensory clusters via a coevolution with ParP and CheA. Intriguingly, both TlpT and ParP play a ParB-like role in controlling the activity of PpfA and ParC, and link these ParA homologues to their cargos. This may represent a general evolutionary mechanism for bacteria to adopt different ParA homologues for the positioning of diverse cargos. The versatility of ParA-like systems, indeed, is clearly demonstrated by the partitioning of cytoplasmic chemosensory clusters in *R. sphaeroides* and membrane chemosensory clusters in vibrios.

10.4 Conclusions and Future Perspectives

Taken together, this study shows that very different mechanisms are employed by *R. sphaeroides* to ensure daughter cells inherit two homologous chemosensory systems during cell division. The membrane chemosensory system relies on the random diffusion of unit-clusters and polar trapping via cell geometry. The

cytoplasmic system depends on a ParA-like system and might coordinate with chromosome segregation. The FtsZ and MreB cytoskeleton are not anchors for the positioning of both chemosensory systems. FtsZ has cell-cycle specific localisation in *R. sphaeroides*, with polar spots moving to midcell to produce nodes from which the Z-ring develops.

The spatiotemporal organisation of the bacterial cell is one of the most active areas in microbiology, producing paradigms that reveal mechanisms of cellular dynamics relevant to all cell types. It is now clear that the cytoskeleton is no longer a unique feature of eukaryotes. However, the studies of prokaryotic cytoskeleton are still greatly motivated by the richness of eukaryotic cytoskeleton research. Nevertheless, studies of bacterial cytoskeletal proteins have greatly improved our understandings of the eukaryotic counterparts. The ease of working with bacterial models and quick development in super-resolution imaging might make the studies of bacterial cytoskeleton and other aspects of spatial organisation become increasingly important to eukaryotic cell biology. The identifications of prokaryotes-specific cytoskeletal proteins further highlight the unique role of bacteria in cell biology.

Besides the cytoskeleton, cell signalling and membrane organisation are the other two important areas of eukaryotic cell biology. One theme that connects these two fields is protein clustering. The discovery of bacterial chemosensory unit-clusters may provide a route to explore common mechanisms of protein clustering by studying bacteria.

Future researches on the *in vivo* organisation of FtsZ assemblies and chemosensory unit-clusters, using a combination of quantitative super-resolution imaging and computer modelling, might be exciting paths to pursue. Simultaneous observations of divisome components may identify FtsZ-interacting proteins which participate in the reorganisation of different FtsZ assemblies. *In vitro* reconstruction and microfabrications (Dogterom and Surrey, 2013; Martos et al., 2012; Vignaud et al., 2012) of FtsZ assemblies are also promising approaches.

For sure, bacteria are not just “bags of enzymes”, but “bags of surprises”!

Bibliography

Aaron, M., Charbon, G., Lam, H., Schwarz, H., Vollmer, W., and Jacobs-Wagner, C. (2007). The tubulin homologue FtsZ contributes to cell elongation by guiding cell wall precursor synthesis in *Caulobacter crescentus*. Mol Microbiol 64, 938-952.

Aarsman, M.E.G., Piette, A., Fraipont, C., Vinkenvleugel, T.M.F., Nguyen-Distèche, M., and den Blaauwen, T. (2005). Maturation of the *Escherichia coli* divisome occurs in two steps. Mol Microbiol 55, 1631-1645.

Abhayawardhane, Y., and Stewart, G.C. (1995). *Bacillus subtilis* possesses a second determinant with extensive sequence similarity to the *Escherichia coli mreB* morphogene. J Bacteriol 177, 765-773.

Adachi, S., Hori, K., and Hiraga, S. (2006). Subcellular positioning of F plasmid mediated by dynamic localization of SopA and SopB. J Mol Biol 356, 850-863.

Adams, D.W., and Errington, J. (2009). Bacterial cell division: assembly, maintenance and disassembly of the Z ring. Nat Rev Microbiol 7, 642-653.

Adams, D.W., Wu, L.J., Czaplewski, L.G., and Errington, J. (2011). Multiple effects of benzamide antibiotics on FtsZ function. Mol Microbiol 80, 68-84.

Addinall, S.G., and Lutkenhaus, J. (1996). FtsZ-spirals and -arcs determine the shape of the invaginating septa in some mutants of *Escherichia coli*. Mol Microbiol 22, 231-237.

Alberts, B., Johnson, A., Lewis, J., Raff, M., Roberts, K., and Walter, P. (2007). The Cytoskeleton. In *Molecular Biology of the Cell*, 5th ed. (New York: Garland Publishing).

Alexandre, G. (2010). Coupling metabolism and chemotaxis-dependent behaviours by energy taxis receptors. Microbiology 156, 2283-2293.

Allard, J.F., and Cytrynbaum, E.N. (2009). Force generation by a dynamic Z-ring in *Escherichia coli* cell division. Proc Natl Acad Sci USA 106, 145-150.

Alley, M.R., Maddock, J.R., and Shapiro, L. (1992). Polar localization of a bacterial chemoreceptor. Genes Dev 6, 825-836.

Alyahya, S.A., Alexander, R., Costa, T., Henriques, A.O., Emonet, T., and Jacobs-Wagner, C. (2009). RodZ, a component of the bacterial core morphogenic apparatus. Proc Natl Acad Sci USA 106, 1239-1244.

Amster-Choder, O. (2011). The compartmentalized vessel: the bacterial cell as a model for subcellular organization (a tale of two studies). Cell Logist 1, 77-81.

Anderson, D.E., Gueiros-Filho, F.J., and Erickson, H.P. (2004). Assembly dynamics of FtsZ rings in *Bacillus subtilis* and *Escherichia coli* and effects of FtsZ-regulating proteins. J Bacteriol 186, 5775-5781.

Aquino, G., Clausznitzer, D., Tollis, S., and Endres, R.G. (2011). Optimal receptor-cluster size determined by intrinsic and extrinsic noise. Phys Rev E Stat Nonlin Soft Matter Phys 83, 021914.

Arai, H., Roh, J.H., and Kaplan, S. (2008). Transcriptome dynamics during the transition from anaerobic photosynthesis to aerobic respiration in *Rhodobacter sphaeroides* 2.4.1. J Bacteriol 190, 286-299.

Armitage, J., and Scott, K. (2013). Bacterial Behavior. In *The Prokaryotes*, E. Rosenberg, E. DeLong, S. Lory, E. Stackebrandt, and F. Thompson, eds. (Heidelberg: Springer), pp. 289-316.

Armitage, J.P., Pitta, T.P., Vigeant, M.A.-S., Packer, H.L., and Ford, R.M. (1999). Transformations in flagellar structure of *Rhodobacter sphaeroides* and possible relationship to changes in swimming speed. J Bacteriol 181, 4825-4833.

Armitage, J.P., and Schmitt, R. (1997). Bacterial chemotaxis: *Rhodobacter sphaeroide* and *Sinorhizobium meliloti* - variations on a theme? Microbiology 143, 3671-3682.

Atmakuri, K., Cascales, E., Burton, O.T., Banta, L.M., and Christie, P.J. (2007). *Agrobacterium* ParA/MinD-like VirC1 spatially coordinates early conjugative DNA transfer reactions. EMBO J 26, 2540-2551.

Aylett, C.H.S., Löwe, J., and Amos, L.A. (2011). New insights into the mechanisms of cytomotive actin and tubulin filaments. Int Rev Cell Mol Biol 292, 1-71.

Baker, M.D., Wolanin, P.M., and Stock, J.B. (2006). Systems biology of bacterial

chemotaxis. Curr Opin Microbiol 9, 187-192.

Bardy, S., and Maddock, J. (2007). Polar explorations: recent insights into the polarity of bacterial proteins. Curr Opin Microbiol 10, 617-623.

Bardy, S.L., and Maddock, J.R. (2005). Polar localization of a soluble methyl-accepting protein of *Pseudomonas aeruginosa*. J Bacteriol 187, 7840-7844.

Barilla, D., Rosenberg, M.F., Nobbmann, U., and Hayes, F. (2005). Bacterial DNA segregation dynamics mediated by the polymerizing protein ParF. EMBO J 24, 1453-1464.

Bean, G.J., and Amann, K.J. (2008). Polymerization properties of the *Thermotoga maritima* actin MreB: roles of temperature, nucleotides, and ions. Biochemistry 47, 826-835.

Bean, G.J., Flickinger, S.T., Westler, W.M., McCully, M.E., Sept, D., Weibel, D.B., and Amann, K.J. (2009). A22 disrupts the bacterial actin cytoskeleton by directly binding and inducing a low-affinity state in MreB. Biochemistry 48, 4852-4857.

Begg, K.J., and Donachie, W.D. (1985). Cell shape and division in *Escherichia coli*: experiments with shape and division mutants. J Bacteriol 163, 615-622.

Ben-Yehuda, S., and Losick, R. (2002). Asymmetric cell division in *B. subtilis* involves a spiral-like intermediate of the cytokinetic protein FtsZ. Cell 109, 257-266.

Bendezú, F.O., and de Boer, P.A.J. (2008). Conditional lethality, division defects, membrane involution, and endocytosis in *mre* and *mrd* shape mutants of *Escherichia coli*. J Bacteriol 190, 1792-1811.

Bendezu, F.O., Hale, C.A., Bernhardt, T.G., and de Boer, P.A.J. (2009). RodZ (YfgA) is required for proper assembly of the MreB actin cytoskeleton and cell shape in *E. coli*. EMBO J 28, 193-204.

Berepiki, A., Lichius, A., and Read, N.D. (2011). Actin organization and dynamics in filamentous fungi. Nat Rev Microbiol 9, 876-887.

Berg, H.C., and Purcell, E.M. (1977). Physics of chemoreception. Biophys J 20, 193-219.

Berlatzky, I.A., Rouvinski, A., and Ben-Yehuda, S. (2008). Spatial organization of a replicating bacterial chromosome. Proc Natl Acad Sci USA 105, 14136-14140.

Bermudes, D., Hinkle, G., and Margulis, L. (1994). Do prokaryotes contain microtubules? Microbiol Mol Biol Rev 58, 387-400.

Bernhardt, T.G., and de Boer, P.A.J. (2005). SlmA, a nucleoid-associated, FtsZ binding protein required for blocking septal ring assembly over chromosomes in *E. coli*. Mol Cell 18, 555-564.

Bi, E., and Lutkenhaus, J. (1991). FtsZ ring structure associated with division in *Escherichia coli*. Nature 354, 161-164.

Bisicchia, P., Arumugam, S., Schwille, P., and Sherratt, D. (2013). MinC, MinD, and MinE drive counter-oscillation of early-cell-division proteins prior to *Escherichia coli* septum formation. mBio 4, e00856-13.

Biteen, J.S. (2012). Extending the tools of single-molecule fluorescence imaging to problems in microbiology. Mol Microbiol 85, 1-4.

Biteen, J.S., Goley, E.D., Shapiro, L., and Moerner, W.E. (2012). Three-dimensional super-resolution imaging of the midplane protein FtsZ in live *Caulobacter crescentus* cells using astigmatism. ChemPhysChem 13, 1007-1012.

Biteen, J.S., and Moerner, W.E. (2010). Single-molecule and superresolution imaging in live bacteria cells. Cold Spring Harb Perspect Biol 2, a000448.

Biteen, J.S., Thompson, M.A., Tselentis, N.K., Bowman, G.R., Shapiro, L., and Moerner, W.E. (2008). Super-resolution imaging in live *Caulobacter crescentus* cells using photoswitchable EYFP. Nat Meth 5, 947-949.

Boberek, J., Stach, J., and Good, L. (2010). Genetic evidence for inhibition of bacterial division protein FtsZ by berberine. PLoS One 5, e13745.

Bolte, S., and Cordelieres, F.P. (2006). A guided tour into subcellular colocalization analysis in light microscopy. J Microsc 224, 213-232.

Bork, P., Sander, C., and Valencia, A. (1992). An ATPase domain common to prokaryotic

cell cycle proteins, sugar kinases, actin, and hsp70 heat shock proteins. Proc Natl Acad Sci USA 89, 7290-7294.

Bouet, J.-Y., Ah-Seng, Y., Benmeradi, N., and Lane, D. (2007). Polymerization of SopA partition ATPase: regulation by DNA binding and SopB. Mol Microbiol 63, 468-481.

Bowman, G., Comolli, L., Zhu, J., Eckart, M., Koenig, M., Downing, K., Moerner, W., Earnest, T., and Shapiro, L. (2008). A polymeric protein anchors the chromosomal origin/ParB complex at a bacterial cell pole. Cell 134, 945-955.

Bramkamp, M., and van Baarle, S. (2009). Division site selection in rod-shaped bacteria. Curr Opin Microbiol 12, 683-688.

Brandt, F., Etchells, S.A., Ortiz, J.O., Elcock, A.H., Hartl, F.U., and Baumeister, W. (2009). The native 3D organization of bacterial polysomes. Cell 136, 261-271.

Bray, D., Levin, M.D., and Morton-Firth, C.J. (1998). Receptor clustering as a cellular mechanism to control sensitivity. Nature 393, 85-88.

Brehm-Stecher, B.F., and Johnson, E.A. (2004). Single-cell microbiology: tools, technologies, and applications. Microbiol Mol Biol Rev 68, 538-559.

Briegel, A., Ladinsky, M.S., Oikonomou, C., Jones, C.W., Harris, M.J., Fowler, D.J., Chang, Y.-W., Thompson, L.K., Armitage, J.P., and Jensen, G.J. (2014). Structure of bacterial cytoplasmic chemoreceptor arrays and implications for chemotactic signalling. eLife 3, e02151.

Briegel, A., Li, X., Bilwes, A.M., Hughes, K.T., Jensen, G.J., and Crane, B.R. (2012). Bacterial chemoreceptor arrays are hexagonally packed trimers of receptor dimers networked by rings of kinase and coupling proteins. Proc Natl Acad Sci USA 109, 3766-3771.

Briegel, A., Ortega, D.R., Tocheva, E.I., Wuichet, K., Li, Z., Chen, S., Müller, A., Iancu, C.V., Murphy, G.E., Dobro, M.J., et al. (2009). Universal architecture of bacterial chemoreceptor arrays. Proc Natl Acad Sci USA 106, 17181-17186.

Brown, P.J.B., de Pedro, M.A., Kysela, D.T., Van der Henst, C., Kim, J., De Bolle, X., Fuqua, C., and Brun, Y.V. (2012). Polar growth in the Alphaproteobacterial order

Rhizobiales. Proc Natl Acad Sci USA 109, 1697-1701.

Browning, D.F., Grainger, D.C., and Busby, S.J.W. (2010). Effects of nucleoid-associated proteins on bacterial chromosome structure and gene expression. Curr Opin Microbiol 13, 773-780.

Buss, J., Coltharp, C., Huang, T., Pohlmeyer, C., Wang, S.-C., Hatem, C., and Xiao, J. (2013). In vivo organization of the FtsZ-ring by ZapA and ZapB revealed by quantitative super-resolution microscopy. Mol Microbiol 89, 1099-1120.

Cabeen, M., Charbon, G., Vollmer, W., Born, P., Ausmees, N., Weibel, D., and Jacobs-Wagner, C. (2009). Bacterial cell curvature through mechanical control of cell growth. EMBO J 28, 1208-1219.

Cabeen, M., and Jacobs-Wagner, C. (2010). The bacterial cytoskeleton. Annu Rev Genet 44, 365-392.

Campos, M., and Jacobs-Wagner, C. (2013). Cellular organization of the transfer of genetic information. Curr Opin Microbiol 16, 171-176.

Carballido-López, R. (2006). The bacterial actin-like cytoskeleton. Microbiol Mol Biol Rev 70, 888-909.

Carballido-Lopez, R., and Errington, J. (2003). The bacterial cytoskeleton: in vivo dynamics of the actin-like protein Mbl of *Bacillus subtilis*. Dev Cell 4, 19-28.

Carballido-López, R., and Formstone, A. (2007). Shape determination in *Bacillus subtilis*. Curr Opin Microbiol 10, 611-616.

Cava, F., Kuru, E., Brun, Y.V., and de Pedro, M.A. (2013). Modes of cell wall growth differentiation in rod-shaped bacteria. Curr Opin Microbiol 16, 731-737.

Cebecauer, M., Spitaler, M., Sergé, A., and Magee, A.I. (2010). Signalling complexes and clusters: functional advantages and methodological hurdles. J Cell Sci 123, 309-320.

Charbon, G., Brustad, E., Scott, K.A., Wang, J., Løbner-Olesen, A., Schultz, P.G., Jacobs-Wagner, C., and Chapman, E. (2011). Subcellular protein localization by using a genetically encoded fluorescent amino acid. ChemBioChem 12, 1818-1821.

Charbon, G., Cabeen, M.T., and Jacobs-Wagner, C. (2009). Bacterial intermediate filaments: in vivo assembly, organization, and dynamics of crescentin. Genes Dev 23, 1131-1144.

Chastanet, A., and Carballido-Lopez, R. (2012). The actin-like MreB proteins in *Bacillus subtilis*: a new turn. Front Biosci (Schol Ed) 4, 1582-1606.

Chiu, S.-W., Chen, S.-Y., and Wong, H.-C. (2008). Localization and expression of MreB in *Vibrio parahaemolyticus* under different stresses. Appl Environ Microbiol 74, 7016-7022.

Chiu, S.-W., and Leake, M.C. (2011). Functioning nanomachines seen in real-time in living bacteria using single-molecule and super-resolution fluorescence imaging. Int J Mol Sci 12, 2518-2542.

Chiu, S.-W., Roberts, M.A.J., Leake, M.C., and Armitage, J.P. (2013). Positioning of chemosensory proteins and FtsZ through the *Rhodobacter sphaeroides* cell cycle. Mol Microbiol 90, 322-337.

Cho, H., McManus, H.R., Dove, S.L., and Bernhardt, T.G. (2011). Nucleoid occlusion factor SlmA is a DNA-activated FtsZ polymerization antagonist. Proc Natl Acad Sci USA 108, 3773–3778.

Chory, J., Donohue, T.J., Varga, A.R., Staehelin, L.A., and Kaplan, S. (1984). Induction of the photosynthetic membranes of *Rhodopseudomonas sphaeroides*: biochemical and morphological studies. J Bacteriol 159, 540-554.

Choudhary, M., Mackenzie, C., Donohue, T.J., and Kaplan, S. (2008). Purple Bacterial Genomics. In *The Purple Phototrophic Bacteria*, C.N. Hunter, F. Daldal, M.C. Thurnauer, and J.T. Beatty, eds. (Netherlands: Springer), pp. 691-706.

Choudhary, M., Zanhua, X., Fu, Y.X., and Kaplan, S. (2007). Genome analyses of three strains of *Rhodobacter sphaeroides*: evidence of rapid evolution of chromosome II. J Bacteriol 189, 1914-1921.

Chudakov, D.M., Matz, M.V., Lukyanov, S., and Lukyanov, K.A. (2010). Fluorescent proteins and their applications in imaging living cells and tissues. Physiol Rev 90, 1103-1163.

Coltharp, C., and Xiao, J. (2012). Superresolution microscopy for microbiology. Cell Microbiol 14, 1808-1818.

Corbin, B.D., Yu, X.-C., and Margolin, W. (2002). Exploring intracellular space: function of the Min system in round-shaped *Escherichia coli*. EMBO J 21, 1998-2008.

Costa, T., Priyadarshini, R., and Jacobs-Wagner, C. (2008). Localization of PBP3 in *Caulobacter crescentus* is highly dynamic and largely relies on its functional transpeptidase domain. Mol Microbiol 70, 634-651.

Cowles, K.N., and Gitai, Z. (2010). Surface association and the MreB cytoskeleton regulate pilus production, localization and function in *Pseudomonas aeruginosa*. Mol Microbiol 76, 1411-1426.

Dajkovic, A., Lan, G., Sun, S.X., Wirtz, D., and Lutkenhaus, J. (2008). MinC spatially controls bacterial cytokinesis by antagonizing the scaffolding function of FtsZ. Curr Biol 18, 235-244.

Daniel, R.A., and Errington, J. (2003). Control of cell morphogenesis in bacteria: two distinct ways to make a rod-shaped cell. Cell 113, 767-776.

de Boer, P.A. (2010). Advances in understanding *E. coli* cell fission. Curr Opin Microbiol 13, 730-737.

Defeu Soufo, H.J., and Graumann, P. (2005). *Bacillus subtilis* actin-like protein MreB influences the positioning of the replication machinery and requires membrane proteins MreC/D and other actin-like proteins for proper localization. BMC Cell Biol 6, 10.

Defeu Soufo, H.J., and Graumann, P.L. (2003). Actin-like proteins MreB and Mbl from *Bacillus subtilis* are required for bipolar positioning of replication origins. Curr Biol 13, 1916-1920.

Defeu Soufo, H.J., and Graumann, P.L. (2004). Dynamic movement of actin-like proteins within bacterial cells. EMBO Rep 5, 789-794.

Defeu Soufo, H.J., and Graumann, P.L. (2006). Dynamic localization and interaction with other *Bacillus subtilis* actin-like proteins are important for the function of MreB. Mol Microbiol 62, 1340-1356.

den Blaauwen, T. (2013). Prokaryotic cell division: flexible and diverse. Curr Opin Microbiol 16, 738-744.

den Blaauwen, T., Aarsman, M.E.G., Vischer, N.O.E., and Nanninga, N. (2003). Penicillin-binding protein PBP2 of *Escherichia coli* localizes preferentially in the lateral wall and at mid-cell in comparison with the old cell pole. Mol Microbiol 47, 539-547.

Dillon, S.C., and Dorman, C.J. (2010). Bacterial nucleoid-associated proteins, nucleoid structure and gene expression. Nat Rev Microbiol 8, 185-195.

Ditkowski, B., Troć, P., Ginda, K., Donczew, M., Chater, K.F., Zakrzewska-Czerwińska, J., and Jakimowicz, D. (2010). The actinobacterial signature protein ParJ (SCO1662) regulates ParA polymerization and affects chromosome segregation and cell division during *Streptomyces* sporulation. Mol Microbiol 78, 1403-1415.

Dogterom, M., and Surrey, T. (2013). Microtubule organization in vitro. Curr Opin Cell Biol 25, 23-29.

Doi, M., Wachi, M., Ishino, F., Tomioka, S., Ito, M., Sakagami, Y., Suzuki, A., and Matsuhashi, M. (1988). Determinations of the DNA sequence of the *mreB* gene and of the gene products of the *mre* region that function in formation of the rod shape of *Escherichia coli* cells. J Bacteriol 170, 4619-4624.

Domínguez-Escobar, J., Chastanet, A., Crevenna, A.H., Fromion, V., Wedlich-Söldner, R., and Carballido-López, R. (2011). Processive movement of MreB-associated cell wall biosynthetic complexes in bacteria. Science 333, 225-228.

Douglass, A.D., and Vale, R.D. (2005). Single-molecule microscopy reveals plasma membrane microdomains created by protein-protein networks that exclude or trap signaling molecules in T Cells. Cell 121, 937-950.

Downing, K.H. (2000). Structural basis for the interaction of tubulin with proteins and drugs that affect microtubule dynamics. Annu Rev Cell Dev Biol 16, 89-111.

Drew, D., Koch, G., Vellante, H., Talati, R., and Sanchez, O. (2009). Analyses of mechanisms for force generation during cell septation in *Escherichia coli*. Bull Math Biol 71, 980-1005.

Duke, T., and Graham, I. (2009). Equilibrium mechanisms of receptor clustering. Prog Biophys Mol Biol 100, 18-24.

Dunham, T.D., Xu, W., Funnell, B.E., and Schumacher, M.A. (2009). Structural basis for ADP-mediated transcriptional regulation by P1 and P7 ParA. EMBO J 28, 1792-1802.

Dworkin, J. (2009). Cellular polarity in prokaryotic organisms. Cold Spring Harb Perspect Biol 1, a003368.

Dziadek, J., Madiraju, M.V.V.S., Rutherford, S.A., Atkinson, M.A.L., and Rajagopalan, M. (2002). Physiological consequences associated with overproduction of *Mycobacterium tuberculosis* FtsZ in mycobacterial hosts. Microbiology 148, 961-971.

Ebersbach, G., and Gerdes, K. (2004). Bacterial mitosis: partitioning protein ParA oscillates in spiral-shaped structures and positions plasmids at mid-cell. Mol Microbiol 52, 385-398.

Ebersbach, G., Ringgaard, S., Møller-Jensen, J., Wang, Q., Sherratt, D.J., and Gerdes, K. (2006). Regular cellular distribution of plasmids by oscillating and filament-forming ParA ATPase of plasmid pB171. Mol Microbiol 61, 1428-1442.

Egan, A.J.F., and Vollmer, W. (2013). The physiology of bacterial cell division. Ann NY Acad Sci 1277, 8-28.

Eils, R., and Athale, C. (2003). Computational imaging in cell biology. J Cell Biol 161, 477-481.

Endres, R., Oleksiuk, O., Hansen, C., Meir, Y., Sourjik, V., and Wingreen, N. (2008). Variable sizes of *Escherichia coli* chemoreceptor signaling teams. Mol Syst Biol 4, 211.

Endres, R.G. (2009). Polar chemoreceptor clustering by coupled trimers of dimers. Biophys J 96, 453-463.

Eraso, Jesus M., and Margolin, W. (2011). Bacterial cell wall: thinking globally, actin locally. Curr Biol 21, R628-R630.

Erhardt, M., Namba, K., and Hughes, K.T. (2010). Bacterial nanomachines: the flagellum and type iii injectisome. Cold Spring Harb Perspect Biol 2, a000299.

Erickson, H.P. (1995). FtsZ, a prokaryotic homolog of tubulin? Cell 80, 367-370.

Erickson, H.P. (2001). Cytoskeleton: evolution in bacteria. Nature 413, 30.

Erickson, H.P. (2009). Modeling the physics of FtsZ assembly and force generation. Proc Natl Acad Sci USA 106, 9238-9243.

Erickson, H.P., Anderson, D.E., and Osawa, M. (2010). FtsZ in bacterial cytokinesis: cytoskeleton and force generator all in one. Microbiol Mol Biol Rev 74, 504-528.

Errington, J. (2003). Dynamic proteins and a cytoskeleton in bacteria. Nat Cell Biol 5, 175-178.

Esue, O., Cordero, M., Wirtz, D., and Tseng, Y. (2005). The assembly of MreB, a prokaryotic homolog of actin. J Biol Chem 280, 2628-2635.

Esue, O., Wirtz, D., and Tseng, Y. (2006). GTPase activity, structure, and mechanical properties of filaments assembled from bacterial cytoskeleton protein MreB. J Bacteriol 188, 968-976.

Eswaramoorthy, P., Erb, M.L., Gregory, J.A., Silverman, J., Pogliano, K., Pogliano, J., and Ramamurthi, K.S. (2011). Cellular architecture mediates DivIVA ultrastructure and regulates Min activity in *Bacillus subtilis*. mBio 2, e00257-11.

Fan, J., Sammalkorpi, M., and Haataja, M. (2010). Formation and regulation of lipid microdomains in cell membranes: theory, modeling, and speculation. FEBS Letters 584, 1678-1684.

Fenton, A.K., and Gerdes, K. (2013). Direct interaction of FtsZ and MreB is required for septum synthesis and cell division in *Escherichia coli*. EMBO J 32, 1953-1965.

Fenz, S.F., and Sengupta, K. (2012). Giant vesicles as cell models. Integr Biol 4, 982-995.

Fiebig, A., Keren, K., and Theriot, J. (2006). Fine-scale time-lapse analysis of the biphasic, dynamic behaviour of the two *Vibrio cholerae* chromosomes. Mol Microbiol 60, 1164-1178.

Figge, R.M., Divakaruni, A.V., and Gober, J.W. (2004). MreB, the cell shape-determining

bacterial actin homologue, co-ordinates cell wall morphogenesis in *Caulobacter crescentus*. Mol Microbiol 51, 1321-1332.

Fisher, J.K., Bourniquel, A., Witz, G., Weiner, B., Prentiss, M., and Kleckner, N. (2013). Four-dimensional imaging of *E. coli* nucleoid organization and dynamics in living cells. Cell 153, 882-895.

Fogel, M.A., and Waldor, M.K. (2005). Distinct segregation dynamics of the two *Vibrio cholerae* chromosomes. Mol Microbiol 55, 125-136.

Formstone, A., and Errington, J. (2005). A magnesium-dependent *mreB* null mutant: implications for the role of *mreB* in *Bacillus subtilis*. Mol Microbiol 55, 1646-1657.

Foss, M.H., Eun, Y.-J., and Weibel, D.B. (2011). Chemical–biological studies of subcellular organization in bacteria. Biochemistry 50, 7719-7734.

Francis, N.R., Wolanin, P.M., Stock, J.B., DeRosier, D.J., and Thomas, D.R. (2004). Three-dimensional structure and organization of a receptor/signaling complex. Proc Natl Acad Sci USA 101, 17480-17485.

Frank, V., and Vaknin, A. (2013). Prolonged stimuli alter the bacterial chemosensory clusters. Mol Microbiol 88, 634-644.

Fu, G., Huang, T., Buss, J., Coltharp, C., Hensel, Z., and Xiao, J. (2010). In vivo structure of the *E. coli* FtsZ-ring revealed by photoactivated localization microscopy (PALM). PLoS One 5, e12680.

Gahlmann, A., and Moerner, W.E. (2014). Exploring bacterial cell biology with single-molecule tracking and super-resolution imaging. Nat Rev Microbiol 12, 9-22.

Galán, B., Dinjaski, N., Maestro, B., de Eugenio, L.I., Escapa, I.F., Sanz, J.M., García, J.L., and Prieto, M.A. (2011). Nucleoid-associated PhaF phasin drives intracellular location and segregation of polyhydroxyalkanoate granules in *Pseudomonas putida* KT2442. Mol Microbiol 79, 402-418.

Galloway, J. (2010). Helical imperative: paradigm of growth, form and function. eLS: http://onlinelibrary.wiley.com/doi/10.1002/9780470015902.a0003673.pub2/full.

Gamba, P., Veening, J.-W., Saunders, N.J., Hamoen, L.W., and Daniel, R.A. (2009). Two-step assembly dynamics of the *Bacillus subtilis* divisome. J Bacteriol 191, 4186-4194.

Garcia Vescovi, E., Sciara, M., and Castelli, M. (2010). Two component systems in the spatial program of bacteria. Curr Opin Microbiol 13, 210-218.

Garner, E.C., Bernard, R., Wang, W., Zhuang, X., Rudner, D.Z., and Mitchison, T. (2011). Coupled, circumferential motions of the cell wall synthesis machinery and MreB filaments in *B. subtilis*. Science 333, 222-225.

Geissler, B., Shiomi, D., and Margolin, W. (2007). The *ftsA** gain-of-function allele of *Escherichia coli* and its effects on the stability and dynamics of the Z ring. Microbiology 153, 814-825.

Gerdes, K., Howard, M., and Szardenings, F. (2010). Pushing and pulling in prokaryotic DNA segregation. Cell 141, 927-942.

Gerding, M.A., Ogata, Y., Pecora, N.D., Niki, H., and De Boer, P.A.J. (2007). The trans-envelope Tol–Pal complex is part of the cell division machinery and required for proper outer-membrane invagination during cell constriction in *E. coli*. Mol Microbiol 63, 1008-1025.

Gerlich, D., and Ellenberg, J. (2003). 4D imaging to assay complex dynamics in live specimens. Nat Cell Biol Suppl, S14-19.

Gestwicki, J.E., and Kiessling, L.L. (2002). Inter-receptor communication through arrays of bacterial chemoreceptors. Nature 415, 81-84.

Gestwicki, J.E., Lamanna, A.C., Harshey, R.M., McCarter, L.L., Kiessling, L.L., and Adler, J. (2000). Evolutionary conservation of methyl-accepting chemotaxis protein location in bacteria and archaea. J Bacteriol 182, 6499-6502.

Giepmans, B.N.G., Adams, S.R., Ellisman, M.H., and Tsien, R.Y. (2006). The fluorescent toolbox for assessing protein location and function. Science 312, 217-224.

Gilson, P.R., and Beech, P.L. (2001). Cell division protein FtsZ: running rings around bacteria, chloroplasts and mitochondria. Res Microbiol 152, 3-10.

Gitai, Z. (2005). The new bacterial cell biology: moving parts and subcellular architecture. Cell 120, 577-586.

Gitai, Z. (2009). New fluorescence microscopy methods for microbiology: sharper, faster, and quantitative. Curr Opin Microbiol 12, 341-346.

Gitai, Z., Dye, N., Reisenauer, A., Wachi, M., and Shapiro, L. (2005). MreB actin-mediated segregation of a specific region of a bacterial chromosome. Cell 120, 329-341.

Gitai, Z., Dye, N., and Shapiro, L. (2004). An actin-like gene can determine cell polarity in bacteria. Proc Natl Acad Sci USA 101, 8643-8648.

Golding, I., and Cox, E.C. (2004). RNA dynamics in live *Escherichia coli* cells. Proc Natl Acad Sci USA 101, 11310-11315.

Goley, E.D. (2013). Tiny cells meet big questions: a closer look at bacterial cell biology. Mol Biol Cell 24, 1099-1102.

Goley, E.D., Dye, N.A., Werner, J.N., Gitai, Z., and Shapiro, L. (2010). Imaging-based identification of a critical regulator of FtsZ protofilament curvature in *Caulobacter*. Mol Cell 39, 975-987.

Goley, E.D., Yeh, Y.-C., Hong, S.-H., Fero, M.J., Abeliuk, E., McAdams, H.H., and Shapiro, L. (2011). Assembly of the *Caulobacter* cell division machine. Mol Microbiol 80, 1680-1698.

Gonzalez, D., and Collier, J. (2013). DNA methylation by CcrM activates the transcription of two genes required for the division of *Caulobacter crescentus*. Mol Microbiol 88, 203-218.

Govindarajan, S., Elisha, Y., Nevo-Dinur, K., and Amster-Choder, O. (2013). The general phosphotransferase system proteins localize to sites of strong negative curvature in bacterial cells. mBio 4, e00443-13.

Govindarajan, S., Nevo-Dinur, K., and Amster-Choder, O. (2012). Compartmentalization and spatiotemporal organization of macromolecules in bacteria. FEMS Microbiol Rev 36, 1005-1022.

Green, M.R., and Sambrook, J. (2012). *Molecular Cloning: A Laboratory Manual* 4th ed. (New York: Cold Spring Harbor Laboratory Press).

Greenfield, D., McEvoy, A.L., Shroff, H., Crooks, G.E., Wingreen, N.S., Betzig, E., and Liphardt, J. (2009). Self-organization of the *Escherichia coli* chemotaxis network imaged with super-resolution light microscopy. PLoS Biol 7, e1000137.

Gregory, J.A., Becker, E.C., and Pogliano, K. (2008). *Bacillus subtilis* MinC destabilizes FtsZ-rings at new cell poles and contributes to the timing of cell division. Genes Dev 22, 3475-3488.

Gündoğdu, M.E., Kawai, Y., Pavlendova, N., Ogasawara, N., Errington, J., Scheffers, D.J., and Hamoen, L.W. (2011). Large ring polymers align FtsZ polymers for normal septum formation. EMBO J 30, 617-626.

Güvener, Z.T., Tifrea, D.F., and Harwood, C.S. (2006). Two different *Pseudomonas aeruginosa* chemosensory signal transduction complexes localize to cell poles and form and remould in stationary phase. Mol Microbiol 61, 106-118.

Haeusser, D., and Levin, P. (2008). The great divide: coordinating cell cycle events during bacterial growth and division. Curr Opin Microbiol 11, 94-99.

Hall, B.A., Armitage, J.P., and Sansom, M.S.P. (2012). Mechanism of bacterial signal transduction revealed by molecular dynamics of Tsr dimers and trimers of dimers in lipid vesicles. PLoS Comput Biol 8, e1002685.

Hallez, R., Bellefontaine, A.F., Letesson, J.J., and De Bolle, X. (2004). Morphological and functional asymmetry in alpha-proteobacteria. Trends Microbiol 12, 361-365.

Hamer, R., Chen, P.-Y., Armitage, J., Reinert, G., and Deane, C. (2010). Deciphering chemotaxis pathways using cross species comparisons. BMC Systems Biol 4, 3.

Hansen, C.H., Sourjik, V., and Wingreen, N.S. (2010). A dynamic-signaling-team model for chemotaxis receptors in *Escherichia coli*. Proc Natl Acad Sci USA 107, 17170-17175.

Harrison, D.M., Skidmore, J., Armitage, J.P., and Maddock, J.R. (1999). Localization and environmental regulation of MCP-like proteins in *Rhodobacter sphaeroides*. Mol Microbiol 31, 885-892.

Hatano, T., Yamaichi, Y., and Niki, H. (2007). Oscillating focus of SopA associated with filamentous structure guides partitioning of F plasmid. Mol Microbiol 64, 1198-1213.

Hazelbauer, G.L., Falke, J.J., and Parkinson, J.S. (2008). Bacterial chemoreceptors: high-performance signaling in networked arrays. Trends Biochem Sci 33, 9-19.

Hazelbauer, G.L., and Lai, W.-C. (2010). Bacterial chemoreceptors: providing enhanced features to two-component signaling. Curr Opin Microbiol 13, 124-132.

Henning, U., Rehn, K., Braun, V., and Hohn, B. (1972). Cell envelope and shape of *Escherichia coli* K12. Properties of a temperature-sensitive rod mutant. Eur J Biochem 26, 570-586.

Henry, J.T., and Crosson, S. (2013). Chromosome replication and segregation govern the biogenesis and inheritance of inorganic polyphosphate granules. Mol Biol Cell 24, 3177-3186.

Hinner, M.J., and Johnsson, K. (2010). How to obtain labeled proteins and what to do with them. Curr Opin Biotechnol 21, 766-776.

Holden, S.J., Pengo, T., Meibom, K.L., Fernandez Fernandez, C., Collier, J., and Manley, S. (2014). High throughput 3D super-resolution microscopy reveals *Caulobacter crescentus* in vivo Z-ring organization. Proc Natl Acad Sci USA 111, 4566-4571.

Holtje, J.V. (1998). Growth of the stress-bearing and shape-maintaining murein sacculus of *Escherichia coli*. Microbiol Mol Biol Rev 62, 181-203.

Hou, S., Wieczorek, S.A., Kaminski, T.S., Ziebacz, N., Tabaka, M., Sorto, N.A., Foss, M.H., Shaw, J.T., Thanbichler, M., Weibel, D.B., et al. (2012). Characterization of *Caulobacter crescentus* FtsZ protein using dynamic light scattering. J Biol Chem 287, 23878-23886.

Howard, J., and Hyman, A.A. (2007). Microtubule polymerases and depolymerases. Curr Opin Cell Biol 19, 31-35.

Howard, M., and Gerdes, K. (2010). What is the mechanism of ParA-mediated DNA movement? Mol Microbiol 78, 9-12.

Hsin, J., Gopinathan, A., and Huang, K.C. (2012). Nucleotide-dependent conformations of FtsZ dimers and force generation observed through molecular dynamics simulations. Proc Natl Acad Sci USA 109, 9432-9437.

Huang, K.-H., Durand-Heredia, J., and Janakiraman, A. (2013). FtsZ-ring stability: of bundles, tubules, crosslinks and curves. J Bacteriol 195, 1859-1868.

Huang, K.C., and Ramamurthi, K.S. (2010). Macromolecules that prefer their membranes curvy. Mol Microbiol 76, 822-832.

Hui, M.P., Galkin, V.E., Yu, X., Stasiak, A.Z., Stasiak, A., Waldor, M.K., and Egelman, E.H. (2010). ParA2, a *Vibrio cholerae* chromosome partitioning protein, forms left-handed helical filaments on DNA. Proc Natl Acad Sci USA 107, 4590-4595.

Huitema, E., Pritchard, S., Matteson, D., Radhakrishnan, S.K., and Viollier, P.H. (2006). Bacterial birth scar proteins mark future flagellum assembly site. Cell 124, 1025-1037.

Imhoff, J. (2006). The Phototrophic Alpha-Proteobacteria. In *The Prokaryotes*, M. Dworkin, S. Falkow, E. Rosenberg, K.-H. Schleifer, and E. Stackebrandt, eds. (New York: Springer), pp. 41-64.

Imhoff, J.F. (2008). Systematics of Anoxygenic Phototrophic Bacteria. In *Sulfur Metabolism in Phototrophic Organisms*, R. Hell, C. Dahl, D. Knaff, and T. Leustek, eds. (Netherlands: Springer), pp. 269-287.

Ind, A.C., Porter, S.L., Brown, M.T., Byles, E.D., de Beyer, J.A., Godfrey, S.A., and Armitage, J.P. (2009). Inducible-expression plasmid for *Rhodobacter sphaeroides* and *Paracoccus denitrificans*. Appl Environ Microbiol 75, 6613-6615.

Ingerson-Mahar, M., Briegel, A., Werner, J.N., Jensen, G.J., and Gitai, Z. (2010). The metabolic enzyme CTP synthase forms cytoskeletal filaments. Nat Cell Biol 12, 739-746.

Ingerson-Mahar, M., and Gitai, Z. (2012). A growing family: the expanding universe of the bacterial cytoskeleton. FEMS Microbiol Rev 36, 256-267.

Iwai, N., Nagai, K., and Wachi, M. (2002). Novel S-benzylisothiourea compound that induces spherical cells in *Escherichia coli* probably by acting on a rod-shape-determining protein(s) other than penicillin-binding protein 2. Biosci Biotechnol Biochem 66,

2658-2662.

Jain, A., Liu, R., Ramani, B., Arauz, E., Ishitsuka, Y., Ragunathan, K., Park, J., Chen, J., Xiang, Y.K., and Ha, T. (2011). Probing cellular protein complexes using single-molecule pull-down. Nature 473, 484-488.

Jain, I.H., Vijayan, V., and O'Shea, E.K. (2012). Spatial ordering of chromosomes enhances the fidelity of chromosome partitioning in cyanobacteria. Proc Natl Acad Sci USA 109, 13638-13643.

Jakimowicz, D., Żydek, P., Kois, A., Zakrzewska-Czerwińska, J., and Chater, K.F. (2007). Alignment of multiple chromosomes along helical ParA scaffolding in sporulating *Streptomyces* hyphae. Mol Microbiol 65, 625-641.

Jennings, P.C., Cox, G.C., Monahan, L.G., and Harry, E.J. (2011). Super-resolution imaging of the bacterial cytokinetic protein FtsZ. Micron 42, 336-341.

Jensen, S.O., Thompson, L.S., and Harry, E.J. (2005). Cell division in *Bacillus subtilis*: FtsZ and FtsA association is Z-ring independent, and FtsA is required for efficient midcell Z-ring assembly. J Bacteriol 187, 6536-6544.

Jiménez, M., Martos, A., Cabré, E.J., Raso, A., and Rivas, G. (2013). Giant vesicles: a powerful tool to reconstruct bacterial division assemblies in cell-like compartments. Environ Microbiol 15, 3158-3168.

Jones, C.W. (2013). *Dynamics, formation and segregation of the cytoplasmic chemoreceptor cluster in* Rhodobacter sphaeroides. Thesis, University of Oxford.

Jones, L.J.F., Carballido-López, R., and Errington, J. (2001). Control of cell shape in bacteria: helical, actin-like filaments in *Bacillus subtilis*. Cell 104, 913-922.

Judd, E.M., Comolli, L.R., Chen, J.C., Downing, K.H., Moerner, W.E., and McAdams, H.H. (2005). Distinct constrictive processes, separated in time and space, divide *Caulobacter* inner and outer membranes. J Bacteriol 187, 6874-6882.

Justice, S.S., Hunstad, D.A., Cegelski, L., and Hultgren, S.J. (2008). Morphological plasticity as a bacterial survival strategy. Nat Rev Microbiol 6, 162-168.

Kahng, L.S., and Shapiro, L. (2003). Polar localization of replicon origins in the multipartite genomes of *Agrobacterium tumefaciens* and *Sinorhizobium meliloti*. J Bacteriol 185, 3384-3391.

Karczmarek, A., Baselga, R.M.-A., Alexeeva, S., Hansen, F.G., Vicente, M., Nanninga, N., and Den Blaauwen, T. (2007). DNA and origin region segregation are not affected by the transition from rod to sphere after inhibition of *Escherichia coli* MreB by A22. Mol Microbiol 65, 51-63.

Katzmann, E., Müller, F.D., Lang, C., Messerer, M., Winklhofer, M., Plitzko, J.M., and Schüler, D. (2011). Magnetosome chains are recruited to cellular division sites and split by asymmetric septation. Mol Microbiol 82, 1316-1329.

Keffer, J.L., Huecas, S., Hammill, J.T., Wipf, P., Andreu, J.M., and Bewley, C.A. (2013). Chrysophaentins are competitive inhibitors of FtsZ and inhibit Z-ring formation in live bacteria. Bioorg Med Chem 21, 5673-5678.

Kentner, D., and Sourjik, V. (2010). Use of fluorescence microscopy to study intracellular signaling in bacteria. Annu Rev Microbiol 64, 373-390.

Kholodenko, B., Hancock, J., and Kolch, W. (2010). Signalling ballet in space and time. Nat Rev Mol Cell Biol 11, 414-426.

Khursigara, C., Lan, G., Neumann, S., Wu, X., Ravindran, S., Borgnia, M., Sourjik, V., Milne, J., Tu, Y., and Subramaniam, S. (2011). Lateral density of receptor arrays in the membrane plane influences sensitivity of the *E. coli* chemotaxis response. EMBO J 30, 1719-1729.

Kiekebusch, D., Michie, Katharine A., Essen, L.-O., Löwe, J., and Thanbichler, M. (2012). Localized dimerization and nucleoid binding drive gradient formation by the bacterial cell division inhibitor MipZ. Mol Cell 46, 245-259.

Kiley, P.J., and Kaplan, S. (1988). Molecular genetics of photosynthetic membrane biosynthesis in *Rhodobacter sphaeroides*. Microbiol Mol Biol Rev 52, 50-69.

Kim, S.Y., Gitai, Z., Kinkhabwala, A., Shapiro, L., and Moerner, W.E. (2006). Single molecules of the bacterial actin MreB undergo directed treadmilling motion in *Caulobacter crescentus*. Proc Natl Acad Sci USA 103, 10929-10934.

Kirkpatrick, C.L., and Viollier, P.H. (2010). Poles apart: prokaryotic polar organelles and their spatial regulation. Cold Spring Harb Perspect Biol 1, a006809.

Kirkpatrick, C.L., and Viollier, P.H. (2011). New(s) to the (Z-)ring. Curr Opin Microbiol 14, 691-697.

Kitagawa, M., Ara, T., Arifuzzaman, M., Ioka-Nakamichi, T., Inamoto, E., Toyonaga, H., and Mori, H. (2006). Complete set of ORF clones of *Escherichia coli* ASKA library (A Complete Set of *E. coli* K-12 ORF Archive): unique resources for biological research. DNA Res 12, 291-299.

Kovar, D.R., Sirotkin, V., and Lord, M. (2011). Three's company: the fission yeast actin cytoskeleton. Trends Cell Biol 21, 177-187.

Krell, T., Lacal, J., Muñoz-Martínez, F., Reyes-Darias, J.A., Cadirci, B.H., García-Fontana, C., and Ramos, J.L. (2011). Diversity at its best: bacterial taxis. Environ Microbiol 13, 1115-1124.

Kremers, G.-J., Gilbert, S.G., Cranfill, P.J., Davidson, M.W., and Piston, D.W. (2011). Fluorescent proteins at a glance. J Cell Sci 124, 157-160.

Kruse, T., Moller-Jensen, J., Lobner-Olesen, A., and Gerdes, K. (2003). Dysfunctional MreB inhibits chromosome segregation in *Escherichia coli*. EMBO J 22, 5283-5292.

Kumar, M., Mommer, M.S., and Sourjik, V. (2010). Mobility of cytoplasmic, membrane, and DNA-binding proteins in *Escherichia coli*. Biophys J 98, 552-559.

Kusumi, A., Fujiwara, T.K., Chadda, R., Xie, M., Tsunoyama, T.A., Kalay, Z., Kasai, R.S., and Suzuki, K.G.N. (2012). Dynamic organizing principles of the plasma membrane that regulate signal transduction: commemorating the fortieth anniversary of Singer and Nicolson's Fluid-Mosaic Model. Annu Rev Cell Dev Biol 28, 215-250.

Kysela, D.T., Brown, P.J.B., Huang, K.C., and Brun, Y.V. (2013). Biological consequences and advantages of asymmetric bacterial growth. Annu Rev Microbiol 67, 417-435.

Laloux, G., and Jacobs-Wagner, C. (2014). How do bacteria localize proteins to the cell pole? J Cell Sci 127, 11-19.

Lam, H., Schofield, W.B., and Jacobs-Wagner, C. (2006). A landmark protein essential for establishing and perpetuating the polarity of a bacterial cell. Cell 124, 1011-1023.

Lamanna, A.C., Ordal, G.W., and Kiessling, L.L. (2005). Large increases in attractant concentration disrupt the polar localization of bacterial chemoreceptors. Mol Microbiol 57, 774-785.

Lan, G., Daniels, B.R., Dobrowsky, T.M., Wirtz, D., and Sun, S.X. (2009). Condensation of FtsZ filaments can drive bacterial cell division. Proc Natl Acad Sci USA 106, 121-126.

Lan, G., Wolgemuth, C.W., and Sun, S.X. (2007). Z-ring force and cell shape during division in rod-like bacteria. Proc Natl Acad Sci USA 104, 16110-16115.

Latch, J.N., and Margolin, W. (1997). Generation of buds, swellings, and branches instead of filaments after blocking the cell cycle of *Rhizobium meliloti*. J Bacteriol 179, 2373-2381.

Le Quéré, B., and Ghigo, J.-M. (2009). BcsQ is an essential component of the *Escherichia coli* cellulose biosynthesis apparatus that localizes at the bacterial cell pole. Mol Microbiol 72, 724-740.

Lee, T.K., Tropini, C., Hsin, J., Desmarais, S.M., Ursell, T.S., Gong, E., Gitai, Z., Monds, R.D., and Huang, K.C. (2014). A dynamically assembled cell wall synthesis machinery buffers cell growth. Proc Natl Acad Sci USA 111, 4554-4559.

Lefman, J., Zhang, P., Hirai, T., Weis, R.M., Juliani, J., Bliss, D., Kessel, M., Bos, E., Peters, P.J., and Subramaniam, S. (2004). Three-dimensional electron microscopic imaging of membrane invaginations in *Escherichia coli* overproducing the chemotaxis receptor Tsr. J Bacteriol 186, 5052-5061.

Leisch, N., Verheul, J., Heindl, N.R., Gruber-Vodicka, H.R., Pende, N., den Blaauwen, T., and Bulgheresi, S. (2012). Growth in width and FtsZ ring longitudinal positioning in a gammaproteobacterial symbiont. Curr Biol 22, R831-832.

Lenarcic, R., Halbedel, S., Visser, L., Shaw, M., Wu, L., Errington, J., Marenduzzo, D., and Hamoen, L. (2009). Localisation of DivIVA by targeting to negatively curved membranes. EMBO J 28, 2272-2282.

Leonard, T.A., Butler, P.J., and Lowe, J. (2005). Bacterial chromosome segregation: structure and DNA binding of the Soj dimer - a conserved biological switch. EMBO J 24, 270-282.

Levin, P.A., Margolis, P.S., Setlow, P., Losick, R., and Sun, D. (1992). Identification of *Bacillus subtilis* genes for septum placement and shape determination. J Bacteriol 174, 6717-6728.

Lewis, P.J. (2004). Bacterial subcellular architecture: recent advances and future prospects. Mol Microbiol 54, 1135-1150.

Li, M., and Hazelbauer, G.L. (2004). Cellular stoichiometry of the components of the chemotaxis signaling complex. J Bacteriol 186, 3687-3694.

Li, M., and Hazelbauer, G.L. (2011). Core unit of chemotaxis signaling complexes. Proc Natl Acad Sci USA 108, 9390-9395.

Li, X., Fleetwood, A.D., Bayas, C., Bilwes, A.M., Ortega, D.R., Falke, J.J., Zhulin, I.B., and Crane, B.R. (2013a). The 3.2 Å resolution structure of a receptor:CheA:CheW signaling complex defines overlapping binding sites and key residue interactions within bacterial chemosensory arrays. Biochemistry 52, 3852-3865.

Li, Y., Hsin, J., Zhao, L., Cheng, Y., Shang, W., Huang, K.C., Wang, H.-W., and Ye, S. (2013b). FtsZ protofilaments use a hinge-opening mechanism for constrictive force generation. Science 341, 392-395.

Li, Z., Trimble, M.J., Brun, Y.V., and Jensen, G.J. (2007). The structure of FtsZ filaments in vivo suggests a force-generating role in cell division. EMBO J 26, 4694-4708.

Lim, G.E., Derman, A.I., and Pogliano, J. (2005). Bacterial DNA segregation by dynamic SopA polymers. Proc Natl Acad Sci USA 102, 17658-17663.

Lim, S.-K., Kim, S.J., Cha, S.H., Oh, Y.-K., Rhee, H.-J., Kim, M.-S., and Lee, J.K. (2009). Complete genome sequence of *Rhodobacter sphaeroides* KD131. J Bacteriol 191, 1118-1119.

Lippincott-Schwartz, J., Altan-Bonnet, N., and Patterson, G. (2003). Photobleaching and photoactivation: following protein dynamics in living cells. Nat Cell Biol Suppl, S7-14.

Liu, J., Hu, B., Morado, D.R., Jani, S., Manson, M.D., and Margolin, W. (2012). Molecular architecture of chemoreceptor arrays revealed by cryoelectron tomography of *Escherichia coli* minicells. Proc Natl Acad Sci USA 109, E1481–E1488.

Livny, J., Yamaichi, Y., and Waldor, M.K. (2007). Distribution of centromere-like *parS* sites in bacteria: insights from comparative genomics. J Bacteriol 189, 8693-8703.

Loose, M., and Mitchison, T.J. (2014). The bacterial cell division proteins FtsA and FtsZ self-organize into dynamic cytoskeletal patterns. Nat Cell Biol 16, 38-46.

Lopez, D., and Kolter, R. (2010). Functional microdomains in bacterial membranes. Genes Dev 24, 1893-1902.

Lopez-Montero, I., Mateos-Gil, P., Sferrazza, M., Navajas, P.L., Rivas, G., Velez, M., and Monroy, F. (2012). Active membrane viscoelasticity by the bacterial FtsZ-division protein. Langmuir 28, 4744-4753.

Lopian, L., Elisha, Y., Nussbaum-Shochat, A., and Amster-Choder, O. (2010). Spatial and temporal organization of the *E. coli* PTS components. EMBO J 29, 3630-3645.

Losick, R., and Shapiro, L. (1999). Changing views on the nature of the bacterial cell: from biochemistry to cytology. J Bacteriol 181, 4143-4145.

Lowe, J. (1998). Crystal structure determination of FtsZ from *Methanococcus jannaschii*. J Struct Biol 124, 235-243.

Lowe, J., and Amos, L.A. (1998). Crystal structure of the bacterial cell-division protein FtsZ. Nature 391, 203-206.

Lowe, J., van den Ent, F., and Amos, L.A. (2004). Molecules of the bacterial cytoskeleton. Annu Rev Biophys Biomol Struct 33, 177-198.

Lu, C., Reedy, M., and Erickson, H.P. (2000). Straight and curved conformations of FtsZ are regulated by GTP hydrolysis. J Bacteriol 182, 164-170.

Lutkenhaus, J. (2012). The ParA/MinD family puts things in their place. Trends Microbiol 20, 411-418.

Lutkenhaus, J., Pichoff, S., and Du, S. (2012). Bacterial cytokinesis: from Z ring to divisome. Cytoskeleton 69, 778-790.

Lux, R., Jahreis, K., Bettenbrock, K., Parkinson, J.S., and Lengeler, J.W. (1995). Coupling the phosphotransferase system and the methyl-accepting chemotaxis protein-dependent chemotaxis signaling pathways of *Escherichia coli*. Proc Natl Acad Sci USA 92, 11583-11587.

Müller, F.D., Raschdorf, O., Nudelman, H., Messerer, M., Katzmann, E., Plitzko, J.M., Zarivach, R., and Schüler, D. (2014). The FtsZ-like protein FtsZm of *Magnetospirillum gryphiswaldense* likely interacts with its generic homolog and is required for biomineralization under nitrate deprivation. J Bacteriol 196, 650-659.

Männik, J., Wu, F., Hol, F.J.H., Bisicchia, P., Sherratt, D.J., Keymer, J.E., and Dekker, C. (2012). Robustness and accuracy of cell division in *Escherichia coli* in diverse cell shapes. Proc Natl Acad Sci USA 109, 6957-6962.

Ma, X., Ehrhardt, D.W., and Margolin, W. (1996). Colocalization of cell division proteins FtsZ and FtsA to cytoskeletal structures in living *Escherichia coli* cells by using green fluorescent protein. Proc Natl Acad Sci USA 93, 12998-13003.

Macara, I.G., and Mili, S. (2008). Polarity and differential inheritance - universal attributes of life? Cell 135, 801-812.

Mackenzie, C., Eraso, J.M., Choudhary, M., Roh, J.H., Zeng, X., Bruscella, P., Puskás, Á ., and Kaplan, S. (2007). Postgenomic adventures with *Rhodobacter sphaeroides*. Annu Rev Microbiol 61, 283-307.

Madabhushi, R., and Marians, K.J. (2009). Actin homolog MreB affects chromosome segregation by regulating topoisomerase IV in *Escherichia coli*. Mol Cell 33, 171-180.

Maddock, and Shapiro, L. (1993). Polar location of the chemoreceptor complex in the *Escherichia coli* cell. Science 259, 1717-1723.

Madigan, M.T., and Jung, D.O. (2008). An Overview of Purple Bacteria: Systematics, Physiology, and Habitats. In *The Purple Phototrophic Bacteria*, C.N. Hunter, F. Daldal, M.C. Thurnauer, and J.T. Beatty, eds. (Netherlands: Springer), pp. 1-15.

Maiato, H., Sampaio, P., and Sunkel, C.E. (2004). Microtubule-associated proteins and their essential roles during mitosis. Int Rev Cytol 241, 53-153.

Margalit, D.N., Romberg, L., Mets, R.B., Hebert, A.M., Mitchison, T.J., Kirschner, M.W., and RayChaudhuri, D. (2004). Targeting cell division: small-molecule inhibitors of FtsZ GTPase perturb cytokinetic ring assembly and induce bacterial lethality. Proc Natl Acad Sci USA 101, 11821-11826.

Margolin, W. (2004). Bacterial shape: concave coiled coils curve *Caulobacter*. Curr Biol 14, R242-R244.

Margolin, W. (2009). Sculpting the bacterial cell. Curr Biol 19, R812-R822.

Margolin, W. (2012). The price of tags in protein localization studies. J Bacteriol 194, 6369-6371.

Martin, A.C., Wadhams, G.H., and Armitage, J.P. (2001). The roles of the multiple CheW and CheA homologues in chemotaxis and in chemoreceptor localization in *Rhodobacter sphaeroides*. Mol Microbiol 40, 1261-1272.

Martos, A., Jiménez, M., Rivas, G., and Schwille, P. (2012). Towards a bottom-up reconstitution of bacterial cell division. Trends Cell Biol 22, 634-643.

Matsumoto, K., Kusaka, J., Nishibori, A., and Hara, H. (2006). Lipid domains in bacterial membranes. Mol Microbiol 61, 1110-1117.

Mauriello, E.M.F., Astling, D.P., Sliusarenko, O., and Zusman, D.R. (2009). Localization of a bacterial cytoplasmic receptor is dynamic and changes with cell-cell contacts. Proc Natl Acad Sci USA 106, 4852-4857.

Mauriello, E.M.F., Mouhamar, F., Nan, B., Ducret, A., Dai, D., Zusman, D.R., and Mignot, T. (2010). Bacterial motility complexes require the actin-like protein, MreB and the Ras homologue, MglA. EMBO J 29, 315-326.

Mayer, B.J. (2001). SH3 domains: complexity in moderation. J Cell Sci 114, 1253-1263.

Mayer, J.A., and Amann, K.J. (2009). Assembly properties of the *Bacillus subtilis* actin, MreB. Cell Motil Cytoskeleton 66, 109-118.

Meier, E.L., and Goley, E.D. (2014). Form and function of the bacterial cytokinetic ring. Curr Opin Cell Biol 26, 19-27.

Meier, V.M., and Scharf, B.E. (2009). Cellular localization of predicted transmembrane and soluble chemoreceptors in *Sinorhizobium meliloti*. J Bacteriol 191, 5724-5733.

Michie, K.A., and Löwe, J. (2006). Dynamic filaments of the bacterial cytoskeleton. Annu Rev Biochem 75, 467-492.

Mika, J.T., and Poolman, B. (2011). Macromolecule diffusion and confinement in prokaryotic cells. Curr Opin Biotechnol 22, 117-126.

Milne, J.L.S., and Subramaniam, S. (2009). Cryo-electron tomography of bacteria: progress, challenges and future prospects. Nat Rev Microbiol 7, 666-675.

Min, H., Guo, H., and Xiong, J. (2005). Rhythmic gene expression in a purple photosynthetic bacterium, *Rhodobacter sphaeroides*. FEBS Letters 579, 808-812.

Mingorance, J., Tadros, M., Vicente, M., González, J.M., Rivas, G., and Vélez, M. (2005). Visualization of single *Escherichia coli* Ftsz filament dynamics with atomic force microscopy. J Biol Chem 280, 20909-20914.

Mishra, M., Kashiwazaki, J., Takagi, T., Srinivasan, R., Huang, Y., Balasubramanian, M.K., and Mabuchi, I. (2013). In vitro contraction of cytokinetic ring depends on myosin II but not on actin dynamics. Nat Cell Biol 15, 853-859.

Monahan, L.G., and Harry, E.J. (2013). Identifying how bacterial cells find their middle: a new perspective. Mol Microbiol 87, 231-234.

Monahan, L.G., Liew, A.T.F., Bottomley, A.L., and Harry, E.J. (2014). Division site positioning in bacteria: one size does not fit all. Front Microbiol 5, 19.

Morris, D., and Jensen, G. (2008). Toward a biomechanical understanding of whole bacterial cells. Annu Rev Biochem 77, 583-613.

Moseley, J.B., and Goode, B.L. (2006). The yeast actin cytoskeleton: from cellular function to biochemical mechanism. Microbiol Mol Biol Rev 70, 605-645.

Muñoz-Espín, D., Daniel, R., Kawai, Y., Carballido-López, R., Castilla-Llorente, V., Errington, J., Meijer, W.J.J., and Salas, M. (2009). The actin-like MreB cytoskeleton organizes viral DNA replication in bacteria. Proc Natl Acad Sci USA 106, 13347-13352.

Muchová, K., Chromiková, Z., and Barák, I. (2013). Control of *Bacillus subtilis* cell shape by RodZ. Environ Microbiol 15, 3259-3271.

Mueller, N., Wedlich-Soldner, R., and Spira, F. (2012). From mosaic to patchwork: matching lipids and proteins in membrane organization. Mol Membr Biol 29, 186-196.

Mukherjee, A., Saez, C., and Lutkenhaus, J. (2001). Assembly of an FtsZ mutant deficient in GTPase activity has implications for FtsZ assembly and the role of the Z ring in cell division. J Bacteriol 183, 7190-7197.

Murat, D., Byrne, M., and Komeili, A. (2010). Cell biology of prokaryotic organelles. Cold Spring Harb Perspect Biol 2, a000422.

Nanninga, N. (1998). Morphogenesis of *Escherichia coli*. Microbiol Mol Biol Rev 62, 110-129.

Natale, P., Pazos, M., and Vicente, M. (2013). The *Escherichia coli* divisome: born to divide. Environ Microbiol 15, 3169-3182.

Nelson, W.J. (2003). Adaptation of core mechanisms to generate cell polarity. Nature 422, 766-774.

Nereng, K.S., and Kaplan, S. (1999). Genomic complexity among strains of the facultative photoheterotrophic bacterium *Rhodobacter sphaeroides*. J Bacteriol 181, 1684-1688.

Neumann, S., Grosse, K., and Sourjik, V. (2012). Chemotactic signaling via carbohydrate phosphotransferase systems in *Escherichia coli*. Proc Natl Acad Sci USA 109, 12159-12164.

Nevo-Dinur, K., Govindarajan, S., and Amster-Choder, O. (2012). Subcellular localization of RNA and proteins in prokaryotes. Trends Genet 28, 314-322.

Niederman, R. (2006). Structure, Function and Formation of Bacterial Intracytoplasmic

Membranes. In *Complex Intracellular Structures in Prokaryotes*, J. Shively, ed. (Heidelberg: Springer), pp. 193-227.

Niederman, R.A. (2010). Eukaryotic behaviour of a prokaryotic energy-transducing membrane: fully detached vesicular organelles arise by budding from the *Rhodobacter sphaeroides* intracytoplasmic photosynthetic membrane. Mol Microbiol 76, 803-805.

Niki, H., and Hiraga, S. (1997). Subcellular distribution of actively partitioning F plasmid during the cell division cycle in *E. coli*. Cell 90, 951-957.

Nogales, E. (2000). Structural insights into microtubule function. Annu Rev Biochem 69, 277-302.

Norris, V., den Blaauwen, T., Cabin-Flaman, A., Doi, R.H., Harshey, R., Janniere, L., Jimenez-Sanchez, A., Jin, D.J., Levin, P.A., Mileykovskaya, E., et al. (2007). Functional taxonomy of bacterial hyperstructures. Microbiol Mol Biol Rev 71, 230-253.

Nurse, P., and Marians, K.J. (2013). Purification and characterization of *Escherichia coli* MreB protein. J Biol Chem 288, 3469-3475.

O'Connell, D. (2005). Exploiting the genome: DNA motifs. Nat Rev Microbiol 3, 830-830.

O'Connor, J.R., Kuwada, N.J., Huangyutitham, V., Wiggins, P.A., and Harwood, C.S. (2012). Surface sensing and lateral subcellular localization of WspA, the receptor in a chemosensory-like system leading to c-di-GMP production. Mol Microbiol 86, 720-729.

Oh, D., Yu, Y., Lee, H., Wanner, Barry L., and Ritchie, K. (2014). Dynamics of the serine chemoreceptor in the *Escherichia coli* inner membrane: a high-speed single-molecule tracking study. Biophys J 106, 145-153.

Oliva, M., Halbedel, S., Freund, S., Dutow, P., Leonard, T., Veprintsev, D., Hamoen, L., and Lowe, J. (2010). Features critical for membrane binding revealed by DivIVA crystal structure. EMBO J 29, 1988-2001.

Oliva, M.A., Cordell, S.C., and Lowe, J. (2004). Structural insights into FtsZ protofilament formation. Nat Struct Mol Biol 11, 1243-1250.

Oliva, M.A., Trambaiolo, D., and Löwe, J. (2007). Structural insights into the conformational variability of FtsZ. J Mol Biol 373, 1229-1242.

Osawa, M., Anderson, D.E., and Erickson, H.P. (2008). Reconstitution of contractile FtsZ rings in liposomes. Science 320, 792-794.

Osawa, M., Anderson, D.E., and Erickson, H.P. (2009). Curved FtsZ protofilaments generate bending forces on liposome membranes. EMBO J 28, 3476-3484.

Osawa, M., and Erickson, H.P. (2013). Liposome division by a simple bacterial division machinery. Proc Natl Acad Sci USA 110, 11000-11004.

Osborn, M.J., and Rothfield, L. (2007). Cell shape determination in *Escherichia coli*. Curr Opin Microbiol 10, 606-610.

Overmann, J., and Garcia-Pichel, F. (2006). The Phototrophic Way of Life. In *The Prokaryotes*, M. Dworkin, S. Falkow, E. Rosenberg, K.-H. Schleifer, and E. Stackebrandt, eds. (New York: Springer), pp. 32-85.

Padilla-Parra, S., and Tramier, M. (2012). FRET microscopy in the living cell: different approaches, strengths and weaknesses. BioEssays 34, 369-376.

Pallen, M.J., and Matzke, N.J. (2006). From The Origin of Species to the origin of bacterial flagella. Nat Rev Microbiol 4, 784-790.

Parton, Daniel L., Klingelhoefer, Jochen W., and Sansom, Mark S.P. (2011). Aggregation of model membrane proteins, modulated by hydrophobic mismatch, membrane curvature, and protein class. Biophys J 101, 691-699.

Pearson, M.M., Rasko, D.A., Smith, S.N., and Mobley, H.L.T. (2010). Transcriptome of swarming *Proteus mirabilis*. Infect Immun 78, 2834-2845.

Pemberton, J.M., Horne, I.M., and McEwan, A.G. (1998). Regulation of photosynthetic gene expression in purple bacteria. Microbiology 144, 267-278.

Penfold, R.J., and Pemberton, J.M. (1992). An improved suicide vector for construction of chromosomal insertion mutations in bacteria. Gene 118, 145-146.

Perez-Cheeks, B.A., Planet, P.J., Sarkar, I.N., Clock, S.A., Xu, Q., and Figurski, D.H. (2012). The product of *tadZ*, a new member of the *parA/minD* superfamily, localizes to a pole in *Aggregatibacter actinomycetemcomitans*. Mol Microbiol 83, 694-711.

Peters, P.C., Migocki, M.D., Thoni, C., and Harry, E.J. (2007). A new assembly pathway for the cytokinetic Z ring from a dynamic helical structure in vegetatively growing cells of *Bacillus subtilis*. Mol Microbiol 64, 487-499.

Pfeiffer, D., and Jendrossek, D. (2012). Localization of poly(3-hydroxybutyrate) (PHB) granule-associated proteins during PHB granule formation and identification of two new phasins, PhaP6 and PhaP7, in *Ralstonia eutropha* H16. J Bacteriol 194, 5909-5921.

Pfeiffer, D., Wahl, A., and Jendrossek, D. (2011). Identification of a multifunctional protein, PhaM, that determines number, surface to volume ratio, subcellular localization and distribution to daughter cells of poly(3-hydroxybutyrate), PHB, granules in *Ralstonia eutropha* H16. Mol Microbiol 82, 936-951.

Pichoff, S., and Lutkenhaus, J. (2005). Tethering the Z ring to the membrane through a conserved membrane targeting sequence in FtsA. Mol Microbiol 55, 1722-1734.

Pilhofer, M., and Jensen, G.J. (2013). The bacterial cytoskeleton: more than twisted filaments. Curr Opin Cell Biol 25, 125-133.

Pilizota, T., Brown, M.T., Leake, M.C., Branch, R.W., Berry, R.M., and Armitage, J.P. (2009). A molecular brake, not a clutch, stops the *Rhodobacter sphaeroides* flagellar motor. Proc Natl Acad Sci USA 106, 11582-11587.

Ping, L., Weiner, B., and Kleckner, N. (2008). Tsr-GFP accumulates linearly with time at cell poles, and can be used to differentiate 'old' versus 'new' poles, in *Escherichia coli*. Mol Microbiol 69, 1427-1438.

Piro, O., Carmon, G., Feingold, M., and Fishov, I. (2013). Three-dimensional structure of the Z-ring as a random network of FtsZ filaments. Environ Microbiol 15, 3252-3258.

Pollard, T.D., Blanchoin, L., and Mullins, R.D. (2000). Molecular mechanisms controlling actin filament dynamics in nonmuscle cells. Annu Rev Biophys Biomol Struct 29, 545-576.

Pontius, W., Sneddon, M.W., and Emonet, T. (2013). Adaptation dynamics in densely clustered chemoreceptors. PLoS Comput Biol 9, e1003230.

Porter, S.L., and Armitage, J.P. (2002). Phosphotransfer in *Rhodobacter sphaeroides* chemotaxis. J Mol Biol 324, 35-45.

Porter, S.L., and Armitage, J.P. (2004). Chemotaxis in *Rhodobacter sphaeroides* requires an atypical histidine protein kinase. J Biol Chem 279, 54573-54580.

Porter, S.L., Wadhams, G.H., and Armitage, J.P. (2007). In vivo and in vitro analysis of the *Rhodobacter sphaeroides* chemotaxis signaling complexes. Methods Enzymol 423, 392-413.

Porter, S.L., Wadhams, G.H., and Armitage, J.P. (2008). *Rhodobacter sphaeroides*: complexity in chemotactic signalling. Trends Microbiol 16, 251-260.

Porter, S.L., Wadhams, G.H., and Armitage, J.P. (2011a). Signal processing in complex chemotaxis pathways. Nat Rev Microbiol 9, 153-165.

Porter, S.L., Wilkinson, D.A., Byles, E.D., Wadhams, G.H., Taylor, S., Saunders, N.J., and Armitage, J.P. (2011b). Genome sequence of *Rhodobacter sphaeroides* strain WS8N. J Bacteriol 193, 4027-4028.

Potluri, L.-P., de Pedro, M.A., and Young, K.D. (2012). *Escherichia coli* low-molecular-weight penicillin-binding proteins help orient septal FtsZ, and their absence leads to asymmetric cell division and branching. Mol Microbiol 84, 203-224.

Pratto, F., Cicek, A., Weihofen, W.A., Lurz, R., Saenger, W., and Alonso, J.C. (2008). *Streptococcus pyogenes* pSM19035 requires dynamic assembly of ATP-bound ParA and ParB on *parS* DNA during plasmid segregation. Nucleic Acids Res 36, 3676-3689.

Pruyne, D., and Bretscher, A. (2000). Polarization of cell growth in yeast. J Cell Sci 113, 571-585.

Ptacin, J., Lee, S., Garner, E., Toro, E., Eckart, M., Comolli, L., Moerner, W., and Shapiro, L. (2010). A spindle-like apparatus guides bacterial chromosome segregation. Nat Cell Biol 12, 791-798.

Ptacin, J.L., and Shapiro, L. (2013). Chromosome architecture is a key element of bacterial cellular organization. Cell Microbiol 15, 45-52.

Quardokus, E.M., Din, N., and Brun, Y.V. (2001). Cell cycle and positional constraints on FtsZ localization and the initiation of cell division in *Caulobacter crescentus*. Mol Microbiol 39, 949-959.

Rafelski, S.M., and Marshall, W.F. (2008). Building the cell: design principles of cellular architecture. Nat Rev Mol Cell Biol 9, 593-602.

Ramamurthi, K.S. (2010). Protein localization by recognition of membrane curvature. Curr Opin Microbiol 13, 753-757.

Ramamurthi, K.S., Lecuyer, S., Stone, H.A., and Losick, R. (2009). Geometric cue for protein localization in a bacterium. Science 323, 1354-1357.

Ramos, A., Letek, M., Campelo, A.B., Vaquera, J., Mateos, L.M., and Gil, J.A. (2005). Altered morphology produced by *ftsZ* expression in *Corynebacterium glutamicum* ATCC 13869. Microbiology 151, 2563-2572.

Ranjit, D.K., and Young, K.D. (2013). The Rcs stress response and accessory envelope proteins are required for de novo generation of cell shape in *Escherichia coli*. J Bacteriol 195, 2452-2462.

Rapsomaniki, M.A., Kotsantis, P., Symeonidou, I.-E., Giakoumakis, N.-N., Taraviras, S., and Lygerou, Z. (2012). easyFRAP: an interactive, easy-to-use tool for qualitative and quantitative analysis of FRAP data. Bioinformatics 28, 1800-1801.

Reimold, C., Defeu Soufo, H.J., Dempwolff, F., and Graumann, P.L. (2013). Motion of variable-length MreB filaments at the bacterial cell membrane influences cell morphology. Mol Biol Cell 24, 2340-2349.

Renner, L.D., Eswaramoorthy, P., Ramamurthi, K.S., and Weibel, D.B. (2013). Studying biomolecule localization by engineering bacterial cell wall curvature. PLoS ONE 8, e84143.

Renner, L.D., and Weibel, D.B. (2011). Cardiolipin microdomains localize to negatively curved regions of *Escherichia coli* membranes. Proc Natl Acad Sci USA 108, 6264-6269.

Reyes-Lamothe, R., Nicolas, E., and Sherratt, D.J. (2012). Chromosome replication and segregation in bacteria. Annu Rev Genet 46, 121-143.

Rico, A.I., García-Ovalle, M., Palacios, P., Casanova, M., and Vicente, M. (2010). Role of *Escherichia coli* FtsN protein in the assembly and stability of the cell division ring. Mol Microbiol 76, 760-771.

Rico, A.I., Krupka, M., and Vicente, M. (2013). In the beginning, *Escherichia coli* assembled the proto-ring: an initial phase of division. J Biol Chem 288, 20830-20836.

Ringgaard, S., Schirner, K., Davis, B.M., and Waldor, M.K. (2011). A family of ParA-like ATPases promotes cell pole maturation by facilitating polar localization of chemotaxis proteins. Genes Dev 25, 1544-1555.

Ringgaard, S., van Zon, J., Howard, M., and Gerdes, K. (2009). Movement and equipositioning of plasmids by ParA filament disassembly. Proc Natl Acad Sci USA 106, 19369-19374.

Ringgaard, S., Zepeda-Rivera, M., Wu, X., Schirner, K., Davis, B.M., and Waldor, M.K. (2014). ParP prevents dissociation of CheA from chemotactic signaling arrays and tethers them to a polar anchor. Proc Natl Acad Sci USA 111, E255-E264.

Roberts-Galbraith, R.H., and Gould, K.L. (2008). Stepping into the ring: the SIN takes on contractile ring assembly. Genes Dev 22, 3082-3088.

Roberts, M.A.J., Wadhams, G.H., Hadfield, K.A., Tickner, S., and Armitage, J.P. (2012). ParA-like protein uses nonspecific chromosomal DNA binding to partition protein complexes. Proc Natl Acad Sci USA 109, 6698-6703.

Robertson, G.T., Doyle, T.B., Du, Q., Duncan, L., Mdluli, K.E., and Lynch, A.S. (2007). A novel indole compound that inhibits *Pseudomonas aeruginosa* growth by targeting MreB is a substrate for MexAB-OprM. J Bacteriol 189, 6870-6881.

Rodríguez, A.D., Lear, M.J., and La Clair, J.J. (2008). Identification of the binding of sceptrin to MreB via a bidirectional affinity protocol. J Am Chem Soc 130, 7256-7258.

Rokney, A., Shagan, M., Kessel, M., Smith, Y., Rosenshine, I., and Oppenheim, A.B. (2009). *E. coli* transports aggregated proteins to the poles by a specific and

energy-dependent process. J Mol Biol 392, 589-601.

Romagnoli, S., Packer, H.L., and Armitage, J.P. (2002). Tactic responses to oxygen in the phototrophic bacterium *Rhodobacter sphaeroides* WS8N. J Bacteriol 184, 5590-5598.

Rudner, D.Z., and Losick, R. (2010). Protein subcellular localization in bacteria. Cold Spring Harb Perspect Biol 2, a000307.

Salje, J. (2010). Plasmid segregation: how to survive as an extra piece of DNA. Crit Rev Biochem Mol Biol 45, 296-317.

Santra, M.K., Beuria, T.K., Banerjee, A., and Panda, D. (2004). Ruthenium red-induced bundling of bacterial cell division protein, FtsZ. J Biol Chem 279, 25959-25965.

Sarcina, M., and Mullineaux, C.W. (2000). Effects of tubulin assembly inhibitors on cell division in prokaryotes in vivo. FEMS Microbiol Lett 191, 25-29.

Sass, P., and Brötz-Oesterhelt, H. (2013). Bacterial cell division as a target for new antibiotics. Curr Opin Microbiol 16, 522-530.

Sato, M., Mogi, Y., Nishikawa, T., Miyamura, S., Nagumo, T., and Kawano, S. (2009). The dynamic surface of dividing cyanelles and ultrastructure of the region directly below the surface in *Cyanophora paradoxa*. Planta 229, 781-791.

Savage, D.F., Afonso, B., Chen, A.H., and Silver, P.A. (2010). Spatially ordered dynamics of the bacterial carbon fixation machinery. Science 327, 1258-1261.

Schafer, A., Tauch, A., Jager, W., Kalinowski, J., Thierbach, G., and Puhler, A. (1994). Small mobilizable multi-purpose cloning vectors derived from the *Escherichia coli* plasmids pK18 and pK19: selection of defined deletions in the chromosome of *Corynebacterium glutamicum*. Gene 145, 69-73.

Schofield, W.B., Lim, H.C., and Jacobs-Wagner, C. (2010). Cell cycle coordination and regulation of bacterial chromosome segregation dynamics by polarly localized proteins. EMBO J 29, 3068-3081.

Schulmeister, S., Ruttorf, M., Thiem, S., Kentner, D., Lebiedz, D., and Sourjik, V. (2008). Protein exchange dynamics at chemoreceptor clusters in *Escherichia coli*. Proc Natl Acad

Sci USA 105, 6403-6408.

Scott, K.A., Porter, S.L., Bagg, E.A.L., Hamer, R., Hill, J.L., Wilkinson, D.A., and Armitage, J.P. (2010). Specificity of localization and phosphotransfer in the CheA proteins of *Rhodobacter sphaeroides*. Mol Microbiol 76, 318-330.

Shaevitz, J.W., and Gitai, Z. (2010). The structure and function of bacterial actin homologs. Cold Spring Harb Perspect Biol 2. a000364.

Shaner, N., Steinbach, P., and Tsien, R. (2005). A guide to choosing fluorescent proteins. Nat Methods 2, 905-909.

Shaner, N.C., Patterson, G.H., and Davidson, M.W. (2007). Advances in fluorescent protein technology. J Cell Sci 120, 4247-4260.

Shapiro, L., McAdams, H.H., and Losick, R. (2009). Why and how bacteria localize proteins. Science 326, 1225-1228.

Shebelut, C.W., Jensen, R.B., and Gitai, Z. (2009). Growth conditions regulate the requirements for *Caulobacter* chromosome segregation. J Bacteriol 191, 1097-1100.

Shih, Y.-L., Kawagishi, I., and Rothfield, L. (2005). The MreB and Min cytoskeletal-like systems play independent roles in prokaryotic polar differentiation. Mol Microbiol 58, 917-928.

Shih, Y.-L., and Zheng, M. (2013). Spatial control of the cell division site by the Min system in *Escherichia coli*. Environ Microbiol 15, 3229-3239.

Shiomi, D., Banno, S., Homma, M., and Kawagishi, I. (2005). Stabilization of polar localization of a chemoreceptor via its covalent modifications and its communication with a different chemoreceptor. J Bacteriol 187, 7647-7654.

Shiomi, D., Sakai, M., and Niki, H. (2008). Determination of bacterial rod shape by a novel cytoskeletal membrane protein. EMBO J 27, 3081-3091.

Shiomi, D., Yoshimoto, M., Homma, M., and Kawagishi, I. (2006). Helical distribution of the bacterial chemoreceptor via colocalization with the Sec protein translocation machinery. Mol Microbiol 60, 894-906.

Shively, J.M., Cannon, G.C., Heinhorst, S., Fuerst, J.A., Bryant, D.A., Gantt, E., Maupin-Furlow, J.A., Schüler, D., Pfeifer, F., Docampo, R., et al. (2009). Intracellular Structures of Prokaryotes: Inclusions, Compartments and Assemblages. In *Encyclopedia of Microbiology* (3rd ed), M. Schaechter, ed. (Oxford: Academic Press), pp. 404-424.

Sieber, J.J., Willig, K.I., Kutzner, C., Gerding-Reimers, C., Harke, B., Donnert, G., Rammner, B., Eggeling, C., Hell, S.W., Grubmüller, H., et al. (2007). Anatomy and dynamics of a supramolecular membrane protein cluster. Science 317, 1072-1076.

Slivka, P.F., and Falke, J.J. (2012). Isolated bacterial chemosensory array possesses quasi- and ultrastable components: functional links between array stability, cooperativity, and order. Biochemistry 51, 10218-10228.

Slovak, P.M., Porter, S.L., and Armitage, J.P. (2006). Differential localization of Mre proteins with PBP2 in *Rhodobacter sphaeroides*. J Bacteriol 188, 1691-1700.

Slovak, P.M., Wadhams, G.H., and Armitage, J.P. (2005). Localization of MreB in *Rhodobacter sphaeroides* under conditions causing changes in cell shape and membrane structure. J Bacteriol 187, 54-64.

Snapp, E. (2009). Fluorescent proteins: a cell biologist's user guide. Trends Cell Biol 19, 649-655.

Sourjik, V., and Armitage, J.P. (2010). Spatial organization in bacterial chemotaxis. EMBO J 29, 2724-2733.

Sourjik, V., and Wingreen, N.S. (2012). Responding to chemical gradients: bacterial chemotaxis. Curr Opin Cell Biol 24, 262-268.

Southward, C.M., and Surette, M.G. (2002). The dynamic microbe: green fluorescent protein brings bacteria to light. Mol Microbiol 45, 1191-1196.

Sowa, Y., and Berry, R.M. (2008). Bacterial flagellar motor. Q Rev Biophys 41, 103-132.

Specht, M., Dempwolff, F., Schätzle, S., Thomann, R., and Waidner, B. (2013). Localization of FtsZ in *Helicobacter pylori* and consequences for cell division. J Bacteriol 195, 1411-1420.

Spira, F., Mueller, N.S., Beck, G., von Olshausen, P., Beig, J., and Wedlich-Soldner, R. (2012). Patchwork organization of the yeast plasma membrane into numerous coexisting domains. Nat Cell Biol 14, 640-648.

Srinivasan, R., Mishra, M., Wu, L., Yin, Z., and Balasubramanian, M.K. (2008). The bacterial cell division protein FtsZ assembles into cytoplasmic rings in fission yeast. Genes Dev 22, 1741-1746.

Srivastava, P., Demarre, G., Karpova, T.S., McNally, J., and Chattoraj, D.K. (2007). Changes in nucleoid morphology and origin localization upon inhibition or alteration of the actin homolog, MreB, of *Vibrio cholerae*. J Bacteriol 189, 7450-7463.

Stachowiak, J.C., Schmid, E.M., Ryan, C.J., Ann, H.S., Sasaki, D.Y., Sherman, M.B., Geissler, P.L., Fletcher, D.A., and Hayden, C.C. (2012). Membrane bending by protein–protein crowding. Nat Cell Biol 14, 944-949.

Strahl, H., and Hamoen, L.W. (2012). Finding the corners in a cell. Curr Opin Microbiol 15, 731-736.

Strauss, M.P., Liew, A.T., Turnbull, L., Whitchurch, C.B., Monahan, L.G., and Harry, E.J. (2012). 3D-SIM super resolution microscopy reveals a bead-like arrangement for FtsZ and the division machinery: implications for triggering cytokinesis. PLoS Biol 10, e1001389.

Sun, Q., and Margolin, W. (1998). FtsZ dynamics during the division cycle of live *Escherichia coli* cells. J Bacteriol 180, 2050-2056.

Sun, S.X., and Jiang, H. (2011). Physics of bacterial morphogenesis. Microbiol Mol Biol Rev 75, 543-565.

Suwanto, A., and Kaplan, S. (1989). Physical and genetic mapping of the *Rhodobacter sphaeroides* 2.4.1 genome: presence of two unique circular chromosomes. J Bacteriol 171, 5850-5859.

Suzuki, K.G. (2012). Lipid rafts generate digital-like signal transduction in cell plasma membranes. Biotechnol J 7, 753-761.

Swulius, M.T., Chen, S., Jane Ding, H., Li, Z., Briegel, A., Pilhofer, M., Tocheva, E.I.,

Lybarger, S.R., Johnson, T.L., Sandkvist, M., et al. (2011). Long helical filaments are not seen encircling cells in electron cryotomograms of rod-shaped bacteria. Biochem Biophys Res Commun 407, 650-655.

Swulius, M.T., and Jensen, G.J. (2012). The helical MreB cytoskeleton in *Escherichia coli* MC1000/pLE7 is an artifact of the N-terminal yellow fluorescent protein tag. J Bacteriol 194, 6382-6386.

Szardenings, F., Guymer, D., and Gerdes, K. (2011). ParA ATPases can move and position DNA and subcellular structures. Curr Opin Microbiol 14, 712-718.

Takacs, C.N., Poggio, S., Charbon, G., Pucheault, M., Vollmer, W., and Jacobs-Wagner, C. (2010). MreB drives de novo rod morphogenesis in *Caulobacter crescentus* via remodeling of the cell wall. J Bacteriol 192, 1671-1684.

Takeuchi, S., DiLuzio, W., Weibel, D., and Whitesides, G. (2005). Controlling the shape of filamentous cells of *Escherichia coli*. Nano Lett 5, 1819-1823.

Tan, Q., Awano, N., and Inouye, M. (2011). YeeV is an *Escherichia coli* toxin that inhibits cell division by targeting the cytoskeleton proteins, FtsZ and MreB. Mol Microbiol 79, 109-118.

Thanbichler, M. (2010). Synchronization of chromosome dynamics and cell division in bacteria. Cold Spring Harb Perspect Biol 2, a000331.

Thanbichler, M., and Shapiro, L. (2006). MipZ, a spatial regulator coordinating chromosome segregation with cell division in *Caulobacter*. Cell 126, 147-162.

Thanedar, S., and Margolin, W. (2004). FtsZ exhibits rapid movement and oscillation waves in helix-like patterns in *Escherichia coli*. Curr Biol 14, 1167-1173.

Thiem, S., Kentner, D., and Sourjik, V. (2007). Positioning of chemosensory clusters in *E. coli* and its relation to cell division. EMBO J 26, 1615-1623.

Thiem, S., and Sourjik, V. (2008). Stochastic assembly of chemoreceptor clusters in *Escherichia coli*. Mol Microbiol 68, 1228-1236.

Thompson, S.R., Wadhams, G.H., and Armitage, J.P. (2006). The positioning of

cytoplasmic protein clusters in bacteria. Proc Natl Acad Sci USA 103, 8209-8214.

Tocheva, E.I., Li, Z., and Jensen, G.J. (2010). Electron cryotomography. Cold Spring Harb Perspect Biol 2, a003442.

Tonthat, N.K., Arold, S.T., Pickering, B.F., Van Dyke, M.W., Liang, S., Lu, Y., Beuria, T.K., Margolin, W., and Schumacher, M.A. (2011). Molecular mechanism by which the nucleoid occlusion factor, SlmA, keeps cytokinesis in check. EMBO J 30, 154-164.

Tonthat, N.K., Milam, S.L., Chinnam, N., Whitfill, T., Margolin, W., and Schumacher, M.A. (2013). SlmA forms a higher-order structure on DNA that inhibits cytokinetic Z-ring formation over the nucleoid. Proc Natl Acad Sci USA 110, 10586-10591.

Toro, E., and Shapiro, L. (2010). Bacterial chromosome organization and segregation. Cold Spring Harb Perspect Biol 2, a000349.

Treuner-Lange, A., Aguiluz, K., van der Does, C., Gómez-Santos, N., Harms, A., Schumacher, D., Lenz, P., Hoppert, M., Kahnt, J., Muñoz-Dorado, J., et al. (2013). PomZ, a ParA-like protein, regulates Z-ring formation and cell division in *Myxococcus xanthus*. Mol Microbiol 87, 235-253.

Tu, Y. (2013). Quantitative modeling of bacterial chemotaxis: signal amplification and accurate adaptation. Annu Rev Biophys 42, 337-359.

Tucker, J.D., Siebert, C.A., Escalante, M., Adams, P.G., Olsen, J.D., Otto, C., Stokes, D.L., and Hunter, C.N. (2010). Membrane invagination in *Rhodobacter sphaeroides* is initiated at curved regions of the cytoplasmic membrane, then forms both budded and fully detached spherical vesicles. Mol Microbiol 76, 833-847.

Typas, A., Banzhaf, M., Gross, C.A., and Vollmer, W. (2012). From the regulation of peptidoglycan synthesis to bacterial growth and morphology. Nat Rev Microbiol 10, 123-136.

Ursell, T.S., Nguyen, J., Monds, R.D., Colavin, A., Billings, G., Ouzounov, N., Gitai, Z., Shaevitz, J.W., and Huang, K.C. (2014). Rod-like bacterial shape is maintained by feedback between cell curvature and cytoskeletal localization. Proc Natl Acad Sci USA 111, E1025-E1034.

van den Ent, F., Amos, L.A., and Lowe, J. (2001). Prokaryotic origin of the actin cytoskeleton. Nature 413, 39-44.

van den Ent, F., Johnson, C.M., Persons, L., de Boer, P., and Löwe, J. (2010). Bacterial actin MreB assembles in complex with cell shape protein RodZ. EMBO J 29, 1081-1090.

van Teeffelen, S., Shaevitz, J.W., and Gitai, Z. (2012). Image analysis in fluorescence microscopy: bacterial dynamics as a case study. BioEssays 34, 427-436.

van Teeffelen, S., Wang, S., Furchtgott, L., Huang, K.C., Wingreen, N.S., Shaevitz, J.W., and Gitai, Z. (2011). The bacterial actin MreB rotates, and rotation depends on cell-wall assembly. Proc Natl Acad Sci USA 108, 15822-15827.

Varley, A.W., and Stewart, G.C. (1992). The *divIVB* region of the *Bacillus subtilis* chromosome encodes homologs of *Escherichia coli* septum placement (*minCD*) and cell shape (*mreBCD*) determinants. J Bacteriol 174, 6729-6742.

Varma, A., de Pedro, M.A., and Young, K.D. (2007). FtsZ directs a second mode of peptidoglycan synthesis in *Escherichia coli*. J Bacteriol 189, 5692-5704.

Varma, A., and Young, K.D. (2004). FtsZ collaborates with penicillin binding proteins to generate bacterial cell shape in *Escherichia coli*. J Bacteriol 186, 6768-6774.

Varma, A., and Young, K.D. (2009). In *Escherichia coli*, MreB and FtsZ direct the synthesis of lateral cell wall via independent pathways that require PBP 2. J Bacteriol 191, 3526-3533.

Vats, P., and Rothfield, L. (2007). Duplication and segregation of the actin (MreB) cytoskeleton during the prokaryotic cell cycle. Proc Natl Acad Sci USA 104, 17795-17800.

Vecchiarelli, A.G., Han, Y.-W., Tan, X., Mizuuchi, M., Ghirlando, R., Biertümpfel, C., Funnell, B.E., and Mizuuchi, K. (2010). ATP control of dynamic P1 ParA–DNA interactions: a key role for the nucleoid in plasmid partition. Mol Microbiol 78, 78-91.

Vecchiarelli, A.G., Mizuuchi, K., and Funnell, B.E. (2012). Surfing biological surfaces: exploiting the nucleoid for partition and transport in bacteria. Mol Microbiol 86, 513-523.

Vecchiarelli, A.G., Neuman, K.C., and Mizuuchi, K. (2014). A propagating ATPase gradient drives transport of surface-confined cellular cargo. Proc Natl Acad Sci USA 111, 4880-4885.

Vendeville, A., Larivière, D., and Fourmentin, E. (2010). An inventory of the bacterial macromolecular components and their spatial organization. FEMS Microbiol Rev 35, 395–414.

Vignaud, T., Blanchoin, L., and Théry, M. (2012). Directed cytoskeleton self-organization. Trends Cell Biol 22, 671-682.

Vollmer, W., and Holtje, J.V. (2001). Morphogenesis of *Escherichia coli*. Curr Opin Microbiol 4, 625-633.

Wachi, M., Doi, M., Okada, Y., and Matsuhashi, M. (1989). New *mre* genes *mreC* and *mreD*, responsible for formation of the rod shape of *Escherichia coli* cells. J Bacteriol. 171, 6511–6516.

Wachi, M., Doi, M., Tamaki, S., Park, W., Nakajima-Iijima, S., and Matsuhashi, M. (1987). Mutant isolation and molecular cloning of *mre* genes, which determine cell shape, sensitivity to mecillinam, and amount of penicillin-binding proteins in *Escherichia coli*. J Bacteriol 169, 4935-4940.

Wachi, M., and Matsuhashi, M. (1989). Negative control of cell division by *mreB*, a gene that functions in determining the rod shape of *Escherichia coli* cells. J Bacteriol. 171, 3123-3127.

Wadhams, G.H., and Armitage, J.P. (2004). Making sense of it all: bacterial chemotaxis. Nat Rev Mol Cell Biol 5, 1024-1037.

Wadhams, G.H., Martin, A.C., and Armitage, J.P. (2000). Identification and localization of a methyl-accepting chemotaxis protein in *Rhodobacter sphaeroides*. Mol Microbiol 36, 1222-1233.

Wadhams, G.H., Martin, A.C., Warren, A.V., and Armitage, J.P. (2005). Requirements for chemotaxis protein localization in *Rhodobacter sphaeroides*. Mol Microbiol 58, 895-902.

Wadhams, G.H., Warren, A.V., Martin, A.C., and Armitage, J.P. (2003). Targeting of two

signal transduction pathways to different regions of the bacterial cell. Mol Microbiol 50, 763-770.

Wagner, J.K., Galvani, C.D., and Brun, Y.V. (2005). *Caulobacter crescentus* requires RodA and MreB for stalk synthesis and prevention of ectopic pole formation. J Bacteriol 187, 544-553.

Wahl, A., Schuth, N., Pfeiffer, D., Nussberger, S., and Jendrossek, D. (2012). PHB granules are attached to the nucleoid via PhaM in *Ralstonia eutropha*. BMC Microbiol 12, 262.

Waidner, B., Specht, M., Dempwolff, F., Haeberer, K., Schaetzle, S., Speth, V., Kist, M., and Graumann, P.L. (2009). A novel system of cytoskeletal elements in the human pathogen *Helicobacter pylori*. PLoS Pathog 5, e1000669.

Wang, H., Wingreen, N.S., and Mukhopadhyay, R. (2008a). Self-organized periodicity of protein clusters in growing bacteria. Phys Rev Lett 101, 218101.

Wang, J., Galgoci, A., Kodali, S., Herath, K.B., Jayasuriya, H., Dorso, K., Vicente, F., Gonzalez, A., Cully, D., Bramhill, D., et al. (2003). Discovery of a small molecule that inhibits cell division by blocking FtsZ, a novel therapeutic target of antibiotics. J Biol Chem 278, 44424-44428.

Wang, S., Arellano-Santoyo, H., Combs, P.A., and Shaevitz, J.W. (2010). Actin-like cytoskeleton filaments contribute to cell mechanics in bacteria. Proc Natl Acad Sci USA 107, 9182-9185.

Wang, W., Li, G.-W., Chen, C., Xie, X.S., and Zhuang, X. (2011). Chromosome organization by a nucleoid-associated protein in live bacteria. Science 333, 1445-1449.

Wang, X., Reyes-Lamothe, R., and Sherratt, D. (2008b). Visualizing genetic loci and molecular machines in living bacteria. Biochem Soc Trans 36, 749-753.

Ward, J.E., and Lutkenhaus, J. (1985). Overproduction of FtsZ induces minicell formation in *E. coli*. Cell 42, 941-949.

Weart, R.B., Lee, A.H., Chien, A.-C., Haeusser, D.P., Hill, N.S., and Levin, P.A. (2007). A metabolic sensor governing cell size in bacteria. Cell 130, 335-347.

Weidel, W., Frank, H., and Martin, H.H. (1960). The rigid layer of the cell wall of *Escherichia coli* strain B. J Gen Microbiol 22, 158-166.

Werner, J.N., Chen, E.Y., Guberman, J.M., Zippilli, A.R., Irgon, J.J., and Gitai, Z. (2009). Quantitative genome-scale analysis of protein localization in an asymmetric bacterium. Proc Natl Acad Sci USA 106, 7858-7863.

White, C.L., and Gober, J.W. (2012). MreB: pilot or passenger of cell wall synthesis? Trends Microbiol 20, 74-79.

White, E.L., Suling, W.J., Ross, L.J., Seitz, L.E., and Reynolds, R.C. (2002). 2-Alkoxycarbonylaminopyridines: inhibitors of *Mycobacterium tuberculosis* FtsZ. J Antimicrob Chemother 50, 111-114.

Wiggins, P.A., Cheveralls, K.C., Martin, J.S., Lintner, R., and Kondev, J. (2010). Strong intranucleoid interactions organize the *Escherichia coli* chromosome into a nucleoid filament. Proc Natl Acad Sci USA 107, 4991-4995.

Wilkinson, D.A., Chacko, S.J., Vénien-Bryan, C., Wadhams, G.H., and Armitage, J.P. (2011). Regulation of flagellum number by FliA and FlgM and role in biofilm formation by *Rhodobacter sphaeroides*. J Bacteriol 193, 4010-4014.

Willemse, J., Borst, J.W., de Waal, E., Bisseling, T., and van Wezel, G.P. (2011). Positive control of cell division: FtsZ is recruited by SsgB during sporulation of *Streptomyces*. Genes Dev 25, 89-99.

Willemse, J., and van Wezel, G.P. (2009). Imaging of *Streptomyces coelicolor* A3(2) with reduced autofluorescence reveals a novel stage of FtsZ localization. PLoS ONE 4, e4242.

Wilson, M.Z., and Gitai, Z. (2013). Beyond the cytoskeleton: mesoscale assemblies and their function in spatial organization. Curr Opin Microbiol 16, 177-183.

Winkler, J., Seybert, A., Konig, L., Pruggnaller, S., Haselmann, U., Sourjik, V., Weiss, M., Frangakis, A.S., Mogk, A., and Bukau, B. (2010). Quantitative and spatio-temporal features of protein aggregation in *Escherichia coli* and consequences on protein quality control and cellular ageing. EMBO J 29, 910-923.

Winters, P., Caldwell, R., Enfield, L., and Ferrari, E. (1996). The *ampS-nprE* (124

degrees-127 degrees) region of the *Bacillus subtilis* 168 chromosome: sequencing of a 27 kb segment and identification of several genes in the area. Microbiology 142, 3033-3037.

Woronowicz, K., and Niederman, R.A. (2010). Proteomic Analysis of the Developing Intracytoplasmic Membrane in *Rhodobacter sphaeroides*; During Adaptation to Low Light Intensity. In *Recent Advances in Phototrophic Prokaryotes*, P.C.C. Hallenbeck, ed. (New York: Springer), pp. 161-178.

Wu, K., Walukiewicz, H.E., Glekas, G.D., Ordal, G.W., and Rao, C.V. (2011). Attractant binding induces distinct structural changes to the polar and lateral signaling clusters in *Bacillus subtilis* chemotaxis. J Biol Chem 286, 2587-2595.

Wu, L.J., and Errington, J. (2004). Coordination of cell division and chromosome segregation by a nucleoid occlusion protein in *Bacillus subtilis*. Cell 117, 915-925.

Wu, L.J., and Errington, J. (2011). Nucleoid occlusion and bacterial cell division. Nat Rev Microbiol 10, 8-12.

Wu, L.J., Ishikawa, S., Kawai, Y., Oshima, T., Ogasawara, N., and Errington, J. (2009). Noc protein binds to specific DNA sequences to coordinate cell division with chromosome segregation. EMBO J 28, 1940-1952.

Yamaichi, Y., Bruckner, R., Ringgaard, S., Möll, A., Cameron, D.E., Briegel, A., Jensen, G.J., Davis, B.M., and Waldor, M.K. (2012). A multidomain hub anchors the chromosome segregation and chemotactic machinery to the bacterial pole. Genes Dev 26, 2348-2360.

Yanofsky, C. (1991). What will be the fate of research on prokaryotes? Cell 65, 199-200.

Yao, S., Helinski, D.R., and Toukdarian, A. (2007). Localization of the naturally occurring plasmid ColE1 at the cell pole. J Bacteriol 189, 1946-1953.

Yeates, T.O., Kerfeld, C.A., Heinhorst, S., Cannon, G.C., and Shively, J.M. (2008). Protein-based organelles in bacteria: carboxysomes and related microcompartments. Nat Rev Microbiol 6, 681-691.

Yeh, Y.-C., Comolli, L.R., Downing, K.H., Shapiro, L., and McAdams, H.H. (2010). The *Caulobacter* Tol-Pal complex is essential for outer membrane integrity and the positioning of a polar localization factor. J Bacteriol 192, 4847-4858.

Yonetani, A., Lustig, R.J., Moseley, J.B., Takeda, T., Goode, B.L., and Chang, F. (2008). Regulation and targeting of the fission yeast formin cdc12p in cytokinesis. Mol Biol Cell 19, 2208-2219.

Young, K.D. (2003). Bacterial shape. Mol Microbiol 49, 571-580.

Young, K.D. (2006). The selective value of bacterial shape. Microbiol Mol Biol Rev 70, 660-703.

Young, K.D. (2010). Bacterial shape: two-dimensional questions and possibilities. Annu Rev Microbiol 64, 223-240.

Youngren, B., Nielsen, H.J., Jun, S., and Austin, S. (2014). The multifork *Escherichia coli* chromosome is a self-duplicating and self-segregating thermodynamic ring polymer. Genes Dev 28, 71-84.

Yu, X.C., and Margolin, W. (1998). Inhibition of assembly of bacterial cell division protein FtsZ by the hydrophobic dye 5,5'-Bis-(8-anilino-1-naphthalenesulfonate). J Biol Chem 273, 10216-10222.

Yu, X.C., Margolin, W., Gonzalez-Garay, M.L., and Cabral, F. (1999). Vinblastine induces an interaction between FtsZ and tubulin in mammalian cells. J Cell Sci 112, 2301-2311.

Zeilstra-Ryalls, J., Gomelsky, M., Eraso, J.M., Yeliseev, A., O'Gara, J., and Kaplan, S. (1998). Control of photosystem formation in *Rhodobacter sphaeroides*. J Bacteriol 180, 2801-2809.

Zhang, P., Khursigara, C.M., Hartnell, L.M., and Subramaniam, S. (2007). Direct visualization of *Escherichia coli* chemotaxis receptor arrays using cryo-electron microscopy. Proc Natl Acad Sci USA 104, 3777-3781.

Zimmerberg, J., and Kozlov, M.M. (2006). How proteins produce cellular membrane curvature. Nat Rev Mol Cell Biol 7, 9-19.

Zupan, J.R., Cameron, T.A., Anderson-Furgeson, J., and Zambryski, P.C. (2013). Dynamic FtsA and FtsZ localization and outer membrane alterations during polar growth and cell division in *Agrobacterium tumefaciens*. Proc Natl Acad Sci USA 110, 9060-9065.

Appendix: Media and Reagents

LB medium

Ingredients	Quantity per litre
Yeast extract	5 g
Tryptone	10 g
NaCl	5 g

Made up to 1 litre with MilliQ water. Adjusted to pH 7.0. Autoclave.

Succinate medium

Ingredients	Quantity per litre
1M Phosphate buffer (see below)	20 ml
Concentrated base (see below)	20 ml
Growth factors (see below)	2 ml
$(NH_4)_2SO_4$	0.5 g
NaCl	0.5 g
Sodium succinate	2 g
Casamino acids	1 g

Made up to 1 litre with MilliQ water, pH adjust to 7.2 with KOH, autoclave.

1M Phosphate buffer pH 7.0

Ingredients	Quantity per litre
K_2HPO_4 1M	174.18 g
KH_2PO_4 1M	136.09 g

Adjust to pH 7.0 with KOH, autoclave and store at 4°C.

Concentrated base

Ingredients	Quantity per litre
Nitrilotiracetic acid	5.94 g
Metals 44 solution (see below)	25 ml
$MgSO_4 \cdot 7H_2O$	14.5 g
$CaCl_2 \cdot 2H_2O$	1.67 g
$FeSO_4 \cdot 7H_2O$	50 mg
Ammonium molybdate $4H_2O$	4.6 mg or 0.2 ml of 23 mg/ml
Casamino acids	1 g

Dissolve nitrilotiracetic acid first and adjust pH with KOH to pH 5.0, it won't dissolve until very near pH 5. This allows $FeSO_4$ to dissolve. Add all the other ingredients. Adjust pH to 6.8 with KOH. Autoclave and store at 4°C.

Metals 44 solution

Ingredients	Quantity per litre
Tetrasodium versenate (EDTA)	2.5 g
$ZnSO_4 \cdot 7H2O$	11 g
$FeSO_4 \cdot 7H2O$	5 g
3M sulphuric acid	1.5 ml
$MnSO_4 \cdot 4H2O$	3 g
$CuSO_4 \cdot 5H2O$	0.39 g
H_3BO_3	0.12
$CoCl_2 \cdot 6H2O$	0.2 g

Filter sterilise and store at 4°C.

Growth factor

Ingredients	Quantity per litre
Biotin	20 mg
$NaHCO_3$	500 mg
Niacin	1 g
Thiamine HCl	500 mg

Autoclave and store at 4°C.

M22

Ingredients	Quantity per litre
1 M phosphate buffer	20 ml
Concentrated base	20 ml
Growth factor	2 ml
$(NH_4)_2SO4$	0.5 g
NaCl	0.5 g

Made up to 1 litre with MilliQ water. Adjust pH to 7.2 with KOH, autoclave.

10 × TBE

Ingredients	Quantity per litre
Tris base	108 g
Boric acid	55 g
EDTA	7.4 g

Made up to 1 litre with MilliQ water. Adjust pH to 8.3.

TFB I

Ingredients	Quantity per litre
Potassiun acetate	30 mM
$RbCl_2$	100 mM
$CaCl_2 \cdot 2H_2O$	10mM
$MnCl_2 \cdot 4H_2O$	50 mM
Glycerol	15% (v/v)

Adjust pH to 5.8 with 0.2 M acetic acid. Filter sterilize.

TFB II

Ingredients	Quantity per litre
PIPES	10 mM
$RbCl_2$	10 mM
$CaCl_2 \cdot 2H_2O$	75 mM
Glycerol	15% (v/v)

Adjust pH to 6.8 with HCl. Filter sterilise.